Diagnostic Imaging of Foreign Bodies and Compartmentalization in the Canine Manus

by

Christopher P. Ober, DVM
Diplomate, ACVR

Dissertation submitted to the faculty of the Virginia Polytechnic Institute and State University in partial fulfillment of the requirements for the degree of

Doctor of Philosophy

in

Biomedical and Veterinary Sciences

Jeryl C. Jones, DVM, PhD, Dipl. ACVR, Chair
Allen D. Elster, MA, MD, MBA
Otto I. Lanz, DVM, Dipl. ACVS
Martha Moon Larson, DVM, MS, Dipl. ACVR
Christopher L. Wyatt, PhD

17 March 2009
Blacksburg, Virginia

Keywords: Computed tomography, magnetic resonance imaging, myofascial compartment, soft-tissue space, ultrasound

Diagnostic Imaging of Foreign Bodies and Compartmentalization in the Canine Manus

Christopher P. Ober

Abstract

Injury of the manus is an important cause of morbidity and function loss in dogs, especially working breeds. These injuries may cause foreign body retention and can lead to persistent infection. Accurate methods for diagnosis and localization of pathology in this anatomically complex region are critical to minimize patient morbidity, guide surgical planning, and improve case outcomes.

The anatomy of the canine manus was evaluated with computed tomography (CT), magnetic resonance imaging (MRI), and transverse anatomic sections. Most structures identified on transverse sections were visible on both CT and MRI images. Detail in the osseous structures was better in CT images, while MRI provided increased contrast of soft-tissue structures.

To test the hypothesis that diagnostic accuracies of CT, MRI, and ultrasound differ for detection of acute wooden foreign bodies in the canine manus, we inserted wooden splinters into canine cadaver manus and imaged each manus with all three modalities. Receiver operating characteristic curve analysis demonstrated that CT was most accurate for detection of acute wooden foreign bodies, followed in turn by ultrasound and MRI.

Diseases in the human hand and foot are often confined by soft-tissue spaces, but similar structures have not been described in the dog. To determine if these spaces are present in the canine manus, we injected contrast medium into likely spaces and compartments in cadaver specimens, imaged the limbs with CT, and dissected the injected manus specimens. We found thirteen discrete soft-tissue spaces and five myofascial compartments that are similar to those described in the human hand.

To test the hypothesis that spread of disease in the canine manus can be modeled and predicted, we injected cadaver interdigital web spaces with contrast medium, imaged them with CT, and dissected them. We found that the pattern of contrast agent spread, as a model of infection, was predictable and unique to the initial injection site.

Findings from these cadaver studies improve our understanding of anatomy, imaging of wooden foreign bodies, and likely patterns of disease extension in the canine manus. Future studies are needed to test the utility of this information for surgical planning in affected clinical patients.

Dedication

For Sheri, who has supported me with love and without question throughout this entire process, and who has willingly made more sacrifices than any person could possibly be expected to make.

For Spot, who started me down this pathway those many years ago.

And for Phoenix and Sierra, who remind me on a daily basis what it really means to be a vet.

Acknowledgements

No endeavor that is half a decade and tens of thousands of words in the making could get off the ground without an awesome supporting cast, and you won't find any exceptions here. This is a huge thank-you to all of those individuals who knowingly or unwittingly helped me out throughout this project.

My parents, (Dr.) Patrick and Cathy Ober: The greatest parents anyone could hope for. For thirty-some years they have provided me with everything I've ever needed (and even that Super Nintendo that I didn't dare ask for).

Dr. Sarah Davies and Dr. Diane Saulnier: My fellow residents have a great sense of humor, and have always been there to bounce ideas off of, complain with, and gossip with (not necessarily in that order).

Dr. Steve Holladay: He doesn't get his name plastered all over this thing, but as my external reviewer, he still had to read it all.

Susie Ayers, Valerie Ishman, and Becky Calfee: This trio of radiology technologists was invaluable in getting all of the imaging done.

Pam Arnold: She has the greatest attitude of anyone I've ever asked to help slice up countless numbers of dog paws.

The shelter dogs: None of this research would have been possible without the sacrifices of these animals.

Virginia Veterinary Medical Association: This group gets a special thanks for providing the funding for the study of wooden foreign bodies in the canine manus.

American Kennel Club Canine Health Foundation: This organization particularly deserves my gratitude for providing the funding for the studies evaluating spaces & compartments and modeling of infection spread in the manus.

The Virginia Tech Veterinary Teaching Hospital and Office of Research and Graduate Studies: Even as the economy tanked, these folks were committed enough to my research to make sure my paycheck continued to arrive.

Table of Contents

List of Tables

List of Figures

Chapter I

Introduction

This dissertation includes four experiments evaluating the best imaging techniques for detection of foreign objects within the canine manus and determining the extent of soft-tissue spaces and myofascial compartments within the manus. This dissertation contains an extensive overview of the human and veterinary literature and four chapters in manuscript format relating the design, procedures, and results of four individual experiments. Three appendices are also included: the first of these is an anatomic atlas of sectional anatomy of the canine manus in three planes, the second is a listing of previous research evaluating the visibility of retained foreign objects, and the third is a pictorial case series representing common imaging findings seen when foreign objects are retained in different parts of the body.

This work represents the collaborative efforts of multiple individuals. The primary author was responsible for producing the dissertation, individual manuscripts, and appendices. Dr. Jeryl Jones, the graduate committee chair, assisted in experimental design, image interpretation, and manuscript review. Dr. Martha Larson served as a committee member and also assisted in experimental design and image interpretation. Dr. Allen Elster and Dr. Christopher Wyatt also served as committee members and further contributed to experimental design. Statistical analysis support was provided by Dr. Stephen Werre, and Dr. Larry Freeman provided assistance in identification of anatomic structures.

1. Background and Significance

Injuries of the distal extremity, including both the manus and the pes, are important causes of morbidity in dogs. Injuries of the distal extremities include lacerations, abrasions, and retention of foreign bodies, and are some of the most common ailments seen in working dogs.[1,2] Foreign body penetration is especially problematic, as these objects may be difficult to identify and can lead to complications ranging from neuropraxia to abscessation and osteomyelitis.[3] Foreign objects often harbor infectious agents, and resolution of clinical signs generally requires recognition and removal of the foreign body. Exploratory surgery can be used to attempt to diagnose and treat suspected foreign bodies, but multiple procedures are required in many cases,[4] and surgery can induce further morbidity.

Diagnosis of some foreign bodies, such as metallic objects, can be made based on radiography. However, foreign objects affecting the distal extremities are commonly composed of wood or other plant material,[5,6] and these objects are generally not visible using radiography.[7-10] Thus, other means of diagnosing wooden foreign bodies are required to limit patient morbidity and improve surgical outcomes. Ultrasonography (US), magnetic resonance imaging (MRI), and computed tomography (CT) have been previously described as sensitive techniques for identifying foreign objects that are not radiographically visible. However, each modality has limitations and there are contradictions in the literature regarding their relative sensitivities. Ultrasound is commonly used in the emergency department to search for embedded foreign objects and in surgical planning for removal of identified foreign bodies,[11-15] but the diagnostic accuracy is variable because sonography is highly operator dependent.[15,16] Foreign objects may also be obscured when they are surrounded by bone, air, dense fibrous tissue, or other tissue

interfaces.[3,10] MRI produces excellent soft-tissue contrast resolution,[16] but the spatial resolution with this modality is generally worse than that seen with the other modalities,[17] which may be a significant limitation when looking for a small embedded object. Additionally, low-signal structures such as calcifications or tendons may produce a false-positive diagnosis when searching for low-intensity foreign objects.[16] Computed tomography has an intermediate spatial resolution relative to ultrasound and MRI,[17] though the soft tissue contrast resolution, while better than that of conventional radiography, is somewhat limited.[16] Like MRI, superimposition of structures does not pose a problem for CT,[3] but failure to recognize a wooden foreign body is somewhat common using CT, as these objects often have a density confused for that of air.[9,18-20] Among the comparative diagnostic imaging studies performed previously, only a small number used distal extremity specimens to test these modalities in regions of appropriate anatomic complexity,[5,7,8,21-24] and all of these were in human subjects, rather than animals. Additionally, only three studies have evaluated US, MRI, and CT simultaneously, but these studies were not performed in the distal extremity and their results do not entirely agree with each other.[9,25,26] Therefore, determination of the most accurate imaging modality for detection of wooden foreign bodies in the canine manus would be beneficial to efficiently diagnose foreign object retention, improve surgical planning, and minimize patient morbidity.

Foreign bodies and infectious processes have a tendency to migrate and spread throughout the affected region.[6,27-29] Because of the likelihood of spread, exploratory surgery often requires a large field, which increases patient morbidity. Also, if the full extent of the spread is not recognized, additional surgical interventions may be required. Because advanced imaging is not always available for evaluation of the distal extremity in injured dogs, especially working dogs in the field, the ability to predict the path of extension would be beneficial in minimizing the

required surgical field and thus decreasing patient morbidity. Discrete soft-tissue spaces and myofascial compartments are recognized in the human hand[30-33] and foot,[34-36] and these structures often determine the spread of inflammation, infection, and neoplasia in the human hand and foot.[37-40] Because disease tends to remain confined to a soft-tissue space or myofascial compartment, surgical intervention can be narrowly directed, and generalized exploration of the distal extremity is often not required in human patients.[38,40,41] While recognition of similar structures in the canine manus would be beneficial in targeting therapy to a specific region, analogous soft-tissue spaces and myofascial compartments have not been identified in the distal extremity of the dog.

2. Research Objectives

This investigation included two observational and two critical studies of the canine manus. The objectives for the first observational study (Chapter III) were to describe the sectional anatomy of the canine manus, determine the visibility of structures using computed tomography and magnetic resonance imaging, and develop an anatomic atlas for use in characterization of lesions. The objectives for the first critical study (Chapter IV) were to compare the diagnostic sensitivities and accuracies of ultrasound, computed tomography, and magnetic resonance imaging in detection of wooden foreign objects in the canine manus, and to develop practice guidelines for use of those modalities when foreign body retention is suspected. We hypothesized that ultrasound would be the most sensitive modality for detection of wooden foreign bodies, and that all modalities would demonstrate some of the foreign objects.

The objective for the second observational study (Chapter V) was to describe the normal extent and locations of soft-tissue spaces and myofascial compartments in the canine manus, using previously described structures in the human hand as a guide. The objectives for the second critical study (Chapter VI) were to describe the extent of involvement of the soft tissues of the manus in a model of injury to the interdigital web spaces, to evaluate if the initial site of injury could be used to predict likely extension of inflammation, and to determine whether patterns of extension caused by injury were unique to each interdigital web space. Hypotheses for this experiment were that the extension of inflammation could be predicted based on the known initial site of injury, and that the patterns of extension stemming from each individual injury site could be differentiated from each other.

Chapter II

Review of the Literature

1. Normal Anatomy of the Canine Manus

1.1 Bones

The manus consists of the bones of the carpus, metacarpus, phalanges, and associated sesamoid bones. The carpus includes two rows of bones. In the proximal row (or antebrachial row), the medially-located radial carpal bone (or intermedioradial carpal bone)[42] represents a fusion of the radial and intermediate carpal bones;[42-45] fusion of the cartilage progenitors of these two bones occurs in the fetus around day 35 of gestation.[46] The ulnar carpal bone is located laterally within the proximal row.[42,43,45] Palmar to the ulnar carpal bone is the accessory carpal bone.[43,45] In the fetus, an intercarpal row consisting of the central carpal cartilage lies between the proximal and distal carpal rows.[45] However, the central carpal is not a separate structure in adults of domestic species and is generally incorporated into the intermedioradial carpal cartilage of dogs between 35 and 42 days of gestation,[46] though fusion may occur several weeks after birth.[45] The distal row (or metacarpal row) of carpal bones consists of 4 numbered cuboidal bones (the first, second, third, and fourth carpal bones, with numbering progressing from medial to lateral), each of which articulates distally primarily with the respectively numbered metacarpal bone.[42,43,45] The fourth carpal bone also articulates with metacarpal V.[42,43,45] The size of the

bones in the distal row increases from medial to lateral.[45] Just medial to the radial carpal bone lies a spherical sesamoid bone within the insertion tendon of the abductor pollicis longus muscle[43,45] (extensor carpi obliquus muscle).[44] Two small cartilages are also described on the palmar surface of the carpus at the level of the middle carpal joint;[42] others refer to these as sesamoid bones, but consider their presence variable.[45]

The metacarpal region of the manus consists of five numbered cylindrical metacarpal bones. The proximal portion of a metacarpal bone is referred to as the base, and the distal part is the head. The first metacarpal bone is considerably shorter than the others, and is generally present even in those dogs that do not have an externally visible first digit.[42,43] The longest metacarpal bones are metacarpal III and metacarpal IV.[43] These two longer metacarpal bones are rectangular in cross-section, while the shorter metacarpal bones (II and V) are triangular in cross-section.[45] The metacarpal bones slightly diverge distally.[42,43] Two elongated proximal sesamoid bones are present just palmar to the heads of the second through fifth metacarpal bones, with a single proximal sesamoid bone located palmar to the head of the first metacarpal bone.[42,43] The proximal sesamoid bones of digits II-V are located within the tendons of insertion of the interosseous muscles, just deep to the digital flexor tendons,[47] and are found within the deep tissues of the metacarpal pad.[44] The proximal sesamoid bone of digit I can be the insertion site of the flexor pollicis brevis muscle.[47] Additionally, a small spherical dorsal sesamoid bone is located in each of the four primary branches of the common digital extensor tendon just dorsal to the distal metacarpal bones II-V,[43] though these sesamoids are also described as being within the metacarpophalangeal joint capsules[42,48] with the extensor tendons found immediately superficial to the sesamoid bones.[48,49] These dorsal sesamoids may also be cartilaginous.[45]

Distal to each metacarpal bone is a digit. The first digit (dewclaw) consists of a proximal and distal phalanx and is present to a varying extent in dogs; the remaining four digits include proximal, middle, and distal phalanges.[42,43,45] The longest digits are digits III and IV; digit I is the shortest digit and does not contact the ground.[42,45] The most distal part of the distal phalanx is the porous ungual process, to which the claw is attached.[42,43] A cartilaginous distal sesamoid is found at the distal interphalangeal joint of each digit, attached to the palmaroproximal margins of the distal phalanges, between the phalanx and the deep digital flexor tendon;[44,45,49] this sesamoid is the equivalent of the navicular bone of the equine digit. Nodular cartilages are present in the dorsal aspect of the proximal interphalangeal joint capsules[42,45] and on the dorsal aspect of the distal interphalangeal joints.[43]

1.2 Muscles and tendons

Muscles of the manus can be subdivided into those which are extrinsic to the paw and those which are intrinsic to the paw. The tendons of six extrinsic muscles are located on the dorsal surface of the manus. The *common digital extensor muscle* originates on the distal part of the lateral epicondyle of the humerus.[47,48,50] A compound (four-part) tendon extends from the muscle belly over the distal half of the radius and over the dorsal surface of the carpus.[47,50] As it passes over the distal antebrachium and carpus, the common digital extensor tendon is contained within a tendon sheath which is held in place by the extensor retinaculum.[48] At the level of the proximal metacarpus, the tendon divides into four individual tendons which extend to the distal phalanges of the second through fifth digits.[47,48,50] The insertion of the tendon is on the extensor processes of the respective distal phalanges.[48,50] At the level of the proximal phalanges, each common digital extensor tendon receives a component of the tendons of the interosseous muscles.[48,50] The

lateral digital extensor muscle originates from the lateral epicondyle of the humerus, the cranial margin of the lateral collateral ligament of the elbow, and the lateral tuberosity of the radius.[47,48,50] A double tendon extends distally from the muscle belly over the distal half of the antebrachium and the carpus.[47] A common tendon sheath contains the lateral digital extensor tendons as they pass over the carpus in approximately 50% of dogs.[48] The caudal (lateral) tendon extends to the distal phalanx of digit V, fusing with the corresponding tendon of the common digital extensor muscle.[47,48,50] The more cranial (medial) tendon splits further into two branches which unite with the common digital extensor tendon branches terminating on the distal phalanges of digits III and IV.[47,48,50] Insertion of the lateral digital extensor tendons on the proximal parts of the proximal and distal phalanges of digits III, IV, and V is also described.[50] The *abductor digiti I (pollicis) longus muscle* originates on the lateral surfaces of the radius and ulna and the interosseous ligament.[47,48,50] The tendon is enclosed by a tendon sheath at the level of the distal radius.[48] Its tendon inserts on the proximomedial aspect of metacarpal I, where a small sesamoid bone is embedded.[47,50] The small *extensor digiti I (pollicis) et II muscle* (previously known as extensor pollicis longus et indicis proprius) originates from the middle of the dorsolateral margin of the ulna.[47,50] The tendon sheath of the common digital extensor tendon also encloses the tendon of this muscle as it passes over the distal forelimb.[48] It gives off a tendon proximal to the carpus; this tendon bifurcates at the proximal metacarpus and the branches extend to distal metacarpal I (a site of attachment) and digit II, respectively.[47,50] The tendon to digit II fuses with the corresponding common digital extensor tendon.[47,50] The *extensor carpi radialis muscle* lies on the cranial margin of the radius.[47] This muscle has two distal tendons: one inserts on the dorsal base of metacarpal II, the other on the dorsal base of metacarpal III.[47] The *extensor carpi ulnaris muscle* (previously known as the ulnaris lateralis

muscle) is found on the lateral aspect of the ulna. The largest part of the insertion tendon of this muscle attaches on the lateral portion of the base of metacarpal V, though some fibers also attach to the accessory carpal bone.[47]

Five extrinsic muscle tendons are present on the palmar aspect of the manus. The *superficial digital flexor muscle* originates via a tendon from the caudal part of the medial epicondyle of the humerus.[47,50] The tendon of insertion begins just proximal to the carpus.[47,50] This tendon travels medial to the accessory carpal bone, but it is superficial to the flexor retinaculum and is not enclosed within the carpal synovial sheath.[47,48,50] The distal tendon divides into four parts in the proximal metacarpal region; these four tendinous branches course to digits II-V.[47,48] At the level of the metacarpophalangeal joints, the respective deep digital flexor tendons perforate the superficial digital flexor tendons at the manica flexoria (tube-like sheath) of the superficial tendons, and distal to this the superficial digital flexor tendons lie deep to the tendons of the deep digital flexors.[47,48] The superficial digital flexor tendons insert on the proximal margin of the middle phalanges of the respective digits.[47,50] The *deep digital flexor muscle* is composed of 3 heads (humeral, radial, and ulnar) which lie on the caudal aspect of the antebrachium.[47,48] The distal tendons of these 3 heads fuse just proximal to the carpus to form the deep digital flexor tendon.[47,50] This tendon crosses the carpus within the carpal canal (which is formed by the flexor retinaculum).[47,48,50] A small tendon to digit I diverges in the proximal metacarpal region; subsequently, the primary tendon divides into four branches which run to digits II-V.[47,48] The individual digital flexor tendons pass through the manica flexoria as previously described and insert on the palmar tuberosities on the proximal margins of the distal phalanges.[47,50] The tendons of the deep and superficial digital flexor muscles to digits II-V are enclosed by common tendon sheaths beginning at the level of the proximal sesamoid bones;

distal to the manica flexoria, these sheaths include only the deep digital flexor tendons.[48,50] The deep digital flexor tendon to digit I is also contained within its own tendon sheath extending from mid-metacarpal I to the flexor tuberosity on the distal phalanx of the first digit.[48] The *interflexorius muscle* originates from the humeral head of the deep digital flexor muscle.[48] It crosses the carpus between the superficial and deep digital flexor tendons.[47,48] Its tendinous branches fuse with the tendons of the superficial digital flexor proximal to the metacarpophalangeal joints.[48] The *flexor carpi radialis muscle* is found on the medial aspect of the antebrachium, superficial to the deep digital flexor muscle. The distal tendon splits into a pair of tendons which insert on the palmar surfaces of the proximal diaphyses of metacarpals II and III, respectively.[47] The *flexor carpi ulnaris muscle* is composed of two muscle bellies lying on the caudolateral portion of the antebrachium. The distal tendons of both of these muscle bellies terminate on the accessory carpal bone.[47]

Multiple intrinsic muscles of the manus are located on the palmar surface; none are located dorsally. The largest intrinsic muscles of the manus are the four *interosseous muscles* which lie immediately palmar to metacarpal bones II-V.[47,48,50] These muscles originate on the proximal aspects (bases) of the respective metacarpal bones and insert via two tendons on the proximal portion of the proximal phalanges of the respective digits.[47] Each of these two distal tendons contains a proximal sesamoid bone.[47,50] Part of each tendon also passes over the collateral surfaces of the metacarpophalangeal joint to join with the associated common digital extensor tendon.[48,50] Three *lumbrical muscles* are associated with the deep digital flexor tendons, lying between the tendons to digits II-V, and act to flex the metacarpophalangeal joints.[47,50] The other small muscle of flexion found between the deep and superficial digital flexor tendons is the *flexor digitorum brevis muscle*, which originates on the lateral aspect of the fifth superficial

digital flexor tendon and inserts on the annular ligament of the metacarpophalangeal joint.[47,48,50] The first digit has three weak muscles associated with it, sometimes referred to as the special muscles of digit I: the *abductor pollicis brevis*, *flexor pollicis brevis*, and *adductor pollicis muscles*.[47,50] These three muscles originate on the palmar carpal ligament and insert on the proximal sesamoid or proximal phalanx of digit I.[50] The *abductor digiti V muscle* originates on the accessory carpal bone and inserts on the palmaroproximal aspect of the proximal phalanx of the fifth digit.[47,50] The *flexor digiti V muscle* originates on the ligament connecting the accessory carpal bone to metacarpal IV, and its small tendon fuses with that of abductor digiti V.[47] The *adductor digiti II and V muscles* originate on the flexor retinaculum (palmar carpal ligament). Adductor digiti II inserts via a tendon on the proximolateral (proximal and axial) margin of the proximal phalanx of digit II; the distal tendon of adductor digiti V inserts on the distomedial (distal and axial) margin of metacarpal V and on the proximal phalanx of digit V.[47,50]

1.3 Ligaments and joints

The carpus consists of 3 joints: from proximal to distal, these are the antebrachiocarpal joint, the middle carpal joint, and the carpometacarpal joint.[45,51] Each of these joint cavities possesses its own synovial membrane.[45] The antebrachiocarpal joint does not communicate with the two more distal joints.[44] However, the middle carpal and carpometacarpal joints communicate between third and fourth carpal bones.[45] Joints between carpal bones in each row are known as the intercarpal joints.[45,51] There are no true collateral ligaments in the canine carpus, as no ligaments span the entire joint.[45,51] However, there are many small special ligaments of the carpus. The most significant of these ligaments include the short radial collateral ligaments, which extend from the distal radius (including the medial styloid process) to the

medial aspect of the radial carpal bone, and the short ulnar collateral ligaments, which extend from the lateral styloid process to the ulnar carpal bone.[51,52] Other antebrachiocarpal and intercarpal ligaments tend to cross only one joint, run longitudinally or obliquely, and tend to be named by their position and attachments.[45] The ligaments on the palmar aspect of the carpus include the palmar ulnocarpal, palmar radiocarpal, palmar radiocarpal-metacarpal, accessorioulnar, accessorioulnocarpal, accessorioquartile, and accessoriometacarpal ligaments; multiple palmar intercarpal and palmar carpometacarpal ligaments are also present.[51-53] Dorsal carpal ligaments include the radioulnar ligament, dorsal radiocarpal ligament, dorsal intercarpal ligaments, and dorsal carpometacarpal ligaments.[51,53]

The metacarpophalangeal joints represent articulations between the five metacarpal bones and their respective digits, each with a joint capsule.[49,51] The palmar portion of the joint capsule extends further proximally than does the dorsal part.[45] Each of the second through fifth metacarpophalangeal joints also has two proximal sesamoid bones which articulate with the palmar part of the joint.[45,51] Only a single proximal sesamoid bone is present at the first metacarpophalangeal joint.[45,51] Medial and lateral collateral ligaments are present at each metacarpophalangeal joint, spanning the space between each metacarpal bone and its respective proximal phalanx,[45,51] though these ligaments are considered indistinct from the joint capsule.[49] Dogs do not have proximal sesamoidean ligaments, such as the equine suspensory ligament, as stabilization of the sesamoids is performed by the tendons of the interosseous muscles.[45] The middle sesamoidean ligaments consist of the lateral and medial collateral sesamoidean ligaments, which extend from the metacarpal bone to the lateral and medial proximal sesamoids, respectively, and from each proximal sesamoid to the proximal phalanx.[45,51] Also included in the middle sesamoidean ligament classification is the intersesamoidean ligament[51] (also called the

transverse or palmar ligament),[45] which connects the two proximal sesamoid bones within each pair (this ligament is obviously absent in digit I, which only has a single proximal sesamoid bone).[45,51] Several distal sesamoidean ligaments are also present in the canine manus. The straight distal sesamoidean ligament extends from the distal end of each sesamoid pair to the palmar aspect of the proximal phalanx.[45,51] The cruciate ligaments of the sesamoid bones attach to the bases of the sesamoid bones and cross each other to attach on the opposite tubercles of the proximal aspect of the proximal phalanx.[45,51] The distal portions of the tendons of the interosseous muscles in digits II-V also effectively act as distal sesamoidean ligaments.[45] Oblique distal sesamoidean ligaments and short sesamoidean ligaments, as are found in the horse,[45] are not present in the dog.

At the sites of articulation of the phalanges, there are proximal interphalangeal joints and distal interphalangeal joints, each of which has a joint capsule.[45,49,51] Medial and lateral collateral ligaments span each of the interphalangeal joints.[45,49,51] Additionally, in the distal interphalangeal joint an elastic dorsal ligament extends from the proximal portion of each middle phalanx to the ungual crest on the proximal portion of the respective distal phalanx: this ligament serves to keep the claws elevated when the deep digital flexor is relaxed, but is weaker in the dog than in the cat.[44,45,49]

On the palmar surface of the manus, at approximately the level of the metacarpophalangeal joints, three interdigital ligaments help prevent spreading of digits II through V.[49] Two of these ligaments, the deep transverse metacarpal ligaments, cross the metacarpophalangeal joints (one for digits II-III, one for digits IV-V) and blend with respective annular ligaments of the metacarpophalangeal joints.[45,49] The third ligament, the V-shaped suspensory ligament of the metacarpal pad (or middle deep transverse metacarpal ligament), attaches to the two previously-

mentioned ligaments and to the metacarpal pad.[45,49] Proximal, middle, and distal annular ligaments bind the digital flexor tendons to the deeper osseous structures at the level of the metacarpophalangeal joint, the distal aspect of the proximal phalanx, and the proximal aspect of the middle phalanx, respectively.[50]

1.4 Arteries and veins

The arteries of the manus are divided into dorsal and palmar divisions. The primary blood supply to the palmar side of the manus is via the median artery which extends from the antebrachium across the carpus,[44,54] passing through the carpal canal.[44] The median artery is located relatively superficially, and gives off the palmar common digital artery I to the first digit. It then branches into the palmar common digital arteries II, III, and IV to the respective digits.[54] These common digital arteries are found between the superficial and deep digital flexor tendons. In the deep palmar tissues, at the level of the proximal metacarpus, the palmar branch of the radial artery and the caudal interosseous artery anastomose to form the deep palmar arch.[54] This arch gives off the palmar metacarpal arteries I, II, III, and IV;[54,55] arteries II-IV run between and deep to the interosseous muscles.[54] The palmar metacarpal arteries then anastomose with the respective palmar common digital arteries just proximal to the level of the metacarpophalangeal joints. These arteries then branch into the axial and abaxial palmar proper digital arteries.[54]

On the dorsal aspect of the front limb, the cranial superficial antebrachial artery extends over the carpus and bifurcates to form medial and lateral branches.[55] The dorsal common digital arteries II, III, and IV extend from the lateral branch.[54,55] Dorsal common digital artery I extends from the medial branch of the cranial superficial antebrachial artery.[54] These arteries are found superficial to and between the common digital extensor tendons. In the deep dorsal tissues, the

medial branch of the cranial superficial antebrachial artery, the dorsal carpal branches of the radial and ulnar arteries, and the dorsal branch of the caudal interosseous artery form the dorsal carpal rete.[55] The dorsal metacarpal arteries I, II, III, and IV extend from the dorsal carpal rete and are found between the metacarpal bones.[54,55] Distally, the dorsal metacarpal arteries anastomose with the dorsal common digital arteries. Subsequently, these branches divide into axial and abaxial dorsal proper digital arteries.[54]

The veins of the manus are divided into dorsal and palmar groupings, but are not further divided into superficial and deep groupings. In the palmar tissues, the most distal veins are the palmar proper digital veins II, III, IV, and V.[56] After anastomoses, the palmar proper digital veins form the palmar common digital veins II, III, and IV. These vessels then further anastomose with dorsal veins and form the superficial palmar venous arch, which lies deep to the metacarpal pad at the level of the metacarpophalangeal joints.[56] Blood flow then progresses proximally via the cephalic vein to the deep palmar venous arch at the proximal metacarpus. Drainage can then continue through the cephalic vein, radial vein, or common interosseous vein.[56]

Venous drainage on the dorsal digits begins in the dorsal proper digital veins II, III, IV, and V, and which continue proximally as dorsal common digital veins II, III, and IV. The common digital veins are found superficial to the common digital extensor tendons, and fuse in the region of the mid-metacarpus to form the accessory cephalic vein.[56] Other smaller veins in the dorsal manus include the dorsal metacarpal veins II, III, IV, and V, and the dorsal venous rete of the carpus.[56] Drainage is ultimately via the accessory cephalic vein.[56]

1.5 NERVES

Dorsally, the radial nerve is represented by the medial and lateral branches of the superficial radial nerve,[44,57] which reach the paw alongside the accessory cephalic vein.[44] The medial branch continues as the dorsal common digital nerve I, then divides into axial dorsal proper digital nerve I and abaxial dorsal proper digital nerve II.[57,58] The larger lateral branch is located approximately on the of the axis of the carpus dorsally, and is adjacent to the cranial superficial artery and accessory cephalic vein.[57] This nerve divides into the dorsal common digital nerves II, III, and IV at the level of the carpometacarpal joint.[57,58] The dorsal common digital nerves further bifurcate at approximately the level of the metacarpophalangeal joints, forming the axial and abaxial dorsal digital nerves II-V.[57] However, abaxial dorsal proper digital nerve II is formed by the medial branch of the superficial radial nerve (as described previously), and abaxial dorsal digital nerve V extends from the dorsal branch of the ulnar nerve.[57]

The median nerve is located on the palmaromedial aspect of the carpus alongside the median artery in the carpal canal,[44] and divides into medial and lateral branches at approximately the level of the middle carpal joint, between the superficial and deep digital flexor tendons.[57,58] The medial branch gives off abaxial palmar digital nerve I and continues distally as palmar common digital nerve I, and the lateral branch divides into palmar common digital nerves II and III.[57,58]

The ulnar nerve, located caudolaterally, branches in the antebrachial region into the dorsal and palmar branches. The dorsal branch is located laterally and ultimately continues as abaxial dorsal digital nerve V.[57,58] The palmar branch is the larger of the two branches and gives off palmar metacarpal nerves I, II, III, and IV.[57] The palmar metacarpal nerves (from the ulnar nerve) communicate with the palmar common digital nerves (from the median nerve) at the distal

portion of the metacarpal region, and continue distally as palmar common digital nerves I, II, III, and IV.[57,58] Distally, the palmar common digital nerves branch into axial and abaxial palmar proper digital nerves. It should be noted that ulnar innervation alone is responsible for the axial and abaxial palmar digital nerves V and the abaxial palmar proper digital nerve IV.[57,58]

1.6 Integument

The pads of the foot are cushions upon which animals bear weight. They consist predominantly of collagen and elastic fibers mixed with adipose tissue, and are covered by relatively thick cornified epidermis. The degree of development of the pads depends on the weight-bearing stance of the animal. The plantigrade bear has prominent and functional digital, metacarpal, and carpal pads, while ungulates only possess digital pads (e.g. the frog of the horse's digit).[44] While humans have additional adipose tissue to provide cushioning at points of contact with the environment, such as the fingertips and calcaneus,[59] these areas are not as well developed as the pads in animals.

In the dog, pads are present in three regions of the palmar surface of the manus. The carpal pad is located immediately distomedial to the accessory carpal bone,[60-62] and does not contact the ground under normal weight bearing.[44,62,63] The metacarpal pad is trilobed, with two abaxial lobes and an apex[61] (representing a fusion of three metacarpal pads),[62] and is located palmar to the metacarpophalangeal joints.[44,61] Each digit possesses a digital pad shaped like a rounded triangle palmar to the distal interphalangeal joint.[44,61,62] The pad of digit I is very small or vestigial.[61-63] The metacarpal and digital pads (with the exception of the pad of digit I) do contact the ground and support their associated joints during weight bearing.[44,61,64] More weight is borne by the pads of digits III and IV than those of the abaxial digits (II and V),[63,64] although in some

cases the pad of digit V may support an amount of weight equal to that borne by digits III and IV.[64] The metacarpal pad also bears a significant amount of weight, essentially intermediate between digital pads III and IV and digital pad V.[64] The skin of the pads is thick and generally the toughest skin found in the dog.[60,61] Multiple highly keratinized conical papillae are present on the pads.[60-62] The deep portion of the pad is known as the digital cushion, which is composed of adipose tissue as well as collagen and elastic fibers.[60,61] As a dog ages, the adipose tissue of the digital pads is replaced by fibrous tissue.[62]

Proximal to the level of the digital pads, interdigital skin webbing is present between the primary digits of the manus (II-III, III-IV, and IV-V).[44] This skin is a common location for infection and cyst formation.[44]

1.7 Differences relative to human anatomy

One difference between humans and dogs is their posture. The manus of the bipedal human is not a weight-bearing structure, while dogs, as quadrupeds, do bear weight on the manus. Additionally, humans have a plantigrade stance, as the entire foot contacts the ground, while dogs have a digitigrade stance, with only the digits contacting the ground.[45] Dogs do not have the considerably differentiated muscles of the manus seen in primates, and the small muscles responsible for moving individual digits are not well developed.[48] The canine digits cannot move independently, and they are all closely interconnected by skin, fascia, ligaments, and pads.[48] Additionally, the interosseous muscles in the canine manus are neither analogous nor homologous to those of the human: the interosseous muscles in the human are found between the metacarpal bones,[31,59] as the name would suggest, while in the dog these muscles are palmar to the metacarpal bones.[47] The canine interosseous muscles are thought to actually represent the

flexores breves profundi muscles,[47] explaining their action in only flexion of the metacarpophalangeal joints,[47] rather than the actions of metacarpophalangeal joint flexion and digital adduction and abduction seen in the true interosseous muscles of the human.[59] Because of these anatomic differences, it is possible that compartmental anatomy between dogs and humans may also differ.

2. **Compartment Syndrome**

2.1 PATHOPHYSIOLOGY OF COMPARTMENT SYNDROME

Compartment syndrome is a condition in which increased pressure within a confined space, such as an anatomic compartment, causes decreased function and (microvascular) circulation within that space.[41,65-67] This generally occurs when intramuscular pressure increases above the capillary hydrostatic pressure, which is generally equal to diastolic pressure, and causes decreased perfusion of the capillary beds.[41,65,66] This will ultimately lead to necrosis, fibrosis, and contracture of the muscle.[65] If nerves are present within the compartment, injury to these structures will also lead to decreased muscle function, sensory deficits, or pain.[65] Compartment syndrome in humans is most commonly described in the lower leg and forearm,[67,68] though can occur anywhere an anatomic compartment exists.

One mechanism of increased intracompartmental pressure is by increasing the volume of the tissue contained inside the compartment.[65] This most commonly occurs due to direct trauma, especially with fracture.[65,66,69-75] Hemorrhage and hematoma formation increase intracompartmental volume, and contribute to production of compartment syndrome following not only fracture, but muscular trauma or vascular injury.[65,66,68,72] Soft tissue injuries (especially

crushing injuries) cause direct muscular damage and produce edema and swelling.[65,66,68,69,71,75,76] Delayed revascularization of a limb following acute ischemia can also lead to compartment syndrome, especially in reconstruction of arterial injury after more than 8 hours of ischemia, due to production of free radicals causing increased vascular permeability.[66,77] Envenomation by crotalid snakes (pit vipers, including rattlesnakes, copperheads, and water moccasins) can occasionally cause compartment syndrome; however, because the clinical signs of snakebite (such as muscle damage and tissue swelling) are similar to compartment syndrome, diagnosis of compartment syndrome in these patients can be a challenge.[65,66,78] Extravasation of radiographic contrast medium is reported as an iatrogenic cause of compartment syndrome.[79] Pressure irrigation of tissues for debridement and extravasation of intravenous fluids administered with a pressure infusion system have also caused cases of compartment syndrome.[80] However, even administration of intravenous medications without described use of a pressure injector, leading to infiltration of the surrounding soft tissues, has been implicated in causing compartment syndrome in the hand.[68]

The other primary mechanism of compartment syndrome production is through a decrease in the overall size of the compartment, as with constriction of the fascia directly due to fibrosis or secondary to external compression. Tight bandage or cast material does not allow for swelling that may occur following injury, increasing the pressure within the affected compartments.[65,66] Following thermal or electrical burns, circumferential eschar formation of the skin and fascia will prevent expansion of a compartment; when combined with fluid extravasation from injured vessels within the compartment, compartment syndrome ensues.[30,41,65,66] Other sources of external pressure, such as surgical tourniquets and intraoperative positioning, have also been implicated in compartment syndrome.[65,66] Because both fascia and bones are relatively

noncompliant, either increased internal volume or decreased external size of a compartment will cause an overall increase in intracompartmental pressure.[65]

Increasing the pressure within an anatomic compartment causes collapse of veins within the compartment, as the thin-walled veins are the vessels most susceptible to collapse.[65,66] This increases the venous pressure which leads to congestion and, in turn, increased capillary pressure within the compartment.[65,66,73] Because of this, the arteriovenous gradient is decreased, leading to decreased perfusion pressure within the compartment.[65,66] If the pressure in the compartment continues to increase, the capillaries will also become occluded (their normal pressure is between 20 and 30 mmHg).[30] The decrease in tissue perfusion leads to ischemia and necrosis of muscle and nerve tissue;[30,65,66] the most severe necrosis occurs in the central portion of the muscle belly, as there is the least amount of collateral circulation in that part of the muscle.[30] Ischemic necrosis of the muscles has been shown to occur at intracompartmental pressures of 20 mmHg below the diastolic blood pressure.[81] Ischemia of musculature causes formation of reactive oxygen species – especially xanthine oxidase – which are toxic to the vascular endothelium and may assist in recruitment of inflammatory cells.[66] These factors lead to increases in microvascular permeability, further increasing intracompartmental pressure.[66] Additionally, severe decreases in muscle oxygenation cause the release of sodium, potassium, calcium, and myoglobin as the sarcoplasm degrades, promoting inflammation, and release of histamine also further promotes cellular swelling and increases vascular permeability.[75]

Compartment syndrome can be divided into four classifications. Incipient compartment syndrome (impending compartment syndrome) is any condition that will lead to acute compartment syndrome if preventative action is not taken.[66] Increasing pain may be noted, but the intracompartmental pressure at this stage would not be elevated sufficiently to necessitate

fasciotomy.[66] This condition most commonly occurs when a cast or bandage material is too tight, or when there is reperfusion to a limb.[66]

Acute compartment syndrome is seen when intramuscular pressure is greater than capillary blood pressure over an extended time.[65] Necrosis of the confined musculature and nerves will occur if decompression is not performed rapidly.[65,66] This type of compartment syndrome is the most common one seen following trauma, snake bites, burns, and iatrogenic incidents (such as accidental perfusion of material into the tissues).[66]

Chronic compartment syndrome, also referred to as exertional compartment syndrome, is an increase in intramuscular pressure caused by exercise.[65,82] It is more frequently seen in the lower limbs than in the upper limbs.[66,82] This form of compartment syndrome occurs when intramuscular pressure increases due to increased muscular perfusion and subsequent muscle swelling, and microvascular perfusion becomes decreased.[66] Muscular hypertrophy can also serve to increase intracompartmental volume over time, thus exacerbating signs with repetitive exercise.[66] Signs in this form of compartment syndrome include pain and occasionally decreased sensation, though symptoms usually resolve once the exercise is halted.[65,66,82] However, if exercise is continued, this form of compartment syndrome can lead to acute compartment syndrome.[65,66] Diagnosis generally requires reproducible pain caused by certain activity and a reversible increase in intracompartmental pressure after exercise when compared to a reading made prior to exercise.[66,82]

Patients with late compartment syndrome frequently have muscle infarction or necrosis, nerve damage, and subsequent impaired function of the affected compartment or limb.[66] In these cases, the muscle and nervous tissue has already been irreversibly damaged, so fasciotomy may be of minimal benefit.[66] Instead, limb reconstruction and salvage (including contracture release

and joint capsule release), rather than fasciotomy and decompression, is the chief focus of treatment for this form of compartment syndrome.[66,75] Further discussion of contracture found in late compartment syndrome can be found in Section 2.3: Diagnosis, Treatment, and Complications.

2.2 Myofascial compartments in the human hand and foot

In humans, myofascial compartments are defined as discrete spaces containing a muscle or muscles and enclosed by dense structures including fascia, articular cartilage, and cortical bone.[30,37,65] Generally these are muscle bellies surrounded by relatively dense fascia. Myofascial compartments are found in the upper arm, forearm, and hand,[30,37,65,66,75] the thigh,[83] the lower leg,[74,75] and the foot.[34,36,84] Some also consider the carpal canal to be an anatomic compartment, although it contains only flexor tendons and no muscle bellies, as it may act as an enclosed space physiologically.[65,67] Arteries, veins, and nerves may also be found within an anatomic compartment.[30,65] While recognition of compartments is important in diagnosing compartment syndrome, these compartments are also important in defining spread of infection.[34] An MRI study of the foot demonstrated that fascial barriers in the foot could prevent spread of infection to other compartments in some patients,[85] though another MRI study found that the barriers between compartments only variably prevented infection spread, with spread from the forefoot much more common than spread from the hindfoot.[29] Anatomic compartments also play an important role in the spread of neoplasia and thus influence planning for biopsy and surgical resection.[37] Additional spaces in the human hand that do not contain muscles are also important in defining spread of disease; these spaces are discussed further in Section 3: Penetrating Foreign Bodies and Infection.

There is debate as to the number of compartments within the human hand. Some of the discrepancies in the literature likely relate to variation among individuals.[31] Compartments within the human hand include the thenar, hypothenar, and adductor compartments, as well as multiple interosseous compartments.[31,65] The margins of the *interosseous compartments* are the dorsal and palmar interosseous fascia and the respective metacarpal bones.[30] Most consider the hand to have 10 total compartments, as the first interosseous region consists of only a dorsal interosseous muscle compartment while the second, third, and fourth interosseous regions are divided into dorsal and palmar (volar) muscle compartments.[30,31,69,76] In the second through fourth interosseous regions, approximately half to two-thirds of injected hands in one study had separate dorsal and palmar (sub-) compartments.[31] However, an infusion study monitoring tissue pressures found that there was leakage of infusate from the dorsal to the palmar interosseous muscles at a pressure of less than 15 mmHg, suggesting that the two compartments in each interosseous region may not represent clinically discrete structures.[32] Additionally, the interosseous compartments occasionally communicated with the midpalmar space or the carpal canal, indicating that anatomic compartments within the hand may not always be complete.[31] Also, not all consider the interosseous muscles to represent independent compartments, regarding the adductor-interosseous compartment as containing the seven interosseous muscles and the adductor pollicis muscle.[86]

The *thenar compartment*, located in the thenar eminence in the palm proximal to the thumb, is surrounded by the thenar fascia on all sides except dorsally, where the first metacarpal bone acts as the compartment's margin.[30,66] The thenar compartment includes the abductor pollicis brevis, opponens pollicis, and flexor pollicis brevis muscles,[30,31,66] although in approximately half of hands injected in one study, at least two discrete sub-compartments were

found within this compartment.[31] The *hypothenar compartment*, in the hypothenar eminence on the ulnar side of the palm, is bound by the hypothenar fascia and the fifth metacarpal, and includes the abductor digiti minimi, opponens digiti minimi, and flexor digiti minimi muscles.[30,31,66] In 76% of hands injected in one study, there were at least two discrete sub-compartments within the hypothenar compartment.[31] The *adductor compartment*, located in the thenar eminence dorsal to the thenar compartment, is defined by the adductor fascia on the palmar surface and the interosseous fascia dorsally.[30] The adductor compartment contains the adductor pollicis muscle,[30,31] and was a separate structure in 71% of injected hands.[31]

Because of the inclusion of lumbrical muscles within the midpalmar space, some also consider this a myofascial compartment (the central palmar compartment); this space also contains the digital flexor tendons, the superficial and deep palmar arterial arches, the common digital arteries, and distal branches of the median and ulnar nerves.[30,65] However, only one case of hematoma formation in this space mimicking compartment syndrome has been described,[87] and this space is likely not an important player in compartment syndrome. See Section 3.3.3: Soft-Tissue Spaces in the Human Hand for more information regarding the midpalmar space. The digits of the hand do not meet the strict definition of a compartment, although increased pressure within the spaces of the fingers may require release as well.[65,66,76] These spaces in the fingers are created by Cleland's and Grayson's ligaments (fascial bands preventing skin movement during flexion and extension) and the fascia at the flexor creases.[66-68] Pyogenic flexor tenosynovitis is reported to cause increased pressure in the digits (30 mmHg or greater in more than half of patients) and may require a skin incision for decompression.[88]

As with the human hand, there is debate regarding the number of compartments within the human foot. Assertions of compartment number in the human foot include three,[34,71] four,[41]

five,[73,76] six,[36] eight,[35] nine,[70,89,90] and ten.[84] The naming of the compartments varies among authors.[34,36,76] The *medial compartment* is found medial to the medial intermuscular septum, dorsolateral to the plantar aponeurosis, and plantar to the first metatarsal bone.[34,76,89] The medial compartment contains the abductor hallucis muscle,[34,36,41,73,84,85,89] with some also including the flexor hallucis brevis muscle,[41,84,85,89] flexor hallucis longus muscle,[41,73] and flexor digitorum longus[73] in this compartment. The *central (intermediate) compartment* may be considered as one[76,85] or two[34,36,84] individual compartments. The dorsal boundary of the central compartment is the plantar interosseous fascia[76] (also referred to as the horizontal septum),[34] the superficial boundary is the plantar aponeurosis,[34,89] and this compartment is bounded on either side by the medial and lateral intramuscular septa.[34,76,89] An additional septum divides the superficial and middle subcompartments of the central compartment.[34] The superficial subcompartment (superficial central compartment) contains the flexor digitorum brevis muscle[34,36,73,84,89] and flexor digitorum accessorius muscle.[34] Distally, the tendons of the flexor digitorum longus muscle[36,41,89] and the lumbrical muscles[36,73,84,89] are also found within this compartment. The middle subcompartment (deep central compartment, or adductor compartment) includes the adductor hallucis muscle,[36,41,73,84,89] flexor hallucis brevis muscle,[34] and tendon of the flexor hallucis longus muscle.[34,36] Injections of both the superficial and middle subcompartments of the central compartment demonstrates communication with the middle flexor compartment of the distal leg.[34]

The *interosseous compartment* in the foot (also described as the deep subcompartment of the central compartment)[34] is defined by the interosseous fascia in both the dorsal and plantar directions and contains the four interosseous muscle groups,[34,36,41,73,76] although one study evaluating fascial planes with MRI considers each interosseous muscle group (dorsal

interosseous muscle at metatarsal I-II, dorsal and plantar muscles at metatarsals II-III, III-IV, and IV-V) to represent its own compartment.[84] While one injection study found the presence of four individual interosseous compartments,[89] other injection studies indicate that the fascial septae between the interossei (extending from the respective metatarsal bones) are not sufficient to prevent spread of infusate, and these studies find the interosseous compartment to be one single compartment.[34,36] One report also notes that the interosseous compartment (referred to as the deep central forefoot compartment) also contains the distal portions of the adductor hallucis and flexor hallucis brevis muscles.[36] The *lateral compartment* is confined dorsally by the fifth metatarsal bone, laterally by the plantar aponeurosis, and medially by the lateral intermuscular septum.[34,76,89] The flexor digiti minimi (brevis) muscle and abductor digiti minimi muscle are found within the lateral compartment in the forefoot,[34,36,41,73,84,85,89] as is the opponens digiti minimi muscle (when present),[73,85] though only the abductor digiti minimi is present in the lateral compartment in the hindfoot.[36] The *calcaneal compartment* is made up of the quadratus plantae muscle[76,84,89] and is bounded by the medial and lateral intermuscular septae.[89] In one injection study, the calcaneal compartment was found to be continuous with the deep posterior compartment of the leg.[89] However, classification of the calcaneal compartment as a true compartment in the foot has been challenged, as the barrier between the quadratus plantae and the flexor digitorum brevis (superficial central compartment) was insufficient to prevent leakage of infusate between the two muscles at less than 10 mmHg.[35] Thus the quadratus plantae muscle is considered by some to be a part of the (superficial) central compartment.[35,41,73]

The dorsal space of the foot has been referred to as a compartment, although it contains only the tendons of the long extensor muscles (tibialis anterior muscle, extensor digitorum longus muscle, and extensor hallucis longus muscle) and does not contain any muscle bellies.[36]

The dorsal foot space communicates with the anterior compartment of the distal leg.[36] Some also report the skin to represent a compartment: the skin compartment is described as containing the extensor digitorum brevis and extensor hallucis brevis muscles dorsally and the fibrous septae of the heel fat pad on the plantar aspect.[84]

2.3 Diagnosis, treatment, and complications

Compartment syndrome can be mimicked by other diseases, including injury to arteries or nerves, and thus must be differentiated from these disease processes.[65] Initially four P's were used as key signs of what would become known as compartment syndrome: Pain with passive extension, Painless onset, Pallor, and Puffiness.[66] Today this has been expanded into five or six P's which can be utilized to recognize compartment syndrome: Pain (with passive extension), Paresthesia, Paresis/Paralysis, Pink skin color, intact distal Pulses, and Palpable fullness.[65,66,75,91] Late in the disease process, there may be a transition to Pallor and Pulselessness,[66,91] but pulses may remain intact as only a decrease in microcirculation, not arterial flow, is required in the pathogenesis of compartment syndrome.[67] Once all of the classic signs are present, irreparable damage to the tissues has occurred.[91] The pain experienced by the patient is often greater than would be expected from the injury incurred, and is increased by passive stretching of the muscles within the compartment.[41,65,66,70] This increased pain can be the only clinical sign in early compartment syndrome.[66] Complete absence of pain is only seen later in the course of disease and indicates nerve ischemia.[69] When neurologic deficits occur, sensory deficits are generally seen before motor deficits.[65] Marked swelling with extremely taut skin is also highly suggestive of compartment syndrome.[41,70,91] When compartment syndrome is a differential diagnosis, it must be distinguished from arterial injury or primary nerve injury. Compartment syndrome can

be differentiated from arterial injury by the presence of distal pulses, which would not be intact with arterial injury;[65] the presence of pulses in compartment syndrome means that there should also be Doppler signal with initial ultrasound evaluation of the tissues.[73] However, because of increased intracompartmental pressure, capillary refill time may be increased in compartment syndrome.[70] Compartment syndrome can also be distinguished from primary nerve injury because intracompartmental pain would not be seen in patients with nerve injury.[65]

The definition of compartment syndrome is another P: increased Pressure.[65] Thus, the confirmatory test of compartment syndrome is to measure the intracompartmental pressure.[41,65,66] To measure the intracompartmental pressure, a probe must be inserted into the compartment, usually directly into the muscle belly. There are multiple methods for evaluating the interstitial tissue pressure; one of the most commonly used approaches is the slit catheter method, which uses a slit catheter attached to a digital arterial monitoring system by saline-filled intravenous tubing.[66,75] The use of a slit catheter rather than a typical needle is important because standard needles give an artifactually elevated pressure reading due to the relatively small contact area between needle and tissue for equilibrium to occur.[66] The side-port needle method is becoming more widely used today – this uses a needle attached to an inexpensive handheld measurement device.[75] An example of the side-port needle method is the Stryker Surgical Intracompartmental Pressure Monitor System, an easily used system which includes a needle, pressure chamber, and monitoring device.[41] Normally, intracompartmental pressure is between -2 and +8 mmHg.[90,92] Varying cutoff values for pressure are used to confirm a diagnosis of compartment syndrome, but use of 30 mmHg or greater with corresponding clinical signs has been proposed.[65] One prospective study found that a differential pressure (diastolic blood pressure minus intracompartmental pressure) of 30 mmHg was an appropriate threshold, as performing a

fasciotomy in all cases with a pressure differential of less than 30 mmHg led to no missed cases of acute compartment syndrome, and use of only an absolute pressure reading would have led to unnecessary fasciotomies.[93] Other suggested thresholds for fasciotomy include 45 mmHg or 20 mmHg below diastolic blood pressure.[65,66,81] A defined threshold for diagnosis of compartment syndrome in dogs has not been identified to the authors' knowledge.

The purpose of any treatment technique is to decompress the affected compartment or compartments in order to restore microcirculation to the compartment before neuromuscular necrosis occurs.[65,75] Initial management for impending compartment syndrome is nonsurgical.[66] In cases of external compression, the offending structure (e.g. a tight cast or bandage material) should be removed.[65,73] While the affected limb should be somewhat elevated,[73] it should only be elevated to heart level, as elevation of the limb beyond this point decreases perfusion pressure, thus decreasing the arteriovenous gradient and the threshold for compartment syndrome.[66,75] Administration of corticosteroids and anticoagulants can help protect muscle tissue against ischemia in the short term.[75] Hyperbaric oxygen therapy has been shown to markedly reduce muscle edema and necrosis in experimentally induced compartment syndrome in dogs,[94] but there are no reports of use of this treatment in a clinical setting. Mannitol has also been used experimentally in compartment syndrome in the dog, and has been found to assist in decreasing intracompartmental pressures, likely through removal of interstitial edema from injured muscle.[95]

If the patient fails to improve, surgical treatment is required;[65] this is generally considered the treatment standard in acute compartment syndrome.[75] Surgical treatment entails fasciotomy, with incisions made over the affected compartments.[41,65,66,77] Basic principles of decompression include making longitudinal incisions over myofascial compartments and transverse incisions at creases for flexion, excision of necrotic tissue, monitoring of tissue pressures following

decompression, and leaving the incisions open for up to ten days.[66] In the hand, the interosseous compartments are decompressed by making two dorsal incisions, one over metacarpal II and one over metacarpal IV, followed by spreading of the incisions.[65-67] The adductor compartment is decompressed with deep dissection along metacarpal II.[66,67] The thenar compartment is released with a longitudinal incision along the abaxial side of metacarpal I, and the hypothenar compartment is released by a longitudinal incision on the abaxial side of metacarpal V.[65-67] In the foot, the interosseous compartments can be decompressed by making longitudinal incisions dorsal to metatarsal II and metatarsal IV.[41,89,90] The adductor compartment (middle central compartment) is then released through deep dissection extending from the incision over metatarsal II.[89,90] A longitudinal incision made over the medial surface of the heel and midfoot (at the region of the arch) serves to decompress the medial and calcaneal compartments, and deeper dissection allows for release of the superficial central and lateral compartments.[89,90]

Complications of treatment for compartment syndrome include injury to the associated nerves or vessels, wound infection, hematoma formation, and deep vein thrombosis.[75] If compartment syndrome is not treated rapidly, or if injury is severe, (Volkmann's) ischemic contracture will occur.[65,66,72,75] This is the end stage of hypoxic damage to the muscles, nerves, and vessels within the compartment.[65] Muscle tissue can survive ischemia of 4-6 hours' duration without irreparable damage, but 8 hours of ischemia will cause irreversible damage.[67,81,90] Contracture will result from muscle ischemia lasting at least 12 hours.[90] Relatively mild contracture may be seen as replacement of parts of muscle with fibrous tissue with resulting shortening of the muscles. Marked contracture involves severe replacement of muscular tissue with fibrous tissue, marked deformity, joint stiffness, and fibrous replacement of nervous

tissue.[65,70,75] Further possible complications of end-stage compartment syndrome are loss of sensation, chronic pain, weakness, and need for amputation.[75]

2.4 Compartment syndrome in the dog

Compartment syndrome is rarely described in the dog. Clinical compartment syndrome in the dog has been reported in the front limb following rupture of the median artery,[96] in the quadriceps compartment after repair of a femoral fracture,[97] in the quadriceps region directly following femoral fracture,[98] between the fascial planes of the semimembranosus and semitendinosus muscles due to pseudoaneurysm of the femoral artery,[99] and in the infraspinatus muscle of a dog with a three-day history of hunting (postulated as rupture of the muscle caused by overuse).[92] Canine models have also been used experimentally to evaluate the pathophysiology and treatment of compartment syndrome.[81,94,95,100] Two experiments used the craniolateral compartment of the distal hind limb as the model,[81,100] while other studies did not specify the compartment used. However, experimental evaluation in cadaver limbs found four discrete myofascial compartments: the craniolateral and caudal compartments of the distal hind limb, the femoral compartment, and the caudal compartment of the antebrachium.[97] Subsequent infusion of fluid into these compartments to achieve intracompartmental pressures of 60, 90, and 120 mmHg in live dogs produced signs of compartment syndrome, including pathology of the muscles and nerves within the respective compartments, though a cutoff pressure at which compartment syndrome could be expected was not identified.[97]

3. Penetrating Foreign Bodies and Infection

Penetrating foreign objects are commonly seen in dogs and cats as well as humans. These objects tend to affect the integument and musculoskeletal system, though penetration into other structures such as the eye, thoracic cavity, or abdomen can also occur. While foreign bodies in the gastrointestinal tract[101-106] and respiratory tract[101,102,106-111] are also common in dogs, cats, and humans (especially pediatric patients), the pathophysiology of these foreign bodies is different (they are generally the result of ingestion, inhalation, or insertion rather than penetration), and they will not be discussed further except as they relate to penetration of the body.

3.1 Pathophysiologic mechanisms

3.1.1 Inflammatory cascade

Embedded foreign bodies generally lead to the production of granulomatous inflammation. Granulomatous inflammation is a chronic reaction where activated macrophages represent the predominant type of cell. A focus of this type of inflammation is referred to as a granuloma. Granulomas consist of clusters of macrophages with an epithelioid appearance surrounded by lymphocytes and sometimes plasma cells. The epithelioid macrophages may fuse to create giant cells. As a granuloma ages, it may also be characterized by a rim of fibroblasts and connective tissue. The two types of granulomas that are described are foreign body granulomas and immune granulomas. Foreign body granulomas are caused by inert foreign bodies such as talc, suture material, or other fibers that are too large to undergo phagocytosis by a macrophage and do not induce a cell-mediated immune response. In these granulomas, epithelioid and giant cells

encompass the foreign body. Immune granulomas are caused by particles that incite a cell-mediated immune response, where macrophages phagocytose the material and subsequently activate T lymphocytes. These T lymphocytes then activate further T lymphocytes via cytokines such as interleukin-2 (IL-2) and transform macrophages into epithelioid cells and giant cells via interferon gamma (IFN-γ). The classic immune granuloma is caused by tuberculosis.[112]

The foreign body reaction (FBR) is a nonspecific immune response caused by the presence of foreign material. Most studies evaluating the foreign body response have investigated the response to sterile implants; most of the considerations are unchanged when regarding accidental foreign body penetration, though the pathogenesis of infection may also play a role in these penetrations. The FBR can be divided into the onset, progression, and resolution phases. The onset of the FBR begins when tissue is first injured. At this time, blood vessel permeability increases. Coagulation also occurs, and with the destruction of platelets comes the release of inflammatory mediators including vascular endothelial growth factor (VEGF), interleukin-8 (IL-8), and transforming growth factor-β (TGF-β). These inflammatory mediators are chemotactic factors and serve to attract neutrophils and eventually macrophages to the injury site. Local vessel production is also stimulated by the angiogenic factors. If the foreign object is degradable, the FBR will become chronic until the object is degraded; if the material is not degradable, the reaction will progress until a capsule is formed around the object, thus preventing further incitement of the inflammatory response.[113]

The course of the foreign body reaction depends on the surface chemistry of the foreign object. For example, particularly severe inflammatory responses have been reported to result from sea urchin spines, even those considered not to be toxic: while the spines are predominantly made of immunologically inert calcium carbonate, the epithelial surface of the spine may also be

coated by secretions which may promote the inflammatory response.[114] In many cases, the FBR is thought to be at least partially induced by the adsorption of proteins to the foreign body. As coagulation occurs at the site of injury, thrombin hydrolyzes fibrinogen, forming a mesh of fibrin. The small peptides that are formed as by-products during the hydrolysis serve to attract neutrophils and macrophages, and fibrin also causes leukocyte adhesion. Fibrinogen adsorbs to hydrophobic portions of the foreign object, exposing fibrinogen's P1 fragment, which in turn binds to phagocyte integrin complement receptor 3 (CR3) and activates tissue phagocytes. Activation induces the tissue phagocytes to release cytokines and chemokines including IL-1, tumor necrosis factor α (TNFα), VEGF, monocyte chemoattractant protein-1 (MCP-1), and IL-8. These cytokines and chemokines activate angiogenesis and attract leukocytes and fibroblasts, setting up the progression phase of the FBR.[113]

Complement protein C3b can also adsorb to a foreign body, activating the alternative complement pathway. Phagocytes will then recognize the bound C3b. Additionally, complement factor Bb will bind to C3b, forming C3bBb, which in turn splices C3 molecules into C3a and C3b convertase. This process is the beginning of opsonization, which causes the release of C5a, a leukocyte chemoattractant in acute inflammation. The inflammatory response is further promoted as C3a and C5a increase vascular permeability and cause mast cells to release histamine. The classical complement pathway may also be initiated upon implantation of a foreign object if nonspecific binding of antibodies to the object occurs. The antibodies' Fc domain is recognized by factor C1q, which leads to deposition of C3b and a similar response as that seen in the alternative pathway.[113]

The progression phase of the foreign body reaction is the most extensive phase. In order for leukocytes to efficiently reach the foreign object, a sufficient number of blood vessels are

necessary. Thus, angiogenesis is an important component of the FBR. In angiogenesis, new blood vessels sprout from existing blood vessels in response to the presence of various factors. Fibrin strongly stimulates vasodilation and angiogenesis, and fibrin degradation product fragment E is important in the proliferation and differentiation of endothelial cells. The histamine released by activated mast cells further promotes angiogenesis. Activated neutrophils and platelets produce VEGF and fibroblast growth factor, which both initiate angiogenesis. While most of these initial steps occur acutely, angiogenesis is continued as macrophages and fibroblasts move too far away from the vessels for oxygen diffusion: these cells then produce VEGF and platelet-derived growth factor (PDGF) in response to anoxia. Importantly, the wide variety of growth factors is necessary for production of functioning vasculature. PDGF is critical to the maturation of vessels as it is responsible for the migration of smooth muscle cells and fibroblasts. While VEGF is needed, without other factors it will produce only immature, overly permeable vessels.[113]

Extravasation of leukocytes is promoted by such cytokines as IL-1β and TNFα which are, themselves, released by activated leukocytes. These cytokines act by stimulating vascular cell adhesion molecule-1 (VCAM-1), intercellular adhesion molecule-1 (ICAM-1), and E-selectin on endothelial cells. Leukocytes first bind to E-selectin, then roll over the endothelial cells until they bind more completely to VCAM-1 and ICAM-1, at which point the leukocytes can migrate through the endothelium.[113]

Migration of leukocytes to a site of inflammation is directed by chemokines, which are chemoattractive cytokines. Families of chemokines include the CXC, CC, C, and CX_3C families, all of which are based on a cysteine structural component. Generally, chemokines bind to heparin or heparan sulfate components on glycosaminoglycans (GAGs) in the extracellular matrix.

Because chemokines are most concentrated closest to the site of inflammation (the foreign object), leukocytes migrate up the concentration gradient of chemokines within the extracellular matrix. The chemokine system exhibits a large degree of redundancy, as most chemokine receptors can recognize multiple chemokines and most chemokines can bind to multiple receptors. Nonetheless, neutrophils are generally attracted by the CXC family of chemokines, while macrophages are attracted by the CC family. T cells are attracted and activated by multiple different chemokines; once activated, they produce IFN-γ, IL-4, and IL-13, which then activate monocytes and promote formation of giant cells. TGF-β, which is released by platelets, also strongly attracts and activates neutrophils, monocytes, and fibroblasts.[113]

Numerous cytokines, proteins that modify the immune response and activate leukocytes, are involved in the foreign body reaction. However, because of the numerous interactions, the function of these hormones is incompletely understood. Some of the more important, and better understood, cytokines include TNFα, which increases phagocytosis and is a chemoattractant; IFN-γ, which inhibits some cell growth; IL-1, which produces edema and fever and induces fibroblast proliferation; IL-10, a phagocytosis inhibitor; and IL-12, a phagocytosis promoter.[113]

Phagocytosis of foreign bodies is promoted by antibodies, complement factors, and fibrin adsorbed to the object. Fc receptors on phagocytes recognize structures that are bound by IgG; when these receptors bind IgG the phagocyte releases IL-1, IL-6, and TNFα, all of which further the inflammatory response. Complement receptors on macrophages bind complement factors adsorbed to the foreign material and promote phagocytosis of these structures. Some foreign particles are too large for phagocytosis by a single macrophage; when this occurs macrophages will fuse and form giant cells. The Langhans type of giant cell is generally found around indigestible organisms, and their formation is promoted by IFN-γ. The foreign body type of giant

cell (FBGC) forms under the influence of IL-4 or IL-13. Once the foreign object has been degraded, the giant cells disappear.[113]

The extracellular matrix surrounding the foreign material remodels throughout the progression of the foreign body reaction. The matrix is important in maintaining the integrity of the tissues and also allows for adhesion of inflammatory cells. Matrix remodeling is necessary to allow migration of inflammatory cells to the foreign body: remodeling of the matrix is performed by matrix metalloproteinases (MMPs). The first matrix that forms around the foreign object is composed of fibrin. However, the matrix is dynamic, and also includes collagen, cytokines, and chemokines during the foreign body reaction.[113]

Macrophages produce small amounts of TNFα during the progression phase, in turn increasing production of collagenase and inhibiting production of type I collagen. Thus continuation of inflammation is marked by degradation of the extracellular matrix. In the resolution phase of the FBR, TGF-β decreases the inflammatory response by decreasing the production of chemokines by macrophages. Migration of phagocytes into the region is thus diminished, and when the foreign object has been digested the leukocytes migrate away towards the local lymph nodes.[113]

During resolution of the foreign body reaction, TGF-β also promotes production of collagen I, collagen III, fibronectin, and proteoglycans in the region of inflammation. These molecules are produced by fibroblasts and myofibroblasts, and collectively result in fibrosis in the region.[113] Using *in vivo* MR microscopy, one study evaluating capsule formation around silicone implants found that the hyperintense band representing fibrous capsule did not change significantly during the first 2 weeks following implantation of the object, but significantly

increased in thickness over the subsequent 2 weeks, consistent with the delayed nature of fibrous tissue formation in the FBR.[115]

Embedded foreign bodies are a source of infection relatively commonly, even when objects are implanted with aseptic technique (as in orthopedic implants). Infections associated with implants are usually caused by *Staphylococcus sp.*, cause tissue infiltration of numerous neutrophils, and generally cannot be cured without removal of the foreign object. A study performed in a guinea pig model found that tissue neutrophils that had been attracted by a subcutaneous implant had poor bactericidal activity against *S. aureus*. When compared to neutrophils that were not associated with a foreign body, these "foreign body neutrophils" had a marked reduction in superoxide production and had a poorer degranulation response when exposed to stimuli. Thus it has been proposed that the presence of a foreign object may induce a defect in neutrophils' metabolism which may in turn cause increased infection susceptibility in these cases.[116]

3.1.2 Macro- vs. microabscesses

Microabscesses are small accumulations of neutrophils and fibrin. These form at the tips of dermal papillae in dermatitis herpetiformis, or in the superficial epidermis in psoriasis.[112]

A macroabscess (or simply an abscess) is a focal confined collection of suppurative (purulent) inflammation. This suppurative inflammation produces a large quantity of pus, an exudate which is made up of neutrophils, necrotic cells, and edema. Suppurative inflammation is generally caused by certain bacteria, such as staphylococci, which are known as pyogenic bacteria. The center of an abscess is composed of necrotic cells (both neutrophils and cells from the local tissues); this central necrotic region is surrounded by viable neutrophils. More

peripherally there is evidence of healing and repair, including vasodilation and proliferation of fibroblasts and parenchymal cells. Eventually the abscess may become surrounded by fibrous tissue, thus preventing spread.[112]

3.1.3 Phlegmon

A phlegmon is defined as "purulent inflammation and infiltration of connective tissue."[117] While this is similar to an abscess in the presence of purulent or suppurative inflammation, a phlegmon does not include a focal collection of purulent material (pus), and thus may be more diffusely infiltrative.[118] However, a review of inflammation in the psoas muscle in humans found that abscesses and phlegmons were indistinguishable using CT, as both were characterized by enlargement and hypoattenuation of the affected muscle.[118]

3.1.4 Foreign-body carcinogenesis

Induction of sarcoma formation by implanted objects in rats and mice was first recognized in the 1940s, though the mechanism is incompletely understood. Currently the most accepted hypothesis attributes carcinogenesis to the effects of the respiratory burst that occurs at the inflammatory site. In the acute phase of inflammation, TNFα expression is high, and neutrophils and macrophages produce oxygen free radicals and nitric oxide free radicals. These free radicals produce both cytotoxic and mutagenic effects, and cell mutations can ultimately progress to tumor formation. IL-1β may also act as a promoter of carcinogenesis, and activation of VEGF further promotes tumor development. Interestingly, however, the degree of initial inflammation intensity appears to be inversely related to the tumorigenicity of a substance.[119]

Various characteristics of implanted foreign objects have been reported to affect the associated rate of tumor formation. For example, cationic plates produced the most tumors, with anionic plates producing fewer tumors and neutral plates producing fewer still. Hydrophilic plates tend to cause decreased leukocyte adhesion, suggesting that carcinogenesis could also be decreased relative to hydrophobic implants. Additionally, smooth plates caused tumor formation more rapidly than those with a rough surface, and larger plates are more carcinogenic than small ones, though carcinogenesis dramatically decreases if a plate is first broken into small fragments.[119]

There is a wide variety of histologic tumor types associated with subcutaneously implanted foreign objects in experimental studies. The most common tumors are poorly differentiated sarcomas and fibrosarcomas, but other tumor types include liposarcomas, osteogenic sarcomas, rhabdomyosarcomas, and hemangiosarcomas. Because some tumors contain regions with partial differentiation toward different cell lines (e.g. cartilage, bone, and smooth muscle), it has been suggested that these tumors arise from one type of pluripotent cell that then differentiates during tumor growth.[119]

3.2 Common penetrating foreign bodies

Objects made of wood or other plant materials are commonly reported as foreign bodies in dogs and humans, with the specific identity of objects based on regional differences in the growth of plant species. In one study, 80% of foreign objects causing draining sinuses in dogs were composed of natural plant matter (wood fragments, thorns, and grass).[4] One study from California found that grass awns were the offending object in 61% of all cases of foreign objects in dogs and cats.[6] Breeds of dog with increased prevalence of grass awn foreign bodies in one

study included Springer Spaniels, Golden Retrievers, Brittany Spaniels, and Airedale Terriers,[6] and another study found that 48% of affected dogs were hunting dogs.[120] Wooden objects are the most common foreign bodies found in the human hand[5,121] and found in humans generally.[122] Additionally, the incidence of plant foreign bodies is probably considerably higher than reported, as the majority of splinters are likely removed by the injured individual without visiting a physician.[5] Plant matter foreign objects are variably sized, up to 7cm in length,[123] and can be found in any location. Reported locations in humans include the hand,[5,124] foot,[124-126] arm,[124] leg,[124,127] retrobulbar/intraorbital region[123,128-132] temporal musculature,[129] periauricular area,[133] cranial vault,[134] and vertebral canal.[135] While wooden foreign bodies are usually fragments of sticks or natural plant matter,[128,129,131,136-139] toothpicks have been described in the foot,[125] and an intraorbital golf tee[140] and intracranial chopstick[134] have also been described. Plant matter also includes a cactus spine embedded in the cartilaginous part of the tibia in a child,[141] and date palm thorn foreign bodies represented 8% of all pediatric foreign body hospital admissions in one study.[142] Wooden foreign bodies are often associated with infections because wood is porous and organic, and usually associated with the soil, allowing for colonization with bacteria or fungi.[131,138] *Clostridium tetani* is a common contaminant of wooden foreign bodies.[143,144]

Injuries caused by porcupine quills are commonly seen in dogs who live in regions where porcupines are endemic, representing 2.1% of new hospital cases in one study period.[28] Similar to grass awns, porcupine quills have sharp tips and backward-pointing barbs, so quills have a tendency to migrate into deeper tissues, and retrograde motion is prevented.[28] Siberian huskies, Rottweilers, and German Shepherd crosses were overrepresented in the population presented for porcupine quill injury, and 13% of the dogs presented to the hospital for porcupine quill removal more than once.[28]

A wide range of other foreign objects have been described in humans. The composition of material varies widely, and the more common foreign objects include glass/ceramic and metal (needles, nails, screws, metal fragments);[5,15,122,145] the commonality of these objects as the cause of injury is primarily a function of their sharp nature, as two-thirds of patients presenting with embedded foreign bodies were lacerated by or stepped on the foreign object.[122] Included in consideration of metallic foreign bodies are bullets and gunshot pellets – while trauma from bullets is greater than that of most foreign bodies due to the profound kinetic energy that they strike with, once embedded the complications of bullet retention are similar to other foreign objects.[106] Another complicating factor in gunshot trauma is the introduction of hair, dirt, and other debris when the bullet penetrates the tissues. Tumbling of the bullet, rapid expansion/contraction forces, and cavitation created by the abrupt change in the bullet's velocity also cause disruption of vascular supply and ischemic necrosis of surrounding soft tissues.[146] Less common foreign bodies include pencil graphite, plastic, gravel, shells, fish spines, hair, fiberglass, paint chips, and bone.[5,122] Entire broken-off pencils have also been described.[133] Embedded fish spines may come from stingrays, catfish, or needlefish (in this last case the offending structure is actually the broken-off beak rather than a spine),[147] and sea urchin spines are also reported, especially in the foot.[114] Foreign bodies found in the oral cavity in people include a plastic pen cap embedded in the floor of the mouth,[148] a fish bone in the mobile part of the tongue,[149] and a toothpick in the hard palate.[150]

One retrospective study performed in a human emergency room found that 14% of patients presented with an open wound, and 8% of those patients' wounds were caused by glass (windows were responsible for 30% and bottles for 25% of glass-associated injuries).[151] Retained glass foreign bodies were found in 9% of patients with glass-caused wounds (7% of the total

wounds in these patients contained a glass fragment).[151] Glass-caused wounds in the head and foot were more likely to have a retained glass foreign body, while those in the hand were less likely to have retained glass.[151] Motor vehicle accidents and stepping on glass were most likely to cause retention of glass within the wound, and puncture wounds were more likely to have a glass foreign body than lacerations were.[151]

Foreign material can be found in plantar puncture wounds in human patients – these foreign objects are often fibers from socks, fragments of rubber sole, or foam lining from the inside of shoes.[152] The initial soft tissue infections seen with these injuries are commonly due to Staphylococcus and Streptococcus (skin flora); later development of osteomyelitis is usually caused by Pseudomonas.[152] Pseudomonas is more commonly found in plantar puncture wounds from patients who were wearing tennis shoes rather than those who were not wearing shoes, as Pseudomonas is often cultured from worn shoes.[152]

Penetrating foreign objects are less commonly described in horses, but do occur. Puncture wounds of the digit, such as by a nail, are well recognized to cause septic arthritis and bursitis, but can also cause intra-articular retention of metallic fragments.[153] A chronic draining tract mimicking fistulous withers has been caused by a bullet resulting in a foreign body reaction.[154] A wooden foreign body has also been described as a nidus for development of obstructive choledocholithiasis in a horse.[155]

Retained surgical instruments and materials have been described in dogs,[156-158] cats,[156] and humans,[159-170] and can cause a foreign body reaction similar to more classical penetrating foreign bodies. In one study, a surgical foreign object was retained inadvertently in 1 case for every 5,500 surgeries performed.[159] It should be noted that, while most cases of foreign material retention are a result of surgical materials being accidentally left in the body, resorbable and non-

resorbable hemostatic agents that are purposefully left in place to prevent hemorrhage (and generally cause no adverse reactions) have also been reported to cause foreign body reactions.[167] Similarly, self-locking nylon cable bands ("zip ties") used as a ligatures for ovariohysterectomy in dogs have been reported to result in granuloma formation and chronic draining tracts.[171,172] A history of previous surgery is important for definitive diagnosis in these cases, even if surgical intervention was many years previously.[156,158,161,163,166,168-170] Sponges that remain anywhere within the body can cause an aseptic foreign body reaction and ultimately cause the formation of a sterile abscess or granuloma.[156,161,167] A capsule composed of collagen fibers generally forms around the mass; granulomatous inflammation is also a component of the capsule and may include neutrophils, plasma cells, lymphocytes, histiocytes, and foreign body giant cells.[160,165-167] In some cases, marked eosinophil infiltration can also be seen.[167] Organizing granulation tissue may also be described histopathologically.[161] Fiber-like material from the offending sponge can generally still be identified in the center of the mass,[102,156,160,166] and necrosis[160,163] and calcification[160,161] may also be noted in the mass. These masses are commonly referred to as gossypibomas, from the Latin *gossypium* ("cotton") and Swahili *boma* ("place of concealment"),[160,163-165,167,169,170,173] although other terms used include "textiloma,"[163,167,169,173] "cottonballoma,"[161,169] "gauzoma,"[167,169] "muslinoma,"[167] and "cottonoid."[173] The terminology comes from the cotton fibers found in the sponge material; while most surgical sponges today are made of synthetic material, the names remain.[173] Not all retained surgical materials are surgical sponges: a Penrose drain used to treat an abscess has been reported to cause an abscess itself 5 years after resolution of the initial clinical signs,[168] and retention of needles and instruments have also been described.[159] Additionally, while not acceptable in Western medicine, injection of paraffin into body tissues has been used for both therapeutic and aesthetic reasons. One case has

been described with granuloma formation, fibrous reaction, and soft tissue inflammation resulting from injection of paraffin into the soft tissues – the authors dubbed this mass a "paraffinoma."[162]

Ingested foreign objects can occasionally penetrate the wall of the esophagus or gastrointestinal tract and migrate into the surrounding tissues. Perforation of the stomach or intestine by sticks (often wooden skewers) has been described in twelve animals;[174,175] sticks that penetrate the gastric wall may exit the stomach completely or may remain partially within the gastric lumen,[174] and may even puncture the gastric wall and fully retract into the gastric lumen.[176] Migration of a toothpick through the esophagus has also been suspected.[177] Wooden sticks may also penetrate the pharynx in stick-chasing dogs and become retained as parapharyngeal foreign objects.[178] Penetration of the GI tract is not limited to animals, however: human cases of intra-abdominal foreign bodies (such as ball-point pens) from GI tract penetration have also been reported.[179] Clinical signs and findings depend on the organs affected by the migrating object, but include vomiting, lethargy, peritonitis and adhesions, body wall swellings, active periosteal response from adjacent bones, draining tracts, and pneumothorax.[174-176]

General soft tissue infections associated with any type of wound are usually caused by *Staphylococcus sp.* and *Streptococcus sp*., commensal bacteria of the skin.[180,181] Specifically, human hand infections are most commonly caused by *Staphylococcus aureus*, *Streptococcus sp.*, and Gram-negative bacteria.[38] Indeed, in one study evaluating hand infections (17% of which were caused by foreign bodies), 44% were pure *Staphylococcus aureus* infections, with 14% caused by streptococci and 12% mixed infections.[182] Most injuries involve a single Gram-positive species.[38] Infections due to bite wounds, however, are more likely to be polymicrobial,

and may involve Gram-positive, Gram-negative, and anaerobic bacteria (an average of more than 4 bacterial species per wound).[38,183] For example, animal bite and scratch injuries are commonly infected with *Pasteurella multocida* or *Pasteurella canis*;[38,183,184] clinical symptoms from Pasteurella occur rapidly, generally within 24 hours.[185] Bacterial infection may occur in 5-16% of dog bites, while up to 50% of cat bites result in bacterial infection.[183]

In humans, Actinomyces and Propionibacterium are anaerobic bacteria commonly found in foreign body infections.[186] Wood is also frequently colonized by *Clostridium tetani*.[143,144] Toothpick foreign bodies commonly result in infection with mixed aerobic and anaerobic bacteria due to the presence of oral flora on most offending toothpicks; common bacteria cultured in one study in toothpick wounds of the hand included *Streptococcus spp.*, *Staphylococcus sp.*, *Prevotella sp.*, *Bacteroides spp.*, *Enterobacter sp.*, and *Escherichia coli*.[187] A series of cases of toothpick foreign bodies in the human foot isolated one or more of the following in each of the patients: *Stenotrophomonas maltophilia*, *Enterobacter cloacae*, *Staphylococcus aureus*, *Streptococcus intermedius*, and *Fusobacterium varium*.[125] Other bacterial organisms reported as the cause of infection in penetrating wounds in people include *Serratia marcescens*, *Klebsiella sp.*, *E. coli*, *Salmonella typhi*, and *Bacteroides melaninogenicus*.[180] However, not all infections are caused by bacteria. The fungus *Phaeoacremonium sp.* is associated with woody plants and can cause infection in humans.[188] The fungus *Sporothrix schenckii*, the cause of "rose gardener's disease," can also be seen in injuries caused by rose thorns, and results in focal ulceration and granuloma formation.[189-191] It should also be noted that, depending on the composition of the object, foreign bodies themselves can cause an inflammatory reaction (as discussed in Section 3.1.1: Inflammatory Cascade), so the presence of inflammation does not necessarily indicate the presence of infection.[192]

Bacterial culture was performed in approximately 10% of small animal patients with grass awn foreign bodies in one study.[6] In that study, *Streptococcus sp.* and *Staphylococcus aureus* were the most commonly isolated organisms (each in 41% of cases), with *Pasteurella multocida* (35%) and *Actinomyces sp.* (29%) also isolated frequently.[6] More than one bacterial species was isolated in 71% of the patients cultured.[6] In a series of dogs with sublumbar plant matter foreign bodies, infecting species of bacteria were predominantly anaerobic, including mouth flora, and included *Fusobacterium sp.*, *Eubacterium sp.*, *Actinomyces sp.*, *Bacteroides sp.*, *Pasteurella sp.*, and *Propionibacterium sp*.[193]

Infections of the deep spaces in the human hand are most commonly caused by penetrating wound or direct spread from adjacent regions.[38] In one study of 100 infections of the deep spaces of the human hand, 33 cases were due to puncture wounds,[194] a situation that also predisposes to foreign object retention. The most common objects associated with the puncture wounds were wooden splinters (11), pins and needles (6), broken glass (3), and assorted other wooden and metallic objects.[194] In infection of the deep palmar spaces and tendon sheaths of the human hand, *Streptococcus sp.* and *Staphylococcus aureus* are most commonly isolated, though other bacterial species including anaerobes and Gram-negative rods can also be involved.[38,39,152,195]

Pseudomonas aeruginosa is the most common cause of osteomyelitis of the human foot when a puncturing object penetrates the sole of a shoe, as Pseudomonas grows well in the moist layers of used shoes, though it does not grow well in unused shoes.[180]

3.3 COMMON LOCATIONS

3.3.1 Veterinary literature

Foreign objects can be found anywhere within the body, including the musculoskeletal system and body cavities. This is true not only because any portion of the body can be injured or come in direct contact with a foreign object, but also because many foreign objects (such as grass awns) have a tendency to migrate through the tissues.[6,27] For example, plant awns from various species have a sharp end which can easily penetrate the skin, can migrate within the body simply due to movement of the animal host, and have barbs to prevent retrograde motion once they are embedded.[6] The most common site for retention of a grass awn was the external ear canal, representing 51% of all dogs and cats with grass awn foreign bodies.[6] The next most common sites to find grass awns were the interdigital web (22%), conjunctiva (18%), and nasal passages (9%).[6] In another study, the most common locations for grass awn migration were the thoracic wall, lumbar region, and head and neck,[120] and intrathoracic involvement secondary to plant material foreign body migration is seen with some frequency.[27,196,197] Plant material foreign bodies have been found in the sublumbar musculature in multiple hunting dogs; it is postulated that these objects were inhaled and migrated along the diaphragmatic crura to ultimately embed in the hypaxial muscles.[193] Plant material foreign bodies have also been described in the body wall, cerebellum, and retropharyngeal region.[107] Other CNS sites of plant foreign body migration include the brain stem, occipital lobe, and lateral ventricle.[198,199] The interdigital web is the most commonly reported site of foreign body retention in the paw,[6,200] though other sites in the paw with reported foreign bodies include the plantar soft tissues of the metatarsus[201] and the metacarpal pad.[4] While not common, a wooden foreign body has been reported as the cause of

retrobulbar abscessation and exophthalmos in a dog.[123] The pharynx is also a relatively uncommon site of trauma in the dog, but pharyngeal lacerations can be seen in dogs who frequently chase or carry sticks, and wooden foreign bodies have been found in 57% of dogs with pharyngeal injuries.[178,202]

While most dogs who are presented for porcupine quill injury have quills in multiple body regions, the head and neck (90%) and mouth (71%) are most commonly affected.[28] The limbs (31%) and trunk (7%) tend to be less involved in porcupine quill injury.[28]

Injury to the feet of working dogs (such as search-and-rescue dogs) is a constant possibility. While protective booties can be worn to help protect the feet, most dogs (including those at the World Trade Center following the events of September 11, 2001) do not wear this protective gear in order to get better traction on rubble.[1,203] In the search-and-rescue dogs deployed following the terrorist attacks of September 11, 2001, there was a 35% incidence of cuts, abrasions, and punctures, 70% of which were on the distal limbs.[1] This represented 9.2 events per 1,000 dog search hours, the highest system-specific disease incidence rate among deployed search-and-rescue dogs.[1] Similarly, 52% of New York Police Department working dogs experienced cuts and abrasions during their efforts following September 11, 2001, representing 9.3 events per 1,000 active deployment hours; 50% of the injuries were on the lower extremities.[2] While no foreign bodies were reported in these search-and-rescue dogs, and the recovery of the dogs suggests that there was no unreported chronic retention of foreign material, the injuries sustained could predispose to foreign body retention or infection.

Retention of surgical sponges in domestic animals more commonly occurs in the abdomen,[156,158] but retention in the musculoskeletal system has also been reported,[157,158] and thoracic involvement would also be possible.

Foreign objects that penetrate the gastrointestinal tract, including the stomach and small intestine, tend to remain primarily within the abdominal cavity.[174,175] However, these objects may penetrate the body wall[174-176] and can also penetrate the diaphragm, leading to thoracic disease.[175] A case of a toothpick which was suspected to have punctured the esophagus migrated to the level of the costochondral junction and caused a cutaneopulmonary fistula with evidence of focal pneumonia.[177] Additionally, foreign objects found in the retropharyngeal region likely represent migration of ingested objects through the oral or pharyngeal wall.[107,178] While these foreign objects are most commonly wooden,[178,202] a retropharyngeal needle has also been identified in a dog.[107]

3.3.2 Human literature

Hand wounds are one of the most commonly seen injuries in emergency departments,[181] and the hand is a common site of foreign body retention because of its constant interaction with the environment.[3,5,15] Males are more commonly affected than females, and the right hand is more commonly injured than the left hand.[5] Wood, glass, and metallic fragments are the most common foreign objects found in the hand,[5,121,204] although there is a wide spectrum of offending objects described. Other objects described in the hand include needles, pencil lead (graphite), bullets, thorns, BBs, nails, plastic, gravel, screws, fish spines, hair, fiberglass, and bone.[5] Presentation for removal of a foreign object may occur anywhere from the day of injury to 20 years later, and the average time of retention is 7 months.[5] Approximately half of the patients with a foreign body presented because of pain alone, and approximately half presented with a painful mass (3% of the patients were asymptomatic and the foreign object was found incidentally).[5] One important note is that 37.5% of the patients had previously been to a

physician who had missed the diagnosis, and in 77% of those cases the retained object was radiopaque, meaning that radiography would have provided a diagnosis.[5]

The feet are another common site of injury and foreign body retention, especially in individuals who walk without wearing footwear,[3,125] In one study investigating children living in a central urban area of Philadelphia, 34% had been cut at least once while walking outside, and 75% of those were not wearing footwear at the time.[205] Of the lacerations, 81% were caused by glass, 6% by nails, and the rest by other objects.[205] Another study of pediatric emergency department visits found that 0.8% of visits were due to puncture wounds in the foot,[152] and multiple cases of toothpick foreign bodies in the feet are described, especially in children.[124-126,206] Common causes of plantar puncture wounds include nails, needles, glass, wood, plastic, and other metallic objects.[180] The incidence of wounds in the lower extremities is important because 8.5% of wounds in the lower extremities of children treated in the emergency department become infected, a significantly higher rate than any other site in the body.[207] Similar regional results are described in adults, with the highest rate of infection in the legs and feet (6.5%), a lower rate in the arms and hands (3.8%), and a negligible rate elsewhere.[208] Increased incidence of wound infection in the lower extremities has been attributed to a relatively poor blood supply to this region of the body.[207,208] Additionally, wounds greater than 3cm in diameter were significantly more likely to become infected than those less than 3cm in diameter (5.3% vs. 0.4% of the cases in the respective groups became infected).[207]

Wooden foreign bodies are less common in head and neck injuries than in injuries of the extremities, but they can be quite important in this region. Wooden foreign bodies have been found in the orbit,[128,129,131,132] in the temporal musculature,[129,209] in the brain secondary to transorbital penetration,[134,210] and in the cervical soft tissues.[20] Wooden foreign bodies in the

facial region can be especially important because they are commonly misdiagnosed.[20,128,129,210] Motor vehicle accidents commonly lead to foreign body injuries in the head and neck, often involving glass fragments.[145] Embedded intraoral wooden, bone and plastic foreign bodies are also described.[148-150] While less common, foreign bodies in the brain parenchyma[211] have profound implications for the patient.

Retained surgical sponges (gossypibomas) are most common in the abdominal cavity[160,164,165,170,173] and pelvic cavity.[160,163] However, gossypibomas have also been described in the thorax,[173,212] cranial vault,[167] and in the musculature of the leg in patients with a previous history of trauma and subsequent repair.[160,161,166,169]

3.3.3 Soft-tissue spaces in the human hand

Recognition of the soft-tissue spaces in the hand is critical in understanding the spread of infection; no spaces other than the myofascial compartments are identified in the human foot. Spread of disease tends to be along fascial boundaries, and infection and foreign objects can remain within specific anatomic spaces. Myofascial compartments can also be also important in determining extension of disease; these are discussed further in Section 2.2: Myofascial Compartments in the Human Hand and Foot.

The two primary fascial spaces in the palm of the human hand are the midpalmar space and the thenar space.[39,59,213] The shield-shaped *midpalmar space* is found dorsal to the deep digital flexor tendons and lumbrical muscles and palmar to the metacarpal bones and interosseous muscles, spanning the third through fifth metacarpal bones (essentially from the thenar to the hypothenar eminence).[33,39,213-216] The palmar boundaries of the midpalmar space are the palmar aponeurosis and deep palmar membranes (including the flexor tendons and lumbrical muscles);

the dorsal boundary is the palmar interosseous membrane.[33,38,217] The attachment of the palmar fascia to metacarpal V, as the most medial aponeurotic septum or hypothenar septum, limits the space on the ulnar side of the hand and marks the boundary of the hypothenar compartment.[38,39,217] On the radial side of the palm, just radial to metacarpal III, the midpalmar space is separated from the thenar space by a connective tissue barrier, the oblique septum,[33,217] or middle palmar septum,[38,194] which extends from the deep digital flexor tendon of the 2nd digit.[194,213,215] This fascial barrier is also said to extend from the palmar fascia (palmar aponeurosis),[39,217] and extends dorsally to the palmar cortex of metacarpal III at the site of origin of the adductor transversus pollicis.[39,194,217] The proximal extent of the midpalmar space is in the proximal metacarpus, at the level of the distal part of the body of the ulnar bursa and transverse carpal ligament, just distal to the level of the distal flexion crease of the wrist.[33,39,215] The body of the midpalmar space extends distally to the level of the distal transverse crease in the palm.[33,213,215] Some authors note that there are septae subdividing the midpalmar space into four channels distally.[33,194] As many as eleven contiguous subcompartments separated by sagittal septae are described in the distal midpalmar space, with four containing the long digital flexor tendons, four containing the lumbrical muscles, and three for the interdigital vessels and nerves.[218] Small-volume injections were generally confined to one or two of the subcompartments of the midpalmar space,[33] but the clinical significance of this is unknown, as the proximal portion of the midpalmar space is undivided and larger injections still filled the entire midpalmar space.[33] Distal extensions of the midpalmar space, extending distally to the interdigital webs, are found on the deep surfaces of the lumbrical muscles of the 3rd-5th digits, representing the lumbrical canals.[39,213-215,217]

Because of the close association between the midpalmar and thenar spaces, infection of the midpalmar space will commonly spread to the thenar space, especially in an infection of several days' duration.[33,213,215] Pus from the midpalmar space may also extend along the lumbrical muscles to affect one or more interdigital web spaces, and can spread to the dorsal tissues of the hand from there.[213,215] Less commonly, infection in the midpalmar space can extend into the ulnar bursa, or even track dorsally through interosseous muscles where pus is seen on the dorsal surface of the hand.[215] In cases of midpalmar infection, tenderness is found in the middle to ulnar portion of the palm, and swelling of both the palmar and dorsal soft tissues can be seen.[39,40,213] The palmar swelling is generally seen as a bulging of the tissues (rather than the usual concave shape of the palm), and the dorsal swelling, which may be more severe than the palmar swelling, tends to present as a pitting edema.[39,91,194]

The wedge-shaped *thenar space*, referred to as the adductor space by some authors,[33,217] is located in the thenar eminence (proximal to the first digit), palmar to the adductor pollicis (adductor transversus) muscle and dorsal to the palmar fascia.[33,39,213-215] The thenar space is smaller than the midpalmar space, extending mediolaterally from metacarpal III to nearly the flexor tendon of digit I, and proximodistally from the level of the carpometacarpal joint and flexor retinaculum (just distal to the distal flexion crease of the wrist) to the level of the distal transverse crease of the palm.[39,215,217] There is also a distal projection of the thenar space along the lumbrical muscle of the second digit.[39] The palmar margin of the thenar space is the palmar aponeurosis and flexor tendon to the first digit, and the dorsal margin is the palmar epimysium of the adductor pollicis muscle.[38,217] The flexor tendons and lumbrical muscle of digit II are found palmar to the thenar space.[39,213,215] The ulnar wall of the thenar space is the oblique septum, separating the thenar space from the midpalmar space as previously described. The radial wall is

formed by the fascia and muscles of the thenar eminence: the adductor obliquus, opponens pollicis, and flexor pollicis brevis muscles.[38,217] The radial bursa is aligned along the radial margin of the thenar space.[39]

As described previously, the close association of the thenar and midpalmar spaces allows infection to extend from the thenar space to the midpalmar space relatively commonly,[33,215] although infection may have a greater tendency to remain within the thenar space for a longer period than is seen in primary infection of the midpalmar space.[213] Large injections of the thenar space led to extension of injected material into the interdigital tissue and the connective tissue dorsal to the adductor pollicis muscle.[33] In infection of the thenar space, there will be tenderness in the radial aspect of the palm, in the region of the space, and a rapidly progressing bulging of this half of the palm (most notably of the thenar eminence itself) can be seen.[39,40,194] Dorsal swelling between metacarpal I and metacarpal II may also be noted;[40] as with infection of the midpalmar space, this may be a pitting edema[39] and may be more severe than the palmar swelling.[91] One clinical study found that the thenar space infections were twice as common as midpalmar space infections, and the right hand was twice as likely to be affected as the left hand.[194] Extension from one space to another was only found in 2 of the 100 cases, both involving spread from the thenar space to the midpalmar space.[194]

The three *subfascial web spaces* between the fingers are also potential sites of pus collection.[38,214,219] These spaces contain loose fat and are found near the metacarpophalangeal joints.[219] The three web spaces do not communicate with each other as they are separated by the joint capsules and ligaments of the metacarpophalangeal joints and by the extensor tendons.[220] Infection of these spaces tends to remain in the immediate palmar tissues, but can track dorsoproximally to the dorsal metacarpus, proximally into the midpalmar space via the lumbrical

canals, medially or laterally into an adjacent web space, or distally into the tissues of a digit.[219] Secondary infection of the web spaces due to extension from deeper spaces[213,215] was described above.

A dorsal thenar space was previously described (with the current thenar space referred to as the palmar thenar space); its location within the palm was similar to the thenar space, but it was considered to be found dorsal to the adductor pollicis muscle and palmar to the first and second interossei.[215] However, injection experiments demonstrated that injection into the palmar portion of the thenar space led to extension dorsal to the adductor pollicis (adductor transversus) muscle in nearly all cases, indicating that this likely represents a single myofascial compartment.[213] The hypothenar space was historically considered an independent space within the septae of the hypothenar muscles, although it was also considered of doubtful significance as a site of deep infection, as purulent material in this space would extend superficially rather than into the deeper tissues.[213,214] However, even in studies attempting to verify its existence, demonstration of a space was difficult.[213] This space is better classified as a myofascial compartment (the hypothenar compartment), as it represents the intermuscular spaces found in the hypothenar eminence.[33,217] Likewise, the thenar space of one author was defined as "the intermuscular spaces of the thenar eminence,"[33] and thus is best described as the thenar compartment today. See Section 2.2: Myofascial Compartments in the Human Hand and Foot for further discussion of the thenar and hypothenar compartments.

Tendon sheaths and other serous structures are also important sites of infection in the palmar portion of the human hand. The radial and ulnar bursae, sacs lined by serous membranes, are present in the palmaroproximal portion of the manus. It should be noted that some consider the term "bursa" to be a misnomer for these structures, as a bursa is a sac between a bony

tuberosity and skin or muscle, while these structures are serous sheaths associated with tendons.[33] However, the bursa terminology is prevalent in the literature and will be used here. The usual arrangement of the bursae includes an ulnar bursa located in the middle and ulnar portion of the palm and a separate radial bursa located on the radial side of the palm.[59,214,215] However, communication between the radial and ulnar bursae is a common occurance.[59,214,215] This communication may take the form of an intermediate or accessory bursa between the two primary bursae,[33,59,213] or may be a small foramen or lack of a septum between the radial and ulnar bursae.[215] The proportion of individuals with a communication between the two bursae has been described as anywhere from one-third to more than 50% of individuals.[33,213-215]

The *ulnar bursa* extends from a point just proximal to the antebrachiocarpal joint, at the styloid process of the ulna, to the middle of the palm, and it is associated with (wrapped around) the superficial and deep digital flexor tendons over this distance, although the tendons are not completely surrounded by the bursa.[33,215] The distal end of the body of the ulnar bursa is at the level of the origin of the lumbrical muscles from the 2nd-4th flexor tendons.[215] The ulnar bursa then continues distally surrounding the flexor tendons of the 5th digit, acting as a synovial sheath for these tendons.[59,213-215] According to some, the flexor tendon sheath can be separate from the ulnar bursa, but these cases are considered uncommon,[213] possibly occurring in up to one-third of cases.[33] In the proximal metacarpus, the ulnar bursa is directly adjacent to the palmar margins of metacarpals III-V, though more distally the midpalmar space and interosseous muscles are found between the bursa and metacarpal bones.[215] The ulnar bursa is located immediately palmar to the proximal end of the midpalmar space and is also adjacent to a small part of the ulnar and proximal aspect of the thenar space, though these two spaces extend further distally than the ulnar bursa.[215] Given the common communications between the ulnar and radial bursae, pus

within the ulnar bursa commonly spreads to the radial bursa.[215] Pus spreading from the tip of the first digit to the tip of the fifth digit is referred to as a horseshoe abscess due to its appearance.[38] The midpalmar and thenar spaces may also become involved when there is infection of the ulnar bursa, given their proximity to this structure.[215] The palmar margin of the ulnar bursa is covered by the tough palmar fascia, which prevents spread of infection toward the palmar skin.[215] Infection of the ulnar bursa causes pain extending from the distal part of the 5th digit over the ulnar side of the palm to the carpus, and frequently leads to pain over the radial bursa as well.[40]

The *radial bursa* extends from a point just proximal to the antebrachiocarpal joint to the distal phalanx of the first digit: this bursa surrounds the flexor pollicis longus tendon proximally then acts as a tendon sheath for the flexor pollicis longus tendon for approximately the distal half of its extent.[33,59,213-215] As previously mentioned, the radial bursa is in close proximity to, and may communicate with, the ulnar bursa.[59,214,215] The radial bursa is also adjacent to the thenar space, although it is not closely associated with the midpalmar space.[215] Thus, infection in the radial bursa has a high likelihood of spreading to the ulnar bursa, and a moderate probability of spreading to thenar space.[215] Pus in the radial bursa leads to pain extending from the distal end of the 1st digit along the radial aspect of the palm to the carpus; again, pain often continues into the region of the ulnar bursa.[40]

Individual *digital synovial tendon sheaths* surround the flexor tendons in the 2nd-4th digits.[59,213,214] These tendon sheaths originate approximately 2 cm proximal to the respective metacarpophalangeal joints,[213] at the level of the distal transverse crease of the palm,[33] and extend to the distal phalanges of the three digits.[213] However, some argue that the sheaths terminate by the level of the distal interphalangeal joints.[33] Rarely one or more of these tendon sheaths may communicate with the ulnar bursa.[33,213] Injection into the tendon sheaths found the

material to generally be confined to the injected sheath, although larger injections tended to cause rupture proximally into the corresponding subcompartment of the midpalmar space, with still larger injections filling more of the midpalmar space.[33]

The *extensor space* (also referred to as the dorsal subaponeurotic space or dorsal gliding space of the extensor tendons) is a deep soft-tissue space on the dorsal aspect of the hand.[38] An injection study found this space to be a continuous connective tissue space surrounding the extensor tendons, with no communications between the paratendinous connective tissue and the tendon sheaths of the extensor digitorum and extensor indicis muscles.[221] The extensor space is separate from the dorsal subcutaneous space; both of these spaces are considered distinct places in which pus can collect.[213,214] The extensor space is separated from the more superficial loose subcutaneous connective tissue of the hand by a strong dorsal membrane and the extensor tendons, and the dorsal membrane is continuous with the palmar membrane found between the extensor tendons and the metacarpal bones.[38,221] The metacarpal bones and interosseous muscles act as the palmar boundary of the extensor space.[38] In one injection study, the extensor space was found around the tendons of the 2nd, 3rd, and 4th digits; an independent extensor space surrounded the 5th digit extensor tendon, and injected material never incorporated the extensor tendon of the 1st digit.[221] A second injection study found that the injected material extended all the way from metacarpal II to metacarpal V, though injection pressures in this study may have been greater than those in the previous one.[213] In the second study, collection of injected material was confined to the area just deep to the tendons themselves and did not fully surround the tendons.[213] The pattern of infection seen in wounds on the dorsal aspect of the hand, such as human bite wounds, follows the anatomic structure of the extensor space.[221] However, infection of the extensor space causes marked dorsal swelling of the hand, and may be difficult to

differentiate from infection of the dorsal subcutaneous tissues.[38] It should also be noted that extension of pus from the deep palmar tissues, such as the midpalmar space, would lead to involvement of the extensor space.[213]

The *dorsal subcutaneous space* was demonstrated with injection experiments, and the injected material tended to remain in the dorsal tissues without extension abaxial to metacarpal II.[213] Fascial attachment to the bone was not identified, and limitation of spread was thought to be due to decreased looseness of the connective tissue at this point.[213] There was no extension of injected material into the palmar tissues of the hand.[213]

3.4 TREATMENTS

Wounds should be cleaned, but the appropriate level of aggressiveness for wound care is controversial.[152] Conservative management is best for individuals with puncture wounds who present within a day of injury and do not have evidence of a foreign body – recommended management includes intermittent soaking in warm water and cleansing of the skin.[180] Elevation of the affected extremity is also important to decrease edema formation.[222] Use of soap and water will help evaluation of the wound site, and betadine or povidone-iodine solutions may decrease the number of bacteria present without adverse effects on healing.[152,180] Jagged skin edges, especially when there is no sensation in the skin, can be removed.[152] Probing a wound could help identify a rigid foreign object, but requires anesthesia and may force smaller or softer foreign bodies further into the tissues.[152]

When a foreign body is identified, surgery to remove the object is generally required.[192] However, occasionally foreign objects are small and asymptomatic, especially when made of inert substances such as gold,[180] and these foreign bodies can be left in place.[5] The extent of

surgery required is determined by the extent of tissue affected by the foreign object. Findings from imaging studies (including sinography, ultrasound, CT, and MRI) can be used to plan surgery. Abnormal tissues, including fibrous and granulomatous nodules and tracts, are commonly removed, and may reveal the foreign object embedded within.[4,156,160,174,175,177] Lavage is generally indicated,[178] and drainage of abscesses is also necessary.[138] Muscles affected by fibrosis may require excision, and abnormal bone (with either proliferative new bone formation or osteomyelitis) may also have to be removed.[123] Lacerations caused by migrating foreign bodies (as to the soft palate from retropharyngeal foreign objects) must be repaired.[178] When the migration of a foreign body has led to adhesions between multiple organs, or between an organ and the body wall, these adhesions can be broken down.[174,176] Placement of surgical drains may also be necessary.[175] Migration of a thorn into a joint will cause synovitis; while copious irrigation of the joint and removal of the offending object may be sufficient for treatment, partial or complete synovectomy may be required.[223,224]

Most foreign bodies in the canine manus are located on the palmar surface: in the interdigital webs, the metacarpal pad, and palmar soft tissues of the metacarpus.[4,6,200,201] Exploration is difficult because of potential postoperative complications – wounds on the palmar surface of the foot are slower to heal because of the unwillingness of patients to stop using the limb. Care must be made in repair of the palmar tissues to prevent distortion of the weight-bearing surfaces, and splinting of the limb is often necessary to help prevent wound dehiscence due to early weight bearing.[63] Bones are near the surgical site and surface of the manus, making osteomyelitis a greater likelihood. In addition, probable migration of a FB means that the incision may have to be long, and both the palmar and dorsal sides of the paw may be affected and thus need to be explored.

Because the region of exploration in the canine manus may be large, it is important for the surgeon to recognize which structures must be spared and which structures can be sacrificed. Dorsally, the most important vessels are the cranial superficial antebrachial artery and vein; these branch into the dorsal common digital arteries and veins which run between the metacarpal bones. The accessory cephalic vein is also found at the level of the distal radius. Important tendons that are encountered include those of the common digital extensor muscle (4 branches), lateral digital extensor muscle, abductor pollicis longus muscle, and extensor carpi radialis muscle. Tendons and vessels smaller than these are considered small enough in a medium-sized dog that their identification is difficult and their preservation is not necessary.[225] The abductor pollicis longus tendon also may not be necessary to save, as it is transected and not repaired in carpal arthrodesis.[226] When approaching from the palmar surface of the manus, the important tendons include the tendons of the superficial and deep digital flexor tendons superficial (palmar) to each metacarpal bone and digit.[225] Laceration of the superficial digital flexor tendon may be of minimal functional importance, but complete severing of both the superficial and deep digital flexor tendons will result in palmigrade positioning of the affected digits.[226] The important arteries are the median artery and the palmar common digital arteries, while the veins that should be saved (from distal to proximal) are palmar common digital veins, deep palmar venous arch, cephalic vein, radial vein, and ulnar vein.

Emergency surgery is necessary for human patients with deep hand infections.[40] For an infection of the deep spaces and tendon sheaths in the human, incisions are made to allow for drainage of pus. The midpalmar space is generally opened via a palmar incision in the interdigital web space and lumbrical canal between metacarpal III and IV.[39,40,214] A curved incision in the palmar skin beginning at the distal flexion crease between metacarpals III and IV

and extending to the proximal flexion crease over metacarpal IV can also be used to approach the midpalmar space.[39] To treat infection of the thenar space, a longitudinal incision is made dorsally on the abaxial margin of metacarpal II.[38,39,194,214] Alternatively, a palmar incision can be made on the thenar eminence, beginning nearly at the web between the 1st and 2nd digits and extending proximally and axially nearly to the thenar crease.[38,40] For infection in the ulnar bursa, an incision is made on the palmar surface of the 5th digit, along the flexor tendons, and is extended proximally along the ulnar side of the palm.[40] However, others recommend that the incision on the 5th digit should be laterally positioned, and is not necessarily continuous with the incision over the hypothenar eminence.[195] An infection of the radial bursa requires an incision beginning on the palmar (or palmaro-axial) surface of the distal phalanx of the 1st digit, extending proximally over the thenar eminence to the level of the carpus.[40,195] The digital tendon sheaths of the 2nd, 3rd, and 4th digits are incised laterally over the proximal and middle phalanges;[195,214] avoiding an incision on the flexor (palmar) surface is important to minimize loss of function caused by scarring.[195] The extensor space is drained by one or more incisions made dorsally over the spaces between the metacarpal bones;[214]one suggestion is to make a longitudinal incision dorsal to metacarpal II and a second longitudinal incision dorsally between metacarpals IV and V.[38]

For any infection, antibiotic therapy is indicated. Infectious agents are commonly found in wooden foreign body injuries because wood is porous and organic, and usually associated with the soil.[131,138] The specific antibiotic of choice depends on the bacterial species identified with culture and Gram stain.[38] In puncture wounds, if the puncturing agent is considered relatively clean, such as a sewing needle, coverage for skin flora (Staphylococcus and Streptococcus) may be sufficient; a 1st-generation cephalosporin such as cephalexin or cefazolin could be used.[152] For

a Staphylococcus skin infection that has progressed to the point of requiring hospitalization (and thus parenteral antibiotics), nafcillin and oxacillin are the antibiotics of choice.[227] However, puncture wounds often require anaerobic coverage, especially when a foreign object is present; clindamycin or ampicillin/clavulanate can be used to cover for such species as Actinomyces.[152,186,228] Outdoor or rusty metallic agents causing wounds, or other dirty wounds, may require coverage for *Clostridium tetani* (metronidazole, ampicillin or penicillin G) as well as tetanus vaccination or boosting with tetanus toxoid.[152,229-231] If the injuring agent is wet, such as a wet splinter, Pseudomonas coverage is indicated; an antipsuedomonal with a beta-lactamase inhibitor such as piperacillin/tazobactam should be used.[152,232] If the puncturing agent is a rose thorn, Sporotrichosis (rose gardener's disease) is a possibility: itraconazole is the drug of choice.[233] The occurrence of community-associated methicillin-resistant *Staphylococcus aureus* (MRSA) is increasing, and coverage against one of these isolates may be necessary; vancomycin is the first choice of therapy.[38,227,234] For animal bite wounds, a beta-lactam/beta-lactamase inhibitor combination such as ampicillin/sulbactam is indicated for coverage of such bacteria as Pasteurella.[183,184] Multiple antibiotics may be required for mixed infections, such as the mixed aerobic and anaerobic infections often seen in toothpick injuries.[187] In addition to antibiotics, tissue debridement may be required when an infection cannot be suitably controlled medically.[187]

3.5 COMMON COMPLICATIONS

Complications from foreign objects depend on the site to which the foreign body migrates. Migration of objects into the thorax may cause pleural effusion or pneumothorax.[235,236] In dogs with grass awns in the external ear canal, 19% had a ruptured tympanic membrane.[6] One cat with severe otitis media and interna was found to have extension of disease into the cranial vault

adjacent to the cerebellum, and a foxtail was discovered within the lesion, suggesting migration from the ear.[237] Lumbar discospondylitis has been associated with grass awn migration in the lumbar region.[6] Localized abscesses are also seen relatively frequently with grass awn migration,[6,27] and sublumbar abscessation may occur secondary to inhalation of grass awns and subsequent migration along the diaphragm.[193] Wooden foreign bodies can also cause formation of a phlegmon.[143] Because wooden fragments may be small or not recognized initially on imaging studies, they may not be identified with surgery, and multiple surgeries may be required to retrieve all of them.[4,138,140] Indeed, in one study of dogs with draining tracts, patients had undergone a mean of 2 surgeries (range 1-5) to treat the tract prior to referral, and all of these patients had at least one additional surgical intervention at the referral hospital.[4] Similarly, a study of Phoenix date palm thorn foreign bodies in children found that the average patient required 1.3 surgical procedures, excluding those procedures performed at outside clinics (inclusion of which would raise the average to approximately 2 procedures per patient).[142]

Facial nerve paralysis in a dog following retention of a wooden foreign body has been described.[123] Other complications that can be caused by orbital foreign bodies include orbital abscess/cellulitis, damage to the optic nerve and extraocular muscles, and intracranial extension (which carries with it a 48% incidence of brain abscessation and 25% mortality in humans).[137,138] Perforation of the globe requiring enucleation has been described due to an intraorbital foreign object.[140] Facial foreign bodies in people have also resulted in obstruction of the parotid salivary duct, trismus, and erosion of the mandibular condyle.[133] Neurologic complications seen with intracranial foreign bodies depend on the part of the brain affected, but included focal epilepsy and sensations of fear and nausea in one human patient with a chronically embedded glass foreign body.[211] Wooden foreign bodies in the brain of dogs causing bacterial

meningoencephalitis and ventriculitis or abscessation have led to decreased conscious proprioception, obtundation, tetraparesis, tonic-clonic muscular contractions, head pressing, and ataxia.[198,199]

When foreign body retention is secondary to pharyngeal laceration, subcutaneous emphysema and pneumomediastinum can also be seen. If the esophagus has been perforated, ingesta may be found in the soft tissues, and mediastinitis and sepsis can ultimately occur.[178]

Complications were seen in 10.8% of dogs presenting with porcupine quill injury: abscess or cellulitis was diagnosed in 87% of the cases with complications, and there were 2 cases (6%) each of intraarticular migration and intraocular migration.[28] One case of a suspected quill-induced pneumothorax was also reported, and quills were removed from the cranial mediastinum and lung during thoracoscopy.[28] The rate of complications significantly rose with increasing time to presentation: dogs presented more than 24 hours after injury were 5.2 times more likely to experience a complication than dogs presented less than 12 hours from the time of injury.[28] Septic arthritis secondary to porcupine quill migration has also been described in a dog.[238]

In one review of 200 human patients with foreign bodies in the hand, 12.5% presented with complications from that foreign body. The most common complication was infection (64%), but other complications included digital nerve neuropraxia, digital nerve laceration, nail deformities, metacarpal fracture, and formation of an inclusion cyst.[5] Infectious processes can include tetanus, gas gangrene, cellulitis, abscessation, draining sinuses, osteomyelitis, mycetomas, tenosynovitis, monoarticular septic arthritis, and lymphangitis.[3,125] Toothpick injuries in the hand carry complications similar to those of human bite wounds due to the presence of oral flora: infection is extremely common, and will often progress to cellulitis, abscessation, septic arthritis, osteomyelitis, or pyogenic tenosynovitis with possible adhesion formation and necrosis.[187]

Additionally, seven of eight patients in one series had to be hospitalized (average stay 26 days with an average of 3 debridements for infection control), and outcome complications included decreased total active motion, decreased grip strength, and flexion contracture.[187] Progressive ulnar neuropathy has been reported as a complication of slow proximal migration of a wooden foreign object from the carpus to the antebrachium.[239] Tendon rupture can also occur, as in a case where a glass foreign body migrated 4.5 centimeters from the site of initial injury and ruptured the flexor pollicis longus tendon in a person 30 years after initial injury.[240] An embedded glass fragment has been incorporated into a healing metacarpal fracture in one case, causing a focal swelling and symptoms of arthritis in the adjacent metacarpophalangeal joint.[241] Circumferential osteolysis of the radial and ulnar cortices has also been described in a cat who was found to have a tight elastic band embedded in the antebrachial tissues.[242]

A host of complications can result from plantar puncture in humans. Many wounds will heal entirely, without complication. However, complications include cellulitis, abscessation, osteomyelitis, or septic arthritis.[152,206] Systemic effects including fever and polyarthritis have also been described secondary to the presence of a sea urchin spine embedded in a wound that was not infected.[114]

Complications associated with gunshot wounds are largely related to the trauma to surrounding structures, but infection and lead toxicity can also be seen, and severe synovitis is possible if a lead bullet fragment remains within a joint.[106] Additionally, a foreign body reaction can occur and lead to a draining tract; in one equine case this had to be differentiated from fistulous withers (which is caused by *Brucella sp.*).[154]

With retention of a surgical sponge, complications are variable. Clinical signs that develop may be nonspecific (such as depression, weight loss, and chronic vomiting), and the only

abnormalities detected on examination may be palpation of a mass at the site of the granuloma.[156] In one series of retained surgical sponges in dogs, a draining sinus was noted in five of the eight cases.[158] Gossypibomas in the abdomen may cause adhesions between abdominal organs and can lead to intestinal perforation, peritonitis, fistula formation, sepsis, and intestinal or ureteral obstruction.[158,165,170] If a gossypiboma is close to bones, osteolysis can result.[161,169] Other complications in humans are psychological, as these masses generally mimic malignant neoplasms.[160,161,169] A gossypiboma adjacent to the stifle of a dog has also been associated with an extraskeletal osteosarcoma, which presumably developed due to malignant transformation secondary to the inflammatory response.[157]

Migration of skewers out of the gastrointestinal tract can lead to complications associated with the abdominal and thoracic cavities and the body wall. Complications include peritonitis and adhesions, focal body wall swellings, active periosteal response from adjacent bones, draining tracts, and pneumothorax.[174,175,177]

4. Diagnostic Imaging of Inflammation and Foreign Bodies

4.1 Radiography

Radiography utilizes x-rays that are projected through a patient and expose a radiographic film or digital radiography panel to produce an image. X-rays are produced in the x-ray tube by producing electrons at the cathode (a tungsten filament) and accelerating those electrons across a high voltage (up to 120 kV) toward a target. The target, or anode, is made of a tungsten alloy, and interaction of the electrons with the target's nuclei produces x-rays via characteristic and bremsstrahlung radiation. The x-rays then interact with the patient via the photoelectric effect

and Compton scattering, and those x-rays that do not interact with the patient's tissues strike the x-ray film or digital radiography panel and are recorded as part of the produced image.[17] The more x-rays that strike the film or panel, the blacker that region of the image becomes. Objects that absorb most of the x-rays appear white on the image, and are considered to be radiopaque. Radiolucent structures are those which absorb few x-rays and thus appear relatively black on the image.

Radiography's advantages include its wide availability, portability (including in the emergency department, operating room, or in the field), low cost, the speed and ease of making an image, and relatively easy interpretation.[16] The spatial resolution of a conventional radiograph is also relatively high (typical resolution of about 7 lp/mm, and up to about 12 lp/mm), while the spatial resolution of digital radiography is somewhat less (approximately 5 lp/mm up to 7 lp/mm).[17] However, radiography is not well suited to visualizing certain types of foreign objects because this modality is not very sensitive at detecting small differences in the physical density or effective atomic number of substances (e.g. differentiation of tissues from fluids); in other words, the contrast resolution is not as good as many other modalities.[123,243] Another limitation in diagnosis of inflammation or foreign body retention is that soft tissue swelling may not always be recognized, especially in complex areas such as the skull.[123]

Because some foreign objects are radiopaque, radiography is indicated as the initial imaging modality to be performed in any case with suspected foreign body retention.[3,5] The appearance of foreign objects with radiography depends on their composition (including effective atomic number and density), size, and orientation within the body.[16,243] The five basic radiographic opacities, from most radiolucent (black) to most radiopaque (white), are air, fat, water/soft tissue, mineral, and metal.[243] The visibility of an object depends on the difference in

radiopacity between the object and the surrounding tissues.[16] The radiopacity, in turn, is a function of the object's density (due to the effects of Compton scatter) and the cube of its effective atomic number (due to the photoelectric effect, the primary contributor to radiopacity and thus tissue contrast).[7,17] Hence, objects that are embedded in the soft tissues and similar to soft tissues in atomic number are unlikely to be visualized with radiography.[7] Use of a small focal spot, collimation to a small field size, and minimal overexposure have been advocated to help in detection of foreign bodies.[3]

Bullets are radiopaque (metal opacity),[154] and while the composition of a bullet cannot be determined by its radiopacity, lead pellets tend to be deformed and fragmented because they are soft, while steel pellets generally remain spherical.[106,146] Other metal objects such as needles, iron, and galvanized steel are generally easily detected as metal opacities, as well.[8,244] Stones and gravel are radiopaque, visualized as a mineral opacity, though the homogeneity of individual specimens varies.[7-9] Other easily detected radiopaque substances include tooth fragments,[9] amalgam,[9] and asphalt.[9] Most chicken and meat bones are radiopaque, although many fish bones are not radiopaque,[106] likely due to their small size and the relative lack of mineral in fish bones. Plastic[7,8,106,244] and thin aluminum objects[3,106] are generally not radiopaque, though polyethylene may be poorly visualized.[7] Wooden foreign bodies are considered to be undetectable on radiographs in most cases,[5,8,9,25,122,124,126,244] as they are of similar density to the soft tissues,[245] although they are occasionally visualized as linear radiolucent structures (especially when large).[5,19,122,127,245] The type of wood and its water content are likely important factors in determining the visibility of wood: dead (non-green) wood has less water content and more air, and would be expected to be more radiolucent.[245] Visualization of a bamboo foreign body has been attributed to the gas in the center of the shaft.[127] In one study in cadaver hands, the wood

grain of one dry wood specimen allowed for its visualization, but all wet woods were radiographically undetectable.[7] Because graphite is radiopaque,[244] pencil fragments may be visualized as a central radiopaque band (the graphite) surrounded by a radiolucent area (the wood).[8] Porcupine quills are also radiolucent.[238]

Contrary to common belief, all glass is visible on radiographs, as the radiographic density of glass is greater than the density of soft tissue (the density ranges from 1.6 to 3.9 times the density of soft tissue).[5,7-9,19,106,244,246] Some authors incorrectly believe that lead must be present in the glass for visualization.[101,247] The higher radiographic density is due to the higher physical density and effective atomic number of all glass relative to soft tissue.[8] One study evaluated 66 different types of glass embedded in chicken cadaver legs and found that all specimens were radiographically visible, including fragments as small as 0.5mm.[248] Nonetheless, not all glass foreign bodies are identified on radiographs of the hand, possibly because of superimposition of the bones.[5]

Most surgical gauze sponges include radiopaque markers (barium sulfate monofilaments) for easy identification.[101,157] However, older sponges may not have radiopaque markers, making the sponge radiographically undetectable, and a radiopaque marker may not be accurately identified.[160,173] Nonetheless, a focal speckled or whirling gas pattern, sometimes associated with a soft tissue mass, has been described in some patients with gossypibomas.[158] A circumferential elastic foreign object in a cat was seen as a circular opacity within cortical lysis of the ulna.[242]

When radiolucent objects are present, secondary response by the surrounding tissues may be the only radiographic evidence of a foreign body. If there is intra-abdominal migration of a foreign object, loss of serosal margin detail may indicate peritonitis or peritoneal effusion.[174,175] Formation of a granuloma or abscess around a foreign object will cause a mass effect, with

displacement of surrounding structures.[249] Similarly, intrathoracic migration can cause pleural effusion, pneumothorax, or pneumomediastinum,[175,196,197,235,236] and an interstitial or alveolar pulmonary pattern consistent with pneumonia, hemorrhage, or atelectasis may also be seen.[177,196] A mediastinal soft tissue mass has also been associated with grass awn migration in a cat.[27] Soft tissue opacity swellings or masses (which may be heterogeneous) may be present in the body wall or muscles,[4,160,162,169,174,176,193] and may contain focal gas opacities.[4,176] If a foreign body is retained secondary to laceration of the pharynx, cervical soft tissue emphysema and pneumomediastinum can be recognized.[178] Mineralization can be present within foreign-body associated masses, and this mineralization may be rounded and dense or streaky.[150,157,160,162] A calcified rim has also been described in an intra-abdominal gossypiboma.[170] Nearby osseous structures may exhibit active periosteal new bone formation or smoother periosteal thickening as a response to inflammation, depending on the chronicity of the condition.[4,123,160,169,174,175,193] However, one author notes that periosteal response is generally mild, which may help in differentiating foreign bodies from neoplastic conditions.[161] Severe osteolysis of the femur surrounded by a radiopaque rim has also been described in cases of gossypiboma,[161,169] and lysis of the coronoid process of the mandible and the zygomatic arch has been identified in a case of a retrobulbar wooden foreign body.[123] Mild erosion of the humerus has been seen in a person who had a retained wooden foreign body in the nearby tissues.[124]

When the presence of a radiolucent foreign body is suspected, use of a "soft-tissue" radiographic technique has been advocated. Soft tissue techniques employ a lower kVp to attempt to increase image contrast. However, use of a soft tissue technique did not improve visualization of radiolucent foreign bodies relative to conventional radiographic techniques in one study.[250]

Fluoroscopy is the use of continuous radiation to image a body part in real time, i.e. with good temporal resolution.[16] The relative appearance of objects using fluoroscopy is the same as on conventional radiographs, except an inverse grayscale is used. Because of its real-time nature, fluoroscopy can be used to aid surgical guidance of foreign body removal, primarily if the object is radiopaque.[16,251] However, while the mA is kept low in fluoroscopy, the total time of exposure is much longer than with conventional radiography, leading to considerably higher overall radiation exposure.[16] Another disadvantage is that with most systems, only a single image plane is available at a time[16] (though biplane systems do exist, especially for use in angiography).[17] Additionally, the spatial resolution of fluoroscopy is generally somewhat poorer than that of conventional radiography, and the contrast resolution is considerably worse due to the low signal-to-noise ratio.[17]

Xeroradiography is similar to conventional radiography in that it uses x-rays for imaging of anatomy. However, rather than radiographic film or a digital detector, the incident x-rays interact with a plate of amorphous selenium that has a uniform electrostatic charge.[7,252,253] The selenium plate is exposed to x-rays just like a conventional radiographic cassette, which causes a loss of charge that is proportional to the x-ray beam intensity and spatial characteristics, creating a latent electrostatic image.[252,253] Developing of the image occurs by exposing the plate to charged toner (pigment) particles which are attracted to the plate, then the toner is transferred to a receiver sheet of paper and heat-fixed to make a permanent image.[252,253] Xeroradiographs are thus viewed with reflected light, unlike conventional radiographs which are viewed with transmitted light.[253] One advantage of xeroradiography is the long grayscale that it employs, allowing evaluation of many different tissue densities and thicknesses with a single exposure,[253] though current digital radiographic systems also have a long grayscale. Xeroradiography was primarily utilized because

of its edge-enhancement ability, making some low-contrast soft-tissue lesions more evident.[7,253] One *in vitro* study found that relatively radiolucent foreign bodies (such as wood, plastic, graphite, and rubber) may be better visualized with xeroradiography than with conventional radiography.[254] This report also suggests that foreign objects such as graphite, wood, and plastic are best visualized in positive mode (image reversed relative to conventional radiographs), while metal was better visualized on the negative mode due to the profound edge enhancement seen on positive mode.[254] However, while some advocated its use in cases of suspected foreign body retention, it was shown to be no more accurate in detection of retained foreign objects than conventional radiography in cadaver studies.[7,255] Additionally, the radiation exposure is approximately twenty times that of conventional radiography,[13] and the additional equipment costs were considerable.[253] Thus, use of xeroradiography was generally not advocated over radiography for detection of foreign objects, and xeroradiography is generally unavailable today. Other than the effects of edge enhancement and possible mild changes in radiopacity, the appearance of foreign bodies is the same on conventional radiographs and xeroradiographs.[7,254]

4.2 SINOGRAPHY

The terms *sinography* and *fistulography* are often used interchangeably. A fistula is "an abnormal passage from one epithelial surface to another epithelial surface,"[256] or from a "hollow organ or part to the body surface or from one hollow organ or part to another."[257] A sinus is "a narrow elongated tract extending from a focus of suppuration and serving for the discharge of pus,"[258] or can refer to normal structures such as the paranasal sinuses of the skull. Some prefer the term *fistulography*, as fistulas are always abnormal and sinography could be performed in a

normal structure.[247] However, *sinography* is more inclusive, as a fistula is a type of draining sinus,[4] so the term *sinography* will be used here.

Sinography is used to determine the extent of a tract within the soft tissues, communication with body cavities (including thorax, abdomen, joint spaces, and tendon sheaths), presence of foreign objects, and proximity of a lesion to bone, which could indicate the presence of osteomyelitis.[4,247] For this procedure, survey radiographs of the area of interest are first made to allow for full evaluation of the soft tissues and osseous structures before they become obscured with contrast medium.[247] A Foley catheter is pre-filled with iodinated contrast medium, then it is inserted into the tract and the balloon is inflated.[200,247] Use of a Foley catheter prevents leakage of contrast medium onto the skin during injection, which would confuse diagnosis of the extent of the draining tract.[200] Contrast medium is injected until there is back pressure on the syringe, and radiographs are made.[247] Monitoring the pressure during injection is important to prevent iatrogenic rupture of the tract.[4] Sinography can also be performed with computed tomography.[171]

A sharply marginated sinus tract may be identified in some cases, but the contrast medium may also disperse through the tissues in cases with more diffuse cellulitis.[247] In the extremities, communication with tendon sheaths or joints can be confirmed when there is visualization of the sheath or joint capsule.[247] However, if communication with a joint is suspected despite lack of confirmation with sinography, an arthrogram may demonstrate leakage of contrast medium out of the joint into the tissues.[247] Foreign objects should appear as filling defects within the contrast medium.[171,201,247] Wooden fragments may be irregular in shape and margination.[247] Filling defects that could lead to a false positive diagnosis include irregular tissues, blood clots, and air bubbles.[247] A foreign object may not be identified even if one is present.[175] However, even if a discrete object is not identified, the extent of affected tissue can be determined, and a possible

site of origin can be found. For example, contrast medium extending from a draining sinus into the stomach indicates a gastrocutaneous fistula,[176] and contrast medium extending from a draining sinus to the bronchial tree has been described in a case of cutaneopulmonary fistula.[177] While the benefits are apparent, obviously a draining tract is required to perform a sinogram.

In a study of 25 cases with draining sinuses, the neck, head, and paws were the most commonly affected body parts.[4] Retained foreign bodies represented the cause of the draining tract in 60% of the cases in this study, and more than half of these were wooden foreign objects.[4] A definitive diagnosis was achieved in 58% of sinograms performed, with only two foreign objects not detected (sensitivity 87%) and no false positive foreign body diagnoses (specificity 100%).[4] Sinography was also useful in detecting the extent of the lesion, as one dog with a draining sinus on the dorsal metacarpus had a thorn in the metacarpal pad.[4]

4.3 SCINTIGRAPHY

Scintigraphy involves administration of a radioactive substance to a patient and detection of the resultant internalized radiation to produce an image. Radiopharmaceuticals are agents which contain a radionuclide (radioactive atom) and a chemically active molecule.[259] The most commonly used radionuclide in medical imaging is ^{99m}Technetium (^{99m}Tc). The molecule attached to the radionuclide will determine where in the body the radiopharmaceutical will localize, and thus the characteristics of the resultant image.[259] The radioactivity is detected with a gamma camera, which counts the gamma rays emitted from the patient and produces an image based on the locations of the radioactive decay events.[260] An advantage of scintigraphy over other imaging modalities is that the interaction of the radiopharmaceuticals with the body depend on physiologic processes, so targeted physiologic information about a system can be obtained;

image interpretation is not limited to simply anatomic information.[261] Disadvantages relative to other modalities include poor spatial resolution (typical spatial resolution of 2.7-4.2 mm versus 7 lp/mm for screen-film radiography and 1-2 lp/mm for CT)[17] and the fact that the patient will remain radioactive for a time that depends on the physical and biological half-lives of the radiopharmaceutical administered.[262]

Numerous radiopharmaceuticals have been used to attempt to evaluate infection. Bone scans using ^{99m}Tc-MDP (methylene diphosphonate) or ^{99m}Tc-HDP (disodium oxidronate) and imaged in three phases (perfusion, soft-tissue, and bone phases) are commonly used when evaluating for osteomyelitis.[263] Uptake of the radiopharmaceutical in bone is a function of blood flow to the bone and chemiadsorption to hydroxyapatite crystals; this latter relates to the osteoblastic activity in the bone.[264] Osteomyelitis classically appears as focal hyperperfusion, focal hyperemia (increased uptake in the soft-tissue phase), and a marked focal increase in osseous uptake.[263] When foreign objects, or the inflammatory response associated with these objects, are adjacent to bones and causing osseous remodeling, bone scintigraphy will reveal increased uptake in the affected bone, though this uptake may be less severe than in osteomyelitis.[161,169,193,264] While a foreign body itself would not be expected to be visible, the surrounding inflamed soft tissues may have abnormal radiopharmaceutical uptake. One gossypiboma in the musculature imaged with ^{99m}Tc-HDP had mild ring-shaped uptake in the periphery of the mass.[169] Subsequent imaging of this mass with ^{201}Tl (^{201}Thallium) demonstrated decreased uptake in the gossypiboma relative to the surrounding muscles.[169]

Agents intended specifically for the imaging of infection have also been developed. ^{67}Ga-citrate (^{67}Gallium) is a commonly used agent, as uptake of this radiopharmaceutical in areas of inflammation and infection tends to be high. Multiple mechanisms have been advanced for its

uptake in inflammatory sites. Most circulating ^{67}Ga is bound to transferrin in the plasma, so increased blood flow and vascular permeability in sites of inflammation cause increased concentrations of ^{67}Ga (bound to transferrin) at those sites.[263] Additionally, ^{67}Ga binds to lactoferrin, which is generally prevalent at sites of inflammation, ^{67}Ga may be transported by white blood cells, and some bacteria may take up ^{67}Ga.[263] When there is suspicion of osteomyelitis, use of ^{67}Ga can increase the specificity of bone scintigraphy. A patient is considered positive for osteomyelitis when the ^{67}Ga and ^{99m}Tc-MDP uptake patterns are spatially different or if the ^{67}Ga uptake is greater than that of ^{99m}Tc-MDP; the study is negative for osteomyelitis when ^{67}Ga uptake is normal or if its uptake is spatially the same as and less intense than that of ^{99m}Tc-MDP; and the study is equivocal if the uptake of ^{67}Ga and ^{99m}Tc-MDP is the same both spatially and in intensity. The overall accuracy of combined bone and ^{67}Ga imaging is between 65% and 80%.[263] Disadvantages of the technique include the use of two radiopharmaceuticals over the course of 2-3 days and the poor imaging characteristics of ^{67}Ga.[263]

Leukocytes labeled with ^{111}Indium (^{111}In-WBC) and ^{99m}Tc-HMPAO have been used to evaluate infection in people and animals. A study in humans evaluating detection of osteomyelitis found that ^{111}In-WBC imaging produced 27 true positive and 9 true negative results, with only 1 false negative and 2 false positive results (the false negative and positives occurred in patients who had soft tissue infections overlying the area of interest).[265] Another study evaluating human osteomyelitis found that imaging with ^{111}In-WBC produced a 100% sensitivity for detection of acute osteomyelitis, but only 60% in chronic osteomyelitis, and the specificity was 96% overall.[266] ^{111}In-WBC imaging has also been used to identify an abdominal abscess in a horse.[267] However, radiolabeling of leukocytes is time-consuming, as a patient's leukocytes must be removed, labeled, and re-administered.[263] Additionally, while leukocyte

uptake is conceptually quite specific for inflammation, it can be difficult to differentiate inflammation from normal uptake in bone marrow.[263]

Ciprofloxacin is an antibiotic that acts by binding to the DNA gyrase of living bacteria, so ^{99m}Tc-ciprofloxacin has been used to identify foci of active bacterial infection.[268] Because of ciprofloxacin's mechanism of action, there should be pronounced uptake at sites of active infection:[268] *in vitro* and animal experiments demonstrated that ^{99m}Tc-ciprofloxacin will accumulate in abscesses caused by both Gram-positive and Gram-negative bacteria, but not in foci of sterile inflammation or abscesses without living bacteria.[269] In theory, this agent should be more specific for active infection than such agents as radiolabeled leukocytes (which can accumulate in any area of inflammation) or ^{99m}Tc-MDP or -HDP (which can detect areas of bone remodeling, but are not specific for the cause of that remodeling).[268] A prospective study comparing ^{99m}Tc-ciprofloxacin imaging to imaging with both ^{99m}Tc-MDP and ^{67}Ga found that the sensitivity (85%), specificity (92%), and accuracy (88%) of ^{99m}Tc-ciprofloxacin were similar to those of the ^{99m}Tc-MDP/^{67}Ga protocol (78%, 100%, and 90%, respectively), but ^{99m}Tc-ciprofloxacin results could be interpreted at least two days before the ^{99m}Tc-MDP/^{67}Ga protocol.[270] Another study comparing ^{99m}Tc-ciprofloxacin and ^{99m}Tc-HMPAO-labeled WBCs in patients with suspected orthopedic infections found that ^{99m}Tc-ciprofloxacin performed better, with sensitivity 94%, specificity 83%, and accuracy 89%, compared to ^{99m}Tc-WBCs (sensitivity 63%, specificity 96%, and accuracy 77%).[269] The sensitivity and specificity of ^{99m}Tc-ciprofloxacin were found to be 97% and 80% in another human study evaluating possible cases of osteomyelitis.[271] In a study evaluating use of ^{99m}Tc-ciprofloxacin in camelids and a goat, there were three true positive results and one true negative result, but there were also two false

negative cases.[268] False negative results have been attributed to poor blood supply to the lesion or concurrent antibiotic therapy.[268]

Positron emission tomography (PET) can also be used for evaluation of inflammation. The agent most commonly utilized in PET is ^{18}F-fluorodeoxyglucose (FDG), which is a glucose analog.[272] Because of its structure, the FDG enters cells via glucose transporters, where it is phosphorylated by hexokinase into phosphorylated FDG (FDG-6-P).[272] The phosphorylation step normally traps glucose within the cell, and the molecule can then proceed through glycolysis. However, FDG-6-P is not a suitable substrate for the next step in glycolysis (catalyzed by glucose phosphate isomerase), so FDG-6-P is trapped and the radioactivity of the ^{18}F remains in the cell.[272] This is important, because it means that the radioactivity that accumulates over time is proportional to the hexokinase activity, which in turn is directly related to the overall rate of glycolysis in the cell.[272] Inflammatory cells also have high metabolic rates, so regions of inflammation will exhibit increased FDG accumulation, although intensity is generally less than in neoplastic lesions, and the specificity of PET for inflammatory lesions is imperfect.[272] Positron emission tomography can also be used in imaging of foreign body responses, and revealed a rim of ^{18}F-FDG activity around one gossypiboma in the abdomen; the increased uptake was thought to be due to acute and chronic inflammation involving histiocytes and giant cells.[165]

4.4 Ultrasonography

Ultrasonography, or sonography, is the use of ultrasound (high-frequency sound) to produce images.[273] Ultrasound is a beneficial technique to use for identification and localization of foreign bodies because it can detect objects that may be radiopaque, radiolucent or

radiographically invisible, and an object can be localized with reference to specific bones, muscles, or tendons.[16,274] Because of this three-dimensional localization, ultrasound is considered more useful than fluoroscopy for foreign body localization and retrieval.[3] Additionally, ultrasound does not use ionizing radiation and can provide high spatial resolution.[16] At a frequency of 15 MHz, a high frequency commonly used in musculoskeletal imaging, the axial spatial resolution of ultrasound is approximately 10 lp/mm, though this decreases to about 3 lp/mm with use of a 5 MHz ultrasound beam.[273] Partially because of the high spatial resolution that can be achieved when evaluating superficial tissues, such as the palm of the hand, ultrasound has been shown to identify small wood fragments that may not be identified with CT.[275] Ultrasound is not as accurate at detecting foreign bodies located deep in the tissues, especially if they are located adjacent to or deep to bone or gas.[15] However, detection of relatively superficial foreign objects (5-10mm deep) in one *in vitro* study was not affected by the presence of soft tissue gas.[276] Because ultrasound is performed in real-time, even intraoperatively, the findings can easily be used to help guide removal of foreign objects, including foreign objects that may not be visualized by the surgeon, and there are multiple reports of ultrasound's usefulness in the emergency department and for surgical planning in humans and dogs.[11-14,204,277,278] False positive diagnoses can result from echogenic structures, including calcifications, ossified cartilage, scar tissue, fresh hematomas, or soft tissue emphysema, especially if there is distal artifact.[15,24] Also, the quality of the scan and diagnosis are highly dependent on the skill of the sonographer.[15,16]

4.4.1 The transducer

The most visible portion of the ultrasound imaging system is the transducer, the portion that is held in the hand and both transmits ultrasound pulses and receives ultrasound echoes.

Within the transducer is a piezoelectric element, or crystal: this crystal will deform and produce a pressure wave when a voltage is applied, and will produce a voltage when pressure is applied. Thus, application of a voltage will cause production of an ultrasound (pressure) wave, and reception of an ultrasound wave will be transduced into a voltage that depends on the amplitude of the received wave and can be further processed by the ultrasound computer. Transducers contain damping material behind the crystal to decrease the duration of a pulse and the spatial pulse length, thus improving axial spatial resolution. Because the piezoelectric element is more dense than the tissues that will be imaged, a matching layer is present on the face of the transducer; this improves ultrasound transmission from the crystal to the tissues by decreasing the impedance difference between them.[273]

Multiple different transducer configurations are available. One of the more common types is a linear array, a type of sequenced array. Linear arrays consist of a row of rectangular elements, and imaging occurs by sequentially activating groups of these elements. As this occurs, the origin of the ultrasound beam moves from one end of the transducer to the other, multiple times each second, with each end-to-end activation producing one image of the entire scan field. Linear arrays produce a rectangular scan field, while convex arrays (sequenced arrays with a curved line of elements) produce a sector image. The other primary type of transducer configuration is the phased array. This type of transducer consists of a short line of elements, many fewer than in a sequenced array. Here a voltage is applied to all of the elements rather than groups in turn, but there is a slight delay (phasing) between the voltages being applied to each individual element, causing the ultrasound beam to be steered in a certain direction. The time delays are changed with each activation, so the beam sweeps across the scan field and produces a sector image. A vector array is a hybrid of linear (sequenced) and phased array transducers.[273]

Another important consideration for a transducer is its operating frequency. Clinically, the chosen frequency may range from 2 to 15 MHz. A higher frequency allows for improved spatial resolution, but at the cost of decreased penetration. Thus, high-frequency transducers are best for superficial body parts. Conversely, a lower frequency transducer has poorer spatial resolution, but allows for better penetration of the anatomy.[273] Nearly all transducers now can operate at multiple frequencies.

4.4.2 Ultrasound data processing

4.4.2.1 *Ultrasound-tissue interactions*

Clinical ultrasonography is performed using pulsed-wave ultrasound. In this method of imaging, a pulse representing 2-3 ultrasound cycles is transmitted and followed by a time period of no ultrasound transmission. Various parameters are used to describe the characteristics of the imaging method, including pulse repetition frequency (PRF), the number of pulses transmitted per second; pulse repetition period (PRP), the time from the beginning of one pulse to the next one; pulse duration, the time over which one pulse occurs; and spatial pulse length (SPL), the physical distance from the beginning to the end of the pulse. When an ultrasound pulse is produced, the ultrasound wave travels into and interacts with the tissues. Some of the energy is absorbed and converted into heat, or attenuated, in an amount proportional to the frequency of the transducer and the path length of the ultrasound pulse. However, some of the ultrasound beam will be reflected. Reflection occurs where there are differences in impedance between two tissues: impedance is equal to a tissue's density multiplied by the propagation speed of sound in the tissue. Stronger echoes result from greater differences in acoustic impedance. When the echo

returns to the transducer, the echo can only be correctly located in the image if the direction and distance of the reflector are known. To determine the direction, the echo is assumed to originate in the same direction as the emitted ultrasound pulse was sent. Distance is determined by multiplying ½ the propagation speed in soft tissues (1.54 mm/μs) by the round-trip time of the pulse.[273]

4.4.2.2 *Pre-processing and image formation – B-mode*

Production of an image begins with the beam former. Here, the pulser first produces the electric voltage used to activate the elements in the transducer. The frequency of the voltage pulse will determine the frequency of the ultrasound pulse produced, and the amplitude of the voltage pulse determines the intensity of the ultrasound pulse. Pulse delays are entered into the system if a phased array transducer or steering of the ultrasound beam are being utilized. After this, the signal reaches the transmit/receive switch, which sends signals from the pulser to the transducer when transmission is to occur, and sends signals from the transducer to the amplifiers when echoes are being received.[273]

The beam former also functions in the first steps after receiving echoes. After the echoes' (relatively small) voltages from the transducer are transmitted to the transmit/receive switch, the signal is sent to the amplifiers which increase the voltage amplitudes to allow for additional processing. The ratio of output power to input power is referred to as gain, which is expressed in decibels (dB). While the overall gain of an image can be changed, time gain compensation can also be used to selectively increase the signal from deeper reflectors to compensate for the increased attenuation of the beam caused by increasing depth. After amplification, the echo voltages are digitized by the analog-to-digital converter and are modified by echo delay

mechanisms for electronic steering. Finally, the summer adds all of the signal voltages together to create a single scan line. Many of these lines together will ultimately produce the entire sonographic image.[273]

The signal processor receives the signal from the beam former. One operation performed here is bandpass filtering, which is used to help eliminate signal frequencies originating only from electronic noise and not returning echoes. If harmonic imaging is being used, the fundamental frequency signal is also filtered out, with only the second harmonic frequency passed. After this, the voltages are demodulated from radio frequency to a form compatible with video. Finally, the image is compressed. The ratio of the largest amplitude that a system can display to the smallest amplitude that it can detect is known as the dynamic range. While the dynamic range of the amplifiers may be 100 dB (a factor of 10 billion) or more, the dynamic range of the human eye is only about 20 dB (a factor of 100), so even if all possible amplitudes could be displayed, we would only detect a difference in a small percentage of them. Because of this, the differences between the largest and smallest amplitudes are decreased, allowing the observer to detect the full range of signals. The dynamic range can also be changed by the user – a lower dynamic range results in an image with higher contrast.[273]

The final component in creating an ultrasound image is the image processor. Within this component, the scan convertor takes the information about the direction of each scan line (generally vertical or at a diagonal) and the location of echoes within each scan line and determines the location in memory and on the display that each echo should be located. Completion of each set of determinations creates a single frame or image. At this point, before the data are stored in memory, pre-processing occurs. This step includes persistence, the averaging of multiple frames to reduce noise at the expense of frame rate; panoramic imaging,

creating a wider field of view by moving the transducer while obtaining a single "frame;" and spatial compounding, which uses phasing to interrogate structures from multiple angles per frame in order to reduce noise and artifacts.[273]

Finally, the image is stored in memory. When stored in memory, each pixel in the 2-dimensional image is assigned a value relating to the intensity of the echo that was mapped to that location. Storage allows the image to be frozen for further evaluation (freeze-frame), and also allows the user to return to recently-acquired frames for further analysis (cine-loop).[273]

There are three primary means of displaying the data acquired by an ultrasound machine; in all modes the depths of reflecting surfaces are depicted on the vertical axis. A-mode (amplitude-mode) ultrasound is the display of a single scan line. In this mode, echogenic interfaces are displayed as peaks on the line, with the height of the peak along the horizontal axis corresponding to the amplitude of the echo. This mode is used in ophthalmology for precise measurements of the structures of the eye, but is rarely used elsewhere. B-mode (brightness-mode) ultrasound is the most commonly used technique. Here, multiple scan lines (A-lines) are acquired to produce a two-dimensional gray-scale image. Within each line, the echo amplitude at each point is proportional to the brightness of the dot displayed on the screen, and both axes display distance information. M-mode (motion-mode) ultrasound is most commonly used in echocardiography. With this mode, the transducer is kept stationary and a single scan line is produced. Similar to B-mode ultrasound, the echo amplitudes are depicted on the display by dots of varying brightness, but the horizontal axis displays time, so the motion of parts can be evaluated throughout the cardiac cycle (for example).[17]

4.4.2.3 *Doppler ultrasound*

Doppler ultrasound is the real-time imaging of motion in ultrasound, usually focused on blood flow. The Doppler effect is the change of a sound's frequency and wavelength caused by motion; in ultrasound, the Doppler effect occurs due to the motion of reflectors. The most common reflectors imaged are the blood cells. If the reflector is moving toward the transducer (which is both the sound source and receiver), the wavelength of the ultrasound decreases, thus increasing the frequency. The opposite is true if the reflector is moving away from the transducer: the frequency of the ultrasound wave decreases. The Doppler shift is the change in frequency, i.e. (received frequency) – (transmitted frequency). A reflector moving toward the transducer will have a positive Doppler shift, and a reflector moving away will have a negative shift. The Doppler angle is also important, as only movement toward or away from the transducer contributes to the Doppler effect; the flow vector that is perpendicular to the ultrasound beam will not produce the Doppler effect. The Doppler angle is the angle of the motion relative to the path of the ultrasound beam, with a 0-degree angle representing flow directly toward or away from the transducer, and a 90-degree angle indicating perpendicular flow. The velocity of flow can then be calculated using the equation $v = (f_D * c)/(2\ f_0 * \cos\theta)$, where f_D is the Doppler shift, c is the speed of sound in tissue, f_0 is the source frequency, and θ is the Doppler angle.[273]

Color Doppler ultrasound uses pulse-echo imaging to evaluate the Doppler shifts that are caused by motion, generally blood flow. With color Doppler imaging, several echo pulses are produced, and when the data are received the computer can determine the average velocity of the tissues in each small sample region along the path of the ultrasound beam. The direction of the Doppler shift is used to determine the direction of flow. Based on the movement speed and

direction, the corresponding pixels are color-coded and superimposed over the grayscale B-mode ultrasound image. The direction of flow is coded as a color family (e.g. reds for movement toward the transducer and blues for motion away from the transducer), and the shade of the color indicates the magnitude of the velocity (e.g. light red for fast-moving blood and dark red for low velocities). B-mode and color Doppler imaging occur simultaneously, so velocity information relative to the grayscale anatomy is provided in real-time, though the frame rate will be decreased relative to B-mode imaging alone.[279]

Power Doppler imaging is similar to color Doppler ultrasound, except using this technique the power of the Doppler signal in each small sample volume is acquired, not the average Doppler shift. The signal power is solely related to the number of moving reflectors at that sampled point, and thus measures only the number of blood cells there, so information regarding velocity and flow direction are lost. Power Doppler is more sensitive for small signals, and is thus useful for detecting small vessels and low blood flow.[279]

4.4.2.4 *Contrast-enhanced ultrasound*

More recent advancements in ultrasound include the use of contrast agents during imaging. These substances are suspended gas microbubbles, often perfluorocarbons or sulfur hexafluoride contained within shells (frequently made of phospholipids) that are small enough to pass through capillaries.[280,281] Ultrasound contrast agents remain within the vasculature after injection, unlike CT and MRI contrast agents, which diffuse into the surrounding tissues.[282] Presence of the contrast agent will increase the echogenicity of the imaged region because the acoustic impedance of the encapsulated bubbles is different from that of the surrounding tissues (e.g. blood).[273,279,280] The echogenicity also depends on the diameter and concentration of the

microbubbles.[280] Additionally, the expansion and contraction of microbubbles during insonation are unequal, producing echoes that are harmonics of the incident ultrasound frequency. Normal tissues produce harmonic frequencies only weakly, so the contrast between the contrast agent and tissues is increased when the transducer is configured to receive harmonic frequencies (contrast harmonic imaging).[273,279] The increased echo signal from contrast material is on the order of 10-30 dB (10- to 1,000-fold).[282] The lifetime of contrast agents in the blood ranges from 2-3 minutes to 20-30 minutes;[279] the mean time is about 5 minutes.[282] Use of contrast agents is most beneficial when a lesion is similar in echogenicity to the surrounding normal tissue, or when Doppler signals are weak.[273,279] Primary uses for contrast-enhanced ultrasonography in veterinary medicine include evaluation of focal or multifocal lesions in the liver and spleen, evaluation of lymph nodes, and examination of the vascularity in the pancreas and kidneys.[282]

There are two methods of imaging ultrasound contrast agents. The nondestructive method utilizes a low mechanical index (MI < 0.5), causing the microbubbles to oscillate stably in a nonlinear fashion (i.e. producing harmonic frequencies). This is the most commonly used method for recognizing and characterizing lesions within organs. The destructive method uses a high mechanical index (MI = 1.0 or higher). This causes rupture of the microbubbles, leading to a marked production of harmonic frequencies. While the destructive method may temporarily increase tissue contrast relative to the nondestructive method, it cannot be used when following the contrast agent over time (e.g. arterial phase, venous phase, and washout).[280]

4.4.2.5 *Tissue elastography*

Elastography is a new ultrasound technique that can be used to evaluate the viscoelastic properties, or stiffness, of tissues. The information that this technique obtains is analogous to the

information obtained through palpation, such as the identification of firm masses. To evaluate the stiffness of a tissue, the stress (force) placed upon the tissue and the strain (spatial rate of deformation) of the tissue must be considered. The most commonly performed method of ultrasound elastography is strain imaging, which evaluates the displacement of the imaged tissues. With this method, a baseline image of the desired anatomy is first obtained. A small amount of external compression is then applied, and a second image is acquired. The mechanical strain can then be calculated by software that compares the two images and calculates the spatial rate of displacement of the tissues. The axial displacement can be determined more accurately than displacement along the lateral or elevational axes.[283]

Elastography is a promising technique because it will provide additional information about lesions detected with B-mode ultrasonography, and may also help in detection of lesions. For example, fibroadenomas are stiffer than surrounding glandular tissue in the human mammary gland. While these nodules may be identified in the midst of the normal tissue using B-mode ultrasound, they may be more apparent with elastography. Additionally, elastography may help identify which lesions are more likely to be malignant: benign fibroadenomas appear the same size on both conventional B-mode imaging and elastography, while malignant invasive ductal carcinoma tends to appear larger on elastography images than on B-mode imaging because of its effects on the surrounding tissues.[283]

4.4.2.6 *Post-processing*

Post-processing relates to image manipulations that are performed after the image is stored in memory, and affects only how previously-acquired data are displayed. As a general rule, if a function can be performed on a frozen image, then it is post-processing. The most commonly

performed post-processing function is assigning of certain display brightness values to echo amplitude values in memory – a change in the grayscale values on the display may improve conspicuity of lesions, but the echo amplitude values obtained by the system are unchanged. Often rather than just making all pixels more or less bright, the contrast over one set of echo intensity values may be increased (the slope made steeper) at the expense of poorer contrast over other value ranges that may not be as important (e.g. low intensity values).[273] This assigning of image brightness values to pixels based on the echo signal amplitude is the basis of B-mode (or brightness mode) ultrasound, where a two-dimensional image is formed by pixels whose brightness values are generally proportional to the amplitude of the echoes received from that location.[17]

4.4.3 Ultrasound image quality

The spatial resolution, the ability to differentiate two closely-spaced objects, is an important factor in the overall quality of an ultrasound image. Unlike other modalities, the spatial resolution in each dimension is dependent on a different factor. The axial resolution (depth resolution) is the resolution in the direction of the ultrasound beam's travel (generally vertically on the image). To achieve resolution of two objects in this direction, echoes returning from the two objects cannot overlap. For the two echoes to be distinct, the objects must be separated by the distance of at least one-half the spatial pulse length.[17] Lateral resolution is the spatial resolution in the plane of the image perpendicular to the path of the ultrasound beam. The lateral resolution is determined by the diameter of the ultrasound beam, which in turn depends on the width of the transducer elements. The diameter of the beam also depends on the distance from the transducer: the best lateral resolution is in the focal zone, at the boundary between the near

field and the far field.[17] The axial resolution is better than lateral resolution, though the two may be similar in the focal zone.[273] Elevational resolution is resolution perpendicular to the image plane, and relates to the thickness of the ultrasound beam. Spatial resolution in this dimension is determined by the height of the transducer elements. The slice thickness of an array transducer is generally its worst measure of spatial resolution, and can result in slice thickness artifacts.[17] (See Section 4.4.4: Ultrasound Artifacts.)

Choice of transducer operating frequency affects image quality, especially the axial resolution. Because axial resolution depends on the spatial pulse length (SPL), decreasing the SPL will improve spatial resolution. The spatial pulse length is directly proportional to the wavelength of the ultrasound used, so at higher frequency the spatial pulse length will be decreased.[17] However, because attenuation of the ultrasound beam (in dB) is also directly proportional to the transmit frequency, imaging depth will be decreased with a higher frequency transducer.[17,273]

Contrast resolution is the ability to differentiate small differences in echo strength between two adjacent structures. Because the dynamic range of the amplifiers is so great, receiving of echoes does not represent a limiting factor. Rather, the most important factor in contrast resolution is the number of bits assigned to the grayscale value for each pixel in image memory. With a 40 dB dynamic range display (10,000-fold difference between highest and lowest values), 4-bit (16-shade) values require an echo to be about twice as strong as another to be displayed as a different shade. However, with a 6-bit (64-shade) system only a 15% difference is needed, and with an 8-bit (256-shade) system, only a 5% difference in echo intensity is required. Likewise, reducing the dynamic range will increase the contrast and decrease the difference in intensity

required to see a difference, as low values are reassigned as 0 and the remaining values are distributed across the available grayscale.[273]

Temporal resolution describes the ability to differentiate events that are closely spaced in time, and is an important consideration in ultrasound, a real-time modality. Temporal resolution depends on the frame rate, the number of entire images made and stored per second. The higher the frame rate, the more images are stored each second, and thus the closer together two events can be and still be distinguished. Hence high frame rates are most important when imaging moving structures, such as the heart. Because an individual ultrasound pulse is required for each focus in each scan line within a frame, both focus number and line number help determine the frame rate – increasing the number of focuses or number of scan lines will improve spatial resolution while decreasing temporal resolution. Increasing the pulse repetition frequency (PRF) will also improve frame rate by increasing the number of pulses per second, but this also increases the chances of range ambiguity artifact, so increased PRF is only achievable if penetration decreases. Because of this, an increase in scan depth (penetration) will cause the ultrasound machine to decrease the PRF and thus decrease the frame rate and temporal resolution.[273]

An important characteristic of any ultrasound image is the echo pattern seen in the tissues. However, this is not a direct characteristic of the sound reflection and scattering within the tissue, nor does it represent image noise. Rather, it is known as acoustic speckle and is a function of the constructive and destructive interference of echoes as they are scattered from the tissues.[273]

4.4.4 Ultrasound artifacts

Numerous artifacts are described in ultrasonography; those which are most pertinent to imaging of foreign objects and inflammation are discussed here.

Reverberation artifact, also known as multiple reflection artifact, is the appearance of multiple strong echoes (often parallel lines) appearing on the image. This occurs when the ultrasound beam strikes a strong reflector such that much of the pulse returns to the transducer. Some of this echo is then reflected by the transducer, causing it to return to the tissues and strike the strong reflector again, with the procedure continuing until the echoes become too weak to be detected. Because the processing software interprets each successive echo as being a discrete event coming at a later time, these echoes are mapped at successively deeper points on the image, though all but the most superficial reflector are artifactual. Closely spaced discrete reverberation echoes are known as comet tail artifact; this occurs when there are two closely-spaced strong reflecting surfaces that may result in some reflections occurring between them, such as the near and far surfaces of a BB. Similar in appearance is ring-down artifact, which is seen as a continuous echogenic band without discrete echoes extending from a reflector. The occurrence of ring-down artifact is due to resonance occurring in a focus of gas bubbles.[273]

Acoustic shadowing is the reduction in the strength of echoes produced by objects that lie deep to a highly reflective or highly attenuating object. If much of the ultrasound beam is reflected or attenuated by the more superficial structure, there is little of the sound that continues deep to the structure, resulting in weak (thus dark) or no echoes from deeper objects. Mineral (including bone) is a common source of shadowing. Less commonly, shadowing is caused by curved objects that refract and effectively defocus the ultrasound beam rather than through increased attenuation or reflection.[273]

Acoustic enhancement is the opposite of shadowing. In this case, a more superficial object that minimally attenuates the ultrasound beam results in the production of stronger echoes at deeper reflective interfaces. Because more of the ultrasound beam is able to pass to the deeper tissues than normal, resultant deep echoes are higher in amplitude, and thus appear hyperechoic on the image. Fluid-filled structures, including the urinary bladder, gall bladder, and abscesses, are common causes of enhancement artifact.[273]

Slice thickness artifact is the effect of reducing a three-dimensional ultrasound beam into a two-dimensional image. While the primary two dimensions of interest make up the scan plane that is evaluated onscreen, the actual ultrasound beam does have a measurable thickness perpendicular to the scan plane. Because the beam is collapsed into two dimensions for viewing, echoes seen at a given position on the screen could have come from the center of the thickness, as we assume, or from the margin of the beam. Thus, while the center of the beam may be projected through anechoic urine in the bladder, for example, the edge of the beam may be reflected by the bladder wall and these echoes will be mapped to the periphery of the bladder lumen, appearing as echogenic debris within the bladder.[273] A similar appearance could occur at the edge of any collection of fluid, including an abscess.

4.4.5 Ultrasound imaging parameters specific to foreign bodies

Most musculoskeletal foreign bodies are small, so a high-frequency linear transducer is required to maximize spatial resolution,[15,284] and the best spatial resolution is in the near field.[3] When using a 15 MHz ultrasound beam, axial resolution may be as good as 0.10 mm, though lateral spatial resolution is not as good.[273] Because many foreign bodies are found in the most superficial soft tissues, a standoff pad may be necessary for better visualization of the affected

tissues.[14] Tissue harmonic imaging can also improve spatial resolution and contrast resolution while decreasing noise and side-lobe artifacts.[284]

4.4.6 Appearance of inflammation & foreign bodies

Structures imaged with ultrasound are described by the intensity of echoes that are received from the object. Structures that are bright on the image are considered hyperechoic, or echogenic, while dark structures are hypoechoic.

All foreign bodies in the soft tissues are echogenic, regardless of their composition.[8,15] However, the intensity of the echoes is proportional to the difference between the acoustic impedance of the object and the acoustic impedance of the surrounding tissues.[15] Artifacts may occur deep to foreign bodies, and these artifacts are predominantly a function of the surface characteristics of a foreign object rather than its composition.[15] Smooth, flat surfaces or objects with a large radius of curvature (e.g. glass and metal) cause reverberation artifact or "dirty shadowing," and irregular surfaces or curved surfaces with a small radius (e.g. wood fragments) cause "clean shadowing."[8,15,285] Nonetheless, rules regarding distal acoustic shadowing are not constant, as surfaces that are not perpendicular to the ultrasound beam may not produce an artifact, and some objects may produce both distal acoustic shadowing and reverberation artifact.[15] Small objects may not produce any distal artifact.[201]

In one study of 17 dogs with grass awns or wooden foreign bodies, the object was visualized in 82% of the cases.[274] Wooden foreign bodies appear as structures with a linear hyperechoic interface and marked uniform distal acoustic shadowing.[8,24,25,124,174,274,286] If the wooden structure is large enough, only the echogenic near edge will be identified, as the distal surface will be obscured by the acoustic shadowing.[124] The echogenic interface has been

described as only moderately intense compared to other foreign objects, such as glass and stone.[9,286] The sonographic characteristics are most notable when the foreign object is perpendicular to the ultrasound beam,[24] although some note that an obliquely oriented wooden foreign object does not change the degree of distal acoustic shadowing seen.[8] Occasionally a distal acoustic shadow is not identified extending from a wooden foreign object.[274] Grass awns are described as tapering spindle-shaped or cigar-shaped structures with two or three parallel hyperechoic interfaces, representing the seeds and seed covers.[120,274] A feathered end may also be seen on grass awns.[274] Distal acoustic shadowing is only identified in approximately one-quarter to one-half of cases with grass awns; the low frequency of shadowing could be because of the small size of grass awns, or may be associated with the density of the structures.[120,274] Chronicity may influence the sonographic appearance of foreign objects made of plant matter. Acute wooden foreign bodies are echogenic and likely to produce a shadow, but over time they absorb fluids and are enzymatically degraded. This may decrease the differences in acoustic impedance and density between the foreign object and the surrounding tissues and thus decrease the object's echogenicity and likelihood of shadowing.[8,24,274] Porcupine quills are similar in appearance to plant matter foreign objects, and are described as a pair of parallel echogenic lines that taper to a point; no distal acoustic shadowing or reverberation artifacts are described when imaging porcupine quills.[238]

Glass fragments have been described as markedly hyperechoic objects with smooth surfaces and either distal shadowing or reverberation artifact (or comet tail artifact).[8,9,286,287] Small metallic objects such as sewing needles may be difficult to recognize, but are visualized as a small echogenic structure with distal acoustic shadowing.[8] Larger metal foreign bodies, including BBs, nails, and wire, tend to have a smooth strongly echogenic surface and produce

distal reverberation or a comet tail artifact.[8,286] However, in one case report, a deformed bullet with an associated tissue capsule was described as echogenic and produced a distal acoustic shadow.[154] Stones and gravel have a rough, markedly echogenic surface and cause distal acoustic shadowing and possible slight reverberation artifact.[8,9,286] Asphalt is also strongly echogenic and uneven and produces a distal acoustic shadow.[9] Amalgam has a uniform echogenic surface and causes a reverberation artifact.[9] Plastic has been described as less echogenic than other foreign objects, but is still associated with pronounced distal acoustic shadowing.[8,287] Teeth have a moderately reflecting uneven surface and produce a distal acoustic shadow.[9] Graphite has moderate surface echogenicity and moderate distal acoustic shadowing.[286]

While the sonographic appearances of most foreign bodies are similar, some differentiation is possible: metal and glass often produce a comet tail artifact, while gravel, wood, and plastic produce distal acoustic shadowing.[288] However, classification of foreign bodies is limited in a prospective blinded situation, as would be expected in the clinic. In one study, glass and metal were commonly mistaken for each other, as both produced shadowing, reverberation, and a ring-down artifact, though bone was more accurately characterized than either of those two substances as it produced only strong distal acoustic shadowing.[276] When gas was present in the soft tissues, characterization suffered, as all three types of foreign bodies were confused for each other more commonly.[276] It would also be expected that use of other foreign objects (such as wood) would have decreased the accuracy of identification, as wooden and bone foreign bodies would have very similar imaging characteristics and more choices of foreign material would have led to decreased certainty of identification.

A foreign object that is present in the body for at least 24 hours will provoke sufficient inflammatory response to visualize sonographically: this reaction is seen as a hypoechoic rim

surrounding the object, effectively increasing the contrast between the echogenic object and the tissues.[15,24] The affected tissue surrounding a foreign body may also be enlarged or thickened and poorly marginated, and may have complex echogenicity and architecture.[174,193,289] For example, anechoic regions or reticulations representing edema or seroma fluid may be seen in the midst of hyperechoic granulation tissue.[174] Inflamed or edematous musculature is described as hypoechoic without normal striations.[193] Cellulitis is represented by thickened edematous tissues, and has been described as having a marbled appearance with fusiform anechoic or hypoechoic foci throughout a hyperechoic background, or alternating bands of increased and decreased echogenicity.[290,291] A phlegmon is similar, though may also include collections of anechoic fluid within the tissues.[291] Fluid within the tissues around a foreign object may be uniformly anechoic or may have areas of increased echogenicity with focal strong echoes; structures with increased echogenicity could represent fibrinous material, cellular debris, hemorrhage, or air.[274] A hypoechoic collection of fluid is also consistent with an abscess.[249] If a fistulous tract or migration path is present, this may be seen as a tortuous linear or tubular echogenic or hypoechoic path that may be traceable directly to the foreign object.[174,201,274] Using Doppler ultrasound, regions of inflammation will be demonstrated as areas with increased blood flow; Power Doppler is more sensitive for this finding due to its increased sensitivity for the low flow rates that occur in soft tissue inflammation.[292] Regional lymph node enlargement may also be present.[120] Periosteal new bone formation or osseous defects may also be identified with ultrasound.[174] If the foreign object migrates within the abdomen, the mesentery and omentum may appear coarsely textured, heterogeneous, and hyperechoic, indicating peritonitis, and anechoic or echogenic peritoneal effusion may also be present.[174,293] Intrathoracic migration of foreign objects may cause pleural effusion or lung lobe consolidation;[196,197] echogenic septations

may also be seen within the fluid.[197] A migrating intrathoracic grass awn was detected in 4 of 8 animals evaluated with ultrasound.[196]

A granuloma caused by a retained surgical sponge will be identified as a discrete mass, and may be well circumscribed with complex architecture.[156] Gossypibomas may have a hypoechoic outer layer (correlating with a thick fibrous capsule) and a hyperechoic inner layer (suspected to represent the sponge itself, as well as trapped gas) when compared to the echogenicity of the mesenteric fat.[156,158] A hypoechoic center may also be identified within the mass.[156] However, another granuloma caused by retained surgical sponges has been described as homogeneous and intermediate in echogenicity.[156] Marked homogeneous distal acoustic shadowing may also be associated with the gossypiboma; this has been postulated to be due to considerable absorption of the ultrasound beam, as there was no evidence of beam reflection in the image.[156] It may not be possible to differentiate a granuloma from an abscess using ultrasound, though one might expect an abscess to have a central hypoechoic to anechoic region, possibly with focal mobile echoes, and associated distal acoustic enhancement.[156] Signs of peritonitis, including echogenic peritoneal effusion and small intestinal corrugation, can also be seen with intra-abdominal gossypibomas.[158]

4.4.7 Appearance of an abscess

Soft-tissue abscesses are well-defined collections of hypoechoic or anechoic fluid, appearing as cavitated masses. A hyperechoic capsule may be seen around the abscess as it becomes more chronic; the internal portion of the capsule can be irregular. The fluid portion of the abscess may contain echogenic debris, and small hyperechoic foci producing a reverberation artifact are consistent with gas formation. Septae can also be seen within the abscess. The

appearance of an abscess is not specific, and can appear the same as a seroma, hematoma, or necrotic neoplasm.[290,291,294] Increased blood flow around the periphery of an abscess can be detected with power Doppler imaging.[294]

4.4.8 Appearance of an evolving hematoma

The appearance of a hematoma depends on its age. When a hematoma first forms, it appears as a homogeneous cavity filled with echogenic fluid. The fluid will generally be as echogenic as a soft tissue mass, but the echoes will not be stationary in an early hematoma. As the hematoma reaches a subacute phase, hyperechoic blood clots will organize and retract and will be surrounded by anechoic fluid. Chronically, a hyperechoic fibrous capsule forms around the hematoma, and the anechoic fluid will ultimately be resorbed. Some hematomas will also exhibit mineralization, which can be recognized as hyperechoic shadowing foci.[290]

4.5 Magnetic Resonance Imaging

Magnetic resonance imaging (MR imaging, or MRI) is the use of a magnetic field to cause alignment of protons within the body and a radiofrequency signal to produce a signal from the tissues. Planar images, or slices, are obtained with MRI, so superimposition of structures is not a limiting factor. Additionally, images can be acquired in any plane without the need for reformatting or repositioning of the patient. MRI produces the best soft tissue contrast resolution of any imaging modality.[16] However, it is not ideal when searching for metallic foreign bodies due to the prominent artifacts that are produced and the possibility of inducing movement and heating of the object.[16] MRI also has relatively poor spatial resolution, about 1mm, though this can be improved at higher magnetic field strengths.[17] Other disadvantages of MRI include high

cost, more limited availability than most other modalities, and the possibility of interference with other medical devices, such as pacemakers.[16] When searching for low-intensity foreign bodies, a false positive diagnosis may be made when there is scar tissue, calcification, or even tendons.[16] Anesthesia is also required in veterinary medicine due to the relatively long imaging times.

4.5.1 MR components and instrumentation

There is a wide variety in the specifications of current MRI systems. However, all systems are composed of four chief components: the magnet, the gradient coils, the radiofrequency system, and the computer.

For use in MR imaging, the field produced by the magnet must be homogeneous and of consistent amplitude – unchanging over time and space. The strength of a magnetic field is measured in Gauss (G) or Tesla (T) units, with 1T equal to 10,000G. Diagnostic MRI may commonly use field strengths of 0.2 to 1.5T, though higher field strengths such as 3T are becoming more available. (As a reference point, Earth's average magnetic field strength at the surface is 0.5G, or 0.00005T.) The three classes of magnets used in MRI are superconducting magnets, resistive magnets, and permanent magnets. *Superconducting magnets* are based on metals and alloys (such as the commonly-used niobium/titanium alloy) that lose their electrical resistance at low temperatures. Once a superconductor has been energized, current will continue in a loop as long as the superconducting wire is kept below the critical temperature. Thus the advantage of this system is that the constant current will produce a constant magnetic field without need for a power supply, and all systems greater than 0.3T are based on superconducting magnets. The disadvantage is the need for extreme cooling – the niobium/titanium alloy is superconducting at temperatures of 10 Kelvin (K) or less, so liquid nitrogen is used to keep the

magnet at 4K. *Resistive magnets* are electromagnets: the magnetic field is produced by an electric current passing through a wire with numerous turns. Because all wires have resistance to flow of electrons, high power is required to supply the current to the wire, and the current source must be very stable. The heat produced by the resistance must then be removed via running water. Because the power required increases as the square of the current, and the current is proportional to magnetic field strength, resistive magnets cannot be used when high magnetic field strengths are required. Additionally, field homogeneity is poorer than in superconducting magnets. *Permanent magnets* are ferromagnetic materials (e.g. iron, cobalt, nickel, rare earth elements) that are magnetized by an external source and remain magnetized after the removal of that source. However, the magnetic field strength is limited by the saturation field strength of these materials and the divergence of the magnetic field lines in air. The primary advantages of permanent magnets are their low operating costs and the ability to produce open configurations that help decrease feelings of claustrophobia in human patients, but the signal-to-noise ratio is low and field homogeneity is poorer than other types of magnets.[295,296]

The gradient system is composed of three sets of coils. These coils are rapidly switched on and off during a scan and are used for slice selection, phase encoding, and frequency encoding to provide information regarding the location of signals within the patient. Magnetic field gradients are created by these coils along all three axes within the magnet bore. The steepness of the field gradient created (change in magnetic field per unit distance) will determine the slice thickness and the minimum field of view sampled. It is important that the coils produce linear gradients across their length or the image will be distorted. Gradients must also be turned on and off rapidly, with short rise and fall times.[295]

The radiofrequency (RF) system is the portion of the MRI system that generates and receives the MR signals. In order to produce an MR signal, the RF coil forces protons in the main magnetic field to precess by rotating them out of alignment with the primary magnetic field by using a pulsed magnetic field of the correct frequency and amplitude. This magnetic precession then induces a voltage in a receive coil, representing reception of the signal. The transmitter's RF output is hundreds of volts (V), but the input from a single voxel may only be 0.1 μV. A variety of RF coils exist for different uses. Because image noise increases with coil size, and signal decreases with increasing distance from the coil to the anatomy, a snug fit over the part being imaged is essential.[295]

The computer is responsible for all of the commands and controls required in imaging. Functions of the computer in data acquisition include selecting the volume of interest, timing the RF pulses, and turning magnetic gradients on and off. Additionally, while some data are being acquired, other data are being processed into images. Other functions of the computer relate to workflow, including the setup of the study at the operator console and the sending of the images to a Picture Archiving and Communication System (PACS) for storage and later retrieval.[295]

4.5.2 Physics of magnetization

The atomic nucleus is composed of protons and neutrons, and those nuclei with either odd numbers of protons or neutrons (but not both) have spin-angular momentum. These nuclei also possess a magnetic field which is described by the magnetic moment, μ. Under normal circumstances, the magnetic nuclei are randomly oriented. However, when exposed to an external magnetic field (B_0), the magnetic dipoles align with that field. Two possible states of hydrogen nucleus alignment exist: parallel and antiparallel. Because the parallel alignment is a

lower energy state, more of the nuclei will be in this orientation, with the direction of the magnetic field (though the fractional excess in a 1.5T magnetic field is only about 10^{-5}). Alignment of each individual dipole with the external field is not perfect (as dictated by quantum mechanics); there is a transverse component to the magnetic moment. Because of this, each individual dipole experiences a torque from the external magnetic field, and the dipole precesses (or "wobbles") about the B_0 vector at a frequency (the Larmor frequency) determined by the element's gyromagnetic ratio and the strength of B_0. However, because the phase of precession of the hydrogen nucleus is random. Therefore, when the magnetization is considered in aggregate the transverse components cancel out and the parallel magnetization vectors outnumber the antiparallel ones, so the net magnetization, M, is perfectly aligned with B_0. This alignment is referred to as the equilibrium magnetization, M_0.[17,297]

Resonance is the production of transitions between different energy states (e.g. from parallel to antiparallel for the hydrogen nuclei). The energy required to produce this change is equal to the energy difference between the two states, and the energy is applied at the Larmor frequency. As individual magnetic moments are flipped to the higher energy (antiparallel) state, the net longitudinal magnetization is reduced to zero.[297]

Detection of a magnetic resonance signal requires production of a transverse magnetization vector to induce a voltage in a receive coil. Because the longitudinal magnetization (in the direction of B_0) is static, it will not induce a voltage. To create transverse magnetization, an RF field (B_1) is applied perpendicular to the primary magnetic field (B_0); B_1 must also rotate in synchrony with the precession of the nuclei (i.e. at the Larmor frequency) to bring the procession of all the nuclei into phase (phase coherence). In other words, the previously random transverse components of the magnetic moments will be oriented in the same direction. Additionally, the

energy provided by the RF signal causes resonance: the number of antiparallel protons is increased, so the M_z vector is decreased. If the net magnetization vector is allowed to rotate 90 degrees (a 90-degree flip angle), the entire vector will be transversely oriented (M_{xy}) and there will be no component of longitudinal magnetization (M_z). (When discussing movement of the net magnetization vector, a rotating frame of reference is often used for simplicity. Using this frame of reference, the x- and y-axes rotate about B_0 synchronously with B_1, and the net magnetization vector arcs from the z-axis to the x-y plane. In a static frame of reference, the net magnetization vector would spiral from the z-axis to the x-y plane.)[17,297]

After the desired transverse magnetization vector is achieved, the RF pulse is turned off. The magnetization vector (M) then precesses around B_0 at the Larmor frequency. This precession can be detected as a voltage that varies over time (cycling between positive and negative values) and exhibits exponential decay based on the T2 time constant. This induced voltage is called free-induction decay (FID). Decay of the transverse magnetization vector occurs because the individual magnetic moments dephase as they interact with each other and as the local magnetic field varies, changing the precessional frequency. This process is called spin-spin relaxation, or T2 relaxation. (It is important to note that the FID decays quicker than would be expected from only the effects of T2 relaxation. The decay is actually related to T2*, in which magnetic field inhomogeneity also plays a role.) The T2 relaxation time is defined as the time at which the transverse magnetization is equal to 37% of its original value. The T2 relaxation time differs among tissues and describes the rate at which the transverse magnetization vector decreases. Free water has a relatively long T2 relaxation time because rapid free motion reduces field differences, so the transverse magnetization in free water remains large for a long period of time.[17,297]

As previously mentioned, the nuclei absorb energy when the RF pulse is applied, causing them to shift to the excited antiparallel state. To return to the parallel orientation (the ground state), the nuclei must release their excess energy to the surrounding tissue, the lattice. As this energy is transferred, called spin-lattice relaxation or T1 relaxation, the longitudinal component of the magnetization vector returns to its equilibrium value. The T1 relaxation time is defined as the amount of time required for recovery of 63% of the longitudinal magnetization. The rate of regrowth of the longitudinal magnetization depends on the molecules surrounding the hydrogen nuclei. For example, spin-lattice relaxation in fat is rapid as compared to relaxation in water, thus the longitudinal magnetization returns quickly in fat. The strength of the magnetic field also affects the T1 relaxation time.[17,297]

Several important factors can be changed to affect the appearance of the acquired image in MRI. The repetition time (TR) is the time between RF excitation pulses. A long TR allows for more T1 relaxation to occur. The echo time (TE) is the time from the center of the RF pulse to the center of the echo produced in spin-echo imaging. In spin-echo imaging, a 180-degree RF pulse is applied after the normal 90-degree excitation pulse; this serves to reestablish phase coherence, allowing for determination of the T2 relaxation time independent of T2* effects. The 180-degree pulse occurs halfway between the excitation pulse and the echo time. As TE is increased, transverse magnetization decreases; thus, adjusting TE will affect the contrast between tissues with different T2 relaxation times.[17,297]

The contrast weighting of spin echo sequences can be varied by changing the variables mentioned above. The contrast in a T1-weighted sequence emphasizes the T1 relaxation of tissues while diminishing the T2 effects. This is done by using a short TR to maximize differences in longitudinal magnetization and a short TE to minimize differences in transverse

magnetization (i.e. minimal dephasing has occurred). Conversely, the contrast in a T2-weighted sequence emphasizes the T2 relaxation of tissues while diminishing the T1 relaxation. T2-weighted sequences use a long TR to minimize differences in longitudinal magnetization (regrowth is nearly complete in all tissues) and a long TE to maximize the differences in dephasing. Proton density weighted images, based on the number of magnetized protons in the tissue, minimize the effects of T1 and T2 relaxation by using a long TR and short TE, respectively. This results in a good signal-to-noise ratio, but relatively low contrast resolution.[17]

4.5.3 MR data processing

4.5.3.1 *Pre-processing and image formation – spin echo and gradient echo sequences*

The most commonly used pulse sequences in MRI are spin echo sequences. In these sequences, there is an initial RF excitation pulse which is often a 90-degree pulse, though can be less than that. At ½ TE a 180-degree refocusing RF pulse is produced, and the echo is received at TE. At TR, another excitation pulse is produced and a new sequence begins. The times chosen for TE and TR depend on the magnet and the desired contrast weighting as discussed above. Additionally, T2- and proton density weighted images are often obtained simultaneously by producing two different echoes for each TR through use of both a short and long TE.[17]

Inversion recovery sequences are spin echo sequences that are used to null the signal from certain tissues. In these sequences, the initial RF pulse is a 180-degree excitation pulse which inverts the M_0 longitudinal magnetization vector to a $-M_0$ vector. After the time of inversion (TI), a 90-degree RF pulse is used to rotate the recovered longitudinal vector into the transverse plane. At time ½ TE after the 90-degree pulse, a 180-degree refocusing pulse is produced, and

the echo is received at time TE. Because the longitudinal magnetization vector must pass through 0 (the bounce point or tissue null) during regrowth, knowledge of this time for different tissues can be used to eliminate MR signal from those tissues. For example, in Short Tau Inversion Recovery (STIR), the TI is chosen as the time when fat is at the tissue null. Thus, when the 90-degree RF pulse occurs, fat has no longitudinal magnetization vector to convert into a transverse vector, and thus fat produces no signal. Fluid-Attenuated Inversion Recovery (FLAIR) is similar, with TI chosen as the bounce point of water and CSF to reduce the signal from free water.[17]

Gradient (recalled) echo (GE or GRE) pulse sequences are similar to spin echo sequences. However, instead of the 180-degree refocusing RF pulse, the frequency encoding gradient (readout gradient – see below) is initially reversed then returned to normal. This switching of the frequency encoding gradient produces the MR echo. A second phase encoding gradient pulse of opposite polarity (a rewinder pulse) is then required to keep phase relationships constant. The advantage of using a GRE sequence is the fast imaging time: flip angles are generally small and TR and TE can be reduced. However, disadvantages include decreased signal-to-noise ratio and increased magnetic susceptibility artifacts (though this latter point can be used advantageously in cases of suspected hemorrhage: see Section 4.5.9: Appearance of an Evolving Hematoma).[17]

MR images are displayed as two-dimensional planes made up of multiple picture elements, or pixels; most MR images use a matrix of 256x256 pixels. Each of these pixels corresponds to a three-dimensional rectangular space (a voxel) in the patient. The intensity of a pixel in the image is based on the strength of the signal produced in the corresponding voxel in the patient. However, unlike computed tomography, there is no standardized scale for intensities in MRI.[297]

Echo sequences alone are not sufficient to produce the spatial information needed to generate MR images. Precise spatial information in MRI is produced by use of magnetic field

gradients. While the primary magnetic field (B_0) is uniform, magnetic gradient coils are used to produce slight variations in the overall magnetic field. The magnetic field produced by these coils varies linearly in strength over a defined distance. As this field is summed on B_0, the result is a slight decrease in magnetic field strength of B_0 at one end of the gradient and a slight increase at the other end. This causes alterations in the precessional frequency of protons based on their location along the gradient (a higher magnetic field produces a higher precessional frequency). Similar gradients are produced in all three dimensions.[17]

The slice select gradient is used to determine which slice in the body is imaged, as RF pulses themselves cannot be spatially directed. For transverse images, this gradient is applied from cranial to caudal. The precise precessional frequency of a proton is thus based on the location of the proton along the z-axis. When a narrow band RF pulse is applied to the entire volume of tissue in the RF coil, only protons with a precessional frequency equal to the frequency of the RF pulse will absorb energy, and thus a slice is selected. The slice thickness is determined by the bandwidth of the RF pulse (a narrow bandwidth produces a thin slice) and the strength of the gradient (an increased gradient strength produces a wider range of frequencies and thinner slices).[17]

The phase encode gradient is the second gradient applied to the volume and is applied perpendicular to the slice select gradient. When the slice select gradient is applied, the proton spins are all in phase. While the phase encode gradient is turned on, the precessional frequency of the excited protons within the slice varies along the gradient. The precessional frequency returns to the Larmor frequency when the gradient is turned off, but the phase of each nucleus has been shifted by an amount proportional to its location across the gradient. A different phase encode gradient strength is applied to the volume over 256 successive TR intervals in a 256x256

image, and Fourier transformation is required to determine the spatial position of a proton based on its phase characteristics after all of the image data are obtained. Because there are numerous incremental changes in the phase encode gradient during image acquisition, positional changes caused by motion will result in phase changes and thus the appearance of ghost anatomic structures in the phase encode direction.[17]

The frequency encode gradient, or readout gradient, is the third gradient applied and is applied perpendicular to the direction of the other two gradients. It is applied at the time that the echo signal is produced. While the gradient is applied, the processional frequency of a proton is determined by the location of the proton along the gradient. The Fourier transform can then be used to convert the frequencies into the proton positions within the line. Hence, by applying gradients in three dimensions, the three-dimensional location of each signal can be determined.[17]

When MR data are acquired, they are stored in k-space in the frequency domain (i.e. as sine and cosine waves). K-space encodes information about the intensity of edges in the image, not the spatial location of structures. Data encoded in the center of k-space represent low-frequency data, or coarse structures. Conversely, data toward the edges are high-frequency structures, correlating with fine detail. Using only the low-frequency data produces a blurry image. However, the low-frequency information does incorporate most of the overall anatomy in the image. Inverse Fourier transformation is used to convert the k-space data into data in the spatial domain, thus reconstructing the image itself.[297]

4.5.3.2 *Other MR imaging techniques*

Diffusion weighted imaging (DWI) is used to differentiate regions of rapid proton diffusion from those with restricted diffusion. In this technique, two equal gradient pulses are applied; if

the imaged nuclei do not move between the two pulses, the first pulse will dephase them and the second will bring them back into phase. Lack of motion indicates that diffusion is restricted, as may occur in acute stroke, and the signal intensity will be increased. Protons that are free to move will not be influenced by both gradients, so signal intensity in these regions will be low.[298,299] However, because DWI images are somewhat T2-weighted, areas of high T2 signal intensity will also appear hyperintense on a DWI image (T2 shine-through). Because of this, apparent diffusion coefficient (ADC) maps are also produced. With this technique, two sets of images are obtained: one with the diffusion gradient, and one without (the latter will look much like a T2-weighted image). The ADC calculation is a function of the negative logarithm of the ratio between the two image acquisitions. Areas of restricted diffusion are hypointense on ADC images, the reverse of the DWI images.[299]

A problem with DWI and ADC imaging is the inherent assumption that diffusion is free to occur in any direction. However, this is not true in the brain, as the orientation of axonal fibers will dictate the amount of diffusion allowed in different directions. Diffusion that differs in degree with direction is referred to as anisotropic. While ADC imaging along the three axes of the scanner can be performed (requiring 1 image for each of the three axes and 1 control image), these axes do not necessarily correlate to the orientation of the white matter tracts in the brain, so determination of diffusion remains imperfect. To more accurately evaluate diffusion in the brain, diffusion tensor imaging can be performed. This requires a total of seven images to be obtained and post-processed to produce six scalar diffusion elements, and provides the ADC value and the direction of diffusion for each pixel individually.[298,300,301]

Magnetic resonance spectroscopy is a noninvasive method used to measure chemicals in the body. Atoms that can be evaluated with MR spectroscopy include ^{1}H, ^{13}C, and ^{31}P.[302]

Because the local magnetic field influencing each individual nucleus is affected by the electrons in that atom as well as the electrons in the other atoms composing a molecule, each nucleus undergoes a chemical shift and resonates at a distinct frequency based on the composition of its molecule.[303] When a nuclear magnetic resonance spectrum from a specified voxel is produced, these different resonance frequencies are displayed as independent peaks, and the identity of the chemicals present can be determined by the degree of chemical shift given in parts per million (ppm).[303] Thus, MR spectroscopy can be used to identify resonance peaks that are not present in normal tissue or may indicate specific pathology such as neoplasia or infection.[304]

Perfusion MR studies can be performed to characterize blood flow to the brain. Generally these studies are performed with exogenous contrast agents, such as gadolinium, though endogenous techniques are also used. For exogenous perfusion mapping, T2*-weighed images are acquired. Because the paramagnetic properties of gadolinium increase local field inhomogeneities, it will cause rapid dephasing of spins and thus signal loss that will extend outside of the vessels containing the contrast agent, with effects seen as much as a centimeter away from the contrast agent itself. Thus, normally perfused areas will exhibit signal loss due to the presence of gadolinium, and there will be no signal loss or decreased signal loss in ischemic regions. Survey MR images are acquired first, then dynamic T2*-weighted images are obtained immediately after contrast medium administration, during the first pass of blood through the brain. Signal intensity (SI) change of each pixel can then be determined by comparing the pre- and post-contrast images. The change will be high in areas of normal perfusion (low signal on post-contrast images) and the change will be low where there is no perfusion, as there is minimal gadolinium and signal loss in those areas. Because the signal intensity on maps of SI change is

proportional to the signal change, poor perfusion is indicated by areas of low signal intensity.[305,306]

Endogenous evaluation of perfusion also utilizes T2*-weighted sequences to detect differences in blood oxygenation. Differences in brain activity that change blood flow to a region will cause a change in the relative oxygenation of that region, and because deoxyhemoglobin is considerably more paramagnetic than oxyhemoglobin, this will also cause a change in the magnetic susceptibility effects there. Hence, dynamic T2*-weighted sequences can be used to detect changes in perfusion via changes in magnetic susceptibility. This imaging technique is known as blood oxygenation level-dependent (BOLD) imaging.[306] When stimuli are provided to a subject, neural activity in different regions of the brain will change. Where neurons are activated, blood flow increases, and this can be detected using BOLD imaging techniques. The map provided by these images can be used to demonstrate the locations in the brain responsible for various tasks: this is the basis of functional MRI.[307]

4.5.3.3 *Post-processing*

Post-processing in magnetic resonance imaging is relatively limited. The primary means of post-processing is by means of window width and level adjustment. Changing the window width alters the contrast of the image: a narrower window displays a smaller number of intensity levels across the available grayscale, increasing the contrast. Changing the window level changes the brightness of the image by determining which intensity value is displayed as the medium gray value.[305]

Multiplanar and three-dimensional reconstructions are uncommonly performed in MRI. Generally to keep the signal-to-noise ratio at an acceptable level, the slice thickness is large

enough that the spatial resolution in the third dimension on reconstructed images is poor. Additionally, an interslice gap to prevent signal crosstalk is also present in most sequences, further degrading spatial resolution in the slice thickness dimension.[308] Specific acquisitions using thin slices can be made with the intent of later performing reconstructions. However, because initial acquisitions can be made in any plane, this is often of limited value. Nonetheless, three-dimensional gradient echo sequences can be used to obtain thin contiguous slices, and use of oblique or curved multiplanar reconstructions may be beneficial in evaluating curved or oblique linear structures such as tendons and ligaments, though the acquisition of thin slices will decrease the signal-to-noise ratio.[309]

4.5.4 MR image quality

A pixel, short for picture element, is a two-dimensional square in any digital image, and represents the smallest elemental unit of that image. In MRI, each pixel corresponds to a voxel (volume element) in the patient. A voxel is a three-dimensional structure, with the dimensions in the scan plane equal to those of the corresponding pixel, but also including thickness equal to the slice thickness used in the study. In the MR display, each pixel is assigned an intensity value which represents the average signal intensity of all the tissues located within the corresponding voxel. Because a pixel (or voxel) cannot be subdivided, two objects within the same pixel (or voxel) cannot be resolved; thus, pixel size is a determinant of spatial resolution. Smaller pixels increase the likelihood that two objects are not within the same pixel, increasing spatial resolution. To change pixel size (size of the voxel in the x-y plane), one must change either the field of view or the matrix (matrix size). The field of view represents the actual size of the area being imaged. Hence, if a smaller area is imaged with the same number of pixels, each pixel will

be smaller. The matrix size is the number of points (pixels) used in forming the image. Thus, if the matrix size is increased (e.g. from 128x128 to 256x256) while field of view remains constant, each pixel will again be smaller. The only way to change the thickness of the voxel is to change the slice thickness.[17,252]

It is also important to note that relatively large slice thicknesses are not the only factor degrading spatial resolution in the slice thickness dimension. Slice thickness is determined by RF pulse bandwidth during the slice select gradient application. However, the pulse is not precise, so some frequencies above and below the desired range of frequencies will also be included in the RF pulse. Because of this, protons outside the intended slice will also respond to the pulse. The undesired signal that they produce is called slice crosstalk, and serves only to increase the noise in the image. To help prevent this, a gap (interslice gap) is usually left between slices.[252,308]

Another parameter that can be adjusted in MRI is signal averaging (number of averages), also referred to as the number of excitations (NEX). When multiple excitations are used, data are acquired from the same volume multiple times using identical pulse sequences. These data sets are then averaged together to produce the final data set. Increasing the number of excitations increases the acquisition time in a linear fashion while improving the signal-to-noise ratio (SNR) in direct proportion to the square root of NEX. Thus quadrupling the NEX from 1 to 4 will quadruple the acquisition time, and the SNR will only be doubled ($\sqrt{4} = 2$).[17]

Spatial resolution in MRI is important, and can be affected by several factors. Ultimately, spatial resolution is determined by voxel size: smaller voxels allow improved spatial resolution. The voxel size in the image plane (the pixel size) is determined by the field of view and the matrix size, as discussed above. Decreasing the field of view or increasing the matrix size will decrease the size of the pixels, improving spatial resolution. The voxel dimension in the z-axis

(the slice thickness) is determined by the sampling bandwidth, as a narrow bandwidth will excite only a thin slice of tissue when the slice select gradient is activated.[17]

While contrast resolution, especially in the soft tissues, is an advantage of MRI over other imaging modalities, contrast resolution is limited by image noise. Noise is produced by random fluctuations in signal intensity produced in the tissues; increased noise will decrease the visibility of structures with low inherent contrast. To improve the contrast, the signal-to-noise ratio must be improved. To improve the signal-to-noise ratio, one could use larger voxel sizes, as more signal will be produced in a large voxel than in a small one. Increased voxel size can be achieved with decreased matrix size, increased field of view, or increased slice thickness, as discussed above. Increasing the number of excitations will also improve signal-to-noise ratio and thus image contrast. A longer TR interval will improve SNR by allowing for more growth of the longitudinal magnetization, but images will have less T1 weighting. Likewise, a shorter TE interval will improve SNR by minimizing the decrease in the transverse magnetization, but images will have less T2 weighting. Increasing the magnetic field strength will also improve the SNR by at least the factor representing the increase in field strength. However, higher magnetic field strength causes lengthening of T1 relaxation, which actually decreases T1 contrast sensitivity. Thus it can be seen that improving contrast resolution always comes with compromises. Spatial resolution is sacrificed with some improvements in contrast resolution (e.g. increased voxel size), while increased scan time is the result of other changes (increased NEX, increased TR).[17,252]

The use of a surface RF coil is one factor that will improve both spatial resolution and SNR (contrast resolution). These coils are close to the part of interest, so the volume imaged is decreased, improving spatial resolution. The SNR is improved because the amount of noise

produced is a factor of the amount of tissue within the coil – a small amount of tissue means the amount of noise is decreased. The disadvantages of using surface coils are the relatively small field of view available and the increased difficulty in positioning these coils correctly.[252]

4.5.5 MR artifacts

Numerous artifacts are described in magnetic resonance imaging; those which are most pertinent to imaging of foreign objects and inflammation are discussed here.

Partial volume averaging occurs because the signal in an image originates from a voxel of finite volume, and only a single value can be present within a given pixel. If multiple tissues are present within a voxel, the value for that pixel will be a weighted average of the signals from the tissues, and the individual structures cannot be differentiated. To improve spatial resolution, two tissues must be present in different voxels, so smaller pixels or thinner slices must be chosen. However, when the voxels are smaller, the signal produced in each voxel is decreased, so the signal-to-noise ratio is diminished (the image is noisier) and contrast resolution is decreased.[17]

Motion artifacts occur when there is patient motion, either voluntary or involuntary (including breathing and the motion of flowing blood), during the scan. While motion artifact can be seen with any imaging modality, the relatively long scan times in MRI increase the probability of this artifact occurring. Motion artifacts cause a decrease in contrast resolution. These artifacts are seen as multiple ghost images, or faint copies of the part affected by the motion, in the phase encode direction. Motion artifact is seen predominantly in the phase encode direction because adjacent lines of phase encoding are separated by the TR interval, which may be 3000 ms or longer.[17]

Magnetic susceptibility is defined as the ratio of the induced internal tissue magnetization to the external magnetic field. The susceptibility of structures can be divided into three categories: diamagnetic, paramagnetic, and ferromagnetic. *Diamagnetic* materials have a slight negative susceptibility (opposing the external magnetic field), and include water and organic materials (because of the effects of carbon and hydrogen). *Paramagnetic* materials have slight positive susceptibility, thus strengthening the magnetic field, and include O_2 and gadolinium-based contrast agents. Paramagnetic structures have no self-magnetism. *Ferromagnetic* materials have strong positive susceptibility and are often magnetic themselves. Iron, cobalt, and nickel are all ferromagnetic substances. When the magnetic susceptibility in the scanned tissues is essentially constant, the magnetic field is uniform, but marked changes in magnetic susceptibility cause distortion of the magnetic field. In normal tissues, this most commonly happens at a tissue-air interface, where there is decreased T2* signal because of more rapid dephasing at the interface. However, any metal can also cause changes in magnetic susceptibility and thus distort the magnetic field. Magnetic susceptibility is important in determining the age of hemorrhage, as the iron-containing components of blood will cause marked shortening of the T1 and T2 relaxation times of the surrounding protons. Gadolinium-based contrast material also causes shortened T1 relaxation of surrounding tissues, causing increased T1 signal in these tissues.[17] However, while susceptibility effects can be beneficial upon occasion, the severe field distortion caused by metallic foreign bodies or surgical implants can drastically reduce the diagnostic quality of an exam.

The magic angle artifact is seen in tendons and ligaments. These linear structures normally have low signal on both T1- and T2-weighted images because the water in the tissues is bound to collagen, so following excitation there is rapid dephasing of the MR signal. However, dipolar

interactions are decreased when the tendon or ligament is angled at approximately 55 degrees relative to the main magnetic field (B_0). When this occurs, the T2 relaxation time of those hydrogen atoms is increased nearly 100-fold and the structure will appear to have increased signal on conventional imaging sequences.[310,311] This artifactual signal increase may cause tendinous or ligamentous injury or inflammation to be diagnosed incorrectly.[310] While the magic angle effect can be identified in T2-weighted images, it is more apparent in T1-weighted and proton density images.[311] Because the magic angle effect is best seen in sequences with a short TE, increasing the TE will decrease the magic angle effect, though it may also decrease sensitivity for pathologic increases in signal in the tendons or ligaments.[310] Alternatively, repositioning of the patient could help determine if increased signal is pathologic or artifactual,[310] and one can also look for secondary signs of disease, such as associated soft tissue swelling.

4.5.6 MR imaging sequences and parameters specific to foreign bodies

Generally T1-weighted and T2-weighted spin-echo sequences are performed when evaluating for foreign bodies.[25,124,312] Post-contrast T1-weighted sequences will also help demonstrate the surrounding inflammatory response.[124] Because foreign objects are often relatively small, thin slices (e.g. 2mm or less) may be beneficial.[244] Additionally, small pixel sizes may also be useful to improve the spatial resolution: this can be achieved with a small field of view or increased matrix size.

4.5.7 Appearance of inflammation & foreign bodies

Structures on MRI are described relative to the intensity of the signal produced in the corresponding voxels. Structures that appear white are referred to as hyperintense, while black structures are hypointense. On T1-weighted images, structures with short T1 relaxation times are hyperintense; on T2-weighted images, structures with long T2 relaxation times are hyperintense.

Dry wood has a markedly low signal on T1-weighted, T2-weighted, and proton density sequences, is hypointense to skeletal muscle, and may be isointense to air (i.e. a signal void).[7,19,25,124,129,131,134,136,140,209,312,313] While theoretically absorption of fluids would increase the T1 and T2 relaxation times, and thus the T2 signal intensity, of a wooden foreign object over time,[209] this has only been recognized clinically in one case of a cervical wooden foreign body in a dog. In this case, the center of the wooden foreign body was mildly T2-hyperintense and T1-isointense to the surrounding cervical musculature.[314] In an *in vitro* study, the MRI characteristics of wood were unchanged after being soaked in water for 3 days.[313] Similarly, in a cadaver study, both wet and dry woods were visualized as signal voids, although the dry woods were considered slightly easier to detect.[7] Fresh (green) wooden foreign bodies inserted into the orbits of living dogs were not detected with MRI, though the inflammatory response was recognized; the actual intensity of the object is unknown because the object itself was not identified, but lack of visualization suggests that either the intensity was similar to the surrounding tissues or the object was too small to be identified.[315] However, one cadaver study did find that wooden splinters soaked in saline for 3 days or 5 months may have either low or high signal on T2-weighted sequences.[25] Interestingly, the outer ring of a pine branch was seen as markedly hyperintense on T2-weighted images in a model of the orbit.[313] Because of wood's low signal, MRI may be most beneficial in identifying a wooden foreign body when the object is

surrounded by fat, such as within the orbit, as this will provide contrast on T1-weighted sequences.[129,131,313] If surrounded by T2-hyperintense inflammation, a hypointense foreign object would also be more visible. The same would be true for a foreign object surrounded by contrast-enhancing inflammation on T1-weighted images. The elongated shape and sharp margination of a wooden foreign body can also aid in recognition.[131,132,136] However, wood does not produce the susceptibility artifact caused by metallic objects, and a linear low-signal structure could be misidentified as a tendon or other dense fibrous structure.[124]

Glass is seen as a sharply-marginated geometric signal void on MRI.[7,9,19,244] If the glass contains lead, visualization may be reduced due to T1-hyperintense paramagnetic artifacts.[244] Plastic and graphite also produce a signal void on MRI (though the void may not be as apparent as that of glass) and are associated with paramagnetic artifacts.[7,244,316] Other foreign objects described as a signal void on MRI include tooth fragments and asphalt.[9] Gravel may not be well visualized with MRI, as fragments often contain variable amounts of ferromagnetic materials, creating hypointense artifacts with distortion of the surrounding anatomy and hindering discrete localization.[7,9] A similar, even stronger, artifact was described with a fragment of amalgam.[9] Naturally, iron objects produce severe ferromagnetic artifacts, preventing evaluation of these objects.[244]

While foreign objects are almost invariably hypointense on T1- and T2-weighted images, a foreign-body granuloma caused by oil droplets in the soft tissues appeared as round, well-circumscribed, variably-sized T1-hyperintense clustered lesions which exhibited peripheral enhancement after contrast medium administration.[317]

Gossypibomas are variable in their signal characteristics, but tend to be well circumscribed.[166] The T1 signal intensity of these granulomas is usually heterogeneous,[160,161] and

may be hypointense[161] or isointense[166,169] to the surrounding musculature. Focal increased T1 signal intensity associated with the mass suggests hemorrhage.[169] The overall T2 signal intensity also varies, and has been described as mildly increased relative to skeletal muscle[166] or heterogeneous and ranging from low to very high.[169] Tortuous or wavy hypointense linear structures can be seen within a gossypiboma on T2-weighted images: these linear structures are thought to represent folded fabric or gauze fibers, and thus are considered characteristic of a retained surgical sponge.[160,166] Fluid can be seen as a T1-hypointense and T2-hyperintense region within the central portion of a gossypiboma.[166] Contrast enhancement tends to be heterogeneous and peripheral,[160,169] and MR angiography demonstrates neovascularization around the mass.[160] In patients diagnosed with an intracranial gossypiboma following resection of a primary brain tumor, MR imaging revealed the presence of the surgical cavity with rim enhancement in four cases and solid material at the surgery site in three patients; all imaging findings had suggested progression or recurrence of neoplasia.[167]

The inflammatory response caused by a foreign body is apparent on MRI, having low signal intensity on T1-weighted images and medium to high signal intensity on T2-weighted images.[124] Thus, if there is sufficient inflammation, a foreign object may be easily visualized on T2-weighted images due to the contrast between the low-intensity object and the high intensity of the inflamed tissues. Contrast enhancement is also seen in the inflamed tissues,[124,193] and this enhancement may appear as a hyperintense rim around the foreign object, which can markedly improve the visibility of a hypoattenuating foreign body.[210,314] Abscessation in the brain associated with wooden foreign bodies appears as a T1-hypointense, T2-hyperintense mass with heterogeneous rim enhancement.[134,199] A sterile cystic structure walled with granulation tissue has been described surrounding a wooden foreign body; this structure appeared as a T1-

hypointense, markedly T2-hyperintense structure with rim enhancement, and the foreign object could be identified as a hypointense filling defect in the middle of the mass on T2-weighted images.[316] Cellulitis appears as a loss in fat signal intensity on T1-weighted images, T2-hyperintensity of the soft tissues relative to muscle, and enhancement on T1-weighted images following administration of contrast medium.[318] The relatively diffuse contrast enhancement seen in cellulitis is a characteristic that can be used to differentiate this disease process from abscessation, which exhibits only rim enhancement.[319]

Using MRI, osteomyelitis is seen as a focal decrease in the T1 signal intensity of bone marrow with a corresponding increase in signal intensity on fat-suppressed T2-weighted and fast spin echo STIR images.[318] Focal enhancement of the marrow is also seen on post-contrast T1-weighted images.[318] More specifically, acute osteomyelitis has been described as ill-defined homogeneous regions of medullary bone with low or intermediate T1 signal intensity and high T2 signal intensity; similar characteristics were found in the adjacent cortical bone and soft tissues.[320] With increasing chronicity, the affected medullary bone is more heterogeneous, and sequestra and involucra are seen as foci of low or intermediate signal intensity on both T1- and T2-weighted images.[320]

Contrast-enhanced MRI utilizes intravenous administration of a paramagnetic contrast agent (a gadolinium chelate) to improve visualization of blood vessels and lesions, such as inflammation and neoplasia.[305] Paramagnetic substances possess a small magnetic moment that aligns with the external magnetic field when administered. Thus the overall magnetic field is locally increased where the contrast agent is present. This in turn causes a shortening of T1 and T2 relaxation times of surrounding tissues. Because T1 shortening predominates at the relatively low concentrations of contrast medium used in clinical imaging, the final result is increased

signal on T1-weighted images.[305] When imaging the brain, the blood-brain barrier (BBB) prevents passage of contrast media across capillary walls, so normal brain parenchyma does not enhance (the only enhancement is within vessels themselves).[321] However, when there is breakdown of the blood-brain barrier, as with inflammation or oxidation damage seen with hematomas, contrast medium will cross into the brain parenchyma and cause contrast enhancement.[322] Similarly, some neoplasms (such as metastatic disease) form capillaries with fenestrated endothelial cells, so these tumors will enhance, though others (such as low grade gliomas) may produce capillaries with an intact blood-brain barrier, thus preventing enhancement of these tumors.[321] Outside the brain, there is not a barrier preventing leakage of contrast media out of capillaries. However, pathologic tissues such as inflammation or neoplasia will still often exhibit greater contrast enhancement than the surrounding tissues because they frequently possess increased viable vasculature;[323,324] these vessels may also be abnormal or damaged with increased permeability.[325,326] Conversely, areas of necrosis or no perfusion will demonstrate minimal or no contrast enhancement.[323,324] Because steroids protect the blood-brain barrier by decreasing free radical production and increasing repair of membrane damage, the decreased permeability of the BBB in patients given steroids will result in decreased enhancement of the brain parenchyma.[322] Additionally, glucocorticoids generally increase vascular tone, though vessel responses to steroids depend on the local environment.[327] Thus a regional increase in vascular tone may cause a decrease in perfusion and a corresponding decrease in contrast enhancement regardless of the location of a lesion.

4.5.8 Appearance of an evolving abscess

Classically, pyogenic abscesses are isointense or hypointense to the surrounding tissue (e.g. muscle or liver) on T1-weighted images, and are hyperintense with signal equivalent to fluids on T2-weighted images.[318,328,329] Occasionally, abscesses may exhibit a signal void on both T1- and T2-weighted images, indicating gas formation, and fluid-gas levels may also be seen.[328] Some abscesses also contain septations.[328] Following contrast medium administration, abscesses demonstrate marked ring enhancement on T1-weighted images, and both the inner and outer margins of the enhanced rim are generally smooth.[318,328,330] This ring enhancement represents the increased vascularity and the increased vascular permeability in the granulation tissue making up the abscess wall.[330] The abscess wall is often T2-hypointense, possibly due to the presence of dense fibrous tissue or hemosiderin.[330] The tissue surrounding an abscess may be isointense on T1- and T2-weighted images, or may be T1-hypointense and T2-hyperintense with a degree of contrast enhancement.[328]

Despite this generalization, specific imaging characteristics of an abscess depend on both its age and etiology. Brain abscesses are described as advancing through four phases: early cerebritis (1-4 days), late cerebritis (4-10 days), early capsule formation (11-14 days), and late capsule formation (greater than 14 days),[304] though capsule formation can take as long as four weeks.[330] In early cerebritis, an abscess is somewhat T1-hypointense and T2-hyperintense, and contrast enhancement is heterogeneous.[304] However, as the abscess becomes more chronic, the T1-hypointense region becomes better defined and increased T2 signal will be seen both within the abscess cavity and in the surrounding brain parenchyma. Once the capsule forms it will be seen as a T1-hyperintense and T2-hypointense structure, and ring enhancement will also be present.[304]

Masses caused by tuberculosis (tuberculomas) have a variable appearance on spin-echo MRI because they have a variable structure. A solid caseous granuloma is isointense on T1-weighted images and will be either isointense or hypointense on T2-weighted sequences.[331,332] This low T2 signal is due to the presence of the solid caseous material, macrophages and their products of digestion, and fibrosis or gliosis.[331] Noncaseous granulomas and caseating granulomas with a liquid center are identified as having a pattern with low T1 signal intensity and high T2 signal intensity, and could thus be confused for a classic pyogenic abscess.[304,331]

On diffusion-weighted images (DWI), pyogenic abscesses are nearly always demonstrated as homogeneous regions of restricted diffusion (markedly increased signal); for this reason DWI is strongly recommended when there is suspicion of brain abscessation.[304,333] When calculated data are displayed on an apparent diffusion coefficient (ADC) map, abscesses are displayed with low signal.[334] This helps in differentiating an abscess from a necrotic neoplasm, as neoplasia generally does not exhibit restricted diffusion.[304] However, this trend is not universal, as fungal abscesses and tuberculosis lesions may have increased diffusivity and thus low DWI signal.[304] Nonetheless, one study comparing DWI and post-contrast T1-weighted images in their ability to differentiate abscesses and neoplasia found a sensitivity and specificity of 93% and 91%, respectively, for DWI and 60% and 27%, respectively, for post-contrast T1-weighted imaging.[335] A similar study found that the sensitivity and specificity of DWI for distinguishing abscesses and primary brain tumors were both 100%, and the sensitivity and specificity of DWI for distinguishing abscesses and metastatic neoplasia were 100% and 73%, respectively.[336]

Magnetic resonance spectroscopy is beneficial in differentiating abscesses from other cystic lesions.[304] Metabolites recognized with MR spectroscopy that are thought to be specific for abscessation include succinate, acetate, glycine, alanine, cytosolic amino acids (leucine,

isoleucine, and valine), lactate, and possibly lipids; most of these compounds would not be expected in cystic neoplasms,[304,334,337] though lactate and lipid peaks can be seen in metastatic neoplasms.[338] Acetate and succinate may be relatively specific for abscesses caused by anaerobic bacteria.[334] Neoplasia would be expected to exhibit brain metabolites such as *N*-acetylaspartate (NAA), choline, and creatine, which should not be seen in abscesses.[334] The key features used to differentiate an abscess from neoplasia are a lack of an elevated choline peak, presence of an amino acid CH_3 peak, and in some cases the presence of acetate and succinate peaks.[337]

4.5.9 Appearance of an evolving hematoma

The appearance of hemorrhage on spin-echo MR images is highly dependent on the chemical composition, and thus the age, of the hematoma. The sequence of appearance is based on bound-water (protein) effects, paramagnetic effects, and inhomogeneous susceptibility effects. Free water has a high motional frequency and consequently a long T1 relaxation time. However, when proteins are added to the water, water molecules are attracted to charged side groups, decreasing the T1 relaxation time (increasing T1 signal intensity). Additional decreases in T1 relaxation time because of dipole-dipole interactions occur when paramagnetic substances (e.g. gadolinium or methemoglobin) are also added. Similar effects are seen regarding T2 relaxation times: binding to proteins causes a decrease in water's T2 relaxation time (decreasing T2 signal intensity), and even more profound T2 shortening is seen from the magnetic susceptibility caused by paramagnetic agents that are confined to a small region (e.g. within a cell).[339,340]

Five stages of hematoma evolution are described. A hyperacute hematoma (first few hours) contains intracellular oxyhemoglobin. Oxyhemoglobin contains iron in the ferrous state (Fe^{+2}),

and because there are no unpaired electrons in this state, oxygenated hemoglobin is diamagnetic (i.e. not paramagnetic). Hyperacute hematomas are iso- to hypointense to normal gray matter on T1-weighted images because they have a relatively higher water content than the brain parenchyma. While the T1 signal intensity will be slightly higher than that of water due to the presence of proteins, there are no paramagnetic effects. These hematomas are also hyperintense on T2-weighted images because of the high water content relative to the brain parenchyma; again, because oxyhemoglobin is diamagnetic, there are no magnetic susceptibility effects. Because hyperacute hematomas are generally mildly T1-hypointese and T2-hyperintense to the gray matter, the imaging appearance is not specific for a hematoma at this stage.[339,340]

As the oxygenation of the hemoglobin is decreased, deoxyhemoglobin is formed. This is considered the acute stage of the hematoma, which is seen from several hours to the first few days. The loss of oxygen molecules from the ferrous iron ion causes four electrons in the outer shell to be unpaired, making deoxyhemoglobin a paramagnetic substance. However, the iron is sequestered within the hemoglobin molecule, preventing water molecules from approaching closely enough to induce dipole-dipole interactions. Hence, without a paramagnetic effect, the hematoma remains T1-isointense or hypointense to the gray matter. Nonetheless, because the paramagnetic deoxyhemoglobin remains within the erythrocyte, magnetic susceptibility effects are seen. Thus there is shortening of the T2 relaxation times, and the hematoma is markedly hypointense to gray matter on T2-weighted images. The effect of T2 shortening is more notable at higher field strengths.[339,340] The increasing concentration of erythrocytes during this phase due to retraction of the clot and effective increase in hematocrit also contribute to decreased T2 relaxation times, though this is thought to be less important than the process of deoxygenation of the hemoglobin.[339,341]

The early subacute stage of hematoma formation is marked by oxidation of deoxyhemoglobin to methemoglobin and the persistence of intact erythrocytes. This phase is seen from approximately 3-7 days. The iron in methemoglobin is ferric (Fe^{+3}), which is very paramagnetic due to the presence of 5 unpaired electrons in the outer shell. Additionally, the position of the iron ion in the methemoglobin molecule is readily accessible by water, allowing for dipole-dipole interactions. Thus, paramagnetic effects shorten T1 relaxation, and the hematoma is T1-hyperintense. Because the erythrocytes remain intact and methemoglobin is paramagnetic, magnetic susceptibility effects are still seen, and the hematoma remains markedly hypointense to gray matter on T2-weighted images. Theoretically the T2 relaxation should be decreased even relative to the acute phase of the hematoma due to the increase in unpaired iron electrons, but this would be difficult to recognize clinically.[339,340]

In the late subacute stage, beginning at approximately 1 week and extending for up to several months, hemoglobin remains as methemoglobin, but erythrocyte lysis occurs. On T1-weighted images the paramagnetic effects of methemoglobin are unchanged, so the hematoma remains hyperintense to gray matter. However, the methemoglobin is no longer compartmentalized and becomes distributed more uniformly throughout the hematoma. Thus there is no (inhomogeneous) magnetic susceptibility effect and T2 relaxation times are again increased, resulting in hyperintensity on T2-weighted images.[339,340]

The chronic stage of the hematoma begins as early as 2 weeks and may be seen indefinitely. Here macrophages (gitter cells) remove the hemoglobin products from the center of the hematoma. Without iron in the center of the hematoma, all of the substances in this region are diamagnetic, so there are no paramagnetic or susceptibility effects. The center of the hematoma is then essentially just fluid (CSF), so it appears T1-hypointense and T2-hyperintense

to gray matter, though this area may ultimately collapse. In the periphery of the hematoma, the iron is stored as hemosiderin and ferritin within lysosomes in the macrophages themselves. The iron in these molecules is sequestered within the molecule, so there are no dipole-dipole interactions with water and thus no paramagnetic effects. However, the molecules are compartmentalized within cells, so inhomogeneity leads to magnetic susceptibility effects, and the hematoma's rim will be T1-hypointense and very T2-hypointense to the normal gray matter.[339,340,342] A summary of spin-echo imaging characteristics is given in Table 2.1.

Table 2.1: Spin-echo Imaging Characteristics of Intracranial Hematomas

Stage	Time	Iron form	Magnetic Property	Iron Location	T1-weighted signal	T2-weighted signal
Hyperacute	Few hours	Oxy-Hb	Diamagnetic	Intracellular	Iso/Hypo	Hyper
Acute	Few days	Deoxy-Hb	Paramagnetic	Intracellular	Iso/Hypo	Hypo
Early subacute	3-7 days	Met-Hb	Paramagnetic	Intracellular	Hyper	Hypo
Late subacute	1 week – months	Met-Hb	Paramagnetic	Extracellular	Hyper	Hyper
Chronic (center)	2 weeks +	None	Diamagnetic	None	Hypo	Hyper
Chronic (rim)	2 weeks +	Hemosiderin & Ferritin	Paramagnetic	Intracellular	Hypo	Hypo

Note: Data were obtained from references [339,340]

Diffusion-weighted imaging (DWI) can also be performed to evaluate intracranial hematomas. All hematoma regions with intracellular hemoglobin products had no significant differences among apparent diffusion coefficient (ADC) values. Hematomas with intracellular hemoglobin products had significantly decreased diffusion when compared to hematomas with extracellular hemoglobin (lysed erythrocytes). When compared to normal white matter, hematomas with lysed erythrocytes had more diffusion and hematomas with intact erythrocytes had more restricted diffusion.[343] It is important to compare DWI images to ADC images and not use DWI images alone for diagnosis, as changes in T2 relaxation can affect the appearance of a DWI image, so the magnetic susceptibility caused by an acute or early subacute hematoma could artifactually change the appearance of a DWI image.[344]

A particularly useful technique for identification of hemorrhage is gradient echo imaging, or susceptibility-weighted MR imaging. Because gradient echo imaging does not include the 180-degree refocusing pulse used in conventional spin-echo MRI, the gradient echo technique is much more sensitive to magnetic field inhomogeneities (i.e. shortening of T2*).[342] At tissue interfaces, which can be caused by ferromagnetic, paramagnetic, or diamagnetic substances, spinning nuclei precess differently where the local magnetic field is heterogeneous, thus causing a more rapid dephasing and signal loss on T2*-weighted images.[345] The paramagnetic hemoglobin products cause field inhomogeneities that are seen as a marked decrease in intensity on gradient echo images;[342] even the interface of the hematoma and normal brain tissue will cause increased magnetic susceptibility.[345] Indeed, on T2*-weighted gradient echo images, areas of hemorrhage will often be seen as a region of hypointense blooming.[346] Because of this, gradient echo imaging is especially useful for identification of small hemorrhages, as in patients with acute stroke or amyloid angiopathy.[346,347]

4.6 COMPUTED TOMOGRAPHY

Computed tomography (CT) uses x-rays transmitted through a patient at multiple projection angles to produce planar images, or slices, of anatomy.[17] By acquiring numerous slices of a patient, CT can provide multiplanar and three-dimensional images of the body, allowing for better localization of pathologic processes than such modalities as radiography allow.[3,16] CT is also not limited by superimposition of gas or bone, unlike ultrasound and (to a degree) radiography.[3] However, artifacts from patient movement and metallic objects are more pronounced than with radiography.[16] Contrast resolution in the soft tissues is better than with radiography, as soft tissue structures with a density difference as small as 0.5% can be distinguished from each other (as compared to a 5% difference required in radiography),[17,305] but soft tissue contrast resolution is limited when compared to MRI.[16] The spatial resolution of CT is about 2 lp/mm, a little better than MRI, but not as good as digital radiography (5 lp/mm) or conventional screen-film radiography (7 lp/mm).[17] Further disadvantages of CT include the relatively high cost, greater ionizing radiation than other modalities, and the need for sedation or anesthesia in veterinary medicine.[15,16]

4.6.1 CT components and instrumentation

The principle of computed tomography is that an image of an unknown structure can be produced if numerous x-ray projections are made through the object. Thus CT utilizes equipment similar to that used in conventional radiography: an x-ray tube and detectors are required to produce the image. The x-ray tube and detectors are present within the gantry, the large ring-shaped structure that the patient is placed within during a scan. The gantry aperture is the opening in the structure through which the patient moves; the size of the aperture will dictate the

maximum size of body parts that can be imaged. The gantry can be angled up to 30 degrees in some cases, allowing the x-ray beam to be perpendicular to the anatomy in certain applications. The patient is placed on the patient table, or couch, for movement through the gantry aperture. The material used in making the couch must be strong, as the end passing through the gantry aperture is not supported, but the material must also minimally attenuate x-rays, as its presence within the gantry aperture means that many of the x-rays passing through the patient will also pass through the couch. While the x-ray tube (and usually the detectors) within the gantry rotate to produce a single transverse slice of the anatomy, it is the translation of the couch through the gantry aperture that allows for acquisition of multiple slices.[348]

Though the x-ray tube is similar to those used in conventional radiography, modifications are necessary. CT scanners place severe demands on the x-ray tube, as numerous prolonged exposures are required for each acquired slice, and each study contains numerous slices. Thus, the daily output of a CT x-ray tube is considerably higher than one used in conventional radiography, and tube heating is of much greater concern.[348] Also similar to conventional radiography, collimator blades located near the x-ray tube determine the thickness of the x-ray beam produced. While this collimation determines slice thickness in scanners with single detector arrays, this is not true in scanners with multiple detector arrays. In multiple detector arrays, collimation is used to make sure the x-ray beam strikes only the active detector elements, without undue additional patient exposure.[17]

There are two primary types of detectors that can be used in CT. *Xenon detectors* consist of many long thin chambers containing pressurized xenon gas. The low density of gas means that its detection efficiency is relatively low, though these detectors are generally quite thick to compensate for this. Because they are long and thin, xenon detectors can only accept x-rays

coming from a very specific angle – due to this, much scatter radiation is not detected, but these detectors cannot be used in 4th generation CT scanners (see below). Xenon detectors function as ionization detectors: a voltage is applied across metal electrodes placed on either side of the detector, and when x-rays interact with the xenon and cause ionization, the ions move to the electrodes where the charge is collected. The amount of charge is proportional to the intensity of the x-rays striking the detector. More commonly used currently are *solid-state detectors*. These detectors consist of scintillators coupled to photodetectors. When the scintillator is struck by an x-ray photon it emits light. This light is then collected by the photodetector, which produces an electronic signal proportional to the light intensity. As in the xenon detectors, this electronic signal is proportional to the initial x-ray intensity striking the detector. Solid state detectors have higher x-ray absorption efficiency than xenon detectors, potentially increasing contrast resolution (decreasing noise) or decreasing patient dose. However, crosstalk between detectors is an issue, so a gap between detectors is required; this decreases geometric efficiency.[17]

Current CT scanners use multiple detector arrays. These arrays are composed of multiple adjacent solid-state linear detector arrays. Each individual detector element has a finite size, and it is the width that determines the minimum slice thickness available in the system. If thicker slices are desired, multiple adjacent detector elements are electronically linked so that they act as a single detector. Because multiple detector arrays allow the collimator to be open wider than single detector array systems (allowing the x-ray beam to strike more detectors at once), more of the x-ray beam is utilized and scanning is more efficient and faster.[17,349] Additionally, spatial resolution in the longitudinal dimension (z-axis) is markedly improved, and voxels are isotropic (equal sizes in all three dimensions) with current scanners.[349]

Historically the geometry of a computed tomography scanner has been referred to by its generation. *First-generation* CT scanners were those that used a "pencil" x-ray beam and only a single detector for each slice. In these systems, also called rotate/translate systems, the x-ray tube and detector moved linearly across the field of view for one set of projections, then rotated a small amount and moved linearly across the field of view again. This process was repeated numerous times for one slice, so acquisition times were very long. *Second-generation* CT scanners used a narrow fan beam to acquire more data with each projection, but still required the beam to translate across the field of view before rotating. *Third-generation* CT scanners are the most commonly used today. The scanners use a wide fan beam to cover the entire field of view with each projection. Because of this, no translation of the x-ray tube and detectors is necessary, and the system is referred to as a rotate/rotate system as the x-ray tube and detector row rotate in concert. *Fourth-generation* CT scanners were developed to prevent ring artifacts and used an x-ray tube that rotated inside of a 360-degree stationary ring of detectors (a rotate/stationary arrangement). The newest type of CT geometry is the stationary/stationary geometry, or *fifth generation*. In this type of scanner, the gantry has no moving parts as an electron beam is steered around the patient, striking a ring-shaped tungsten target and producing x-rays which travel through the patient. Because the electron beam can be rapidly steered, this type of scanner is mostly used in cardiac studies, where good temporal resolution is critical.[17]

While different geometries of the gantry were developed to make imaging of a single slice faster, old CT scanners still had to pause at the end of each rotation to unwind the wires connecting the rotating components to the stationary components. However, the development of slip ring technology changed this. A slip ring is a circumferential contact with sliding brushes which eliminated the need for wires. With the development of this technology came the

development of helical CT. Helical CT scanners acquire data as the table is moving instead of moving the table incrementally and scanning only when the table is stationary. Helical acquisitions have drastically reduced the times required for a CT scan.[17]

Once the data are acquired, a computer is required to reconstruct the images. This is further discussed in Section 4.6.2: CT Data Processing. Finally, viewing and storage of the images requires them to be sent to a Picture Archiving and Communication System (PACS) and requires viewing workstations to retrieve the images.

4.6.2 CT data processing

4.6.2.1 *Pre-processing and image formation*

The initial phase of creating a CT image is tomographic acquisition. Multiple x-rays are transmitted through a patient and are detected by the detectors opposite the x-ray tube. Each individual transmission measurement made by one detector element at a discrete timepoint is known as a ray. A series of rays passing through the patient at the same time in the same orientation is a projection. In current CT scanning, fan beam geometry is used, meaning that the rays in each projection are divergent. In the acquisition of one axial CT image, there may be 800 rays transmitted through the patient at each of 1000 different projection angles, leading to 800,000 individual transmission measurements. After those transmissions are complete, the patient table moves a small amount, and the process is repeated for the next slice. (Note that table movement is continuous in helical acquisition.)[17]

Multiple preprocessing steps are required prior to reconstruction of CT images. The first set of preprocessing procedures involve calibration of the digital data that are acquired. The

electronic gain of each individual detector is adjusted using calibration data that were previously obtained in air scans. There is also correction of geometric differences caused by misalignments of detectors, which is especially important in fourth generation scanners due to the changing distance between the x-ray tube and the detectors.[17]

The transmission measurements represent the intensity of the x-rays striking the detectors (I_t). The unattenuated x-ray beam intensity (I_o) is also measured by a reference detector. After calibration these two factors can be used to calculate the average linear attenuation coefficient (μ) along the ray with the equation $\ln(I_o/I_t) = \mu t$, where t is the patient thickness along the ray and will ultimately be canceled out. This computation of μ represents another pre-processing step, and results in reconstruction of data that are based on anatomic features, not machine-dependent parameters such as the initial intensity of the x-ray beam.[17]

With helical CT scans, a final step of interpolation must be performed before image reconstruction. This is needed because CT reconstruction algorithms are based on an assumption of axial acquisition, i.e. a circular path of the x-ray tube around the patient rather than a helical one. Thus, the data are converted into planar data sets (mimicking axial acquisitions) by taking the weighted averages of data points on either side of the chosen image planes. An added advantage of this is that images can be reconstructed at any position along the scan length, thus allowing for production of additional overlapping slices without having to rescan the patient. This may increase the sensitivity for small subtle lesions that may not have been centered in a voxel on the initial reconstruction.[17]

Production of the CT images is performed using a CT reconstruction algorithm. There are multiple methods of reconstruction, but the most commonly used type clinically is backprojection. Simple backprojection is essentially a reversal of the data acquisition. For each

ray, the linear attenuation value, the acquisition angle, and the detector's position in the detector array are used to project (essentially superimpose) the value of μ for each ray over the image along the path that the ray initially took. As the hundreds of thousands of rays are layered over the image, areas of similar attenuation reinforce each other, creating an image in the computer. However, simple backprojection tends to cause blurring of objects within the image, so filtered backprojection is more commonly used. In this technique, a mathematical convolution kernel is used to convert the raw projection data, and the converted data are used for the backprojection procedure.[17]

Different reconstruction kernels, or filters, are used in CT image reconstruction depending on the organ of interest. For example, bone filters accentuate high frequencies, thus enhancing edges, though with the cost of increased noise in the image. Bone images have high contrast and a good signal-to-noise ratio, so increased noise is not a significant problem. Conversely, soft tissue filters reduce the amplification of high frequencies, thus softening or smoothing the image and decreasing noise. This is important in soft-tissue imaging, where improved contrast resolution is more important than improved spatial resolution.[17]

Once image reconstruction is complete, each pixel can be represented by a value based on the x-ray attenuation characteristics of the tissues present in the corresponding voxel in the patient. However, before image display and storage, those numbers are normalized to the attenuation coefficient of water using the equation $HU = 1000((\mu_{x,y} - \mu_{water})/\mu_{water})$, where $\mu_{x,y}$ represents the initial attenuation value of the pixel in question and μ_{water} represents the linear attenuation coefficient of water. The normalized values are given as Hounsfield Units (HU), also referred to as the CT number.[17] (Interestingly, older literature uses EMI units rather than HU for attenuation values. While also scaled to water, EMI units were half the value of Hounsfield

units; thus 2 HU = 1 EMI unit.[350]) At the x-ray energies used in CT (average photon energy of 75 keV), Compton scatter is responsible for most of the interactions of x-rays with the patient. Thus, because physical density is the most important component of tissue that influences Compton scatter, the HU value essentially represents physical density. An advantage of using the CT number is that they are quantitative, so measurement of structures' HU values can aid in diagnoses.[17]

4.6.2.2 *Post-processing*

Post-processing functions are performed to improve visibility of both normal and pathologic structures. This need stems partially from the limitations of human vision. The human eye has a profound dynamic range for detecting absolute light intensities, as is apparent given our ability to see on bright days and in dark rooms. However, most of this range comes from changes in the diameter of the pupil affecting the amount of light allowed to enter the eye. At a given light level (i.e. pupil diameter), the relative differences that are detectable are far less.[17] Estimates of the dynamic range of human vision vary, but estimates include 20 dB, meaning that only about 100 different levels of gray can be differentiated,[273] or from 30 to 90 gray shades.[17] Other estimates suggest differentiation of up to 200 gray shades depending on the luminance of the surroundings,[351] though still other tests indicate only 40 shades of gray could be differentiated by a young (approximately 20-year-old) observer versus only about 20 for an older observer.[352] Color differentiation of the human eye is considerably better. When an observer is adapted to the luminance level being tested, approximately 2750 distinct colors can be discriminated, though when the observer is adapted to light at a different level of luminance, as

few as 448 colors can be differentiated.[353] However, when the variety of shades (luminance levels) of each color are accounted for, the human eye can distinguish many thousands of colors.

The most common post-processing functions performed on CT images are windowing and leveling. Generally, CT images have a depth of 12 bits, producing a grayscale of 4096 shades of gray (corresponding to -1000 to +3095 HU). However, not all of these shades can be displayed, as most computer monitors can display only 8 bits (256 shades). Additionally, the human eye is limited in its ability to detect shades of gray as well, as discussed above. Thus, the 12 bits of image depth must be converted to 8 bits of display depth. Adjusting the window width and level is a method of adjusting the grayscale of the image. The window width is essentially the contrast of the image, as it determines the number of HU values that are present between black and white on the display. A narrow window produces increased image contrast, as even a relatively small difference in the HU of two tissues is likely to have a difference of one or more shades of gray. The window level is the HU value at the center of the displayed grayscale, and the number chosen should be the HU value of the organ of interest. Once the window width and level are chosen, values less than the low end of the window will be displayed as black, and values higher than the upper end will be displayed as white.[17] While the window level is chosen as the center of the image, it effectively determines the overall brightness of the image. A lower window level will produce a brighter image than a higher window level, as with a low window level there are more data values that are above the point of the level and are thus displayed as light gray or white. For example, in one study evaluating the luminance achieved when evaluating the Society of Motion Picture and Television Engineers (SMPTE) test pattern at different window levels, the luminance at the 50% digital value was approximately 20 cd/m^2 at a window level of 30 HU and 70 cd/m^2 at a window level of -500 HU.[354]

Another type of post-processing that can be performed is multiplanar reconstruction (MPR). CT images are generally obtained in a transverse orientation, but structures that run cranial to caudal may be better evaluated in a sagittal or dorsal projection. Because the volume data are already available, reformatting is simple. Some workstations also allow use of a curved plane of reconstruction to more fully follow a structure of interest. Usually the spatial resolution of the reformatted images is less than the initial transverse images because z-axis resolution is limited by the slice thickness. Because the slice thickness is usually greater than the dimensions of pixels in the x-y plane, there is a mismatch of spatial resolution, so interpolation of the data is required to maintain the correct aspect ratio. Nonetheless, the actual spatial resolution along the z-axis is still limited by the slice thickness and cannot be improved.[17] However, because current multidetector array scanners can produce isotropic voxels, multiplanar reconstructions on these systems will have the same spatial resolution in all three dimensions.[349] Spatial resolution improvements in the z-axis direction can also be achieved by obtaining overlapping slices, but this also results in oversampling and increases patient radiation exposure.

Three-dimensional reconstruction can also be performed in the post-processing phase of image analysis. This may be particularly useful for surgical planning or planning of radiation therapy, and not necessarily for initial diagnosis. Volume rendering uses segmentation of target structures before performing the reconstruction. Segmentation consists of selection of the target organs, usually by selecting ranges of CT numbers to include in the image – generally tissues above a certain threshold are selected, and this technique works best when there is a large difference in HU value between the target structure and surrounding tissues, as with selection of bone. The rendering software then calculates the theoretical appearance of the selected structures as viewed from a given perspective.[17] Three-dimensional reconstruction has been shown to

improve surgical planning and improve surgeons' confidence in their surgical plans in retrieval of foreign objects from the head and neck because of the improved global visualization of structures.[355]

While reconstruction techniques can be beneficial for displaying lesions relative to pertinent anatomy and for surgical planning, care must be taken in using reconstructed images for a diagnosis. Multiplanar reconstructions should maintain the diagnostic accuracy of the initially acquired images, though some extrapolation of data in the slice thickness dimension is required if isotropic voxels are not used.[356] Curved planar reconstruction is beneficial in following tortuous structures, but anatomic distortion occurs and thus these images cannot be used for measurements.[356] Projection 3D techniques (maximum intensity projection, minimum intensity projection) suffer from partial volume averaging, and subtle lesions may be missed because only the most extreme voxels are used in image creation.[356] Structures such as vessels may also appear to overlap or be truncated, leading to an incorrect diagnosis.[357] Three-dimensional shaded-surface display can be encumbered by misleading data incorporation depending on the exact threshold values selected for inclusion in the final image.[356] Volume rendering of multiple tissues simultaneously may combat this problem, but margins may still be artificial and imprecise.[356] Also, when evaluating vessels opacified with contrast medium, structures such as calcium plaques causing stenosis may actually appear as outpouchings or aneurysms because the vessel and calcifications are displayed with the same level of gray.[357] Measurements are a concern in multiple reconstruction techniques: in a study evaluating multiplanar reconstructions, virtual colonoscopy, shaded-surface display, and Raysum techniques for assessing colorectal carcinoma, only multiplanar reconstructions were accurate in assessing the circumferential involvement of the neoplasm, and only Raysum (and to a lesser

extent, shaded-surface display) were accurate in assessing tumor length.[358] Because of these issues, only windowing and leveling are completely safe post-processing manipulations, as no data are lost or misconstrued.

4.6.3 CT image quality

A pixel, short for picture element, is a two-dimensional square in any digital image, and represents the smallest elemental unit of that image. In CT, each pixel corresponds to a voxel (volume element) in the patient. A voxel is a three-dimensional structure, with the dimensions in the scan plane equal to those of the corresponding pixel, but also including thickness equal to the slice thickness used in the study. In the CT display, each pixel is assigned a Hounsfield Unit value which represents the average x-ray attenuation properties of all the tissues located within the corresponding voxel. Because a pixel (or voxel) cannot be subdivided, two objects within the same pixel (voxel) cannot be resolved; thus, pixel size is a determinant of spatial resolution. Smaller pixels increase the likelihood that two objects are not within the same pixel, increasing spatial resolution. To change pixel size (size of the voxel in the scan plane), one must change either the field of view or the matrix (matrix size). The field of view represents the actual size of the area being imaged. Hence, if a smaller area is imaged with the same number of pixels, each pixel will be smaller. The matrix size is the number of points (pixels) used in forming the image. Thus, if the matrix size is increased (e.g. from 512x512 to 1024x1024) while field of view remains constant, each pixel will again be smaller. The only way to change the thickness of the voxel is to change the slice thickness.[17,252]

The pitch is a parameter used in helical CT scanning. The pitch has an important influence on radiation dose, scan time, and image quality. In a scanner with a single detector array, the

pitch is determined by the collimation (collimator pitch), and equals the table movement (mm) per full rotation of the gantry divided by the collimator width (mm). A pitch of 1.0 means that the number of views is equivalent to the number that would be obtained with axial acquisition of contiguous slices: the amount the table moves is equal to the slice thickness. If the pitch is decreased to less than 1.0, the table is moving less than one slice thickness per rotation. This overscanning will improve spatial and resolution, but scan time and patient radiation dose will be increased. If the pitch is greater than 1.0, partial scanning occurs. This will decrease the scan time and patient dose, though spatial resolution is also decreased. Practically speaking, a pitch of greater than 1.5 will produce an inadequate image, as not enough data acquired are contiguous. In scanners with multiple detector arrays, detector pitch is defined as the table movement (mm) per full rotation of the gantry divided by detector width (mm).[17]

Spatial resolution is the ability to differentiate two closely-spaced objects, and many factors are important in determining the spatial resolution of CT. The detector aperture is the size of one detector element, and smaller detectors will improve spatial resolution in the scanned (x-y) plane. Spatial resolution in the third dimension is determined by the slice thickness: thinner slices improve spatial resolution in the z-axis. The reconstruction kernel is important, as a bone (edge-enhancing) filter provides better spatial resolution, while a soft-tissue filter produces more blurring and thus poorer spatial resolution. The pixel matrix size also influences spatial resolution, as increasing the number of pixels for a given field of view will decrease the size of each one, thus improving spatial resolution. Likewise, decreasing the field of view for a given matrix size will also decrease the size of each pixel, also improving spatial resolution. Patient motion causes blurring, which decreases spatial resolution. As discussed above, increasing the helical pitch will also decrease spatial resolution.[17]

Contrast resolution is the ability to differentiate small differences in x-ray attenuation between two adjacent structures, and is also affected by multiple factors in CT. The mA used determines the number of x-ray photons produced; thus, increasing the mA will increase the number of photons and the signal-to-noise ratio (SNR), improving contrast resolution. Increasing the pixel size also increases the number of x-rays passing through each voxel, also improving the SNR and contrast resolution. This can be achieved by decreasing the matrix size (number of pixels) or increasing the field of view. Thicker slices will also increase the voxel size along the z-axis, also improving contrast resolution. The reconstruction filter used also influences contrast resolution, as soft tissue filters provide better contrast resolution than bone filters.[17] As can be seen, many CT factors involve a tradeoff between spatial resolution and contrast resolution, as improvement of any of these factors other than mA will negatively influence the spatial resolution.

In a single detector array CT system, the slice thickness is determined by the collimation of the x-ray beam by lead sheets, as in conventional radiography. A wider gap between the lead sheets allows for a wider x-ray beam to strike the (static) detectors. The maximum slice thickness available is determined by the width of the detectors, as the portion of a wider x-ray beam will simply not be detected but will increase the dose to the patient and increase the amount of scatter radiation. For CT scanners with multidetector arrays, however, the width of the detectors in the slice thickness dimension determines the slice thickness. The thinnest slice available is determined by the size of a single detector element, but thicker slices can be obtained by binning (electronically linking) multiple adjacent detectors together. The advantage of an increased slice thickness is a linear increase in detected x-ray photons, in turn increasing signal-to-noise ratio (SNR) and contrast resolution. However, this increase in slice thickness also decreases the spatial

resolution in the slice thickness dimension and increases partial volume averaging.[17] Use of thicker slices also decreases the total time of the study, which in turn will decrease motion artifact, though the use of multidetector CT systems has decreased the time required for studies, even with acquisition of thin slices.[349]

Image noise is random signal in an image, and all imaging systems have a noise component in the image. Noise causes addition or subtraction of a variable amount from a measurement, increasing the uncertainty of any measured value. The primary source of noise in CT is quantum noise, or quantum mottle. The amount of noise present in a given pixel is equal to the square root of the number of photons in that pixel, which is also the standard deviation of the number of photons in the pixel. If the total number of photons detected in the pixel is low, the noise represents a significant percentage of the overall signal. As the number of photons increases, the amount of noise increases more slowly, so the signal-to-noise ratio (SNR) increases as well. An increase in the total number of photons by a given factor will increase the SNR by the square root of that factor. Contrast resolution increases with increased SNR.[17]

The overall detectability of a structure on an image is described by the Rose model. The signal-to-noise ratio (SNR) is commonly used to measure image quality and is calculated as the mean signal in the structure of interest divided by the image noise (the standard deviation of the signal in a region outside the body).[359,360] Visibility of one structure relative to another, e.g. the visibility of an organ against the background, can also be described by the contrast-to-noise ratio (CNR): the signal difference between the two structures divided by the image noise, or, equivalently, the difference in the SNR between the two structures.[359,360] However, these strict measurements of the signal and noise are not the only determinants of structure visibility in an image. According to the Rose model, SNR (which some refer to as visibility) can be defined as

CNR (the signal difference between the two structures divided by the image noise) times the square root of the area of the object; this can also be calculated as tissue contrast (signal difference divided by mean background signal) times the square root of the product of area and background signal.[359] Thus, visibility of an object improves as the size of the object (the number of voxels occupied) increases. In order to detect a signal, the threshold SNR to detect a signal is considered to be approximately 4,[361] though this is not precise and estimates place the value between 2 and 6.[359,362]

4.6.4 CT artifacts

Numerous artifacts are described in computed tomography; those which are most pertinent to imaging of foreign objects and inflammation are discussed here.

Partial volume averaging is dependent on the overall size of a voxel, a function of both the two-dimensional measurements in the plane of the acquired image and the slice thickness. The shade of gray displayed within a pixel is based on the CT number of the tissue within the corresponding voxel, which in turn is proportional to the x-ray linear attenuation coefficient (μ) of the tissues in the voxel. If the tissue is all of one type, the CT number is a good representation of the tissue. However, if multiple tissue types (such as bone and soft tissue) are present in a single voxel, the CT number calculated for the corresponding pixel will be based on a weighted average of the different linear attenuation coefficient values and may not accurately represent either tissue that is actually present. Partial volume averaging is most common at the margins of curved structures. Because the slice thickness is usually the largest dimension of a voxel, using thinner slices will help reduce partial volume averaging, though decreasing the voxel dimensions within the slice plane (increased matrix size or decreased field of view) would also help.[17]

Motion artifact occurs when there is patient motion during the CT acquisition. A small movement will cause blurring of the image, while large movements will result in the appearance of double images or ghosting. If motion artifact is severe enough, the patient will need to be re-scanned.[17]

Beam hardening artifact occurs because the x-ray beam used in CT imaging is a polychromatic beam with an average energy around 70 keV. Low-energy photons are more easily attenuated than high-energy photons, so the x-ray beam exiting the patient will have a higher proportion of high-energy photons than the beam entering the patient, and the beam is said to be "hardened." This is important because the linear attenuation coefficient measured in tissues depends on the average energy of the x-ray beam: a hardened (higher average energy) beam will result in a lower measured linear attenuation coefficient of the tissues.[252] While beam hardening occurs in all tissues and can be corrected for to a degree, it is especially pronounced when the x-ray beam passes through a dense structure, such as the petrous temporal bones. The reconstruction algorithm is further confused because rays from some projection angles are hardened more than rays from other angles, and the final result is hypoattenuating streaks extending from the dense structures.[17]

Metallic structures can cause severe hyperattenuating and hypoattenuating streaks in the image. The cause of these artifacts is complex, as they are produced by a combination of beam hardening and edge gradient effects. The edge gradient artifact is seen in dense objects that have sharp borders (i.e. high spatial frequency) and irregular geometry, as different x-ray beam orientations will cause different degrees of x-ray attenuation. Thus, the data acquired by different detectors will seem incompatible with each other during the reconstruction process, and this will produce streaks extending from sharp edges with high density differences.[348]

4.6.5 CT imaging parameters specific to foreign bodies

Wooden foreign bodies are often hypoattenuating and can mimic gas pockets when viewed with a narrow (soft tissue) window.[131,144] Because of this, a wide window width, such as a bone window (e.g. 1000 HU), is recommended for recognition of a wooden object.[124,129,131,139] A lung window can also be used to identify wooden foreign objects:[107] a window width of 1000 HU and window level of -500 HU demonstrates that these hypoattenuating wooden foreign objects are hyperattenuating to gas and easily delineated from the surrounding tissues (which are displayed with a relatively light shade).[131] For evaluation of possible wooden foreign bodies in the orbit, a window width of 1000 HU with a window level of 0 HU or 35 HU has been advocated, as this allows for differentiation of wood from fat.[313] Another study found that dry pine could be most easily differentiated from gas, fat, and fluid at window width 1000 HU and window level -500 HU; this window in combination with window width 214 HU and window level 19 HU has been suggested for differentiating fresh pine from gas, fat, and fluid.[312] With a wide window, striations or reticulations in the wood may also be identified.[129,139]

Three-dimensional CT is beneficial in identifying and localizing foreign objects as it allows for evaluation of the objects in multiple planes.[363] Foreign objects are often best localized relative to palpable landmarks or other structures with the use of multiplanar or three-dimensional reformatting.[107]

4.6.6 Appearance of inflammation & foreign bodies

On CT, structures are described by their x-ray attenuation. Structures that attenuate many x-rays appear white on the image, and are referred to as hyperattenuating (hyperdense in some

literature). Hypoattenuating (hypodense) structures attenuate few x-rays, and are displayed as black.

Wooden foreign objects are variable in their appearance on CT. Small wooden objects, and especially dry wooden objects, are commonly hypoattenuating to the surrounding tissues and can mimic foci of air because much of the volume of dry wood is air.[9,18-20,129,131,139,140,144,210,244,313,364] One study found that dry wood that was imaged with CT less than one day after injury was hypoattenuating to fat, although dry bamboo imaged less than one day following injury was isoattenuating to the surrounding fat.[130] A cadaver study also found that wooden splinters that had been soaked in saline for 3 days prior to insertion were hypoattenuating to the surrounding musculature.[25] Other authors note that the attenuation of plywood increased after soaking in water for 3 days (up to -67 HU), but that soaking of pine and oak had little effect on their CT numbers.[313] While air (-1000 HU) should be markedly hypoattenuating to wood,[244] measurement of the CT number may not help in determining if a small hypoattenuating focus represents air or wood, as partial volume averaging will prevent the acquisition of an accurate value.[128,131,313] Wooden structures may also be hyperattenuating to the surrounding skeletal muscle and fat (often described as greater than 100 HU),[19,123,124,128,129,134,209] especially when they have been present for a long period of time.[123,128,129,134,209] Intraorbital wooden foreign bodies that had been present for at least 8 days prior to CT were hyperattenuating to muscle, including one that had been hypoattenuating to fat when CT was performed less than one day after injury.[130] Similarly, a hypoattenuating wooden foreign body mistaken for air on the day of admission was seen as a hyperattenuating structure on a CT performed on day 4.[210] A bamboo foreign body was recognized as a cylindrical object with a rim that was hyperattenuating to the surrounding musculature (127 to 156 HU) and a hollow air-filled core.[127] The overall attenuation of wood on

CT is described as being due to the amount of air or other materials trapped within the cellulose matrix of the wood,[131] and increased attenuation of wooden foreign bodies within the body over time has been attributed to absorption of fluids (e.g. edema fluid) from the surrounding tissues changing the wood's hydration.[129] Absorption of blood products could also contribute to increased attenuation above 0 HU,[124,209] as could absorption of suppurative material.[209] Some authors claim that absorption of water would explain an increase only from low density to 0 HU (the density of water), and would not increase the density of a foreign object to 100 HU or greater.[128] Nonetheless, in one cadaver study, a soaked toothpick was noted to have the same attenuation as adjacent clotted blood, indicating that absorption of water alone was sufficient to increase the attenuation of the wood over 0 HU.[255] Also, wooden splinters that had been soaked in saline for 5 months before insertion into soft tissues were found to be hyperattenuating to muscle.[25] This finding is understandable if one postulates that partial volume averaging within the wooden object causes the averaging of the absorbed water (0 HU) and the structural components of the wood (e.g. cell walls, likely considerably more attenuating than water), yielding a measurement somewhat greater than water. Calcification of the wood within a foreign body granulomatous reaction could also occur and would be expected to increase the density of the object, but this mechanism has not been confirmed *in vivo*.[128]

Freshly cut (green) wood should have greater attenuation than dry wood due to its increased water content.[139] The CT number of freshly cut tree branches (-274 to -70 HU) was higher than that of dry wood (-984 to -356 HU), though could still be distinguished from a fat background.[313] Other studies have also demonstrated that both fresh and dry woods have CT numbers less than -100 HU.[244] Likely because of the increased attenuation of wet woods to a value more similar to body tissues, dry woods have been described as more easily detected than

wet woods with CT.[7] A study evaluating fresh (green) wood inserted into living dogs' orbits found that the objects could not be identified with CT, though the inflammation was.[315] The type of wood also affects its CT number: hard woods are more attenuating than soft woods.[139] Surface coating or treatment of the wood will also affect its density.[129] As with MRI, the elongated linear shape and sharp margination of a wooden foreign body aid in recognition.[131,144] Wooden foreign bodies are usually cylindrical, so when the object is parallel to the axis of the part scanned, they will appear as circular structures seen in multiple adjacent slices.[107,123] Striations within the wood may also be seen with CT, especially with use of a wide window.[107,129] Additionally, wooden objects may have a target appearance when imaged transversely; this appearance is thought to be due to inflammatory tissue adjacent to the surface of the wood[107] or could represent absorption of fluid by the wood's surface.[143] Certain types of wood may also inherently have this appearance: in one *in vitro* study, both pine and walnut were described as having a hypoattenuating core encircled by hyperattenuating rings.[313] The appearance of grass awns is poorly described, as migrating intrathoracic grass awns were detected with CT in only 4 of 14 cases evaluated.[196]

In studies evaluating CT attenuation of wood *in vitro*, the CT number of individual specimens was found to be quite variable.[143] Values obtained for different types of wood are given in Table 2.2.[143,312,365] As can be seen, soft woods generally have lower attenuation values than hard woods. The density of wood varies markedly by species;[366-369] the density differences in different species of wood may be due to different cell sizes and cell wall composition.[143] The hydration status of wood is also important, as absorption of water causes increased attenuation by wood.[143,365] For example, the surface of a dry spruce plank immersed in water for 28 days changed from -463 HU when dry to -86 HU after immersion, and the inner portion of the wood changed from -473 HU to -205 HU.[143] Other variables reported to affect the density of wood

include the soil in which a tree grows, the stage of life of a tree (old trees have denser wood than young trees), the degree of decay (decay increases porosity), and the season (wood's specific gravity is lower in the spring than in the fall).[143] The density of wood is also higher in the pith of a tree than it is near the bark,[370-372] and fertilization has been shown to decrease the overall density of wood (though the amount of growth was greater in fertilized trees).[370] Wood density also decreases with increasing altitude[368] and increases with increasing temperature and rainfall.[372] Wood density is also dependent on its height within the tree, as density decreases from the butt of the tree to the top.[373] Wood density of a species is negatively correlated with leaf size.[374]

Table 2.2: Attenuation of Different Species of Wood Under Different Conditions

Wood	Lowest density (HU)	Mean density (HU)	Highest density (HU)
Pine (dry)	-649	-461	-136
Pine (dry)		-656	
Pine (fresh)	-550		20
Pine (fresh)		-24	
Pine (soaked 60h)	-644	-376	-61
Spruce (fresh)	-320		-15
Birch (fresh)	-250		130
Aspen (fresh)	-540		-330
Ebony (dry)	-6		289
Live Oak (dry)	-187	-88	-13
Live Oak (soaked 60h)	-117	69	198
Red Cedar (dry)	-436	-320	-129
Red Cedar (soaked 60h)	-328	-218	-79
Dogwood (dry)	-321	-198	-102
Dogwood (soaked 60h)	-8	59	144
Wax Myrtle (dry)	-457	-328	-157
Wax Myrtle (soaked 60h)	11	66	144
Pencil wood (dry)	-748	-394	880
Pencil wood (soaked 60h)	-469	-156	804

Note: Data were obtained from references [143,312,365]

Metallic foreign bodies, such as needles, are easily identified with CT. Metallic structures are markedly hyperattenuating, and their shape is best visualized with a (wide) bone window.[107] Metallic objects also commonly produce streak artifacts, which are more easily recognized on a (narrow) soft tissue window.[107] When there are large metallic objects retained, such as retained surgical instruments, CT will demonstrate a markedly hyperattenuating structure with beam hardening artifact;[363] iron is described as >3000 HU.[244] Similarly, amalgam has been described as hyperattenuating material that produces hyper- and hypoattenuating streak artifacts.[9] Retained glass foreign bodies are easily detected as well defined hyperattenuating objects that may be less attenuating than mineral foreign bodies[7,9] and tend to have a CT number of 1000 to 1300 HU.[244] While glass foreign bodies are generally visible with most modalities, one case report found that fine, sand-like glass fragments were best visualized with CT, and could not be reliably detected with ultrasound.[145] Teeth, asphalt, gravel, and stones are also easily recognized as hyperattenuating structures.[7,9] Graphite is also markedly hyperattenuating, measuring 600 to 800 HU.[244] Plastic can be difficult to identify with CT, but can be detected as a hypoattenuating structure with a density of -55 to -100 HU.[7,244,364]

Gossypibomas are generally described as well circumscribed masses on CT[163,164,173] and are hypointense to the surrounding musculature.[169] The mass may be relatively homogeneous on CT,[163] though multiple coarse dense calcifications may be present within the mass.[169] In one study of 13 cases, all cases had a hyperattenuating, non-enhancing, sharply marginated rim surrounding the gossypiboma,[173] but heterogeneous rim enhancement has also been described in gossypibomas.[164,169] CT imaging characteristics do not necessarily allow for differentiation of a gossypiboma from a hematoma or abscess, and in the previously mentioned retrospective study of 13 gossypibomas evaluated with CT, the authors noted that three cases had been initially

misdiagnosed.[173] Even in the nine cases with radiopaque markers in the sponge, diagnosis was not always conclusive, as the radiopaque filament was misinterpreted as pleural calcification in one case and the mineralized rim of a hematoma in another.[173] However, a "spongiform pattern" of gas bubbles may be useful in leading to a diagnosis of retained surgical sponge: this pattern was present in 7 of 13 cases, and the bubbles did not correlate with intestinal perforation or abscess formation.[173] This gas bubble pattern was also repeated on in vitro CT scans of surgical sponges placed in a water bath.[173] Another feature that is reported as characteristic of a gossypiboma is the "calcified reticulate rind" sign: this sign is described as a mass with a thick mineralized wall and calcified reticulations within the mass, thought to represent a gradual deposition of mineral along the fibers of the foreign object.[170] As with radiography, secondary changes including periosteal thickening in adjacent bones can also be recognized on CT in patients with a gossypiboma.[169]

Foreign objects are generally surrounded by inflammation. The inflammatory reaction surrounding orbital foreign bodies has been described as a homogeneous mass with a density similar to the surrounding muscles (approximately 40 HU); granulomatous tissue and pus could not be differentiated with CT.[128] In some cases, the foreign objects may not be identified, and only the inflammatory mass will be recognized. Poor recognition of foreign bodies may be due to their small size or because the density of the wood (including water content) is the same as the density of the inflammatory response.[132,375] The inflammatory response itself may be difficult to distinguish from surrounding musculature, as the attenuation characteristics may not change significantly, but effacement of fat planes may indicate the presence of inflammation.[124] However, in some cases the inflammatory mass has mixed attenuation characteristics with or without heterogeneous contrast enhancement;[107] foreign body reactions have been described as

having a pseudotumor appearance.[107,124] Soft tissue trauma caused by a foreign body may cause muscle edema; edematous muscle is generally hypoattenuating (average 36 HU) to normal musculature (average 67 HU).[127] Soft tissue tracking of a foreign object may be identified, and the migration path may have contrast-enhancing margins.[196] Secondary changes, such as osteolysis and new bone production on adjacent bones, can also be seen.[107,123] When foreign body migration involves the thoracic cavity, secondary changes seen on CT can include pneumothorax, pleural effusion, pneumomediastinum, lymph node enlargement, and focal interstitial or alveolar pulmonary densities.[196] A body wall mass may also be identified.[196]

Using CT, cellulitis appears as thickening of the skin and superficial fascia with septation of the subcutaneous fat.[376] If cellulitis progresses to necrotizing fasciitis, deeper structures are affected, and there is usually gas seen in the soft tissues due to the presence of gas-forming bacteria.[376] Osteomyelitis appears as areas of decreased attenuation and coarse trabeculae in the medullary cavity, focal lysis of cortical bone, and periosteal reaction with adjacent soft-tissue swelling.[376] Though rare, an extramedullary fat-fluid level is specific for osteomyelitis.[376] CT can also be used to detect sequestra and involucra, although MRI is considered better for determining the viability of a sequestrum.[376]

Contrast-enhanced CT uses intravenous administration of an iodinated contrast agent to improve visualization of blood vessels and lesions, such as inflammation and neoplasia.[305] Because iodine has relatively high x-ray attenuation, tissues and organs in which it collects will appear hyperattenuating to (whiter than) their appearances on pre-contrast images.[305] When imaging the brain, the blood-brain barrier (BBB) prevents passage of contrast media across capillary walls, so normal brain parenchyma is non-enhancing (the only enhancement is within vessels themselves).[321] However, when there is breakdown of the blood-brain barrier, as with

inflammation or oxidation damage seen with hematomas, contrast medium will cross into the brain parenchyma and cause contrast enhancement.[322] Similarly, some neoplasms (such as metastatic disease) form capillaries with fenestrated endothelial cells, so these tumors will enhance, though others (such as low grade gliomas) may produce capillaries with an intact blood-brain barrier, thus preventing enhancement of these tumors.[321] Outside the brain, there is not a barrier preventing leakage of contrast media out of capillaries. However, pathologic tissues such as inflammation or neoplasia will still often exhibit contrast enhancement because they frequently possess increased viable vasculature;[323,324] these vessels may also be abnormal or damaged with increased permeability.[325,326] Conversely, areas of necrosis or no perfusion will demonstrate minimal or no contrast enhancement.[323,324] Because steroids protect the blood-brain barrier by decreasing free radical production and increasing repair of membrane damage, the decreased permeability of the BBB in patients given steroids will result in decreased enhancement of the brain parenchyma.[322] Similarly, glucocorticoids generally increase vascular tone, though vessel responses to steroids depend on the local environment.[327] Thus a regional increase in vascular tone may cause a decrease in perfusion and a corresponding decrease in contrast enhancement regardless of the location of a lesion.

4.6.7 Appearance of an evolving abscess

An abscess appears as a sharply marginated collection of hypoattenuating fluid with a pseudocapsule.[376] The outer layer exhibits rim enhancement following administration of contrast medium.[376]

Specific imaging characteristics of an abscess depend on both its age and etiology. Brain abscesses can be considered to progress through four phases: early cerebritis (1-4 days), late

cerebritis (4-10 days), early capsule formation (11-14 days), and late capsule formation (greater than 14 days).[304] There is often a large amount of hypoattenuating edema surrounding brain abscesses, usually beginning in the late cerebritis phase.[304] In the cerebritis phases, an abscess may be recognized only as a hypoattenuating region with mass effect.[304] However, during the capsule formation stages a rim around the hypoattenuating center can be identified, and uniform ring enhancement is also seen in these stages.[304]

4.6.8 Appearance of an evolving hematoma

It is recognized that hemorrhage is hyperattenuating to surrounding tissues, such as brain tissue. The CT number of blood is directly related to the hematocrit of the blood: for example, in one *in vitro* study, blood with a hematocrit of 10% had an attenuation of 34 HU, while blood with a hematocrit of 50% had an attenuation of 60 HU.[377] Normal human venous blood has been found to be between 48-65 HU.[378] A considerable amount of the x-ray attenuation of blood is due to the effects of the hemoglobin. Most of the attenuation of hemoglobin is due to the protein (globin) component; the iron component contributes only 7-8% of the overall attenuation of hemoglobin.[377] An *in vitro* study found that, like hematocrit in whole blood, hemoglobin concentration has a linear relationship with x-ray attenuation: a hemoglobin concentration of 3g/100mL water had an attenuation of 8 HU, and a hemoglobin concentration of 15g/100mL water had an attenuation of 40 HU.[377] Because serum is considerably less attenuating (24 HU) than the cellular component of blood, and the effective hematocrit of a clot increases over the first 1-2 days as the serum is extruded from the clot and resorbed by the surrounding tissues, an even more hyperattenuating structure is produced as a clot organizes.[377]

Studies have demonstrated that hematomas are initially high in attenuation values, but decrease over time. For example, in one study intracranial hematomas less than 24 hours old had attenuation values of 75 HU, decreasing to approximately 45 HU (equal to the value of cortical gray matter) at 4-9 days, and decreasing further to 35 HU (equal to white matter) at 2-3 weeks.[378] After intracranial hematoma formation, the maximum attenuation value of the hematoma decreased by approximately 1.4 HU per day, and the more attenuating portion of the hematoma decreases in size by 0.65mm per day (though mass effect did not necessarily diminish as rapidly).[379] *In vitro* evaluation of blood clot progression found that the clot began retracting quickly, with clear demarcation between the higher-attenuation clot and the lower-attenuation peripheral serum as early as 3 hours; the maximum attenuation value of the clot (an increase from 60 to 76 HU) was reached in approximately 20 hours.[378] In a study of extracranial hematomas, 87% of those evaluated within the first 72 hours were hyperattenuating, while only 50% were hyperattenuating at 7 days and none were hyperattenuating by 40 days.[380] From 2-8 weeks, hematomas may be isoattenuating or hypoattenuating to brain parenchyma; the decrease in attenuation starts peripherally and progresses toward the center.[377] The decreased attenuation of a hematoma over time is likely due to breakdown of red blood cells and the removal of blood products (e.g. proteins) from the site by phagocytes, though edema fluid may also diffuse through the clot and decrease the attenuation as well.[377] Contrast enhancement due to neovascularization can be seen at the periphery of a hematoma at approximately 4-6 days following the inciting cause; rim enhancement may be visible for up to 6 weeks.[340]

Based on the CT imaging characteristics of resolving intracranial hematomas, six stages of resorption have been identified. Stage I is seen for 1-10 days following the initial onset of symptoms. In this stage, the hematoma is hyperattenuating (70-90 HU) and sharply marginated

with a thin hypoattenuating rim and no enhancement following administration of contrast medium. Stage II hematomas (seen from day 3-20) have decreasing attenuation and are less well marginated than stage I hematomas. The hypoattenuating rim is larger in a stage II hematoma, and ring enhancement is seen with contrast medium administration. This enhancement can be decreased via corticosteroid administration. At stage III (18-64 days), the hematoma is isoattenuating to the surrounding brain parenchyma. Ring enhancement that can be modified with steroids remains. The hematoma is hypoattenuating in stage IV (35-70 days), but the enhancement characteristics remain similar to those in stages II and III. Stage V occurs from 42-84 days, and is seen as a hypoattenuating structure with rim enhancement that is not decreased with steroid administration. Stage VI represents a healed hematoma and may be seen at 84-240 days. This hematoma may be isoattenuating or hypoattenuating without contrast enhancement; calcification and ipsilateral brain atrophy may be recognized.[322]

4.7 Multimodality comparisons for imaging of foreign bodies

Multiple studies have been performed to evaluate the visibility of different foreign bodies in different tissue types and in different anatomic locations using various modalities. However, the conclusions reached from these studies are variable and are often at odds with each other. Ultrasound,[8,9,22,24-26,250,276,286-288,381] computed tomography,[7,9,26,244,255] magnetic resonance imaging,[7,25,313,364] and xeroradiography[254] have all been advocated as beneficial in visualizing radiolucent foreign bodies (though the benefits of xeroradiography were later debunked[5,381]). Digital volume tomography, a method of cone-beam CT allowing for volume acquisitions of data, has also been supported, although this modality performed worse than conventional CT in one study.[382] Nonetheless, clinically applicable studies are limited in number. For example, many

studies were performed using simple tissue models that may not provide the challenge of the anatomic complexity, including vegetable oil,[313] beef cubes,[288] steak strips,[381], cow tongues,[9] and sheep necks.[383] Eyeballs from various species have also been used,[244,364] and while this is an appropriate model for ocular injury, the findings may not correlate with imaging results in more complex anatomic areas (i.e. those containing bones, muscles, tendons, and ligaments). In the interest of creating a model with greater anatomic complexity, animal and human parts with muscle and bone have been used: these include lamb shank,[254] chicken and turkey thighs,[10,26,250,251,286,384], and porcine shoulders,[25] but even these do not contain the multiplicity of small complex structures seen in the distal extremity. Similarly, use of human cadaver limbs[255,287,385] may not account for the importance of the bones as a confounding structure in diagnosis of foreign objects if the test objects are placed superficially. Only three studies have evaluated the conspicuity of foreign objects in the human hand in clinical patients,[5,22,23] and there are four studies evaluating visualization of foreign objects in cadaver human hands and feet.[7,8,21,24] However, these studies are also limited: three of them assess visibility with only a single modality,[22-24] only ultrasound and radiography were compared in another,[8] and only radiography and xeroradiography were evaluated in a fifth.[21] The retrospective nature of one clinical study means that different modalities were not used to attempt to diagnose the same objects.[5] The most comparative of the seven distal extremity studies omits ultrasound, perhaps the most commonly used modality in detection of foreign objects outside of radiography, and used large foreign objects that protruded from the hand and are of questionable clinical applicability due to their size.[7]

Despite advocacy for use of ultrasound, CT, and MRI for diagnosis of radiolucent retained foreign bodies, only three studies evaluate all three of these modalities simultaneously.[9,25,26]

These studies found that the best modalities to use for diagnosis of a foreign body when radiography is inconclusive are ultrasound and CT[9,26] or ultrasound and MRI.[25] However, these studies are also limited, as none of the experiments were performed in specimens as complex as the distal extremity.

Specific details from the visualization studies are presented in Appendix B: Foreign Body Imaging Comparisons in the Literature.

Chapter III

Computed Tomography, Magnetic Resonance Imaging, and Cross-Sectional Anatomy of the Normal Canine Manus

Christopher P. Ober
Larry E. Freeman

A version of this chapter has been accepted by the *American Journal of Veterinary Research*. (Ober CP and Freeman LE. Computed tomography, magnetic resonance imaging, and cross-sectional anatomy of the normal canine manus. *American Journal of Veterinary Research*, in press.)

1. Abstract

Objective – To develop a computed tomography (CT), magnetic resonance (MR) imaging, and sectional anatomic atlas of the normal canine manus.

Animals – Seven normal adult mixed breed dog cadavers weighing between 25 and 30 kg.

Procedures – The front limbs of three large breed dog cadavers were cut into 4mm sections using a band saw, with one limb each sectioned in the transverse, dorsal, and sagittal planes. Sections were then photographed. The front limbs of three additional large breed dog cadavers were imaged transversely using CT. A seventh large breed dog was imaged in the transverse, sagittal, and dorsal planes using MR imaging. CT, MR imaging, and anatomic sections were correlated, and clinically pertinent anatomy was labeled on all images.

Results – Most of the anatomic structures identified on the anatomic sections could also be identified on the CT and MR images. Osseous and musculotendinous structures were easiest to detect, while vascular structures were only rarely identified with the imaging techniques used.

Conclusions and Clinical Relevance – The provided images will allow for improved recognition of normal structures of the canine manus and will be beneficial in surgical planning for diseases of the distal limb.

2. Introduction

The canine paw is a frequent site of disease, especially in working dogs, and common pathologic conditions of the manus and pes include trauma, infection, and neoplasia.[1,2,6,386,387] Because surgical exploration is required for many of these conditions, recognizing the precise location of the disease is of critical importance. This is especially true in the case of foreign objects, where the foreign body may migrate and produce a draining tract distant from the original site of insertion. One study found that patients underwent a mean of two surgical procedures to attempt treatment of a draining tract prior to presentation to a referral hospital.[4] Studies also show that the mean duration of clinical signs in dogs with draining tracts was nearly 10 months prior to referral,[4] and average time of retention of a foreign body in the human hand is 7 months.[5] Accurate and efficient localization of pathology is critical to minimize patient morbidity, and multiple different imaging modalities have been utilized in detecting diseases of the manus. The increasing availability of cross-sectional imaging modalities such as computed tomography (CT) and magnetic resonance (MR) imaging has led to increasing use of these modalities in imaging the canine manus.

The increasing use of CT and MR imaging for the canine manus requires understanding of all of the soft tissue and osseous structures in the distal extremity. However, only one reference known to the authors is available to describe the normal cross-sectional anatomy of the canine manus, and the primary focus in this reference is placed on the osseous structures.[388] The purpose of this study was 1) to produce a CT and MR imaging atlas of the soft tissues and osseous structures of the canine manus and correlate imaging findings to sectional anatomy, and

2) to determine which structures of the canine manus could normally be seen using sectional imaging.

3. Materials and Methods

Six large-breed dog cadavers were obtained from a local animal shelter following euthanasia, and both thoracic limbs of each dog were amputated. Hair on the distal limbs was clipped after amputation. All limbs were harvested within 4 hours of euthanasia, and were frozen in a walk-in freezer immediately following amputation. The limbs remained frozen for variable amounts of time.

Right thoracic limbs from three of the cadavers were used for preparation of anatomic sections. The limbs were sectioned at 4mm intervals while frozen, with one limb each sectioned in the transverse, sagittal, and dorsal planes. Anatomic sections were then cleaned and photographed.

Both thoracic limbs from the remaining three cadavers were allowed to thaw, then were imaged using CT. Computed tomography was performed with a single-slice helical scanner.* For each dog, both thoracic limbs were placed in the gantry with the palmar surface on the table. Transverse images of the manus were obtained using 1.5mm slice thickness and 0.5mm index using a modified extremities protocol (200 mA, 120 kVp, 180 mm field of view, 512x512 matrix, small focal spot, standard reconstruction algorithm). Images of the right thoracic limbs were used for correlation with anatomic sections.

A seventh large-breed dog was euthanized for reasons unrelated to disease of the thoracic limbs, and the body was donated to the Virginia-Maryland Regional College of Veterinary

Medicine. The right thoracic limb was amputated during postmortem examination, and subsequent MR imaging of this limb was performed with a 0.2T magnet.† The manus was placed in an extremity coil with the palmar surface closest to the table. Sequences obtained included transverse, sagittal, and dorsal planar T1-weighted spin echo sequences (2.5mm slice thickness, 0.2mm spacing, TE 26) in the transverse (TR 2250, NEX 2), sagittal (TR 1150, NEX 1), and dorsal (TR 950, NEX 1) planes. A transverse high-resolution gradient echo sequence was also obtained (2.0mm slice thickness, 0.2mm spacing, TE 16, TR 1720, NEX 3). Field of view for all MR sequences was 140mm, and a 256x192 matrix was used.

The CT and MR images were evaluated and matched to the corresponding anatomic sections. CT images were evaluated in both a soft tissue window (window level 40, window width 350) and a bone window (window level 480, window width 2500). Relevant structures were labeled in the CT, MR imaging, and anatomic images.

4. Results

Seven transverse CT and MR images of the right canine manus extending from the proximal phalanges to the distal carpal row were matched with corresponding anatomic sections. Numbered lines on Figure 3.1, a dorsopalmar radiograph, represent the approximate locations of the transverse images (Figs. 3.2-3.8). On the transverse images, lateral (right) is to the reader's left, and dorsal is at the top of the image. Sagittal CT and MR images of the manus through the second metacarpal bone and digit were obtained and correlated with an equivalent anatomic section (Fig. 3.9). On the sagittal images, dorsal is to the reader's left and proximal is at the top of the image. A dorsal MR image of the manus was obtained through the middle of the manus,

and was also correlated with an equivalent anatomic section (Fig. 3.10). On dorsal planar images, lateral (right) is to the reader's left and proximal is at the top of the image. Clinically relevant structures were labeled in all figures, and the legend is available in Table 3.1.

Most osseous structures were easily identified with both imaging modalities. All bones, including the sesamoid bones, were recognized in the CT images as markedly hyperattenuating structures. Cortical bone on MR imaging is identified as a structure with low signal on gradient echo sequences and no signal on spin echo images. The carpal bones, metacarpal bones, and phalanges were easily identified using MR imaging. The proximal sesamoid bones and the sesamoid in the abductor pollicis longus tendon were also identified on MR images. However, the dorsal sesamoid bones were only definitively visualized on the sagittal planar images, and could not be identified on the transverse planar images.

The interosseous muscles II-V, abductor digiti quinti muscle, and special muscles of the first digit could be identified using both CT and MR imaging. However, definitive fascial boundaries between these muscles were generally not seen with either modality. The adductor digiti II and adductor digiti V muscles were difficult to visualize due to their close proximity to the interosseous muscles, but could be seen on CT images in Figures 3.7 and 3.6, respectively, where they were surrounded by less attenuating tissue (likely fat). The smaller muscles of the manus, including the interflexorius muscle, flexor digitorum brevis muscle, lumbricales muscles, and flexor digiti V muscle, could not be identified with either modality due to their small size and the limited spatial resolution of the imaging techniques used in this study. Likewise, the individual muscle bellies of the three special muscles of digit I could not be resolved.

The superficial digital flexor, deep digital flexor, common digital extensor, and lateral digital extensor tendons could be identified throughout most of their length in the manus. These

structures are seen as ovoid structures which were slightly hyperattenuating to the surrounding soft tissues on CT images and markedly hypointense to the surrounding tissues on MR images.

Few vessels were visible using either of the imaging techniques. Palmar common digital artery III could be identified in the distal manus at the level of the metacarpal pad, where the artery is surrounded by sufficient fat to provide contrast. Although other palmar common digital arteries, the palmar interosseous artery, and the median artery could be identified in more proximal anatomic sections, these were not visible using CT or MR imaging.

Visibility of structures was similar on T1-weighted spin echo images and gradient echo images. Gradient echo images produced sharper margins of many structures, which in some cases helped differentiate these structures from the background tissues. However, this mild increase in visibility was generally offset by the apparent increase in anatomic complexity caused by the increased number of margins (e.g. fascial boundaries) seen on gradient echo images.

Table 3.1: Legend to Figures 3.2-3.10

Number	Structure	Number	Structure
1	Abductor digiti quinti muscle	24	Metacarpal I
2	Abductor pollicis brevis, adductor pollicis & flexor pollicis brevis mm.	25	Metacarpal II
		26	Metacarpal III
3	Abductor pollicis longus tendon	27	Metacarpal IV
4	Adductor digiti II muscle	28	Metacarpal V
5	Adductor digiti V muscle	29	Metacarpal pad
6	Carpal bone 1	30	Metacarpophalangeal joint
7	Carpal bone 2	31	Middle phalanx, digit II
8	Carpal bone 3	32	Palmar common digital artery II
9	Carpal bone 4	33	Palmar common digital artery III
10	Carpal pad	34	Palmar common digital artery IV
11	Common digital extensor tendon	35	Palmar (caudal) interosseous artery
12	Deep digital flexor tendon	36	Proximal digital annular ligament
13	Digital pad	37	Proximal interphalangeal joint
14	Distal interphalangeal joint	38	Proximal phalanx, digit II
15	Distal phalanx, digit I	39	Proximal phalanx, digit III
16	Distal phalanx, digit II	40	Proximal phalanx, digit IV
17	Dorsal sesamoid	41	Proximal phalanx, digit V
18	Extensor carpi radialis tendon	42	Proximal sesamoid
19	Interosseous muscle	43	Sesamoid in abductor pollicis longus tendon
20	Intersesamoidean ligament		
21	Lateral digital extensor tendon	44	Superficial digital flexor tendon
22	Manica flexoria	45	Ulnaris lateralis tendon
23	Median artery		

Note: mm = muscles

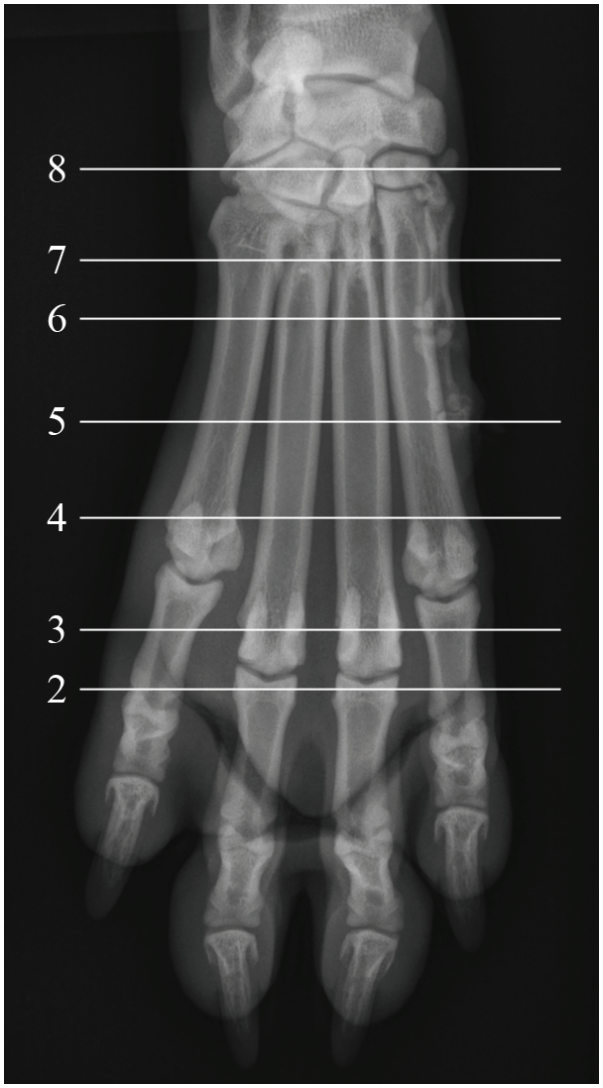

Figure 3.1: Dorsopalmar localizer radiograph of the right manus. Numbered lines correspond to the locations of the transverse images in figures 3.2-3.8.

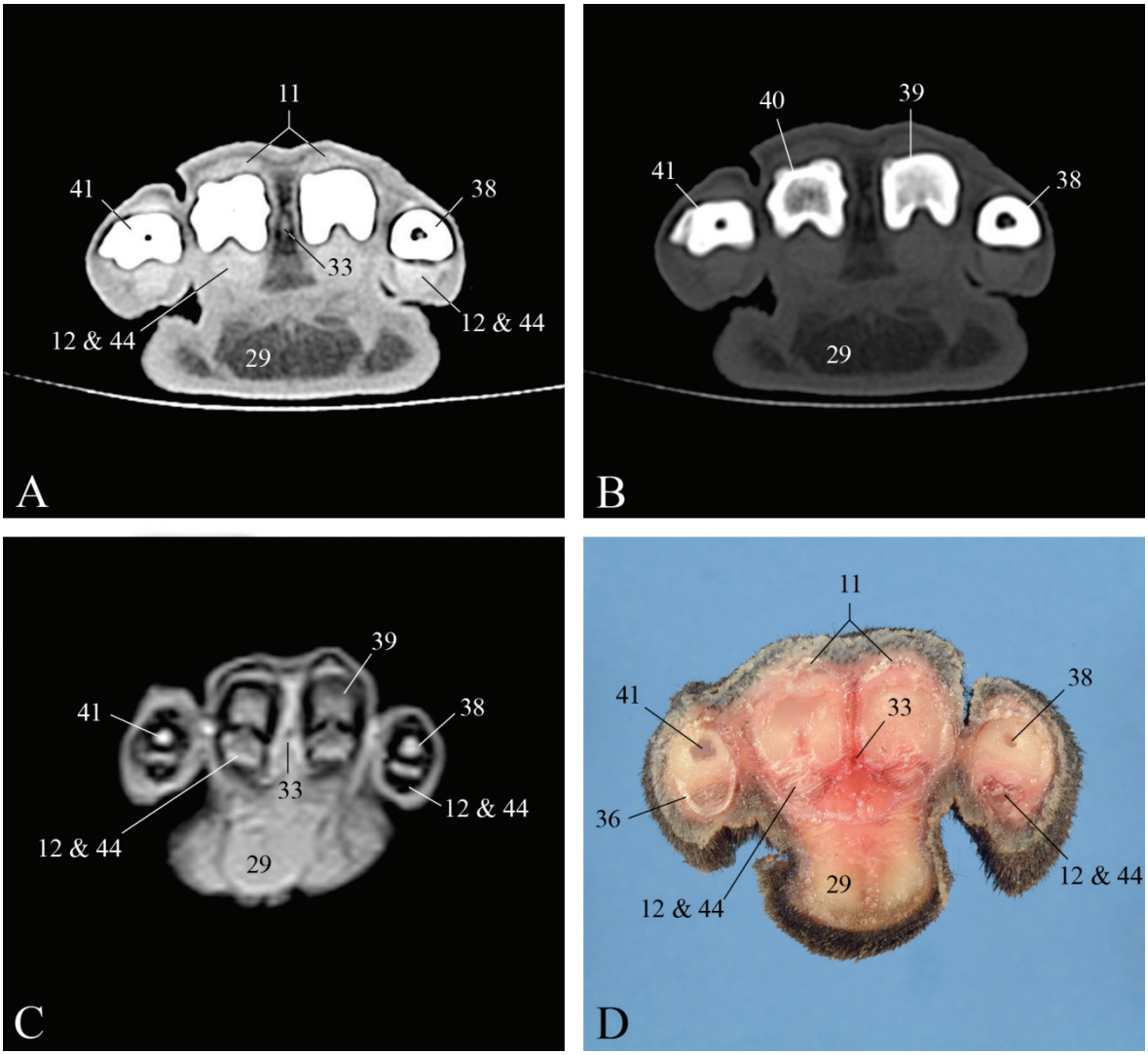

Figure 3.2: Transverse images of the right manus, with medial to the right of the image. (A) CT using soft tissue window, (B) CT using bone window, (C) T1-weighted MRI, (D) anatomic section. See Table 3.1 for legend. Note that the trilobed structure of the metacarpal pad (29) is not apparent in (D) due to the slightly more distal position of the slice through the pad relative to (A-C).

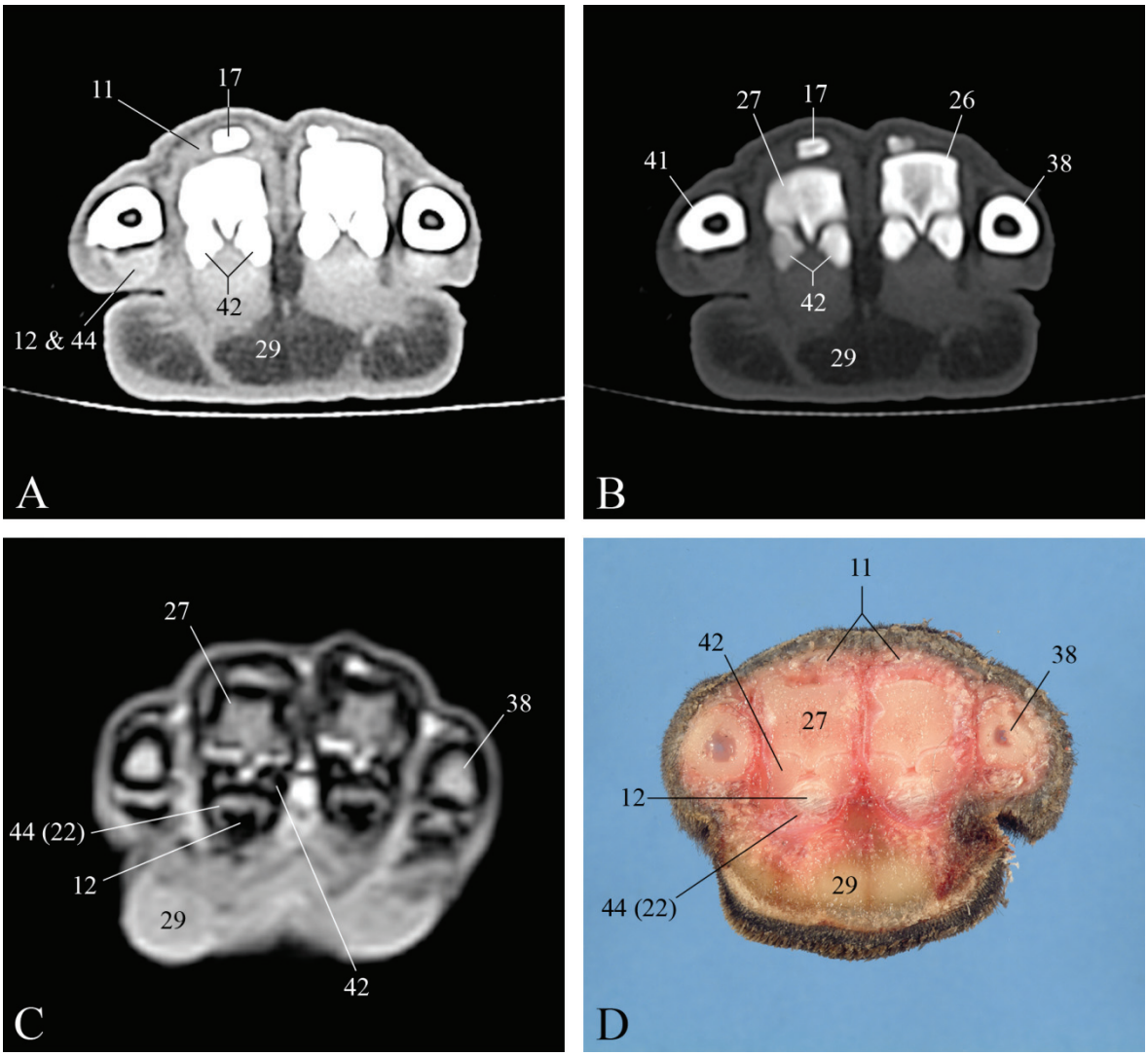

Figure 3.3: Transverse images of the right manus, with medial to the right of the image. (A) CT using soft tissue window, (B) CT using bone window, (C) T1-weighted MRI, (D) anatomic section. See Table 3.1 for legend. Note that the deep digital flexor tendons (12) become superficial to the superficial digital flexor tendons (44) distal to the manica flexoria (22).

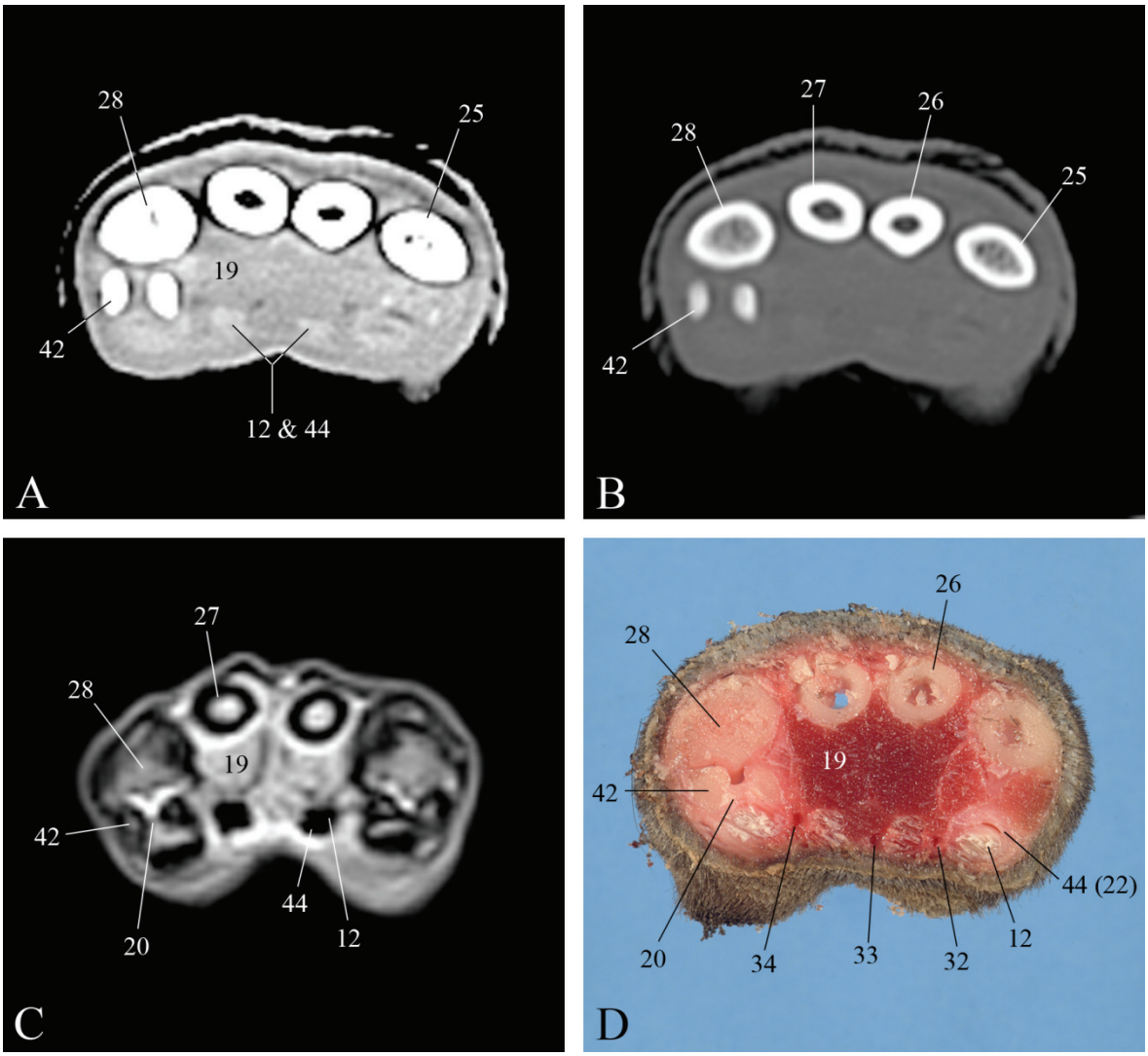

Figure 3.4: Transverse images of the right manus, with medial to the right of the image. (A) CT using soft tissue window, (B) CT using bone window, (C) T1-weighted MRI, (D) anatomic section. See Table 3.1 for legend.

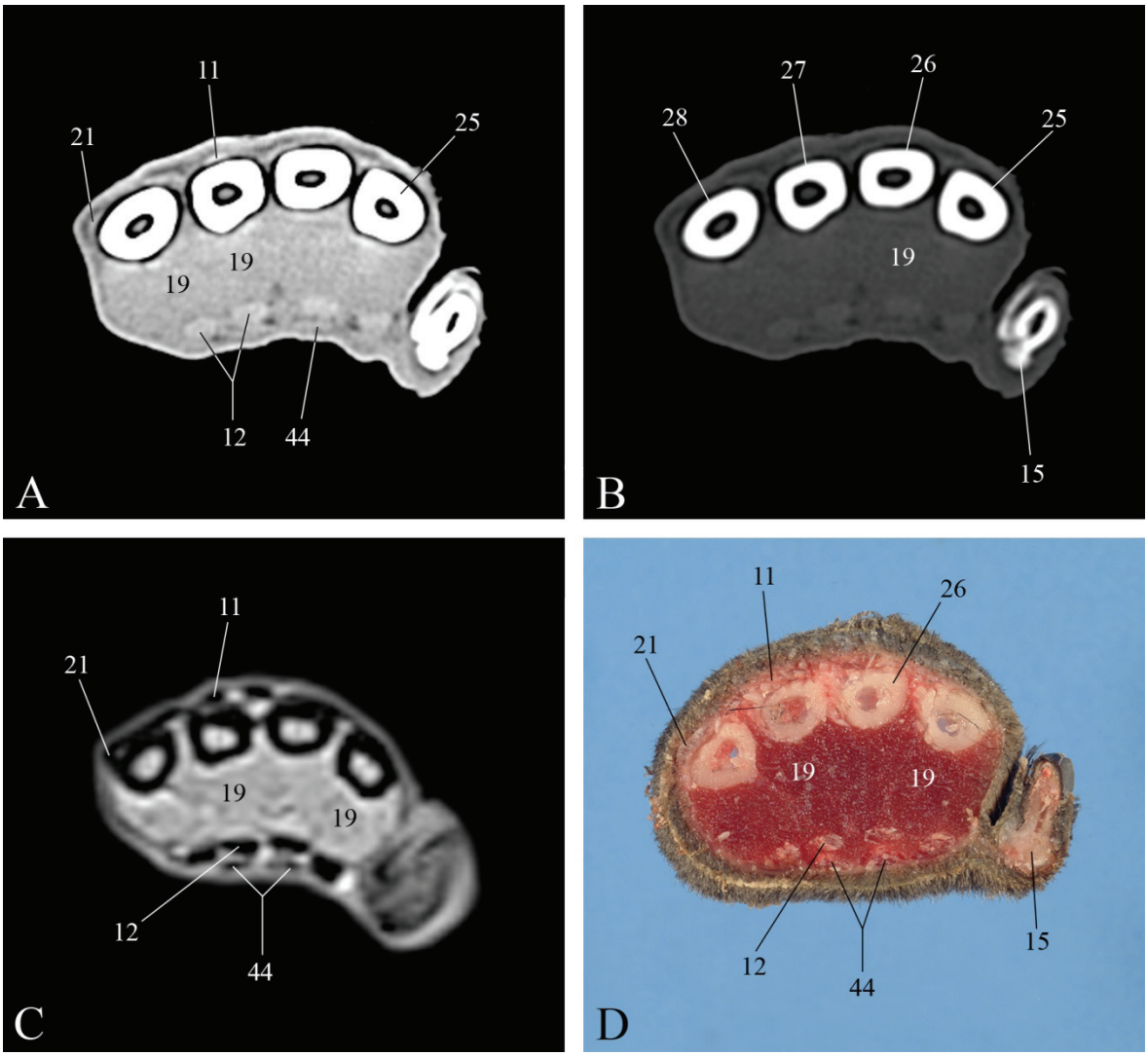

Figure 3.5: Transverse images of the right manus, with medial to the right of the image. (A) CT using soft tissue window, (B) CT using bone window, (C) T1-weighted MRI, (D) anatomic section. See Table 3.1 for legend.

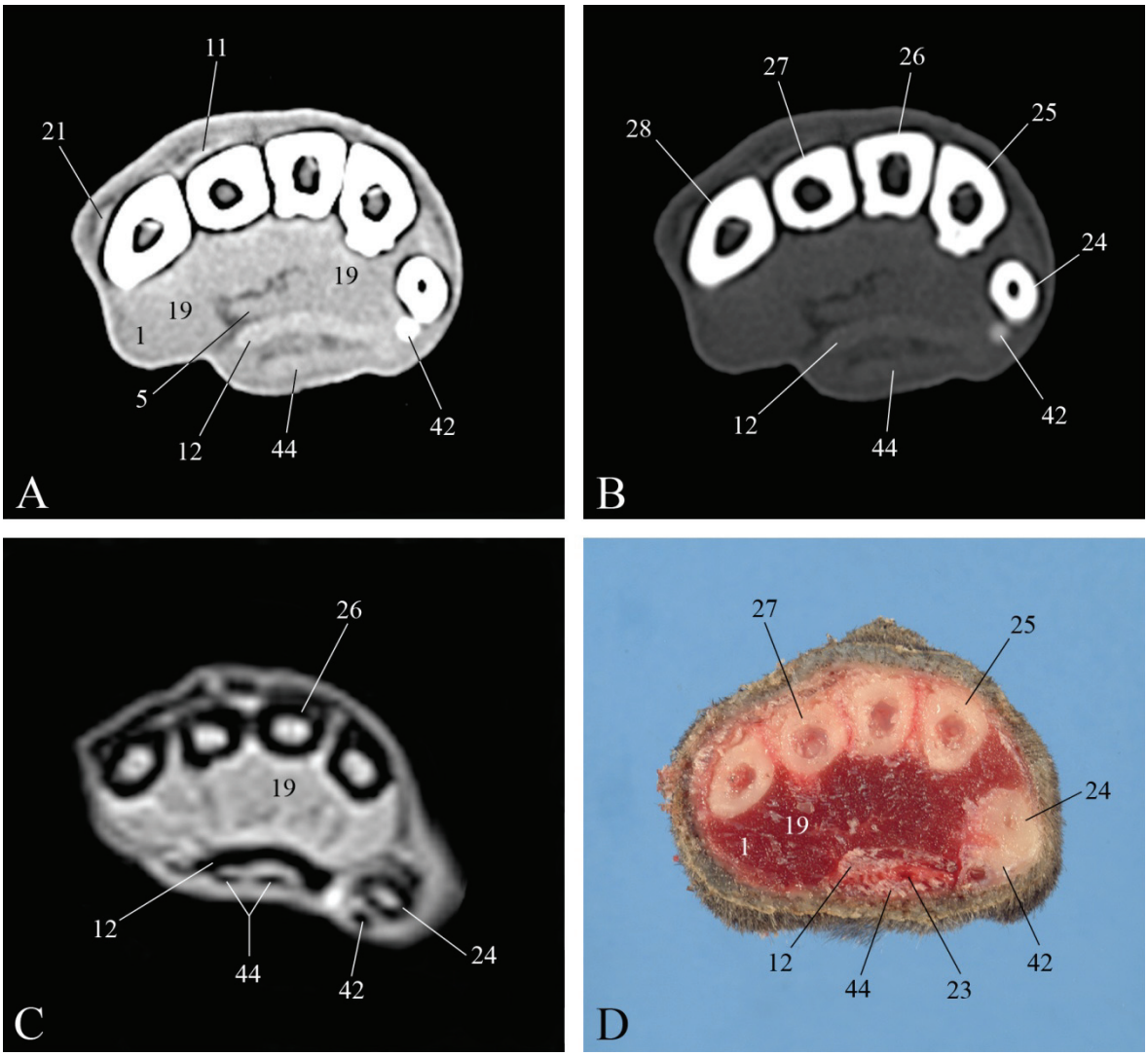

Figure 3.6: Transverse images of the right manus, with medial to the right of the image. (A) CT using soft tissue window, (B) CT using bone window, (C) T1-weighted MRI, (D) anatomic section. See Table 3.1 for legend.

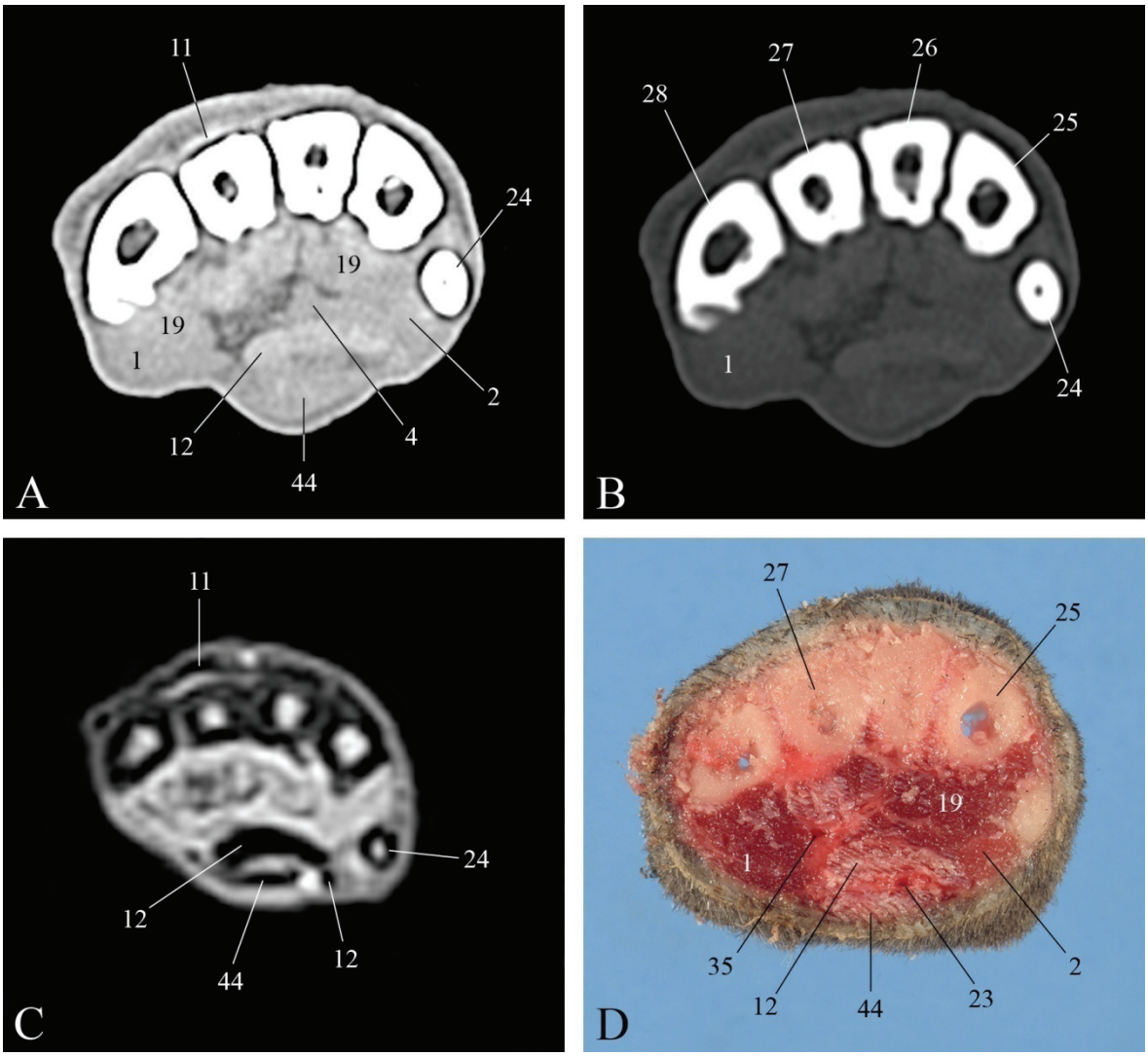

Figure 3.7: Transverse images of the right manus, with medial to the right of the image. (A) CT using soft tissue window, (B) CT using bone window, (C) T1-weighted MRI, (D) anatomic section. See Table 3.1 for legend.

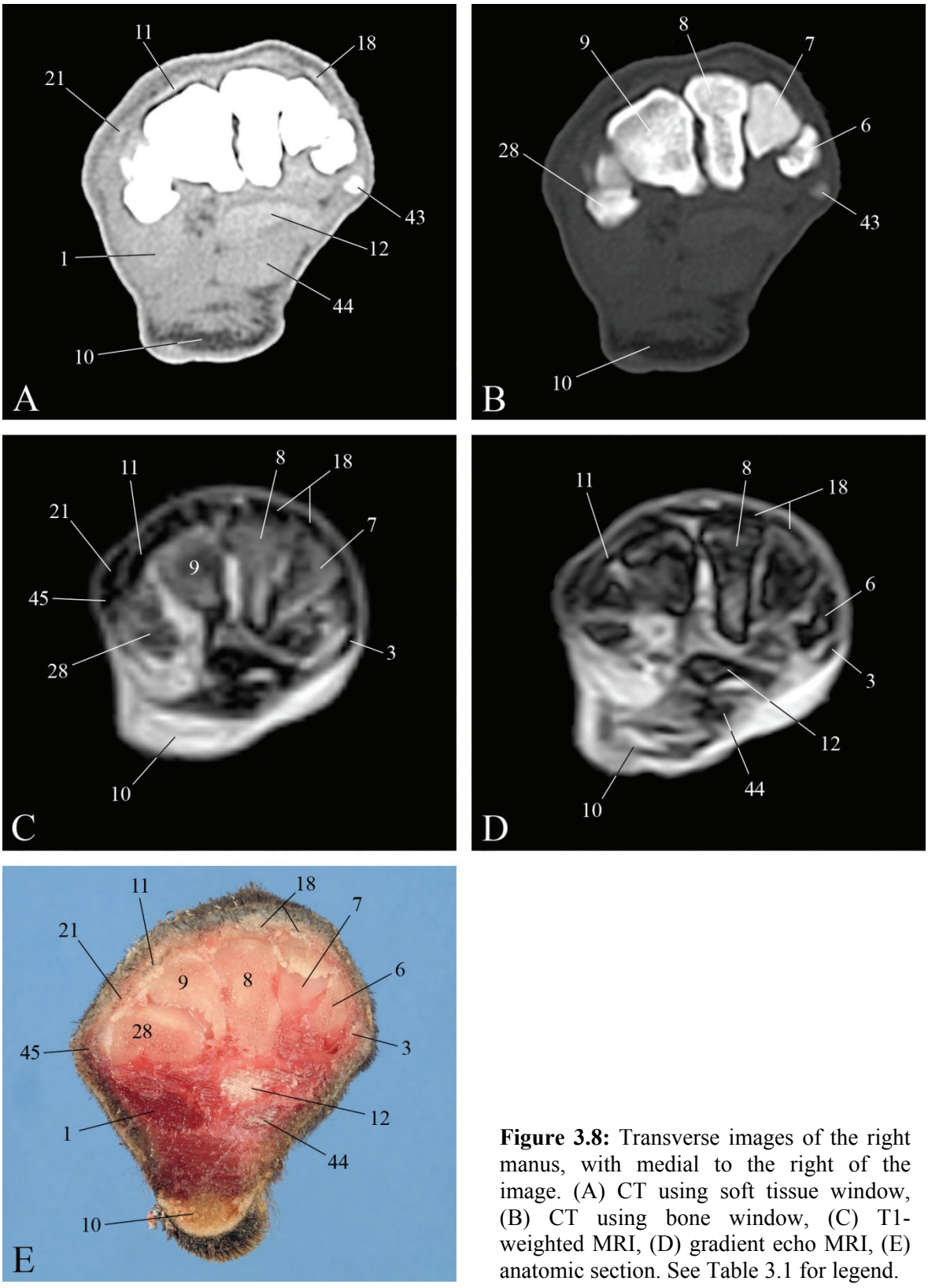

Figure 3.8: Transverse images of the right manus, with medial to the right of the image. (A) CT using soft tissue window, (B) CT using bone window, (C) T1-weighted MRI, (D) gradient echo MRI, (E) anatomic section. See Table 3.1 for legend.

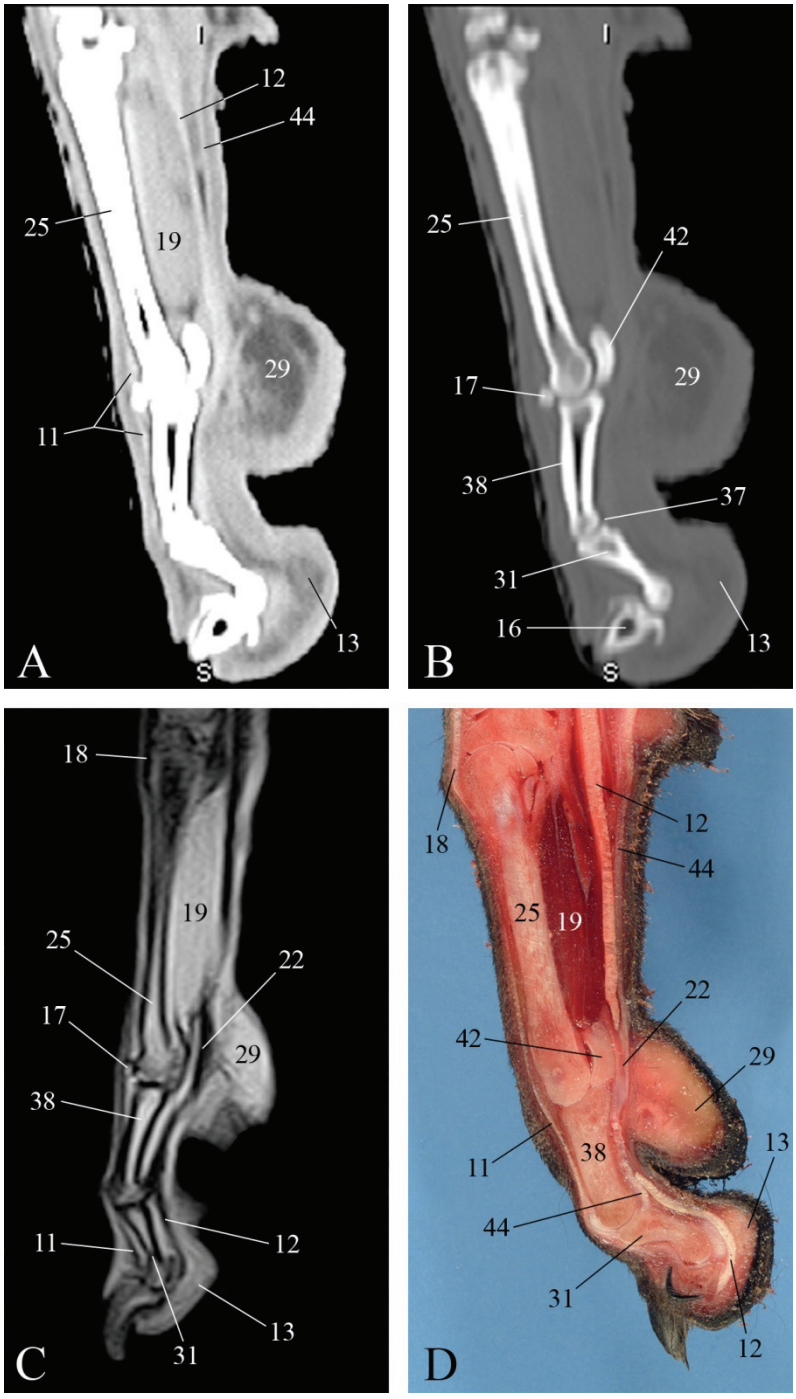

Figure 3.9: Sagittal images of the right manus, with dorsal to the left of the image. (A) CT using soft tissue window, (B) CT using bone window, (C) T1-weighted MRI, (D) anatomic section. See Table 3.1 for legend. Note that the deep digital flexor tendon (12) becomes superficial to the superficial digital flexor tendon (44) distal to the manica flexoria (22).

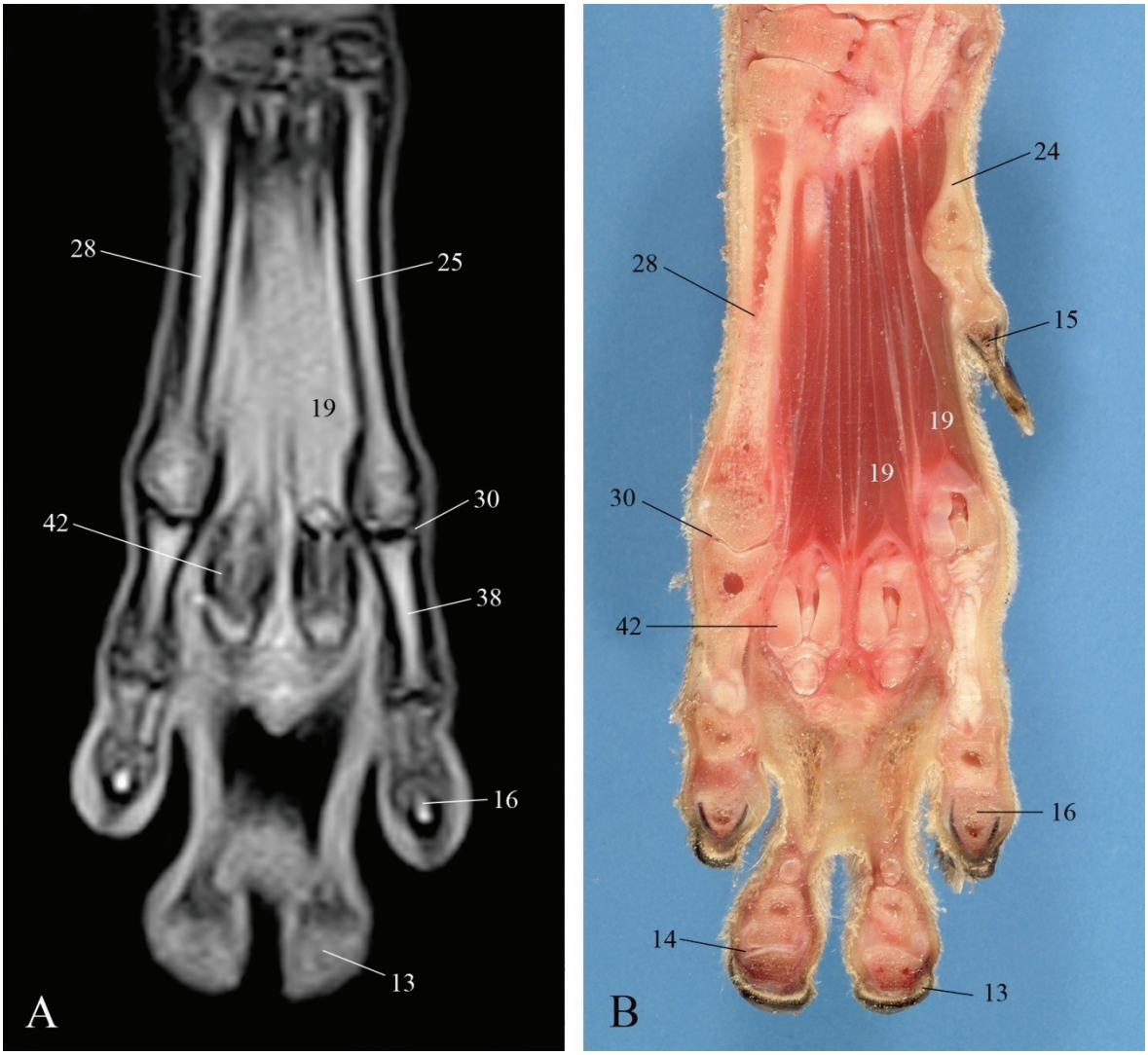

Figure 3.10: Dorsal images of the right manus, with medial to the right of the image. (A) T1-weighted MRI, (B) anatomic section. See Table 3.1 for legend. Note the slight difference in image plane between the two images, as metacarpal 1 (24) and the first digit are visible on the anatomic section.

5. Discussion

Pain, lameness, and swelling localized to the canine manus can be attributed to trauma, infection/inflammation, foreign body retention, or neoplasia.[1,2,6,386,387] Radiography of the manus is generally indicated initially when disease is suspected,[5] but is often of limited use due to the superimposition of multiple osseous structures and the minimal information that can be obtained regarding the soft tissues. Additionally, foreign bodies embedded in the distal extremities are commonly composed of plant material,[5] and are generally not visible radiographically.[7-9] For this reason, further evaluation of the manus with other modalities such as CT is indicated when an embedded foreign object is suspected.[389]

CT and MR imaging can also be beneficial for more detailed evaluation of disease processes that may be visible radiographically. Injuries to the manus and pes are relatively common, and surgical planning requires an understanding of the extent of disease, including bone, ligament, and tendon involvement.[63] While radiography can allow for identification of fractures and soft tissue swelling, sectional imaging can provide a more thorough assessment of osseous and soft tissue structures and can also be used to identify sites of infection.[320,376] Imaging of the distal limb is also indicated in patients with a digital mass, as 61% of these masses are malignant neoplasms.[387] CT and MR imaging can both be used to evaluate the extent of the mass,[390,391] which is necessary to plan a surgical approach.

Because the uses of cross-sectional imaging for complete evaluation of the manus are expanding, it is critical to understand the complex anatomy of the canine manus in multiple planes. However, while detailed descriptions of the general anatomy of the canine manus are

available,[392] depictions of the cross-sectional anatomy of the manus have been limited in their scope.[388]

Both CT and MR imaging can be used to eliminate the diagnostic difficulties resulting from of superimposition of tissues as seen on radiographs. While the spatial resolution of both of these modalities is inferior to radiography, the contrast resolution of both is superior to radiography.[305] This is especially true regarding the soft tissue contrast resolution of MR imaging. Osseous details in this study proved to be easier to identify with CT, especially when viewed in an appropriate bone window. Cortical bone has low to no signal on MR imaging,[299] so subtle structural differences can be more difficult to detect. However, soft tissue structures were more readily differentiated using MR imaging as compared to CT. For example, the low-signal tendons on MR imaging are easy to distinguish from the higher intensity muscle bellies, while on CT all of these structures are very similar in their attenuation characteristics. The improved soft-tissue contrast resolution of MR imaging relative to CT is also important in disease, as characterization and extent of soft-tissue pathology are often more readily determined with MR imaging than with CT.[320,390,391,393]

The difficulties in identifying the dorsal sesamoid bones on the transverse images using MR imaging partially relate to the spatial resolution and slice thickness used with this modality. As improving the spatial resolution of MR imaging leads to a more apparent decrease in signal-to-noise ratio than in CT,[305] a smaller matrix and thicker slices were used in MR images as compared to CT. Because of this, the ability to resolve smaller structures such as the sesamoid bones is diminished as the signal characteristics of small structures are more likely to be averaged with those of adjacent tissues (partial volume averaging artifact). Additionally, both

tendons and cortical bone have very low signal on MR imaging;[299] thus, there is minimal contrast between sesamoid bones and the tendons that contain them.

The poor identification of vessels with CT and MR imaging is likely a function of both spatial resolution and contrast resolution. On CT, the vessels have attenuation characteristics similar to muscle, which explains the visualization of palmar common digital artery III only when it was surrounded by fat. Additionally, the vessels in the manus are relatively small, and the matrix size chosen in our protocols may not have been sufficient to allow differentiation of most vascular structures from the surrounding tissues.

Both CT and MR imaging are valuable in fully evaluating the canine manus; we found that most clinically important structures in the canine manus can be evaluated with both CT and MR imaging. The information in this paper will be useful in clinical evaluation of the front paw.

Footnotes

* Picker PQ5000, Philips Medical Systems, Bothell, WA, USA

† Vet-MR, Esaote S.p.A., Genoa, Italy

Chapter IV

Comparison of Ultrasound, Computed Tomography, and Magnetic Resonance Imaging in Detection of Acute Wooden Foreign Bodies in the Canine Manus

Christopher P. Ober

Jeryl C. Jones, Martha Moon Larson, Otto I. Lanz, Stephen R. Werre

This chapter has previously appeared as a manuscript in *Veterinary Radiology and Ultrasound*, published by Blackwell Publishing. (Ober CP, Jones JC, Larson MM, Lanz OI, and Werre SR. Comparison of ultrasound, computed tomography, and magnetic resonance imaging in detection of acute wooden foreign bodies in the canine manus. *Veterinary Radiology and Ultrasound* 2008, 49(5): 411-418.) The definitive version is available at www.blackwell-synergy.com.

This manuscript received the 2008 American College of Veterinary Radiology Resident-Authored Paper Award.

A portion of this paper was presented at the Annual Scientific Conference of the American College of Veterinary Radiology, Chicago, IL, 2007.

Supported by a grant from the Virginia Veterinary Medical Association Veterinary Memorial Fund.

1. Abstract

We evaluated the diagnostic sensitivity of ultrasound, non-enhanced computed tomography (CT) and non-enhanced magnetic resonance (MR) imaging in detecting wooden foreign bodies in the canine manus. Identical wooden splinters were manually inserted into thirty cadaver canine manus, and the limbs were evaluated using ultrasound, CT, and MR imaging by independent observers. All sites were rated as positive or negative for the presence of a foreign body, and observer certainty was scored on a 1-10 scale. Using receiver operating characteristic (ROC) analysis, CT was the most accurate modality for detection of wooden foreign bodies overall and within each of the three individual regions, followed by ultrasound and MR imaging, respectively. Ultrasound evaluations were most limited in the metacarpal pad, where distal acoustic shadowing from the pad surface hindered evaluation of the tissues in some specimens.

2. Introduction

Foreign bodies affecting the integumentary and musculoskeletal systems are common in domestic animals and humans. While any location can be affected, the distal extremities are among the most common sites.[3,6] Foreign bodies of the manus or pes represent a hazard for active dogs, such as search-and-rescue dogs, and can prevent affected dogs from performing their duties. Radiolucent foreign bodies are a diagnostic challenge because of the complex anatomy of the manus and pes and because of unpredictable migration of foreign objects. In addition, differentiating foreign objects from bones, ligaments, and tendons can be challenging. While exploratory surgery is an option, many dogs undergo multiple procedures,[4] and surgery

brings its own risk of complication and loss of function. Undetected foreign bodies can lead to complications, including neuropraxia, cellulitis, abscessation, and osteomyelitis.[3]

As wood is one of the most common foreign objects found in the distal extremities,[5] a noninvasive technique for detection and localization of wooden foreign bodies is needed to minimize surgical exploration. Wooden foreign bodies have been detected using ultrasound (US), computed tomography (CT), or magnetic resonance (MR) imaging, but little is known about the sensitivity of different modalities for detecting radiolucent foreign bodies[7,8,22,24]

The purpose of this study was to compare the accuracy of ultrasound, CT, and MR imaging for detection of acute wooden foreign bodies in the canine manus.

3. Materials and Methods

Fifteen medium- to large-breed dog cadavers were obtained from a local shelter, and both forelimbs from each dog were amputated. All limbs were harvested within 4 hours of euthanasia, and were immediately frozen following harvesting. The limbs were frozen for variable lengths of time, as order of limb usage was randomly determined. All limbs were thawed for approximately 10 hours before further manipulation.

After limbs were thawed, they were submerged in a water bath and a 14G, 1.5-inch needle was used to create holes in the palmar surface of the manus. Skin puncture was performed with the paw submerged in a water bath to limit the amount of gas allowed to track into the wounds. Three defects were made in each of the following three regions: the interdigital skin (one defect in the skin of each interdigital space between the second and fifth digits), the distal aspect of the metacarpal pad, and the skin palmar to the metacarpal bones. These regions represent the most

common foreign body sites.[4,6,200,201] After creation of needle tracts, pre-cut cylindrical Eastern White Pine (*Pinus strobus*) splinters measuring 1cm in length and 1mm in diameter were placed into some of the created punctures. All splinters had been soaked in water for 24 hours prior to insertion in the paw to mimic absorption of body fluids as would be expected.[7,25] Placement or lack of placement of a foreign body at each site was determined by a coin toss; thus, each paw could have as few as 0 or as many as 9 foreign bodies. Foreign bodies were inserted by manually pushing them along the needle tracts, and all foreign bodies were oriented parallel to the metacarpal bones and digits. The presence or absence of foreign bodies at each site was known only by the person responsible for their placement. After preparation, the specimens were returned to a cooler for approximately 14 hours prior to imaging.

Each manus was evaluated with US, CT, and MR imaging. US and CT were performed at Virginia Tech, and MR imaging was performed at Wake Forest University. Because two facilities were used, US and CT examinations were performed before MR imaging for all paws to minimize the effects of transit and autolysis. The order of CT and US evaluation was randomly determined for each paw.

Each of the nine possible foreign body locations was evaluated using each modality. The images from each modality were read by a single board-certified radiologist, either a veterinarian or physician, with a high degree of expertise in that modality; and each modality had a different reader. For all examinations, the radiologist was unaware of the foreign body status of that specimen: the only information provided was the approximate possible locations of the foreign bodies. The observers recorded whether a foreign body was present or absent at each site. Each reader also recorded the certainty of his or her diagnosis on a scale of 1 to 10, with 1 representing absolute uncertainty, and 10 representing absolute certainty.

US was performed using a 14MHz linear transducer.* A standoff pad was available for use at the sonographer's discretion, and an independent observer assisted with positioning of the specimens to minimize the chances of the sonographer inadvertently palpating the foreign bodies. CT was performed using a single-slice helical scanner.† Both of a single dog's limbs were in the gantry at the same time, with the palmar surface on the table and the distal aspect of the manus closest to the gantry. Transverse images of the manus were obtained using 1.5 mm slice thickness and 0.5 mm slice interval with a modified extremities protocol (200 mA, 120 kVp, standard reconstruction algorithm, small focal spot, 180 image size). CT acquisitions were subsequently evaluated on a dedicated CT workstation.‡

Magnetic resonance imaging utilized a 1.5T magnet.§ Both forelimbs from each dog were positioned as for CT. A phased array (cardiac) coil was used to allow for comparison of both limbs as in a clinical situation, and sequences used included T1-weighted FSE (TE 13, TR 600, NEX 2, FOV 16, matrix 256x256) and proton density/T2-weighted FSE (TE 13/53, TR 5000, NEX 2, FOV 16, matrix 256x192). All images were obtained in a transverse plane with 2 mm slice thickness and 0 mm spacing, and spectral fat saturation was used for both sequences. After the imaging studies, all paws were dissected to verify the location of the foreign bodies.

Sensitivity and specificity were calculated for each modality overall and for each region (interdigital, metacarpal pad, metacarpus). Receiver operating characteristic (ROC) curves were generated using the certainty data, and the area under the curves (AUC) were compared using the correlated z statistic from a dedicated ROC analysis program (Rockit).‖ Categories for use in the ROC curve generation were produced by assigning negative values to certainties for absent foreign bodies and positive values for present foreign bodies, then collapsing the now-20-point scale into 6 categories. Statistical significance was set at $P < 0.05$.

4. Results

Upon dissection, all wooden foreign bodies were found at their respective sites of insertion without migration. Fragmentation of one foreign body was noted, and the fragments remained in apposition with each other.

Using US, the foreign bodies appeared as hyperechoic interfaces with distal acoustic shadowing (Figure 4.1). On CT, the foreign bodies appeared as cylindrical structures that were hypoattenuating to surrounding muscle and fat. When using a narrow window width, these objects appeared similar to gas, which could result in a false negative diagnosis for a wooden foreign body (Figure 4.2A). However, when a wider window width was used, their attenuation was found to be greater than that of air, allowing wooden objects to be distinguished from gas tracts (Figure 4.2B). Foreign bodies were often more easily identified as linear objects using oblique multiplanar reformatting (Figure 4.3). With MR imaging, the wooden foreign bodies were hypointense to surrounding soft tissues in both T1- and T2-weighted sequences, though they were less apparent on the T2-weighted images due to the inherent increase in noise (Figure 4.4).

Sensitivity and specificity were calculated for all three modalities overall and within each region (Tables 4.1 and 4.2). ROC curves were generated for all modalities overall and within each region (Figure 4.5); however, the US ROC curve in the metacarpal region was excluded from AUC analysis because the data were located too close to the vertical axis for valid analysis. The area under the ROC curve for the entire paw was greatest for CT (0.91), followed by ultrasound (0.75) and MR imaging (0.50), indicating that CT was the most accurate modality for detection of acute wooden foreign bodies (all $p < 0.001$). In addition, when evaluating each

region individually, the areas under the CT ROC curves were greater than those of MR imaging (all $p \leq 0.0001$) and US (both $p < 0.05$), and the areas under the ultrasound ROC curves were greater than those of MR imaging (both $p < 0.05$).

Table 4.1: Sensitivity of Ultrasound, Computed Tomography, and Magnetic Resonance Imaging for Detection of Acute Wooden Foreign Bodies

	Overall (%)	Interdigital (%)	Metacarpal Pad (%)	Metacarpus (%)
CT	75.2	76.2	76.1	73.5
US	54.0	71.4	37.0	55.1
MR	2.2	7.1	0.0	0.0

Table 4.2: Specificity of Ultrasound, Computed Tomography, and Magnetic Resonance Imaging for Detection of Acute Wooden Foreign Bodies

	Overall (%)	Interdigital (%)	Metacarpal Pad (%)	Metacarpus (%)
CT	95.5	93.8	95.5	97.6
US	97.0	97.9	93.2	100.0
MR	97.7	95.8	97.7	100.0

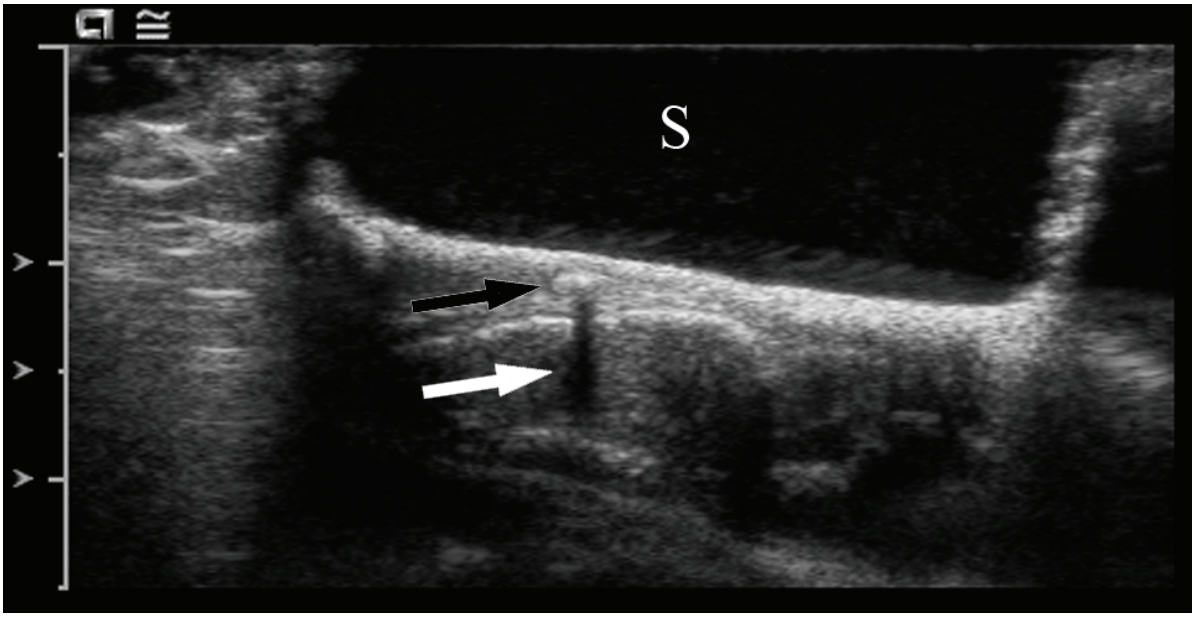

Figure 4.1: Transverse ultrasound image in the interdigital region. A wooden foreign body is seen as an echogenic structure (black arrow) with distal acoustic shadowing (white arrow). A standoff pad (S) was used to maximize image quality.

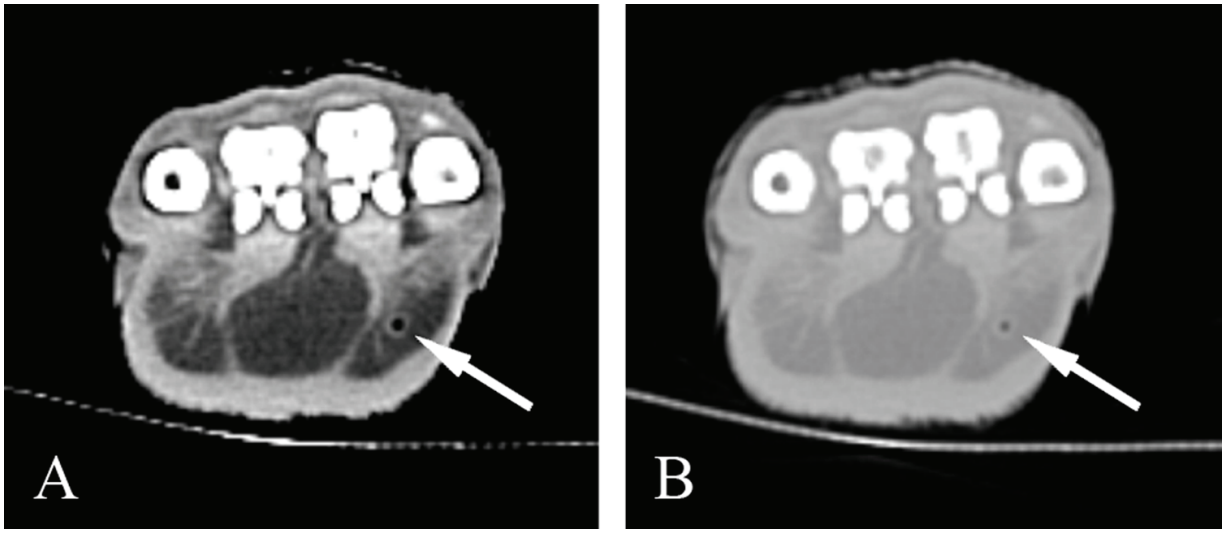

Figure 4.2: Transverse CT images at the level of the metacarpal pad. (A) The wooden foreign body (arrow) appears to have the same attenuation as air in a relatively narrow window (window width 375, window level 40). (B) Same location as (A). With a wider window, the foreign body (arrow) remains hypoattenuating to the surrounding fat, but is hyperattenuating to air (window width 1500, window level -160).

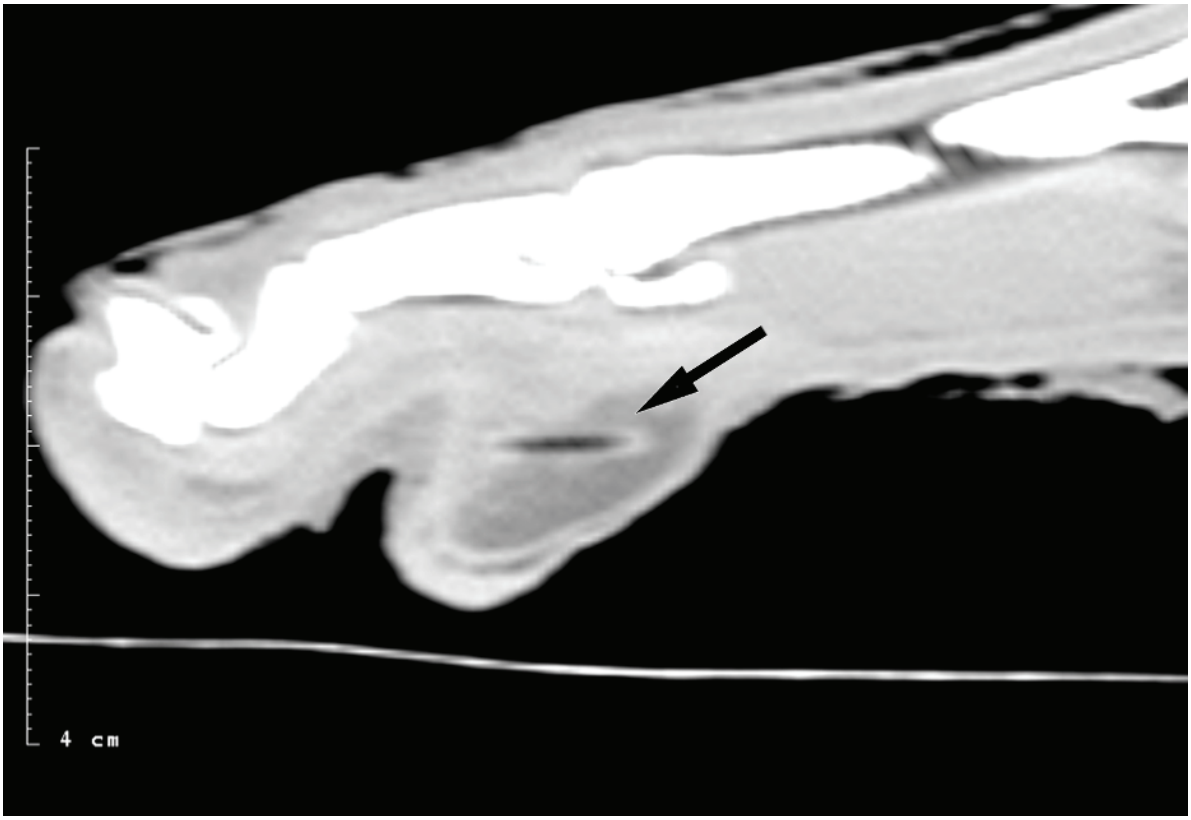

Figure 4.3: Reformatted sagittal CT image. Note the foreign body within the metacarpal pad (arrow).

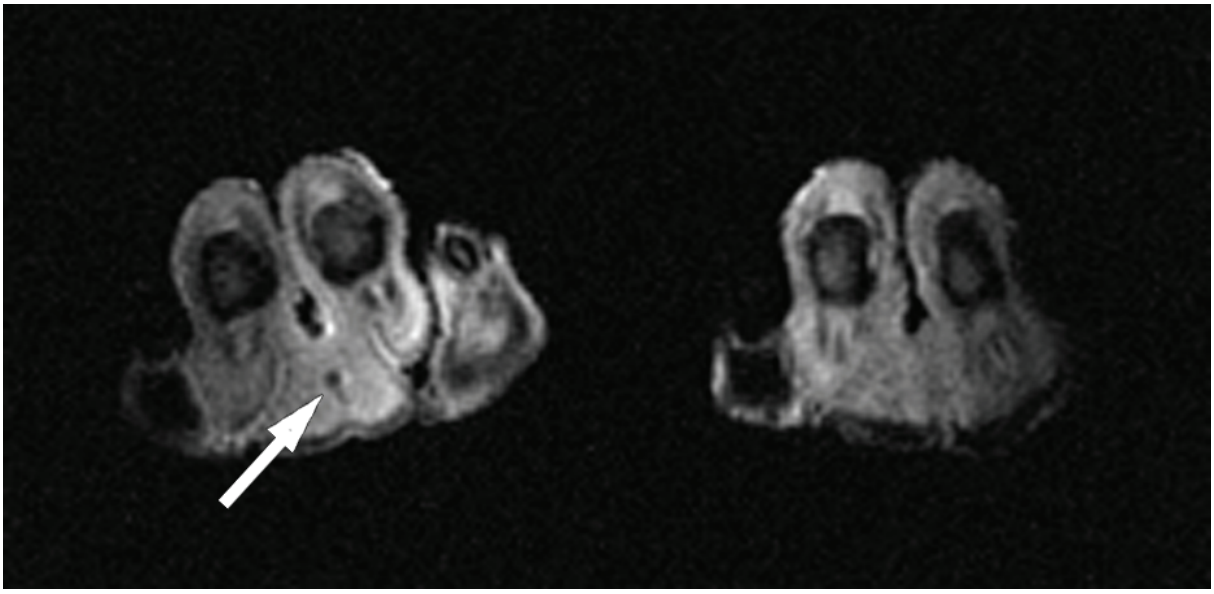

Figure 4.4: Transverse T1-weighted MR image of both front paws at the level of the digits. A wooden foreign body is seen as a signal void within the interdigital tissue between the third and fourth digits (arrow). Note the signal drop-off at the lateral portion of both paws.

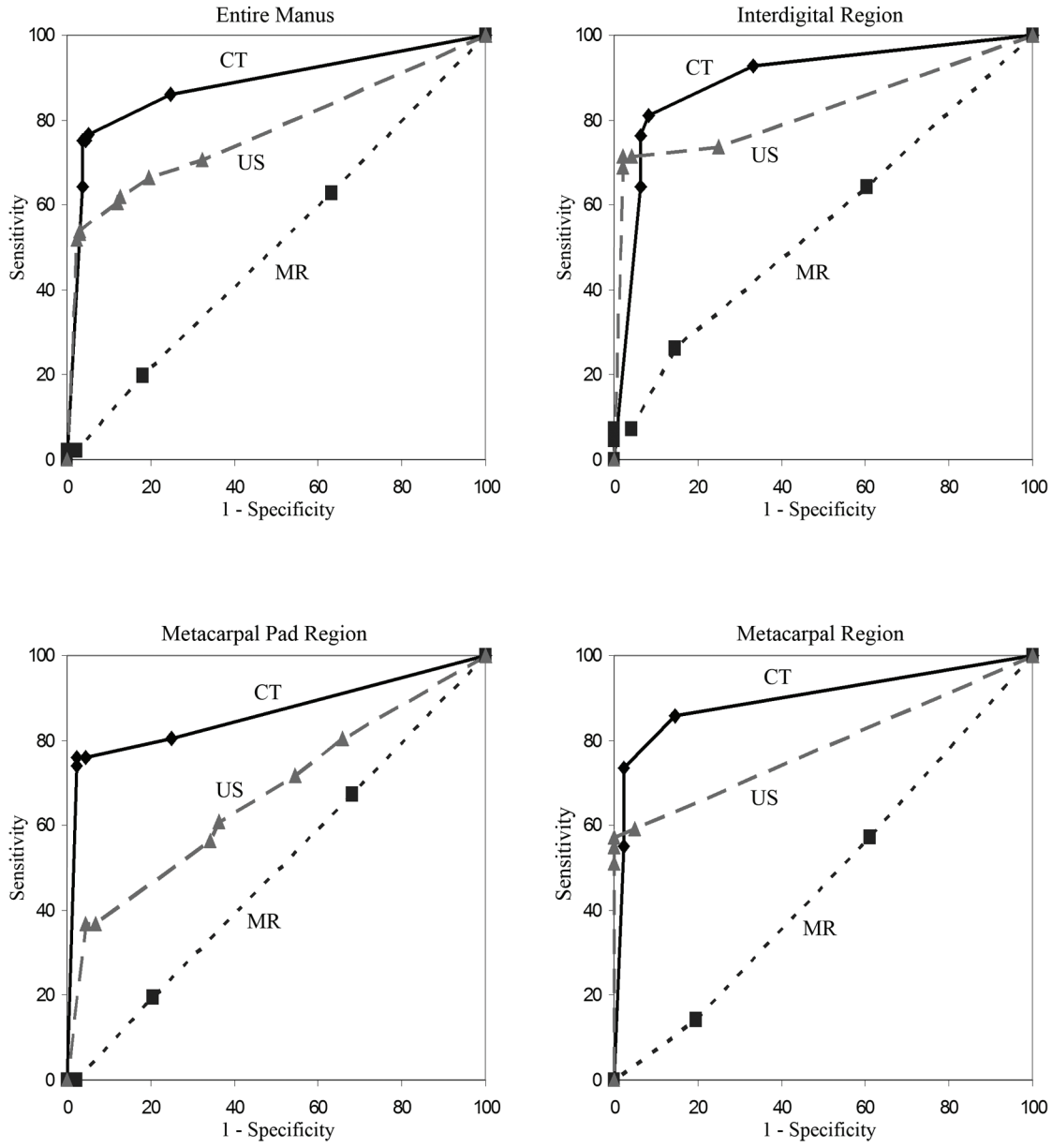

Figure 4.5: Receiver operating characteristic curves for CT, ultrasound, and MR imaging. Curves were generated for the entire manus and for each region individually.

5. Discussion

There are conflicting recommendations for the best imaging modality for diagnosis of radiolucent foreign materials, such as wood. However, there is no direct comparison of US, CT, and MR imaging of wood in the distal extremities, the most clinically pertinent situation in dogs. Various modalities have been assessed in specimens of meat with no bone present, including beef cubes,[288] steak strips,[381] and cow tongue[9]. Chicken thighs[10,26,250,384] and porcine shoulders[25] have also been used as models with increased anatomic complexity. However, none of these models adequately mimic the multiple small bones, tendons, muscles, and other soft tissue structures that compose the distal extremity of dogs.

Three comparisons of US, CT, and MR imaging in model tissues (cow tongue, porcine muscle, and chicken thigh) have been conducted, but there is disagreement regarding the most sensitive modality,[9,25,26] and some of the foreign objects were larger than clinically applicable.[25] Radiography, xeroradiography, CT, and MR imaging were compared regarding their ability to detect various foreign bodies in human cadaver hands, but the conclusions were limited because the foreign objects were relatively large, no control sites were used as true negatives, and US was not evaluated.[7] Omission of US is unfortunate given its wider general acceptance as a valuable bedside test to evaluate for radiolucent foreign bodies.[14,121,204,275] US has been used to evaluate the presence of wooden foreign bodies in the plantar soft tissues of human cadaver feet[8,24] or the soft tissues of the hands of clinical patients,[22] but there was no comparison to CT or MR imaging.

Radiography is the most appropriate initial imaging study to perform when there is suspicion of a foreign body, as this will sometimes provide a definitive diagnosis.[5] Small wooden

foreign bodies, such as splinters, are rarely detectable with radiography,[5,22] and large wooden objects may appear as ill-defined lucencies.[106] However, there are many examples of wood and other plant foreign bodies that were not visible radiographically.[7-10,120,124,125,275] Radiography may still be beneficial for more chronic foreign bodies, as secondary periosteal reaction and osteolysis are sometimes seen.[120,124,125] Sinography can also be beneficial in detecting foreign bodies, but this requires the presence of a draining tract.[4] We designed our study to model an acute situation where there is no tract for administration of contrast medium.

The US appearance of wooden foreign bodies in our study agrees with previous reports, as they are generally described as linear echogenic structures, usually with marked distal acoustic shadowing (Table 4.3).[8,15,24,25,124,249,275] Grass awns are described as linear with parallel echogenic interfaces and rare distal acoustic shadowing.[120] However, US findings are not specific for a certain type of foreign body, as surface characteristics, and not composition, are the most important factors in production of acoustic shadowing,[8] and many types of foreign objects may look similar.[9,288] The echogenicity of wooden foreign bodies may also decrease over time, as ultimately they will be absorbed into the surrounding inflammation.[24] In studies *in vivo*, a hypoechoic rim or region representing inflammation and edema may be found surrounding foreign objects.[15,193] Because our study was modeling acute wooden foreign body penetration, the highly echogenic interface and distal acoustic shadowing with lack of hypoechoic rim are consistent with early findings *in vivo*.

Table 4.3: Common Imaging Characteristics of Wooden Foreign Bodies Using Ultrasound, Computed Tomography, and Magnetic Resonance Imaging

	Acute Wood	Chronic Wood	Inflammation
US	Echogenic surface, marked distal acoustic shadowing, linear or cylindrical	Decreased echogenicity	Hypoechoic surrounding tissues
CT	Hypoattenuating or hyperattenuating to surrounding tissues, linear or cylindrical	Increased attenuation	Isoattenuating or mildly hypoattenuating, contrast-enhancing tissues; effacement of surrounding fat planes
MR	Markedly T1- and T2-hypointense (signal void), linear or cylindrical	T1-hypointense, T2-hypointense or hyperintense	T1-hypointense, T2-hyperintense, contrast-enhancing tissues

Note: Table is summary of references [7-9,15,18-20,24,25,107,124,127,193,210,249,275,314,365,375]

While all of the foreign bodies in our study were hypoattenuating to the surrounding tissues on CT, the reported appearance for wood varies. In CT images, wooden foreign bodies may appear as hypoattenuating[9,18-20,210,365] or hyperattenuating[19,20,107,124,275] linear or cylindrical structures (Table 4.3). Mean attenuation varies by the type of wood, with hardwoods generally being more attenuating than soft woods;[143,365,394] and by water content, with freshly cut wood more attenuating than dry air-filled wood.[139] In addition, wooden foreign bodies in the body tend to increase in attenuation over time due to the absorption of fluid;[20,25,210] thus, the low attenuation values for the wood in our study better model an acute situation. Although we soaked the wooden objects for 24 hours prior to insertion to mimic fluid absorption of 1 day's duration, this would not be expected to cause a clinically apparent change in the attenuation of the wood.[25] Because acute wooden foreign bodies are so similar in attenuation to air, especially at narrow window settings, misdiagnosis is a concern.[18,20,139,144,210] While a narrow window width should be used initially to detect lesions in the soft tissues, the wide window setting proved to be necessary to characterize the lesions as wood or air and thus reduce the chance of a false negative diagnosis.[18,139,144] It should be noted that in some instances the plant material itself cannot be detected, and only the inflammatory response is seen.[107] This inflammatory response is generally characterized as isoattenuating or mildly hypoattenuating to the surrounding tissues and contrast-enhancing with variable effacement of adjacent fat planes.[19,124,127,210,375]

With MR imaging, wooden foreign material is usually T1- and T2-hypointense to the surrounding musculature, often appearing as a signal void (Table 4.3).[7,9,25,124] This corresponds to the imaging characteristics seen in our study. However, long-term soaking of a wooden object may increase its signal intensity on T2-weighted sequences,[25] and fresh wood may also have higher T2 signal than dry wood.[315] One chronic wooden foreign body appeared T1-isointense

and slightly T2-hyperintense to surrounding musculature.[314] In the *in vivo* situation, a T1-hypointense, T2-hyperintense, contrast-enhancing inflammatory response is generally seen,[124,314] though increased T1 signal is also described.[193] The inflammatory response may accentuate the appearance of the foreign body on T2-weighted images unless the foreign object has absorbed enough fluid to sufficiently increase its T2 signal. Because a T2-hyperintense inflammatory response could accentuate an embedded T2-hypointense wooden foreign body in a living patient, we may have underestimated the sensitivity of MR imaging for finding these foreign objects. Our results would thus represent a worst-case scenario for MR imaging, an acute injury with minimal or no inflammatory response. It is also possible that our detection rate may have been higher than that seen in living tissues, where increased wood hydration could reduce the T2 contrast between a wooden foreign body and the tissues,[315] although this was not seen in several clinical patients.[19,124]

CT was the most accurate modality for detecting wooden foreign bodies, and this is most apparent in the imaging of the metacarpal pad region. The lower accuracy of US relative to CT in this region is at least partially due to the acoustic shadowing caused by the metacarpal pad surface in some limbs. While the degree of acoustic shadowing was variable, shadowing was complete in some metacarpal pads (Figure 4.6). This shadowing made complete sonographic evaluation of the pad region impossible in these specimens, though a limited examination could still be performed. In these specimens, the transducer was oriented dorsally and the most proximal or distal skin of the pad was used as an acoustic window, rather than performing the scan with a usual transverse orientation of the transducer and using the palmar surface of the pad as a window. We feel that this shadowing was most likely due to variable keratinization of the

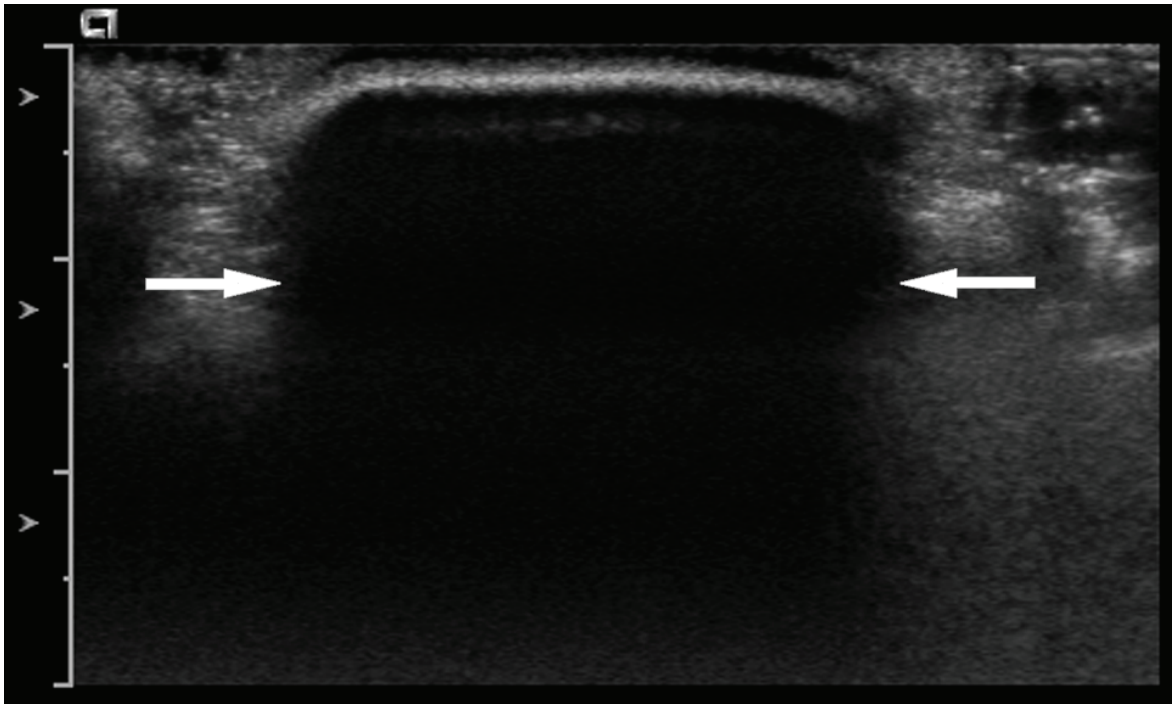

Figure 4.6: Transverse ultrasound image of the metacarpal pad. Note the echogenic skin interface at the surface of the transducer and the complete distal acoustic shadowing extending from the pad surface (arrows).

metacarpal pad skin, as subsequent clinical experience has confirmed variable shadowing in this region, with rougher pads seeming to produce more of a distal acoustic shadow. This possible blind spot for ultrasound detection of foreign bodies in the canine paw is worth emphasizing, as it may contribute to the choice of modality when searching for possible foreign bodies. The freezing of the limbs could have also influenced the acoustic properties of the skin, though we would have expected this to produce an effect in the other regions as well.

The poor accuracy of MR imaging was due to the inability to detect most of the foreign objects: there were only three true positive diagnoses, all in the interdigital region. The ROC curve for MR imaging approximates a diagonal for the manus overall and for each region individually, as would be expected for a test that relies on chance alone. In fact, the most important factor causing differences in accuracy among the three modalities seems to be the sensitivity, the ability to detect a true positive. The specificities of all three modalities were similar at all sites because there were few false positives – detection of actual foreign bodies was a more challenging task than recognition of normal, possibly confounding, structures.

The most significant weakness in our study was the use of cadaver limbs rather than living patients. This prevented the use of contrast media to cause enhancement of inflamed tissue with both CT and MR imaging, and also may have underestimated the sensitivity of MR imaging for detecting wooden foreign bodies because of the lower T2 contrast resolution between foreign body and inflamed tissue than would be expected *in vivo*. However, our model represents an acute situation, in which these inflammatory changes may be minimal and visualization of the foreign body itself is critical. While a more chronic presentation may be more common in practice, our model can be seen as an extreme situation for foreign body detection, as there is no inflammatory response to help the reader with lesion detection and localization.

Direct comparison of diagnostic accuracy among modalities is also limited somewhat by the different spatial resolution used in the three modalities. Based on the parameters we chose, US had the highest spatial resolution and MR imaging the lowest. This may have contributed to the poor performance of MR imaging in our study, as the cross-sectional size of the foreign bodies (1mm) was likely near the lower limit of detection. While scanning only one paw at a time with CT and MR imaging would have allowed use of a smaller field of view and thus improve spatial resolution, we would have lost the ability to compare each limb to the contralateral limb.

Another limitation of our study was that all foreign bodies were identical to limit the effect of size and shape variation in determining sensitivity for each modality. Because of this, the observers knew the size and shape of the objects for which they were looking. This seemed to be most important in CT, where gas tracking in the tissues and foreign objects could mimic each other. The reader for CT could more definitively diagnose some sites as positive or negative based on size and shape rather than the attenuation characteristics. This is consistent with previous studies on detection of wooden foreign bodies in humans and in the canine nasal region, where the non-anatomic shape of the foreign object was found to be important for differentiating the foreign body from gas pockets.[107,124,144,312] However, in a clinical situation where the size and shape of a possible foreign body are unknown, some of these sites may have been considered equivocal due to the similar appearance of wood and gas with partial volume averaging, so we may have overestimated the sensitivity for CT. In addition, use of only pine wood in our study makes extrapolation of results to woods with different characteristics uncertain.

Further studies to be performed include evaluation of all three modalities *in vivo* to determine if sensitivity in clinical patients is similar to that of our acute model, or if the

inflammation seen in these generally more chronic patients plays a significant role in the evaluation of foreign objects. In addition, further evaluation would be necessary to determine the smallest wooden foreign objects that can be detected with each modality.

In summary, CT was the most accurate modality for identification of wooden foreign bodies in the canine manus. While radiography is always indicated as a primary means of evaluation for suspected foreign body penetration of the paw, CT should be considered when radiography is negative and suspicion of a wooden foreign body remains.

Acknowledgements

The authors would like to thank Allen Elster and Susie Ayers for their administrative and technical assistance with this project.

Footnotes

* ACUSON Sequoia 512, Siemens Medical Solutions, Malvem, PA, USA

† Picker PQ5000, Philips Medical Systems, Bothell, WA, USA

‡ Picker Voxel Q Visualization Station, Philips Medical Systems, Bothell, WA, USA

§ GE Twinspeed, GE Medical Systems, Waukesha, WI, USA

|| Rockit, Windows v1.0.1 beta 2, Kurt Rossman Laboratories, University of Chicago, Chicago, IL, USA

Chapter V

Myofascial Compartments and Soft-Tissue Spaces in the Normal Canine Manus

Christopher P. Ober

Jeryl C. Jones, Martha Moon Larson, Otto I. Lanz

A version of this chapter has been accepted by the *American Journal of Veterinary Research*. (Ober CP, Jones JC, Larson MM, and Lanz OI. Myofascial compartments and soft-tissue spaces in the normal canine manus. *American Journal of Veterinary Research*, in press.)

Portions of this study were presented at the 2008 Research Symposium of the Virginia-Maryland Regional College of Veterinary Medicine

Supported by a grant from the American Kennel Club Canine Health Foundation.

1. Abstract

Objective – To determine whether soft-tissue spaces and myofascial compartments present in the human hand and foot are also present in the normal canine manus.

Animals – Thirty-three normal adult medium- to large breed dog cadavers.

Procedures – The manus of each canine front limb was imaged using computed tomography (CT) both before and after injection of a radiopaque, blue-staining contrast medium into locations where soft-tissue spaces and myofascial compartments were predicted based on a pilot study. Two veterinary radiologists reviewed CT images and recorded the presence or absence of a discrete space or compartment at each injection site. Following imaging the paws were dissected or sectioned transversely. Locations of blue-staining contrast medium accumulation were described and compared with locations of CT contrast enhancement. Anatomic structures within each soft-tissue space or myofascial compartment were also described.

Results – Thirteen soft-tissue spaces and five myofascial compartments were present in the canine manus. Dorsal extensions of contrast medium (dorsal spokes) were seen in multiple spaces. Three myofascial structures tested were determined not to be compartments.

Conclusions and Clinical Relevance – In humans, soft-tissue spaces and myofascial compartments are used to map the likely spread of disease in the hand and foot. Understanding the locations and extent of similar structures in the canine manus may improve the effectiveness of surgical interventions for dogs with distal extremity injuries or inflammation. The dorsal spokes seen in multiple spaces could direct disease from a palmar injury to the dorsum of the manus.

2. Introduction

The canine distal extremity is a common site of abrasions, lacerations, and foreign body penetration. Indeed, injuries of the paws and distal limbs are among the most common injuries in working dogs.[1,2] These injuries can lead to chronic infection, and the associated morbidity may result in a permanent loss of working capability for affected dogs. Chronic paw infections commonly require exploratory surgery, and often multiple procedures are needed.[4] Exploration may be extensive because of the tendency of foreign bodies to migrate and the likelihood of infection spreading beyond its initial focus. The large extent of exploration, often coupled with the need for multiple procedures, may produce additional patient morbidity.

In humans, soft-tissue spaces and myofascial compartments in the hand[30-33] and foot[34-36] have been found to be important in limiting and defining the spread of inflammation, infection, and neoplasia.[37-40] Soft-tissue spaces are defined as tissue regions bounded by dense structures such as bone and fascial planes,[39,213] and myofascial compartments are defined as spaces containing a muscle or muscles that are enclosed by dense structures such as cortical bone or fascia.[30,37] While the importance of myofascial compartments is more commonly documented in human patients with compartment syndrome,[72,90] these compartments can also be important in determining the direction of disease spread.[29,37] Recognizing the presence of disease in one of these structures allows for a directed interventional procedure, and prevents the need for generalized exploration of the distal extremity.[38,40,41]

While injuries to the distal extremities of dogs are relatively common, to the authors' knowledge similar spaces and compartments in the canine manus have not been previously described. Thus, when there are chronic disease processes such as inflammation or draining

tracts, a more generalized surgical exploration of the paw is required, increasing morbidity and recovery time. Additionally, a cause of the pathology may not be identified, and further surgical explorations may be required. If soft tissue spaces and myofascial compartments are recognized in the canine manus, this could help the veterinarian in presurgical planning, as the location of disease may help predict the location of the initial insult.

The purpose of this study was to determine if soft-tissue spaces and myofascial compartments equivalent to those previously described in the human hand and foot are present in the canine manus.

3. Materials and Methods

Front limbs were removed from thirty-three medium- to large-breed dogs euthanized for reasons unrelated to front limb disease. Immediately after harvesting, the limbs were frozen. Limbs were allowed to thaw in a walk-in cooler for approximately 16 hours before imaging and further manipulations. Limbs were thawed in seven batches: one for a pilot study and six batches that served as the test groups.

Contrast materials were mixed immediately prior to the first injections of each group. The contrast medium mixture was produced by diluting 5 mL iopromide* and 2 mL indigo blue acrylic ink† in 45 mL 0.9% NaCl. The mixture was shaken approximately every 5 minutes to keep the blue pigment in suspension.

Six cadaver canine manus were used in a pilot study to determine probable locations of soft-tissue spaces and myofascial compartments based on locations previously described in humans. For the purposes of this study, we defined soft-tissue spaces as tissue regions bounded

by bone and/or fascial planes that do not incorporate muscles,[39,213] and myofascial compartments as spaces containing a muscle or muscles enclosed by bone and/or fascia.[30,37] Dissection to individual muscles or spaces was performed to guide injection of the contrast medium mixture into the specimens in the pilot study under direct visualization. Based on the results from this pilot study, 21 predicted soft-tissue spaces and myofascial compartments were identified as injection sites for the test dogs. These spaces and compartments were as follows: digital pads II-V, metacarpal pad (medial, central, and lateral lobes), carpal pad, midpalmar space, flexor space, extensor space, palmar subcutaneous tissues, dorsal subcutaneous tissues, interosseous muscles II-V, special muscles of digit I (abductor pollicis brevis, flexor pollicis brevis, and adductor pollicis muscles), adductor digiti II, adductor digiti V, and abductor digiti V.

The six test groups each consisted of 10 limbs which were imaged simultaneously using a single-slice helical CT scanner.‡ Three front limbs were placed on the couch side-by-side in extension, as for a patient positioned head-first in sternal recumbency. Cardboard platforms were used to support two upper rows of 3 or 4 limbs, and the limbs in these rows were positioned the same as the lower row. The location of individual limbs was determined randomly. Pre-contrast CT scans of the ten front limbs in each group were obtained from the distal ends of the digits through the antebrachiocarpal joint with axial acquisitions of 1.5mm slice thickness and 1.0mm slice interval using a modified extremity protocol (200 mA, 120 kVp, 240 field of view, 512 x 512 matrix, standard reconstruction algorithm).

After pre-contrast scanning, one predicted compartment or space in each manus was injected directly with a 22G needle using either a percutaneous approach or with visualization after dissection to the region of interest. A percutaneous approach was used for the more superficial spaces, such as the pads and subcutaneous regions, where needle placement was

certain. However, when precise localization of the needle tip needed to be verified (as for the muscle bellies and deep palmar spaces), dissection was performed to allow visualization of the needle. During dissection, care was taken to incise only the minimal amount of tissue required to visualize the anatomic part of interest, and the structure itself was not cut. For injection of predicted myofascial compartments, the center of the muscle belly was injected. The amount of contrast injected in each predicted space or compartment was based on the amount required to distend that structure in the pilot study, and this amount produced notable distension of each space or compartment and/or a considerable increase in resistance to injection in test limbs. The amount of contrast medium injected ranged from 0.5 mL in the digital pads to 3 mL in the dorsal and palmar subcutaneous spaces. The interosseous compartments, flexor space, and midpalmar space each received 1 mL of contrast agent. Each of the 21 predicted locations of a soft-tissue space or myofascial compartment was injected in at least two specimens during the study, though not every site was injected in each imaging group.

Following injection of contrast medium, the limbs were returned to their previous positions on the CT couch, and post-contrast CT scans of the limbs were acquired as previously described. The scanning protocol was similar to the pre-contrast protocol, except that a 0.5mm slice interval was used for post-contrast scanning, and the scan did not include the carpus if contrast medium was not visualized in the proximal metacarpus.

Scans for the test dogs were reviewed by two board-certified veterinary radiologists (CPO and JCJ) using a remote diagnostic workstation and commercially available DICOM viewing software.[§] For each manus, presence of a compartment or space was based on a consensus opinion using the following criteria: sharp margination of the area of contrast medium accumulation, homogenous appearance, and confinement of the contrast agent to a discrete

region. Each injection site was graded using a 0-4 scale: (4) contrast medium homogeneous and confined with sharp margins, (3) contrast medium confined and relatively homogeneous, with occasional ill-defined margins, (2) contrast medium heterogeneous and moderately confined, with multiple poorly-defined margins, (1) contrast medium heterogeneous with poor confinement and few well-defined margins, and (0) contrast medium heterogeneous with no definable margins and diffusion into surrounding soft tissues. Soft-tissue spaces or myofascial compartments were considered to be present if the structure received a score of 3 or 4 in at least two manus.

Immediately following CT scanning, all front limbs were frozen again. After the specimens were frozen, some were removed from the freezer for transverse sectioning using a band saw. The other front limbs were later thawed again and dissected conventionally. Selection of paws for transverse sectioning and dissection was random, with at least one specimen from each injection site represented in each of the two groups. Extent of the contrast medium mixture was correlated with imaging findings, and the dissections were also used to identify the structures found in each space or compartment.

4. Results

Of the 21 soft-tissue spaces and myofascial compartments predicted from our pilot study, 18 were found to be present in the test dogs. The special muscles of digit I, adductor digiti II muscle, and adductor digiti V muscle did not meet our imaging criteria for presence of a myofascial compartment. Direct visual evaluation of the dissected and transversely sectioned specimens correlated well with the imaging findings: the contrast medium mixture was retained

in those structures determined to be compartments or spaces and caused distension of those structures. There was no distension of the three muscles that were not compartments, and the contrast medium diffused throughout the surrounding soft tissues after injection of those structures. The contents of the positive soft-tissue spaces and myofascial compartments are given in Tables 5.1 and 5.2, respectively.

Table 5.1: Soft-Tissue Spaces of the Canine Manus

Space	Contents
Digits II-V	Digital pad stroma
	Digital connective tissues
	DDFT and SDFT (distal)
Metacarpal pad (medial lobe)	Pad stroma (medial lobe) and tissue dorsal
	Palmar common digital artery 2
Metacarpal pad (central lobe)	Pad stroma (central lobe) and tissue dorsal
	Palmar common digital artery 3
	Superficial palmar venous arch
Metacarpal pad (lateral lobe)	Pad stroma (lateral lobe) and tissue dorsal
	Palmar common digital artery 4
Carpal pad	Pad stroma
Midpalmar space	Caudal (palmar) interosseous artery
	Palmar common digital artery and nerve 3
	Ulnar nerve – deep branch
Flexor space	DDFTs (through level of carpus)
	SDFTs (not at level of carpus)
	Abductor digiti V tendon (lateral pouch)
	Lumbrical muscles
	Interflexorius muscle
	Flexor digitorum brevis muscle
	Median artery and nerve
	Superficial palmar arterial arch
	Palmar common digital arteries and nerves
	Ulnar nerve – superficial branch
Extensor space	Common digital extensor tendons
	Lateral digital extensor tendons
Palmar subcutaneous space	Cephalic vein
	Superficial palmar venous arch
Dorsal subcutaneous space	Cranial superficial antebrachial artery
	Accessory cephalic vein
	Dorsal common digital arteries, veins, & nerves
	Superficial radial nerve
	Ulnar nerve – dorsal branch

Note: DDFT = deep digital flexor tendon, lig. = ligament, SDFT = superficial digital flexor tendon

Table 5.2: Myofascial Compartments of the Canine Manus

Myofascial Compartment	Contents
Interosseous muscle II	Interosseous muscle II
Interosseous muscle III	Interosseous muscle III
Interosseous muscle IV	Interosseous muscle IV
Interosseous muscle V	Interosseous muscle V
Abductor digiti V	Abductor digiti V muscle
	Caudal (palmar) interosseous artery
	Ulnar nerve

Soft-tissue spaces: Pads

All injections into the digital pads stayed within the respective digits, indicating the presence of four individual digital spaces. However, while occasional injections were confined to the pad stroma, most spread through the soft tissues of the digit, wrapping around the digital flexor tendons and twice (out of ten total injections) extending into the dorsal tissues of the digit (Figure 5.1 A & B). The contrast medium never extended beyond the level of the middle of the proximal phalanx.

When the medial and lateral lobes of the metacarpal pad were injected, distribution of the contrast agent into the central lobe was prevented by septae. The contrast medium extended dorsally between the respective digits (II & III or IV & V) at the level of the metacarpophalangeal joints, and was present in the palmar tissues adjacent to the manica flexoria of the flexor tendons and the palmar annular ligaments (Figure 5.2 A & B). A similar pattern was seen with injection of the central lobe of the metacarpal pad, with the stromal component of the contrast agent remaining in the central lobe and the remainder extending dorsally to a point between the metacarpophalangeal joints and proximal phalanges of the third and fourth digits (Figure 5.2 C & D). The contrast medium did extend a small distance proximally and distally

from the level of the pad with injections of all three lobes of the metacarpal pad. The proximal margin of the central metacarpal pad space was the midpalmar space.

When the carpal pad was injected, all of the contrast medium remained within the pad stroma.

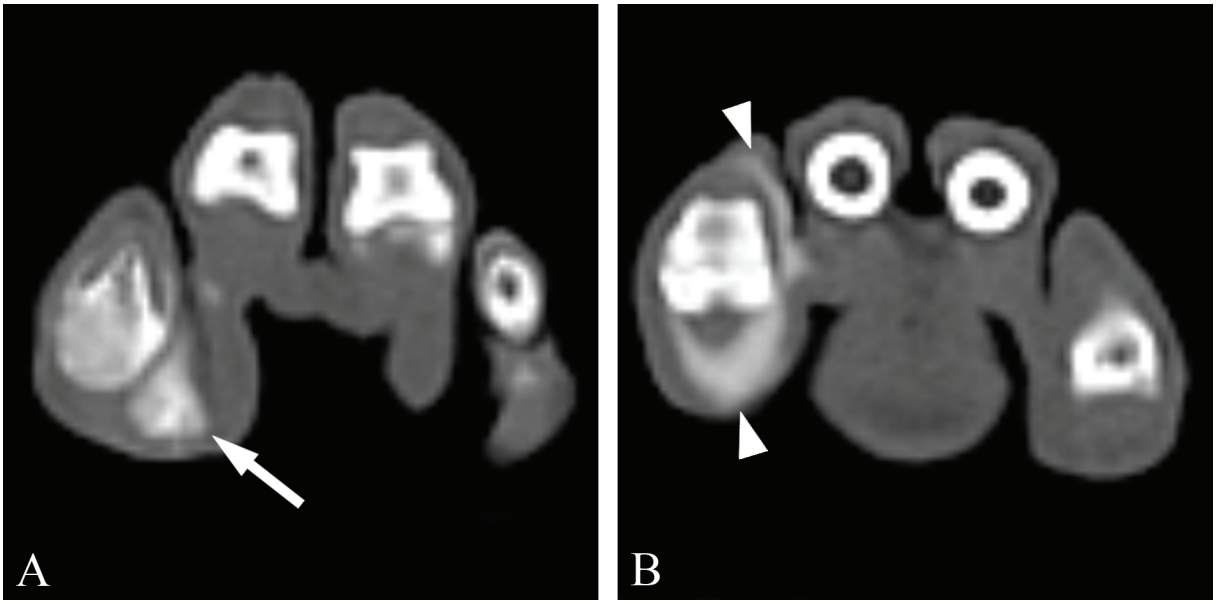

Figure 5.1: Transverse CT images of digital spaces. (A) Contrast medium is mostly contained by the stroma of the digital pad (arrow). (B) The contrast medium extends into the palmar and dorsal soft tissues of the digit (arrowheads).

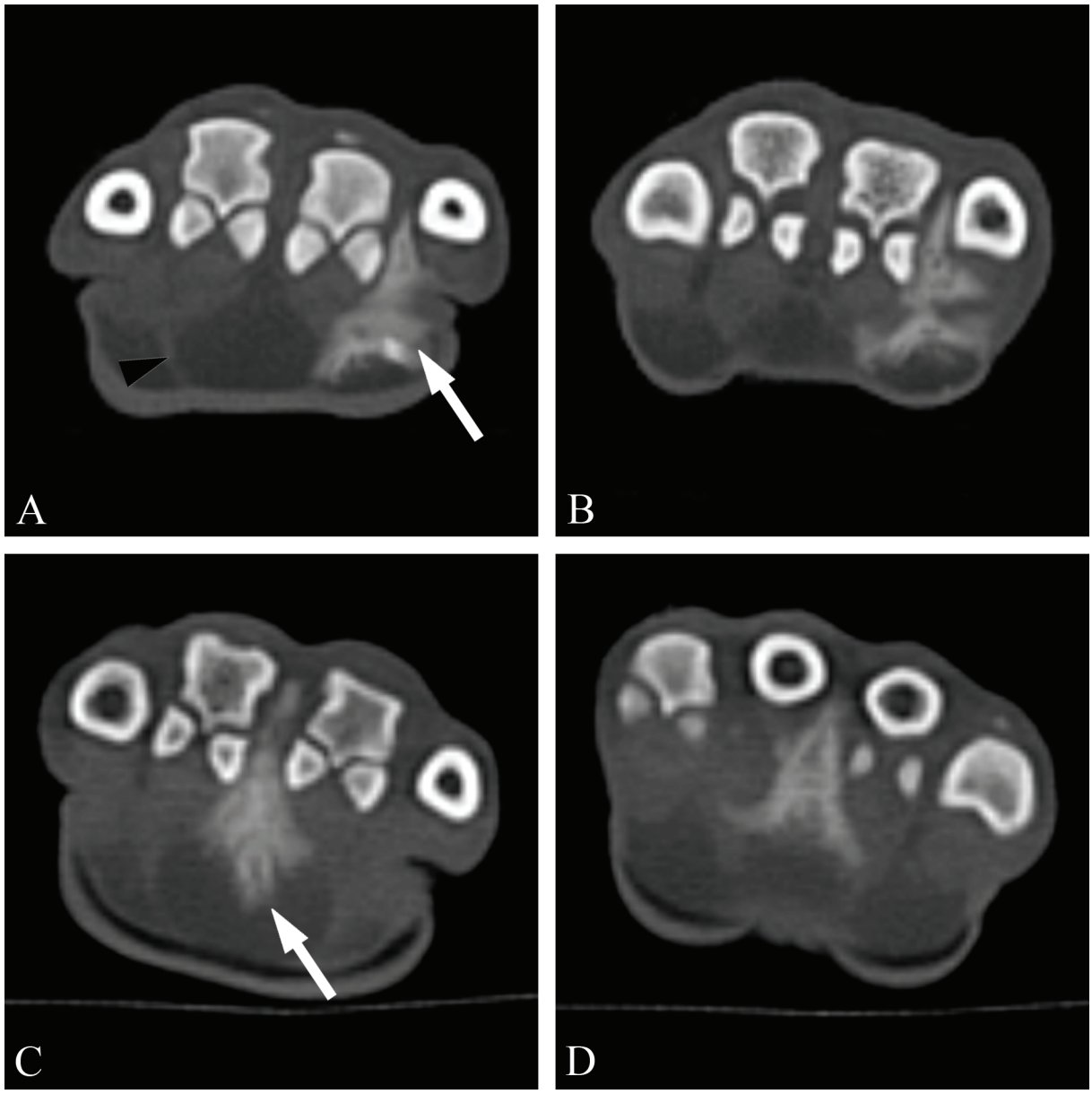

Figure 5.2: Transverse CT images of the metacarpal pad spaces. These spaces extend dorsally between the metacarpophalangeal joints and proximal phalanges. (A) Contrast medium within the lateral metacarpal pad space is indicated by the arrow. Note the septum separating the medial and central lobes of the metacarpal pad (arrowhead). (B) Contrast medium within the lateral metacarpal pad space, more proximal than image A. (C) Contrast medium within the central metacarpal pad space is indicated by the arrow. (D) Contrast medium within the central metacarpal pad space, more proximal than image C.

Soft-tissue spaces: Palmar tissues

Injection into the midpalmar space demonstrated multiple spokes extending primarily around interosseous muscles III and IV and adductor digiti II and V, with a small portion of the space extending adjacent to interosseous muscles II and V (Figure 5.3 A-D). The midpalmar space was on midline of the manus immediately deep to the deep digital flexor tendons and immediately proximal to the central metacarpal pad space: while most of the midpalmar space was proximal to the metacarpal pad, the most distal spoke of the space extended to the level of the metacarpophalangeal joints of the third and fourth digits. The most distal spoke also extended dorsally between metacarpals III and IV at the level of and just proximal to the metacarpophalangeal joints. Proximally the midpalmar space extended to the level of the proximal metacarpal bones (metacarpal bases).

The flexor space contained the tendons of the superficial and deep digital flexors, and was separated from the midpalmar space by a thick fascial plane (Figure 5.4 A-D). Additionally, while the space was predominantly found on midline, in two of the four injected specimens it also had a lateral recess in the proximal half of the metacarpus through which the tendon of the abductor digiti V ran (Figure 5.4D). The flexor space extended proximally to the level of the metacarpal bases, though only the deep digital flexor tendon was incorporated at the most proximal extent. The flexor space extended distally to the level of the distal one-third of the diaphysis of metacarpal III and IV; this corresponded to the level of the second and fifth metacarpophalangeal joints, though the space is not present as abaxially as the second and fifth metacarpal bones distally.

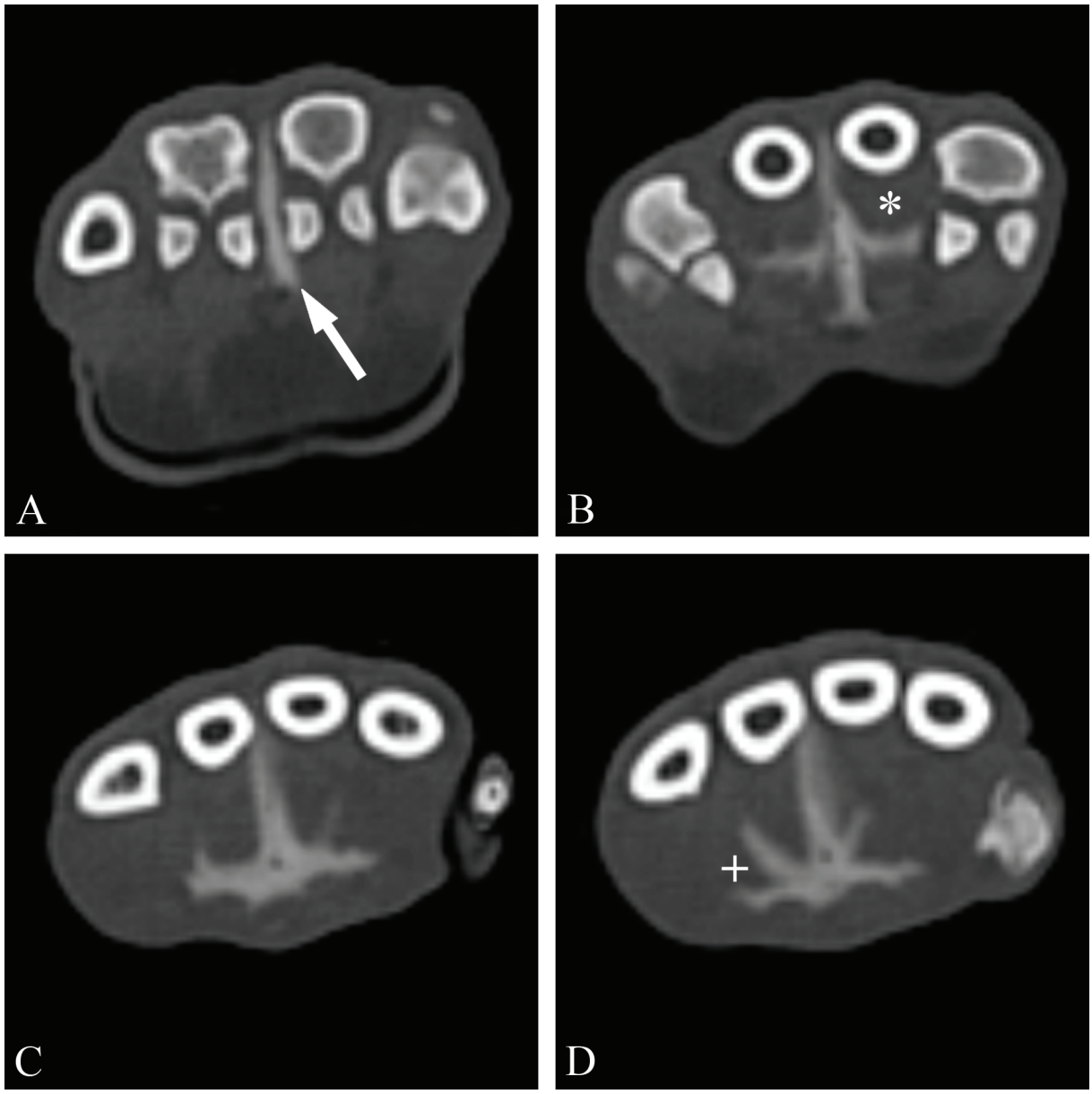

Figure 5.3: Transverse CT images of the midpalmar space. (A) The distal extent of the midpalmar space (arrow), at approximately the same level as the proximal extent of the central metacarpal pad space. (B) Image more proximal than A. Note the midpalmar space wrapping around the interosseous muscles (asterisk). (C) Image more proximal than B. (D) Image more proximal than C. The multiple spokes of the midpalmar space are evident at this level. The adductor digiti V muscle and palmar margin of the fifth interosseous muscle are indicated by +.

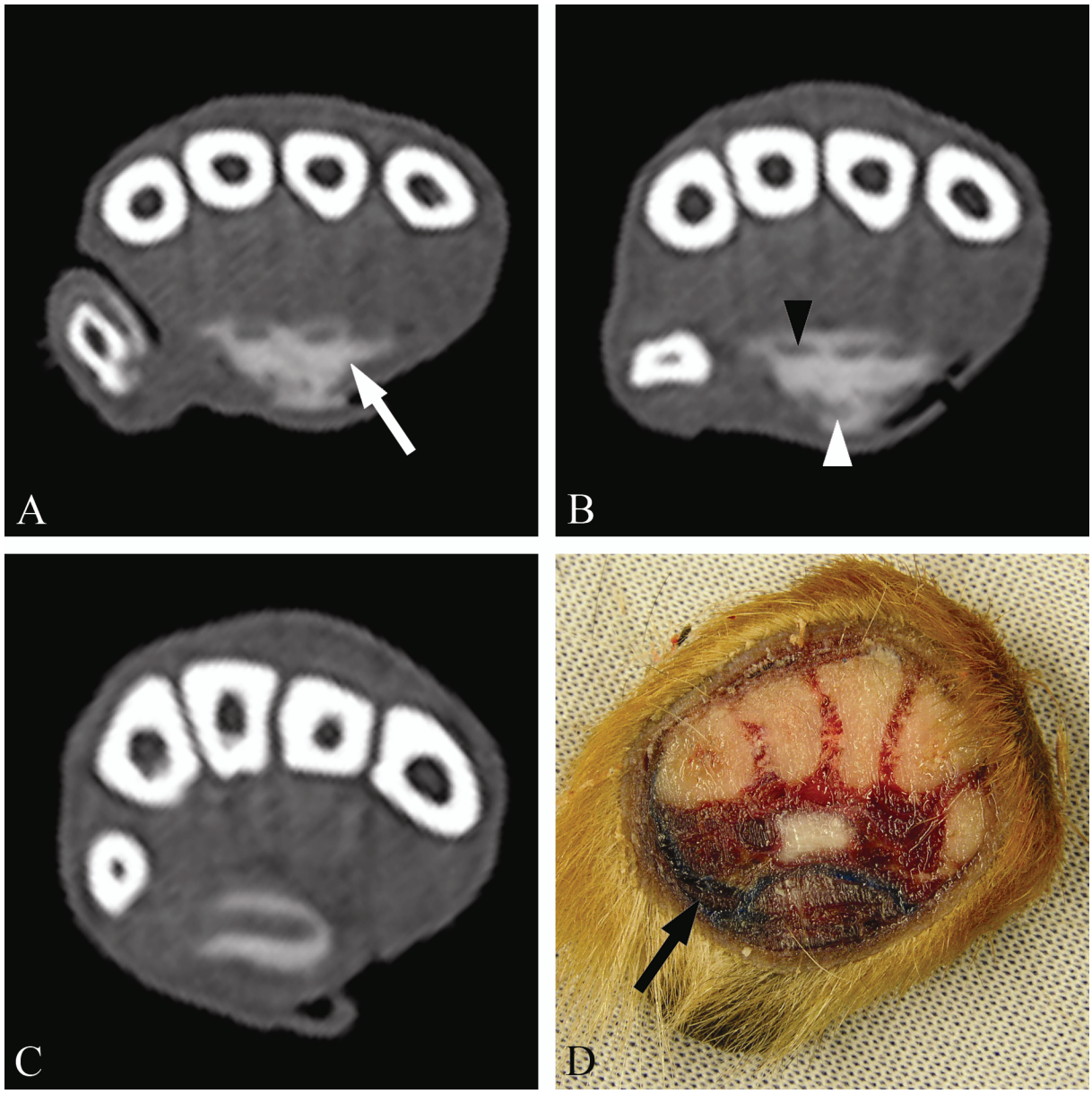

Figure 5.4: Transverse images of the flexor space. (A) CT image with contrast medium within the flexor space (white arrow) in the mid-metacarpus. (B) CT image more proximal than A. The filling defects in the flexor space are caused by the deep digital flexor tendons (black arrowhead) and superficial digital flexor tendons (white arrowhead). Note also the defect in the palmarolateral skin due to the incision made prior to injection. (C) CT image more proximal than B, at the level of the metacarpal bases. Here the flexor space surrounds only the deep digital flexor tendon. (D) Transverse section at approximately the same level as C in a different dog. The lateral recess can be seen surrounding abductor digiti V (black arrow) at the myotendinous junction.

The palmar subcutaneous space was located in the most superficial palmar tissues of the manus, and extended from the carpal pad to the distal portions (heads) of metacarpals III and IV (Figure 5.5 A-B). On midline of the manus, its dorsal (deep) boundary was a fascial plane separating it from the flexor space and superficial digital flexor tendons. Medially and laterally the palmar subcutaneous space extended dorsally near the palmarolateral cortex of metacarpal V and the palmar cortex of metacarpal I, but did not extend to the dorsum of the manus. At the medial and lateral margins of the palmar subcutaneous space, the skin of the manus was closely associated with the metacarpal bones, and there was minimal subcutaneous connective tissue, though there was no discrete structure which could be seen to prevent the extension of the contrast agent dorsally.

Soft-tissue spaces: Dorsal tissues

The extensor space was found on the dorsum of the manus and contained the common digital extensor and lateral digital extensor tendons (Figure 5.6 A-B). However, there was poor filling of the contrast medium around the dorsal aspect of these tendons, as the dorsal surface of the tendons was intimately associated with the fascial plane separating the extensor space from the dorsal subcutaneous space. The extensor space extended proximodistally from the bases of the metacarpal bones to the second through fifth metacarpophalangeal joints. At the distal margin of the space, the extensor space wrapped around the abaxial cortices of the metacarpal bones. (Figure 5.6A).

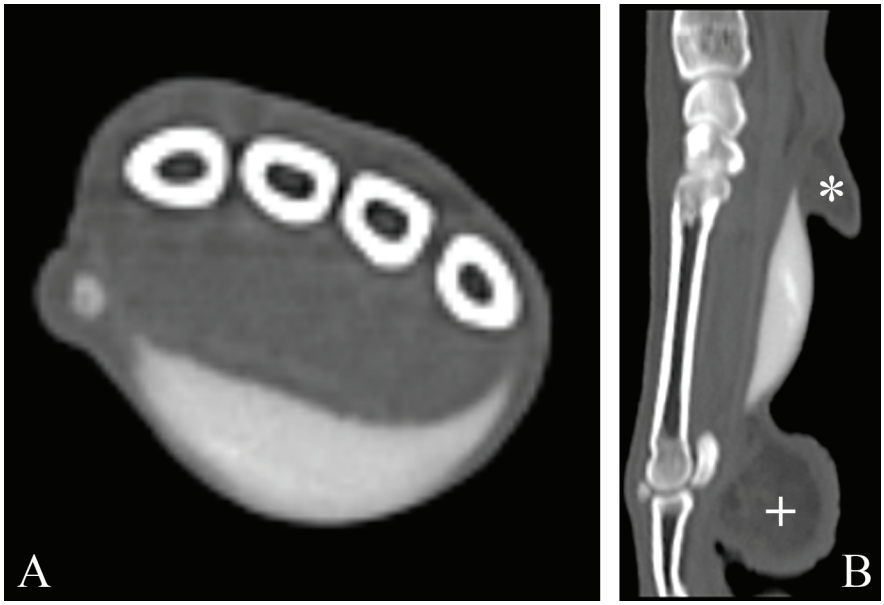

Figure 5.5: The palmar subcutaneous space. (A) Transverse CT image. The palmar subcutaneous space extends nearly to the cortices of the first digit and fifth metacarpal bone. (B) Sagittal CT image. The sharply marginated space extends between the carpal pad (asterisk) and the metacarpal pad (+).

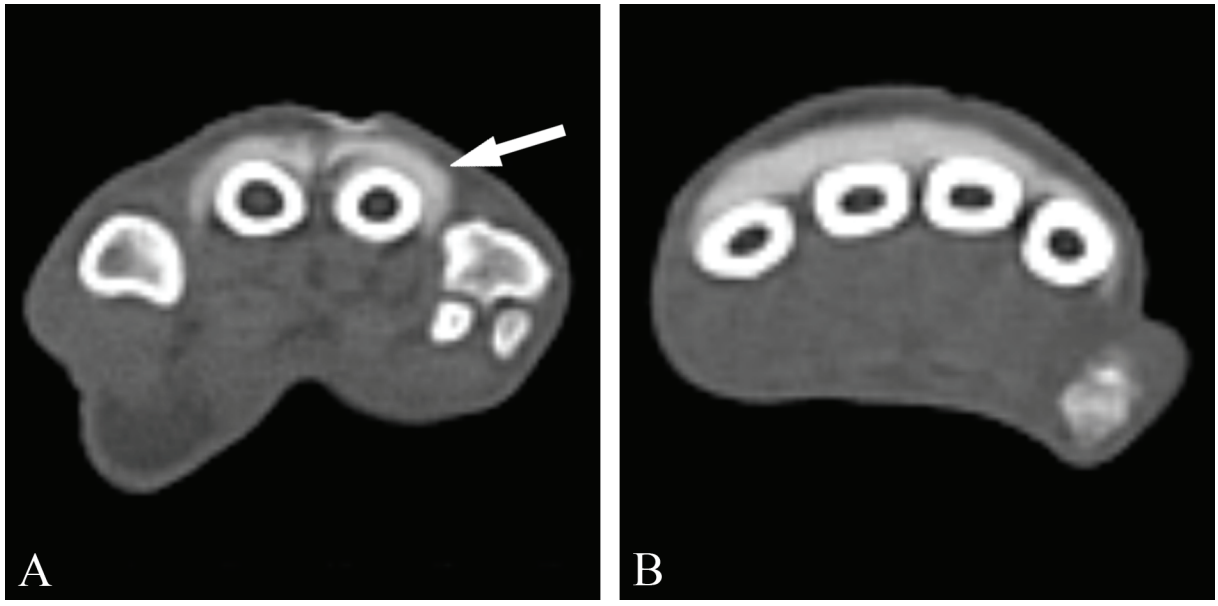

Figure 5.6: Transverse CT images of the extensor space. (A) The distal extent of the extensor space (arrow). Note the extension of the space around the abaxial cortices of metacarpal III and IV. (B) The extensor space in the mid-metacarpus. The contrast medium is in direct contact with the dorsal cortices of metacarpals II-V.

The dorsal subcutaneous space was located in the most superficial dorsal tissues of the manus, extending from the middle of the metacarpus to the metacarpophalangeal joints or proximal phalanges of the second through fifth digits. Its palmar (deep) margin was the fascial plane associated with the dorsal surface of the extensor tendons. The dorsal subcutaneous space extended medially to the dorsomedial margin of metacarpal II and laterally to the dorsal margin of metacarpal V; at these locations the dense fascia associated with the extensor space appeared tightly bound to the skin, likely preventing extension of contrast medium farther in a palmar or abaxial direction (Figure 5.7).

Myofascial compartments

Each of the four interosseous compartments (interosseous II-V) contained only the corresponding interosseous muscle (Figure 5.8A). However, though distension of the muscle was visualized, filling was incomplete in multiple cases: in some cases the filling was heterogeneous, and in some instances there was the appearance of subcompartmentalization of interosseous muscles II and V (Figure 5.8B). It should also be noted that, while the interosseous muscles are almost entirely located palmar to the corresponding metacarpal bones, a small triangular extension of the interosseous muscles extends between the metacarpal bones.

The abductor digiti V compartment primarily enclosed the muscle belly of abductor digiti V, and accordingly extended from the accessory carpal bone to the level of the metacarpal bases. A small amount of tissue immediately surrounding the muscle was also included in this compartment, and medially the caudal (palmar) interosseous artery and ulnar nerve passed through the compartment (Figure 5.9).

Figure 5.7: Transverse CT image of contrast medium within the dorsal subcutaneous space. The image is at the level of the distal one-third of the metacarpus. Note the unfilled space between the contrast medium and the metacarpal bones, representing the extensor space.

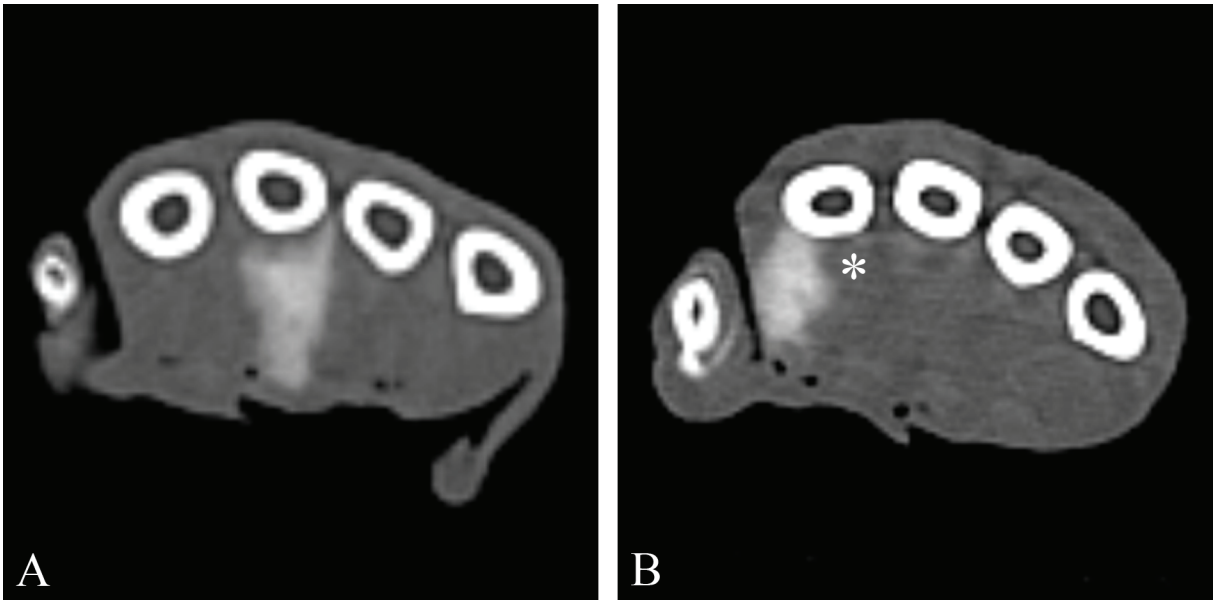

Figure 5.8: Transverse CT images of interosseous compartments. (A) Contrast medium within the third interosseous compartment. Note the relatively homogeneous filling and sharp margins. (B) Contrast medium within the second interosseous compartment. While the filling is homogeneous and the margins are rather sharp, the filled area represents only approximately half of the expected muscle. The unfilled portion of the muscle is indicated by an asterisk, though the precise boundaries cannot be seen due to the contrast resolution constraints of CT.

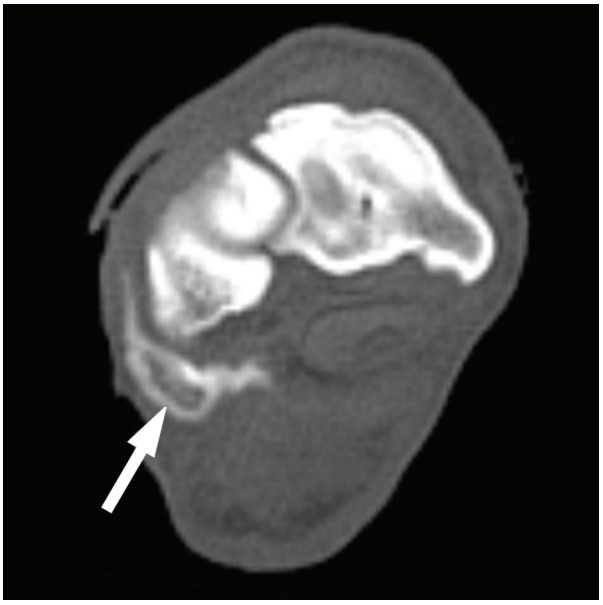

Figure 5.9: Transverse CT image of the abductor digiti V compartment (arrow) at the level of the proximal carpal row. The heterogeneous filling defect represents the muscle belly partially filled with contrast medium.

5. Discussion

Our results indicate that at least eighteen individual soft tissue spaces and myofascial compartments exist in the canine manus. Despite the use of relatively large volumes of contrast medium for the small spaces studied, distention of spaces without leakage of contrast medium was the norm. This finding indicates that, at least acutely, disease processes such as infection may remain relatively confined to the initial site of injury. For example, injection in the digital pads lead to retention of contrast medium within the soft tissues of the digit, and injection into the carpal pad lead to retention solely within the pad stroma. Confinement of the contrast agent emphasizes the need for early detection of disease, before pathology is more likely to spread further.

Perhaps more interesting for future clinical applications in mapping paths of disease spread were the results of injection into the metacarpal pad and midpalmar space. With injection into each lobe of the metacarpal pad, dense connective tissue prevented extension of the contrast medium into the other lobes of the pad. However, the contrast agent extended dorsally from each of the three lobes, terminating between the associated metacarpophalangeal joints. Similarly, the midpalmar space is located predominantly within the palmar tissues in the center of the manus, but one spoke of the space extends dorsally to terminate between the distal aspect of the third and fourth metacarpal bones. Thus, it is plausible that disease of any of these spaces could be directed to the dorsum of the manus, which could easily lead to incomplete resection of disease tissue during a surgical procedure. The subcutaneous spaces, on the contrary, had a relatively regular shape. A large volume of the contrast medium mixture was injected into the dorsal and palmar subcutaneous spaces, and the agent remained confined while causing marked distention

of the tissues, indicating a large capacitance of these tissues. Additionally, communication between the dorsal and palmar subcutaneous tissues was not identified.

The flexor space appears to be analogous to the ulnar bursa in the human hand, as it wraps around the flexor tendons.[59] However, the ulnar bursa in the human is a serous sheath that generally continues distally as the flexor tendon sheath for the fifth digit,[33] while in dogs this space appears to be composed only of connective tissue and bounded by fascial planes. No serous structure has been described in the palmar metacarpal region in dogs,[47] and the flexor space did not communicate with the flexor tendon sheaths of the digits in our study. An interesting finding in the flexor space in our study was the presence of a lateral recess encompassing the proximal aspect of the abductor digiti quinti tendon in two of the four injected specimens. This likely represents an anatomic variant, as variation in the precise morphology of spaces and compartments in the human hand is well recognized.[31,33,213,215] Given the small number of dogs in which we injected this space, the prevalence of the lateral recess cannot be estimated.

The cause of the variable appearance of the digital spaces is unknown. In most of the digital pad injections, the contrast medium spread throughout the soft tissues of the digit. However, occasionally the contrast agent remained in within the stroma of the digital pad with a very high backpressure to injection. In all cases, the tip of the needle was placed just below the keratinized dermal tissue of the pad. We feel the most likely situation is that in those cases with contrast medium retention in the pads themselves, the needle was not fully extended through the dermis into the pad stroma, making injection difficult and preventing spread of the contrast medium. When the needle was fully within the pad stroma, the contrast medium could easily spread throughout the digital soft tissues. However, an alternate theory is that each digital pad is

a discrete space separate from the digital soft tissue space and the needle was passed deep to the pad in those injections where the contrast medium spread more freely. Nonetheless, this second theory is considered unlikely as all needle tips remained superficial and of the stromal area of the pad filled in all cases, which would not be expected if the two spaces were separate and injection were made into the deeper tissues.

The limited proximal extent of the dorsal subcutaneous space is surprising, and a reason for the limited extent despite the relatively large volume of contrast medium administered was not identified. It is possible that the subcutaneous tissues in the region of the dorsal metacarpus become diminished in volume or the skin becomes more tightly adhered to the deeper tissues, thus acting as a barrier to spread. It is also possible that administration of an even larger volume of contrast medium would have allowed for more proximal spread because spread was inhibited by the relatively large capacitance of the more distal tissues into which the contrast medium was injected.

Heterogeneous incomplete filling of some interosseous muscles is understandable, as the contrast medium had to dissect between muscle fibers. However, in one instance each, only the more abaxial portion of interosseous muscles II and V were filled with contrast medium. The margination in both of these cases was relatively sharp, suggesting the existence of a subcompartment within the interosseous muscle. This was not seen in all cases and could represent an anatomic variant or may indicate the presence of a weaker boundary which may not be sufficient to withstand the pressures injected in some cases. Further evaluation would be required to determine the commonality and significance of this finding.

We have chosen to refer to the flexor space as a soft tissue space, though because it contains the lumbrical, interflexorius, and flexor digitorum brevis muscles one could argue for its

inclusion in the list of myofascial compartments. We list it as a soft tissue space for two reasons. First, the lumbrical muscles are present in the midpalmar space in the human hand, and numerous publications refer to this as a space,[33,39,59,213-216] while only one known to the authors considers it a compartment.[30] Second, an underlying premise for the recognition of a myofascial compartment is that it could be a location of compartment syndrome, which is produced by increased intramuscular pressure (often due to muscular swelling). Because the muscle bellies in the flexor space represent only a miniscule percentage of the overall volume of the space, their contribution to compartment syndrome is doubtful.

The adductor digiti II and adductor digiti V muscles are not considered myofascial compartments because the contrast medium leaked out of all sides of the muscle belly into the surrounding tissues, even with a small injection volume, and no distention of the muscle was visualized. Upon close examination, there was minimal to no fascial covering of these muscles to prevent diffusion of the contrast agent. Each muscle was likely considered a compartment on one CT evaluation because of the low volume of contrast medium administered before leakage occurred, though leakage in both cases was confirmed following anatomic sectioning. Similar to the adductor digiti muscles, the grouping of special muscles of digit I was not considered a compartment based on CT findings or anatomic findings. Again, the fascia surrounding these muscles is very thin, and the contrast agent spread throughout the surrounding tissues. Leakage of contrast medium from the needle tract could have confounded interpretation, with a true space or compartment being considered not a true space. However, following injection of other spaces and compartments this was recognized as a focal linear leakage on several CT images (generally resulting in a score of 3 for the space or compartment), and appeared considerably different from

the diffuse spread of contrast medium seen following injection of the adductor digiti II and V muscles and special muscles of digit I.

Because of the strict definition of a 4 on the five-point scale of contrast medium confinement (contrast medium homogeneous and confined, all margins sharp), there were very few spaces that received a score of 4. Only the flexor space, dorsal subcutaneous space, palmar subcutaneous space, and interosseous muscle III would have been considered soft-tissue spaces or myofascial compartments if a score of 4 were required to consider a region positive for confinement of the contrast agent. We chose to count scores of both 3 and 4 as positive for presence of a space or compartment because the category of 3 would include instances of slight leakage of the contrast agent out of the injection site and slightly ill-defined margins caused by partial volume averaging, both of which would be relatively apparent as artifactual occurrences. Additionally, our use of a five-point scale is analogous to five-point scales commonly used in scoring the certainty of a lesion in imaging studies: in these situations, the top two points are used as degrees of a positive score, the middle point as an equivocal score, and the bottom two points as negative scores.[395-397]

One limitation of this study was the use of only medium- to large-breed dogs. Small-breed dogs were excluded due to the small size of the soft-tissue spaces and myofascial compartments and the difficulties of injecting these small spaces without additional damage to the surrounding tissues. However, similar results would be expected in dogs of any size. Additionally, similar results to those found in this study would be expected in a study of the pes, as the anatomy of the canine metatarsus is quite similar to that of the metacarpus.[47] Indeed, such a study would be useful, as injuries to both the manus and the pes are common. However, because of limited

resources and the recognition of compartmental differences in the human hand and foot,[31,33,36,84] we chose to focus on only the canine manus in this study.

We acknowledge that a cadaver study identifying soft tissue spaces and myofascial compartments cannot demonstrate the actual clinical importance of these spaces in a living patient. While the contrast medium remained confined under the conditions of our model, such processes as inflammation could cause degradation of fascial barriers, thus allowing for further spread of disease. In addition, while recognition of tissue distention indicates increased pressure within the tissues, we cannot be certain if this mimics the amount of pressure that may be seen under pathologic conditions. Higher pressures may cause failure of some of the fascial boundaries that remained intact during our study. Pressures within the soft tissue spaces and myofascial compartments were not measured during our study due to the small size of the spaces: accurate pressure readings would require insertion of a second needle into the space, which was not possible without causing undue trauma to the space being studied.

In summary, there are at least eighteen discrete soft tissue spaces and compartments in the canine manus. Recognition of these compartments is important, as they may influence the spread of disease in the canine distal extremity. However, further study to evaluate their importance in clinical disease is required.

Footnotes

* Ultravist®, Berlex, Montville, NJ

† Super Pigmented Acrylic Ink, Speedball Art Products Co., Statesville, NC

‡ Picker PQ5000, Philips Medical Systems, Bothell, WA

§ eFilm Workstation 2.1, Merge Healthcare, Milwaukee, WI

Chapter VI

Modeling Infection Spread in the Canine Manus

Christopher P. Ober

Jeryl C. Jones, Martha Moon Larson, Otto I. Lanz, Stephen R. Werre

A version of this chapter has been accepted by the *American Journal of Veterinary Research*. (Ober CP, Jones JC, Larson MM, Lanz OI, and Werre SR. Modeling infection spread in the interdigital spaces of the canine manus. *American Journal of Veterinary Research*, in press.)

Supported by a grant from the American Kennel Club Canine Health Foundation.

1. Abstract

Objective – To determine if the pattern of extension of modeled infection from the interdigital web spaces is predictable and if the pattern of extension differs among initial injury sites.

Animals – Twenty-three normal adult medium- to large breed dog cadavers.

Procedures – The manus of each canine front limb was imaged using computed tomography (CT) both before and after injection of a radiopaque blue-staining contrast agent into the interdigital web spaces. Two veterinary radiologists reviewed the CT images and described the extent of contrast medium from each site. The paws were dissected or sectioned transversely after imaging, and the extent of contrast medium accumulation was described and compared with locations of CT contrast enhancement. Fisher's exact test was performed to determine if the pattern of contrast extension differed by injection site.

Results – Injections made in the interdigital web spaces of the canine manus led to unique and predictable patterns of extension in the surrounding soft tissues. Extension into the soft tissues primarily affected the soft tissues of the digits, and there was minimal involvement of previously described soft-tissue spaces in the manus.

Conclusions and Clinical Relevance – In humans, knowledge of common extension patterns from infected soft-tissue spaces in the hand is used to predict the spread of disease and develop surgical plans that will minimize patient morbidity. Identifying the common sites of disease spread from the interdigital web spaces in the dog will help improve surgical planning and treatment of infection in the canine manus.

2. Introduction

Abrasions, lacerations, and foreign body penetration are common in the paws of dogs, especially in working dogs. A 35-52% incidence of cuts, abrasions, and punctures in search-and-rescue and police dogs has been reported, and 50-70% of those injuries were on the distal limbs.[1,2] In these reports there were more than 9 events per 1,000 dog deployment hours, the highest system-specific disease incidence rate among deployed dogs.[1,2] Even if wounds are treated, chronic infection can develop from injuries to the paw, and the prolonged morbidity can cause loss of function and the need for rehabilitation. Exploratory surgery and debridement of affected tissues are commonly required in cases of chronic infection in the paw, but it is often difficult to achieve a cure with a single procedure, and multiple surgeries may be required.[4] Exploration generally must be extensive because infection typically extends beyond the site of initial injury. The requirement of a large surgical field and the frequent need for multiple procedures often results in further patient morbidity. A method for predicting the likely path of extension of pathology from a given injury site would help surgeons more efficiently plan their approaches and therefore minimize damage to normal anatomic structures.

Soft-tissue spaces and myofascial compartments in the human hand[30-33] and foot[34-36] are important in confining disease processes such as inflammation, infection, and neoplasia.[37-40] Because inflammation generally does not extend beyond the boundaries of one of these structures, surgical intervention can be directed at the affected structure, and complete exploration of the hand or foot is usually unnecessary.[38,40,41] We have recently identified soft-tissue spaces and myofascial compartments in the canine manus that are similar to those described in humans (see Chapter V). However, to our knowledge, there are no published

descriptions of extension patterns from one anatomic region to another in dogs. Thus, knowledge of the spaces in the canine manus remains of limited use in surgical planning.

The objective of this study was to test the hypothesis that fluid injected into different interdigital spaces as a model of infection will extend into and be confined differently by the surrounding soft tissues. We anticipate that this model will demonstrate a predictable path of disease based on the site of initial injury, with different sites of injury leading to spread of disease into different regions.

3. Materials and Methods

Sample collection

Front limbs were removed from twenty-three medium to large-breed dogs euthanized for reasons unrelated to front limb disease and were frozen immediately after removal. Limbs were to be excluded if there was evidence of orthopedic or soft tissue abnormalities, though none of these abnormalities were identified during the study. Once frozen, the forty-six limbs were divided into five batches of nine or ten limbs for imaging, and each batch was allowed to thaw in a walk-in cooler for approximately 16 hours before imaging. This thawing time allowed the limbs to be easily manipulated and injected during the imaging phase of the study.

Contrast medium preparation

Contrast medium components were mixed immediately prior to the first injections of each batch of limbs. The contrast medium mixture included 5 mL iopromide* and 2 mL indigo blue

acrylic ink[†] diluted in 45 mL 0.9% NaCl. The mixture was shaken approximately every 5 minutes to keep the blue pigment in suspension.

CT scanning and injection protocol

All of the limbs in each batch were imaged simultaneously using a sixteen-slice helical CT scanner.[‡] Three front limbs were placed on the couch side-by-side, in an extended position, as for a patient positioned head-first in sternal recumbency. Cardboard platforms were used to support two upper rows of three or four limbs; the positioning of the limbs in the upper two levels was the same as those in the lower row. Limb location was determined randomly. Pre-contrast CT scans of the front limbs were obtained from the distal ends of the digits through the distal antebrachium with helical acquisitions of 0.5 mm slice thickness using a modified carpus protocol (0.5 second rotation, 300 mA, 120 kVp, 250 mm field of view, 512 x 512 matrix, bone and soft-tissue reconstruction algorithms).

Following pre-contrast CT, one interdigital web space in each paw (medial, central, or lateral) was injected with 3 mL of the contrast agent using a 22G needle. This amount of contrast medium was found to cause repeatable marked distension of the interdigital web space and extension of the contrast agent into the surrounding tissues in all specimens in a pilot study. The injection site was determined randomly for each limb. One limb in the first scan group (the group of ten limbs) was not injected. After injection of the contrast material, the limbs were returned to their previous positions on the CT couch, and CT scans of the limbs were repeated with the same protocol as was used for the pre-contrast scan.

CT data recording

CT scans of the dog limbs were reviewed by two board-certified veterinary radiologists (CPO and JCJ) using a remote diagnostic workstation and commercially available DICOM viewing software.[§] Extension of the contrast agent at eight pre-determined CT slice locations was recorded using line drawings, and contrast medium dispersion was also described relative to recognizable anatomic structures, such as individual phalanges.

Anatomic correlation

The front limbs were frozen again after CT scanning. After freezing, some limbs were removed from the freezer for transverse sectioning using a band saw. The other front limbs were later thawed again for conventional dissection. Selection of paws for transverse sectioning and dissection was random, and all injection sites were represented by multiple specimens in each of the two sectioning methods. Extent of the blue-staining contrast medium was correlated with imaging findings.

Statistical analysis

Outcome was defined as extension of the contrast medium into any of the 5 regions (axial, abaxial, palmar, dorsal, or dorsal subcutaneous space of the metacarpus) associated with each of the 4 digits, or to any of the 3 web spaces (lateral, central, or medial). Thus, a total of 23 regions were considered. Subsequently, data were summarized as contingency tables of injection site (lateral, medial, or central) by digit region or web space. To test the null hypothesis that there is no association between site of injection and contrast medium migration to any of the digit regions or to any of the interdigital web spaces, all the contingency tables were visually

inspected using a Fisher's exact test. Statistical significance was set at $p = 0.05$. All analyses were performed using commercially available statistical software.[‖]

4. Results

CT scanning and injection protocol

Use of our CT scanning protocol allowed good visualization of all limbs. The contrast medium could be easily differentiated from the surrounding tissues, and the spatial resolution was sufficient to localize the extent of the contrast agent.

Sixteen injections were made into the medial interdigital web space, with fifteen made into the central web space and fourteen into the lateral web space. Marked distension of the interdigital spaces resulting in displacement of the associated digits away from the web space was seen with all injections, and increasing resistance to injection was noted over the course of each injection of contrast medium.

CT data recording

No difficulties in identifying the contrast agent were identified during the recording of data. Skin contamination with contrast medium was identified on two limbs, and there was a focus of soft tissue mineralization that was not continuous with the contrast agent in one digit; however, neither of these situations hindered interpretation of contrast medium extent. Gas bubbles were noted as incidental findings at two injection sites.

Anatomic correlation

Nine limbs were sectioned transversely using a band saw. The remaining limbs were dissected using conventional techniques. CT findings and anatomic descriptions were nearly identical in all cases. No discrepancies were found between CT descriptions and the anatomic descriptions of the transverse sections. However, in some cases evaluated with conventional dissection it was difficult to determine if the contrast agent extended into an adjacent interdigital web space or remained within the soft tissues of a digit. Evaluation of this extension was much easier when the paws were viewed transversely (with CT or transverse sectioning).

Statistical analysis

Repeatable and predictable patterns of contrast medium extension were seen with injection of the interdigital web spaces: in nearly all cases, injection of a web space caused filling of that web space and the adjacent margins of the associated digits (see Table 6.1). For example, injection of the medial interdigital web space caused filling of that web space, the axial soft tissues of digit II, and the abaxial soft tissues of digit III. The contrast agent also commonly extended into the palmar and dorsal soft tissues of those digits (Table 6.1). However, in all cases with dorsal extension there was a filling defect immediately dorsal to the phalanges in the location of the digital extensor tendons, and in all cases with palmar extension there was a filling defect immediately palmar to the phalanges in the location of the digital flexor tendons. When a soft-tissue region was involved for a given digit, the region adjacent to the proximal phalanx was almost invariably affected (98.3% of instances), the region adjacent to the middle phalanx was relatively commonly affected (70.8%), and the contrast agent uncommonly extended to the level of the distal phalanx (17.4%). The contrast medium within the web space itself tapered to a point

proximally at approximately the level of the third and fourth metacarpophalangeal joints, though the precise proximodistal location varied by individual. Representative CT images depicting the extent of the contrast agent are given in Figures 6.1 and 6.2, and composite drawings of the typical and predictable extent of spread are shown in Figures 6.3 and 6.4.

The contrast agent extended to the next adjacent interdigital web space (i.e. from a medial or lateral web space injection to the central web space, or from a central web space injection to the medial and/or lateral web spaces) with moderate frequency (Table 6.1). However, in these cases the contrast medium never extended further to affect the next adjacent digit. The contrast material also generally remained confined to the soft tissues of the digits, without extension beyond the level of the metacarpophalangeal joints. Extension of the contrast medium into the most distal portion of the dorsal subcutaneous space, associated with the distal metacarpal bones and dorsal sesamoid bones, occurred in only seven regions following six injections (13.3% of limbs, see Table 6.1 and Figure 6.5). Small tubular structures in the dorsal soft tissues of the manus extended from the most proximal aspect of the injected interdigital web space in all specimens; these were demonstrated to be lymphatic vessels upon dissection. In 7 of the 45 limbs (15.6%), the contrast agent was seen in dorsal lymphatic vessels extending from a web space adjacent to the injected space. Palmar lymphatics containing the contrast agent were identified extending from the injected space in two limbs (4.4%) and from a non-injected space in two other limbs (4.4%).

There were significant differences in the distribution of the contrast agent based on the site of injection (Table 6.1). Contrast medium injected into a given web space was significantly more likely to be found within that web space and the adjacent margins of the associated digits than with injections at other sites (all $p < 0.003$). While the contrast agent also commonly extended

into the dorsal and palmar tissues of the adjacent digits, as well, there were no significant differences in frequency of extension to these areas when comparing injections made in the two web spaces associated with these digits (e.g. extension from the medial and central web spaces to palmar or dorsal digit III, all $p > 0.28$).

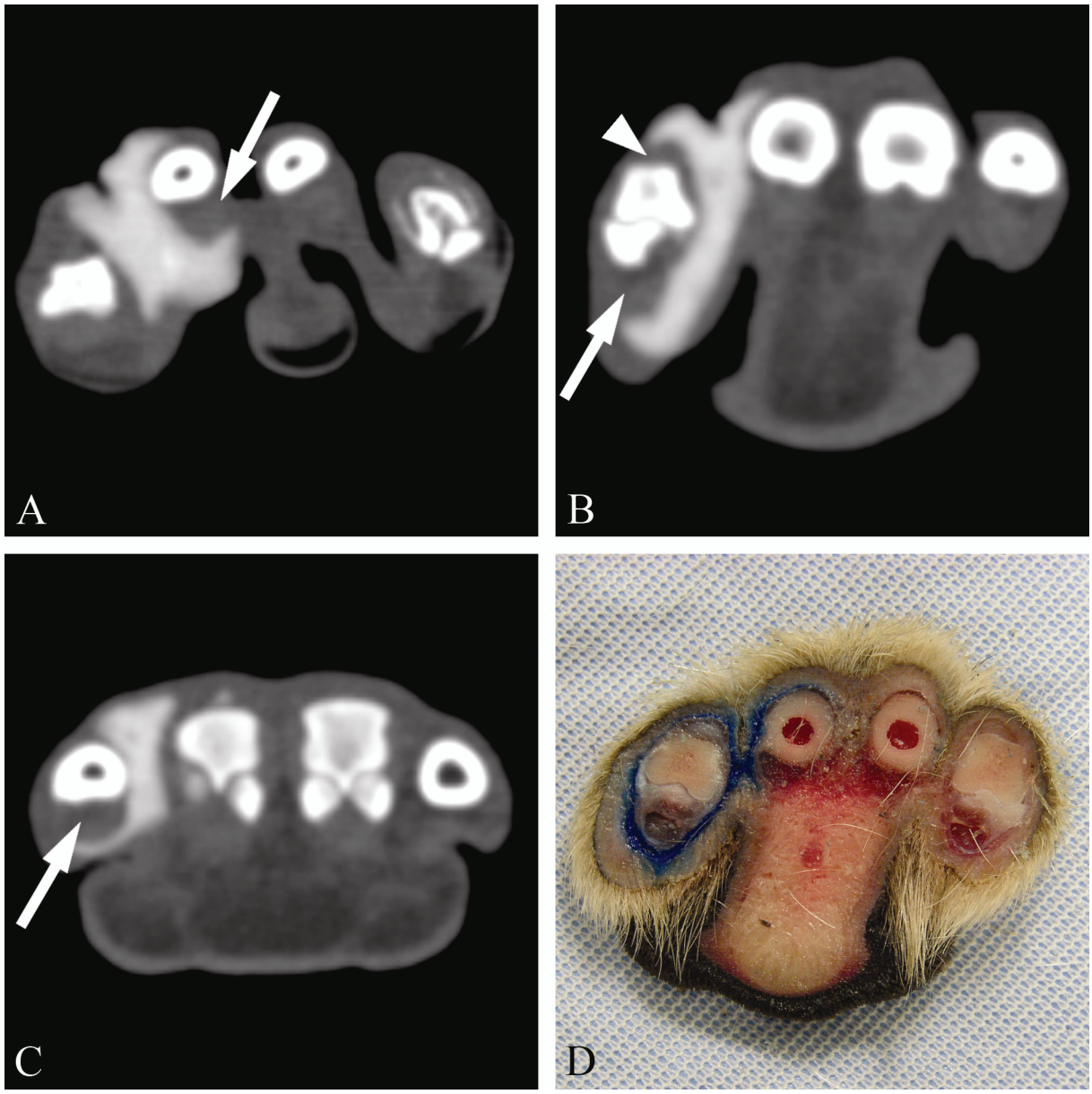

Figure 6.1: Transverse images of canine manus specimens following injection of the medial interdigital web space. An equivalent pattern was seen with injection of the lateral interdigital web space. (A-C) CT images advancing from distal to proximal. Note the marked distension of the injected interdigital web relative to the contralateral web space in A. The contrast medium tracks around the digital flexor tendons (arrows) and digital extensor tendons (arrowhead). (D) Transverse section of a manus at approximately the same level as B. Here the contrast agent surrounds digit II, and the extensor and flexor tendons are not infiltrated by the contrast medium.

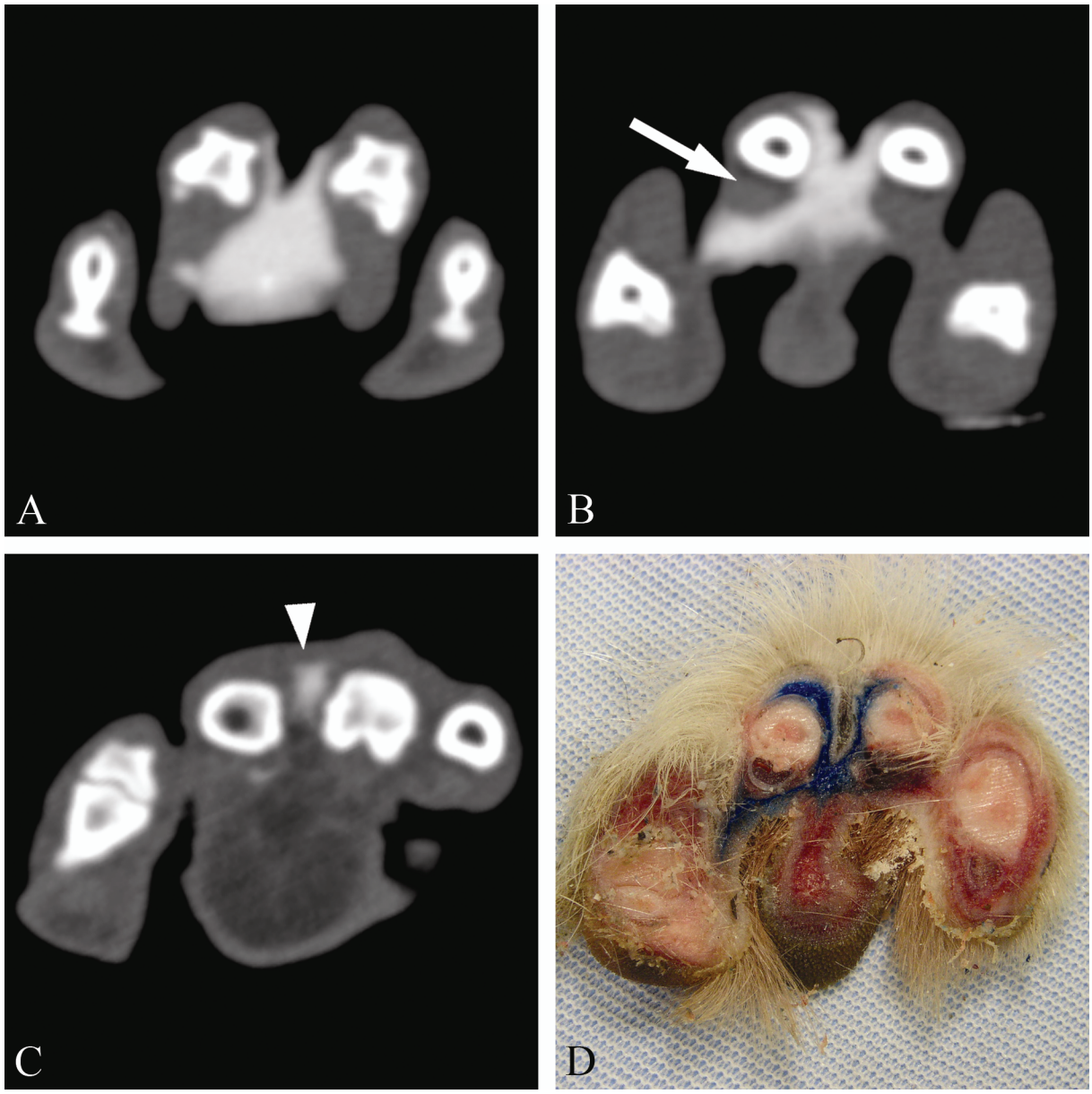

Figure 6.2: Transverse images of canine manus specimens following injection of the central interdigital web space. (A-C) CT images advancing from distal to proximal. Note the marked distension of the injected interdigital web space in A. The contrast medium extends around the digital flexor tendons (arrow). The proximal extent of the contrast medium (arrowhead) is just distal to the metacarpophalangeal joints, more distal than is seen in injection of the medial and lateral web spaces. (D) Transverse section of a manus at approximately the same level as B. The blue material can be seen extending into the adjacent web space on the left side of the image.

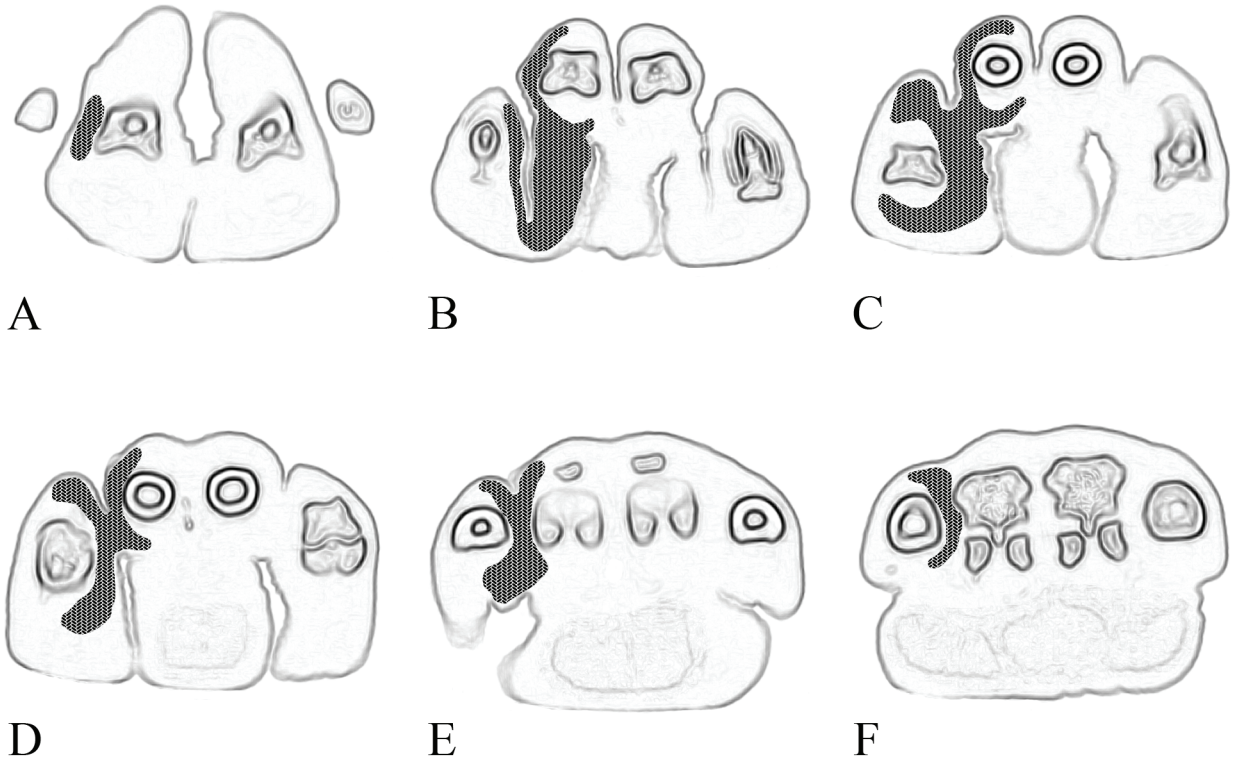

Figure 6.3: (A-F) Schematic transverse images of the canine manus advancing from distal to proximal. The shaded area represents the typical extent of contrast medium following injection of the medial or lateral interdigital web space. The contrast agent collection tapered rapidly in the transverse planes immediately proximal to the plane depicted in image F.

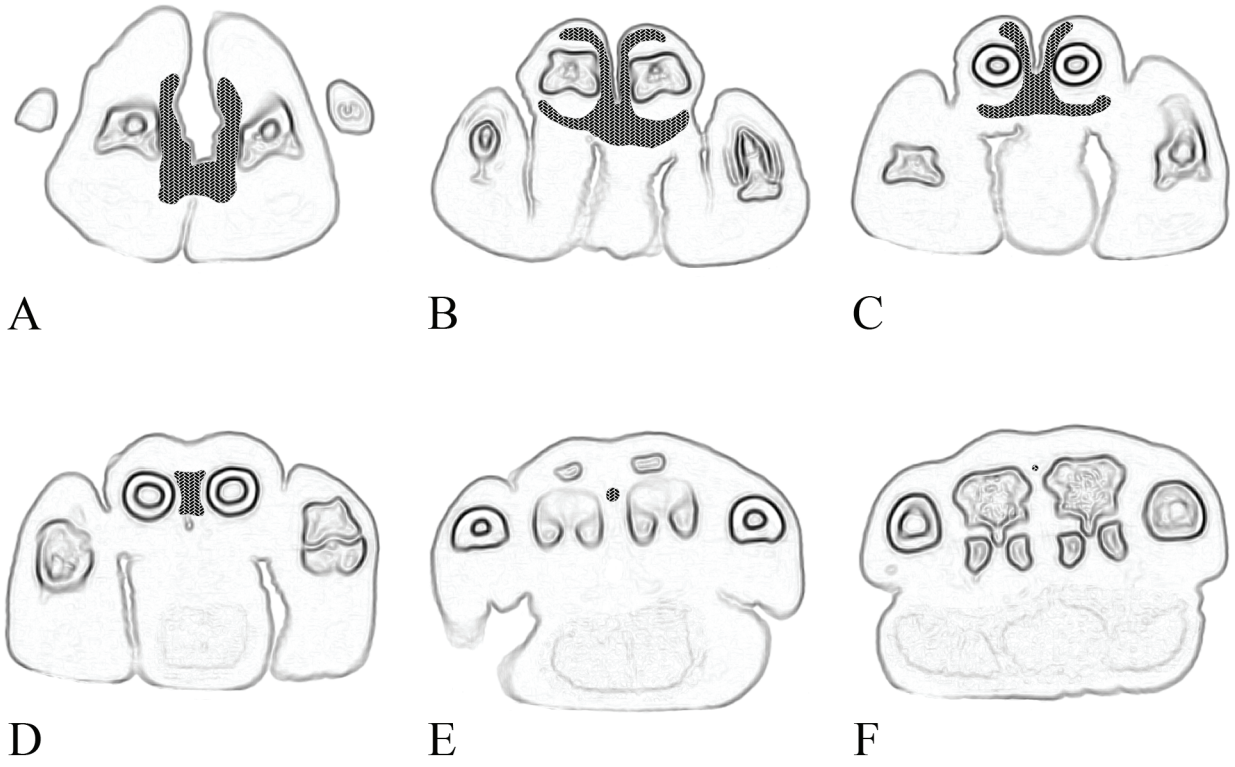

Figure 6.4: (A-F) Schematic transverse images of the canine manus advancing from distal to proximal. The shaded area represents the typical extent of contrast medium following injection of the central interdigital web space. The contrast agent collection tapered rapidly at the level of the metacarpophalangeal joints (E), and usually only a small tubular structure representing a lymphatic vessel could be seen proximal to this (F). When there was extension of the contrast medium to an adjacent web space, this extension invariably occurred at the levels depicted in image B or C.

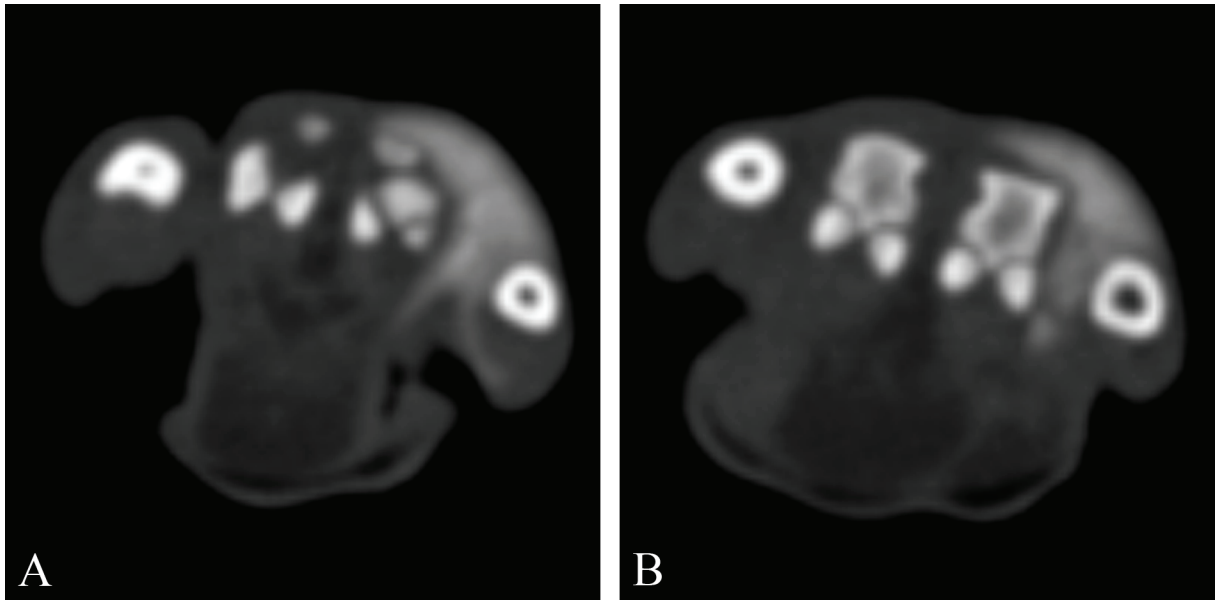

Figure 6.5: Transverse images of a canine manus following injection of the lateral interdigital web space. The contrast medium extends dorsoproximally into the distal aspect of the dorsal subcutaneous space. (A) The contrast agent is dorsal to the dorsal sesamoid bone of metacarpal IV. (B) The contrast agent is dorsal to the distal portion of metacarpal IV, at the level of the proximal margin of the proximal sesamoid bones. The linear filling defect between the contrast medium and the dorsal cortex of metacarpal IV represents the extensor tendons.

Table 6.1: Extension of Contrast Medium Into the Soft Tissues of the Manus by Injection Site (Percent of Cases)

	Digit II					Medial	Digit III					Central
Injection	Abaxial	Palmar	Dorsal	DSQ	Axial	Web	Abaxial	Palmar	Dorsal	DSQ	Axial	Web
Medial	18.8^{A}	75.0^{A}	75.0^{A}	6.2^{A}	100.0^{A}	100.0^{A}	100.0^{A}	93.8^{A}	37.5^{A}	12.5^{A}	6.25^{B}	18.8^{B}
Central	0.0^{A}	0.0^{B}	0.0^{B}	0.0^{A}	0.0^{B}	53.3^{B}	20.0^{B}	86.7^{A}	60.0^{A}	0.0^{A}	86.7^{A}	100.0^{A}
Lateral	0.0^{A}	0.0^{B}	0.0^{B}	0.0^{A}	0.0^{B}	0.0^{C}	0.0^{B}	0.0^{B}	0.0^{B}	0.0^{A}	0.0^{B}	21.4^{B}

	Digit IV					Lateral	Digit V				
Injection	Axial	Palmar	Dorsal	DSQ	Abaxial	Web	Axial	Palmar	Dorsal	DSQ	Abaxial
Medial	0.0^{B}	0.0^{B}	0.0^{B}	0.0^{B}	0.0^{B}	0.0^{C}	0.0^{B}	0.0^{B}	0.0^{B}	0.0^{A}	0.0^{A}
Central	100.0^{A}	86.7^{A}	66.7^{A}	0.0^{B}	6.7^{B}	46.7^{B}	0.0^{B}	0.0^{B}	0.0^{B}	0.0^{A}	0.0^{A}
Lateral	7.1^{B}	92.9^{A}	78.6^{A}	28.6^{A}	100.0^{A}	100.0^{A}	92.9^{A}	71.4^{A}	92.9^{A}	0.0^{A}	21.4^{A}

Note: Within each column, values followed by the same superscript are not significantly different.
DSQ = Dorsal subcutaneous space

5. Discussion

Our results show that injection of contrast medium into the interdigital web spaces results in predictable extension of the material into the surrounding soft tissues of the manus, as we hypothesized. This is important because the interdigital web spaces are among the most common sites for retention of foreign bodies;[6] consequently, recognizing the likely paths of foreign body migration or spread of infection is beneficial for surgical planning. While use of imaging would be beneficial for identification of the extent of inflammation or the presence of a foreign body,[124,204] this is not always possible, and exploratory surgery based on probable extent of disease may be required.

The findings in this study indicate that exploration should begin in the affected interdigital web space, as the web spaces have the capacity to contain a large amount of material. The proximal extent of the interdigital web space is approximately the level of the metacarpophalangeal joints. In our model, spread to the immediately adjacent soft tissues of the related digits occurred almost invariably, and these tissues should be considered to be involved as well. Involvement of the dorsal and palmar soft tissues of the adjacent digits was also common, so exploration of these areas may be required in most cases. While there was no infiltration of the contrast agent into the digital extensor and flexor tendons, these structures could be secondarily affected by dorsal or palmar inflammation through adhesion formation.

Just as pertinent for surgical planning are those sites which were involved less frequently, as failure to recognize spread of disease to these areas would result in continued morbidity and the requirement for additional surgical interventions. There were 21 instances of contrast medium extension to the next interdigital web space in 18 (40.0%) of the limbs (three injections

of the central web space resulted in extension to both the medial and lateral web spaces). Because the amount of material in many of these cases was small, it could easily be overlooked. Likewise, involvement of the dorsal subcutaneous space adjacent to seven metacarpal bones occurred after six injections (13.3% of limbs). This finding indicates that a distal palmar injury could lead to infection in the dorsum of the metacarpus, a site which may not be explored following a more palmar injury.

Statistical differences in the extension of the contrast agent based on site of injection will allow for further discrimination of necessary sites to explore in surgery. For example, if the abaxial tissues of digit III are known to be infected, involvement of the medial interdigital web space is also highly likely. However, contrast medium rarely extended from the central interdigital web space to abaxial digit III, so exploration of the central web space in this case may not be as critical. Additionally, the differences in contrast medium extension from the three interdigital web spaces and the marked distensibility of these spaces indicate that these three structures can likely be considered discrete soft-tissue spaces, similar to those identified in Chapter V. Retention of contrast medium within the web spaces was incomplete because the volume of contrast agent injected was deliberately chosen to cause extension of the contrast agent so that disease spread could be evaluated.

The anatomy of the interdigital web spaces in the manus of the dog appears to be analogous to the anatomy of the human interdigital web space. In the human hand, the interdigital webs are recognized as distinct subcutaneous fascial spaces in which pus may collect.[38,214,219] Indeed, it has been noted that the interdigital web spaces are one of the most common sites of pus collection, second only to the pulp spaces of the finger tips.[219] In the human, the web spaces are not continuous with each other, and are separated by the joint capsule and collateral ligaments of

the intervening metacarpophalangeal joints as well as the digital extensor tendons.[220] However, similar to the findings in our model in dogs, web space infections in humans may spread distally into the digit, medially or laterally into an adjacent web space, or proximally to the dorsum of the metacarpus.[219] A fourth direction of spread from the interdigital web spaces described in the human hand is proximally along a lumbrical canal into the midpalmar space.[219] We did not recognize this last path of spread in our study, possibly because of the differing anatomy between dogs and humans, including the vestigial nature of the lumbrical muscles in dogs,[47] and the association of the lumbrical muscles with the flexor tendons rather than the midpalmar space as in humans (see Chapter V).

While our study provides a model for disease spread in the canine manus, we recognize that further work using live dogs and actual infection would be required to better assess patterns of disease extension. Although soft-tissue structures tend to confine pathologic processes in people, this is not always the case. Depending on the chronicity and severity of infection and the anatomy of the initially affected soft-tissue space, the inflammatory process may extend to a neighboring space.[29,85] It is understood that cadaver models cannot replace clinical experiments and experience, as the conditions of infection and increased pressure in soft-tissue spaces and myofascial compartments cannot be faithfully replicated in cadavers.[32,35] Because of the actions of enzymes released during infection, it is not possible to fully evaluate the resistance of barriers to the spread of disease in a cadaver model: structures recognized as discrete compartments anatomically may not contain disease, especially if an infection is severe or chronic.[29,85] Nonetheless, studies of disease spread performed on human cadaver hands tend to correlate well with clinical experience,[213-215] and we feel that our results likewise represent a meaningful depiction of disease spread from the interdigital web spaces in dogs.

To summarize, extension of disease was highly predictable in our model of infection of the interdigital web spaces of the canine manus, and the most likely regions affected by infection were identified. Further, patterns of extension varied by the site of original injury, indicating that the three interdigital web spaces can be considered discrete soft-tissue spaces. While our results will be beneficial for surgical planning in patients with injury and infection of the web spaces, further work on patients with clinical disease will still be required. With the knowledge obtained from this cadaver model of disease, further work can be performed on clinical cases. Using CT or magnetic resonance imaging (MRI), we would have the background to more thoroughly evaluate the spread of infection or neoplasia *in vivo*, which would then allow us to develop more optimal prognostic and therapeutic techniques.

Footnotes

* Ultravist®, Berlex, Montville, NJ

† Super Pigmented Acrylic Ink, Speedball Art Products Co., Statesville, NC

‡ Aquilion TSX-101A Multislice CT Scanner, Toshiba America Medical Systems, Tustin, CA

§ eFilm Workstation 2.1, Merge Healthcare, Milwaukee, WI

|| SAS version 9.2, SAS Institute, Inc., Cary, NC

Chapter VII

Conclusion

1. Objectives and Findings

Injury and infection of the canine manus are important causes of morbidity, and imaging of the manus is important in affected patients because early detection of pathology is important for minimizing tissue damage. However, the sensitivity of radiography for disease is limited due to poor soft tissue contrast and the presence of multiple small structures within the manus. Other modalities, such as computed tomography (CT) and magnetic resonance imaging (MRI), show promise for use in better evaluating the distal extremity, but the normal sectional anatomy of the canine manus has not previously been described. Thus, the objectives for the first observational study were to describe the sectional anatomy of the canine manus, determine the visibility of structures using computed tomography and magnetic resonance imaging, and develop an anatomic atlas for use in characterization of lesions.

Both computed tomography and magnetic resonance imaging are useful modalities for imaging the normal canine manus. Osseous structures were generally easy to recognize using both modalities, although the dorsal sesamoid bones were more difficult to identify with MRI. Variations in cortical bone were also easier to see with CT, especially with use of different window width and level settings, as cortical bone has minimal to no signal on MRI. While regions of musculature could be recognized, discrete boundaries between muscle bellies were

only rarely resolved with the equipment available at our institution (single-slice CT scanner and 0.2T MRI). Border effacement of adjacent muscles on CT will likely prevent differentiation of individual myofascial compartments or soft-tissue spaces due to the inherent similarities in x-ray attenuation of the tissues, regardless of the technical specifications of the CT scanner itself. However, use of a higher field strength magnet, with corresponding improvements in spatial and contrast resolution, may be beneficial in identifying individual compartments in the canine manus, as 3T MRI has been used to identify compartments in the human foot.[84] Use of T1-weighted spin echo sequences could be used to provide good resolution, with fascial planes appearing as hypointense bands between medium-intensity muscles, and T1-weighted gradient recalled echo images would additionally accentuate tissue boundaries.[84]

While the flexor and extensor tendons in the canine manus could be visualized with both CT and MRI, these structures were only slightly hyperattenuating to the surrounding soft tissues on CT, making them somewhat difficult to distinguish. This was in marked contrast to MRI, where the markedly hypointense tendons were easily differentiated from the medium- to high-intensity surrounding soft tissues. Thus, MRI would likely be more useful than CT when imaging tendinous structures. Vessels were poorly visualized with either CT or MRI. This is likely a function of the spatial resolution of these modalities, especially for MRI, as many vessels are smaller than the corresponding voxels, so partial volume averaging would diminish recognition of these structures. This is especially true in the cadaver limbs that were imaged, as the vessels were not as distended with blood as they might be in a living animal. Additionally, the imaging characteristics of vessels would be expected to be similar to those of the surrounding tissues on both CT and MRI, leading to minimal contrast between the tissues. Thus, in summary, both CT

and MRI demonstrate the anatomy of the canine manus well, with CT demonstrating osseous structures somewhat more clearly and MRI depicting the soft tissues better.

* * *

Injuries to the distal extremities with possible retention of foreign material are significant concerns in dogs, especially working dogs. A retained foreign body should be suspected when there is a non-healing wound or persistent swelling or pain of the paw. Because most retained foreign objects are composed of plant matter, they are not visible on conventional radiographs, and it is difficult to diagnose the presence and exact location of the foreign body. The usual method of diagnosis via exploratory surgery is invasive and often ineffective at providing a diagnosis and fully alleviating clinical signs. Thus, a more effective and non-invasive diagnostic technique was sought. Based on clinical experiences and reports in the medical literature, ultrasound, CT, and MRI all appeared promising in their abilities to detect wooden foreign objects.

The objectives for the first critical study were to compare the diagnostic sensitivity of ultrasound, computed tomography, and magnetic resonance imaging in detection of wooden foreign objects in the canine manus, and to develop practice guidelines for use of those modalities when foreign body retention is suspected. We hypothesized that ultrasound would be the most sensitive modality for detection of wooden foreign bodies, and that all modalities would demonstrate some of the foreign objects.

The appearance of wood in our study was consistent with previous reports. With ultrasound wood appeared as an echogenic focus that produced a distal acoustic shadow, and on MRI the wooden foreign objects were visualized as small signal voids. CT is considered to produce the most variable characteristics of wood; the hypoattenuating appearance of wood in our study (-

100 to -250 HU) was consistent with the previously described appearance of acute wooden foreign bodies. Interestingly, some wooden foreign objects in this study also had a hyperattenuating rim (see Figure 4.2). We have postulated that this may be due to absorption of fluid in the periphery of the foreign object, or could represent compression of the surrounding tissues or introduction of water into the needle track secondary to insertion of the object.

Computed tomography was the most sensitive and most accurate modality for detection of acute wooden foreign bodies in the canine manus. Ultrasound was the second-most accurate modality, and MRI performed poorly. CT was more accurate than the other two modalities overall and in each individual anatomic region (interdigital web spaces, metacarpal pad, and palmar metacarpal tissues), ultrasound performed second-best overall and in all anatomic regions, and MRI was worst in all comparisons, with an accuracy no better than chance. While CT and ultrasound had similar sensitivities in the interdigital region, there was more disparity in the palmar metacarpus, and ultrasound performed worst in the metacarpal pad, likely due to the presence of shadowing seen in multiple specimens. The sensitivity of MRI was remarkably poor, as there were many false negatives and few true positives. Interestingly, no differences were seen in the specificities of the three modalities, as all modalities were good at recognizing true negatives with few false positives.

Although the results of this study were in favor of use of CT for imaging of wooden foreign objects in the canine manus, several caveats must be kept in mind. One important limitation of the study was the use of cadaver limbs in this study, as there was no inflammatory response. While this models an acute foreign-body injury, and as such a worst-case scenario for recognition of a foreign object, it is unlikely that a patient would be presented so soon after an injury as to have no detectable inflammation. An inflammatory response would have been

recognized with all three modalities, allowing the interpreter of the images to focus on a specific area. While the presence of inflammation alone does not indicate a foreign body, it may have changed the conspicuity of a foreign object. On MRI, a hypointense foreign body would be expected to be more visible when surrounded by T2-hyperintense inflammation. Post-contrast T1-weighted images would also cause enhancement of the inflamed tissues, which would also be expected to reveal a hypointense foreign object if one is present. In the initial inflammatory response, ultrasound may also be more sensitive for wooden foreign objects, as the echogenic surface would be more apparent when surrounded by hypoechoic inflammatory tissue. However, with long-standing inflammation the foreign body may become degraded, making it less visible. Similarly, absorption of fluid and enzymatic degradation of wood would change its imaging characteristics on CT, as its attenuation would increase over time. Depending on the degree of increase, this may make it less visible as its x-ray attenuation more closely matched that of the surrounding tissues. Thus, these considerations may have altered the conclusions of the study if imaging of chronic foreign body retention had been performed.

Another limitation of the study was the use of only one reader for each modality. Because these individuals were considered experts in their respective modalities, their results may not be representative of radiologists as a whole. Additionally, each study was only interpreted once, so learning effects could not be evaluated. Use of multiple readers for each modality and multiple interpretations for each reader would have allowed us to determine inter- and intraobserver variability, which could have strengthened the statistics.

* * *

While imaging of the manus would be the ideal method of diagnosing a retained foreign object, modalities such as ultrasound and computed tomography are not always available. This is

especially true for working dogs who are injured in the field. For these patients, exploratory surgery may be required to try to minimize morbidity and rehabilitation time. In these cases, it would be beneficial to be able to predict the path of foreign body migration or infection spread based on the site of initial injury. This would allow surgery to be directed toward the regions of the paw most likely to be affected. Soft-tissue spaces and myofascial compartments that determine the spread of disease in the human hand and foot are recognized, but there are no reports identifying these structures in the canine manus.

The objective for the second observational study was to describe the normal extent and location of soft-tissue spaces and myofascial compartments in the canine manus, using previously described structures in the human hand as a guide.

Based on injection experiments in cadaver limbs, we found thirteen discrete soft-tissue spaces and five myofascial compartments in the canine manus. While the contrast agent remained confined to these structures by definition, the shapes of several soft-tissue spaces suggest the probable direction of disease spread when these spaces are affected. For example, each lobe of the metacarpal pad was found to be a discrete space, without extension of contrast medium into the other lobes of the pad. However, the contrast medium spread dorsally from each of these lobes, coming to a point between the associated digits at the level of the metacarpophalangeal joints, nearly to the dorsum of the manus. Similarly, the midpalmar space has a spoke that extends between the third and fourth metacarpal bones, just proximal to the projection of the central metacarpal pad space. Because the injections in this study were performed in normal cadaver limbs, the tissues were sufficient to contain the contrast agent. However, it is probable that long-standing inflammation would cause degradation of some of the

boundaries, and extension of pus from one of these palmar compartments to the dorsum of the manus would be conceivable.

* * *

Because confinement of pathology to a single small soft-tissue space is unlikely in a chronic infection, recognition of likely sites of extension is important for surgical planning. If extension of infection from a given site of injury is consistent and predictable, and if different injury locations can be differentiated based on the spread of subsequent inflammation, directed surgical interventions will be feasible. In our model of infection spread, we chose to evaluate extension from the three interdigital web spaces in the canine manus, as these are common sites for foreign body retention.

The objectives for the second critical study were to describe the extent of involvement of the soft tissues of the manus in a model of injury to the interdigital web spaces, to evaluate if the initial site of injury could be used to predict likely extension of inflammation, and to determine whether patterns of extension caused by injury were unique to each interdigital web space. Hypotheses for this experiment were that the extension of inflammation could be predicted based on the known initial site of injury, and that the patterns of extension stemming from each individual injury site could be differentiated from each other.

Injection of the interdigital web spaces to a point of severe distension produced repeatable and predictable patterns of contrast medium extension into the surrounding soft tissues. For injection at a given web space, the contrast agent was nearly always present in the adjacent sides of the associated digits, and the dorsal and palmar tissues of those digits were also commonly involved. Filling defects representing the extensor and flexor tendons were always present, indicating that these structures were not infiltrated. Importantly, the contrast agent extended to an

adjacent web space 40% of the time, and extended into the dorsal subcutaneous space in 13% of specimens. Extension of infection in either of these patterns would require more extensive surgical exploration and would be more easily overlooked, likely leading to a need for further procedures.

Significant differences were found in patterns of extension from the three interdigital web spaces. Contrast medium found in the axial or abaxial soft tissues of a digit was significantly more likely to have originated from the adjacent web space than from another space. Based on this finding, if these tissues are infected, it would be appropriate to extend the surgical exploration to the adjacent web space and digit, as this would be a likely site of origin for the infection.

2. Benefits to Canine Health

The results of the foreign body identification study allow us to make recommendations for imaging of the canine manus when foreign body retention is suspected. Radiography remains the initial modality of choice, as this will allow for identification of mineral or metallic foreign objects. However, if conventional radiography is negative for a foreign object, additional imaging should be pursued. Computed tomography would be the best modality to use when there is suspicion of a retained wooden foreign object, based on its superior sensitivity and accuracy for these foreign bodies. Nonetheless, because CT is not widely available and requires sedation or anesthesia, ultrasound could also be performed as a screening test for wooden foreign objects. It should be remembered, though, that ultrasound diagnosis is highly operator-dependent, and even in the hands of an expert a negative test would not exclude the possibility of a foreign

object. Additionally, foreign objects in the metacarpal pad may be missed on ultrasound due to the acoustic shadowing originating from the skin surface. Most important, though, is the need for persistence when searching for foreign objects, as any given modality may not identify a retained object in a specific case.

Identification of multiple soft-tissue spaces and myofascial compartments in the canine manus indicates that disease processes are likely to remain confined to the area of initial pathology, at least acutely. The important implication of this finding is that surgical interventions can likely be directed to specific parts of the manus based on the location of the initial injury or inflammation. However, establishment of disease in living patients is more complex, and a degree of spread would be expected as the disease process becomes more chronic. Nonetheless, recognition of the geometry of the different spaces and compartments may allow us to predict which other structures may become secondarily affected (such as extension to the dorsal tissues following involvement of the midpalmar space).

Recognition of patterns of disease spread from commonly affected anatomic sites, such as the interdigital web spaces, will further aid surgical planning in patients with injury or infection originating from those sites. By predicting the probable spread of disease, a directed surgical intervention can be performed, and exploration may not have to extend to tissues that are unlikely to be affected, thus decreasing patient morbidity. Similarly, tissues that are likely to be involved can be explored even if pathology does not initially seem to extend that into those tissues, helping decrease the chances of missing a nidus of infection, in turn decreasing the likelihood of a need for additional surgical procedures.

3. Future Studies

Based on the results from this dissertation research, computed tomography is a beneficial modality for the identification of acute wooden foreign bodies, soft-tissue spaces, and myofascial compartments in the canine manus. However, all components of the research were limited by the use of cadaver limbs for imaging. Computed tomography was the best modality for identification of acute wooden foreign body retention, but the effects of inflammation could not be evaluated. Similarly, anatomic spaces and compartments were identified through injection of those structures, and a model of disease spread following injection was also studied, but neither of these studies could mimic the effects of inflammation and enzymatic degradation of tissues caused by infection.

Future research will entail evaluation of diseases of the canine manus in clinical patients. Prospective multimodality evaluation of patients with suspected foreign bodies in the manus could be performed to determine which imaging modality is most sensitive for identification of foreign bodies in the presence of inflammation. This would also allow for identification of the extent of inflammation caused by foreign objects, which could be correlated with surgical findings. Similarly, dogs with any inflammation or infection of the manus can be evaluated with pre- and post-contrast computed tomography or magnetic resonance imaging. With identification of the extent of disease, the importance of fascial boundaries in influencing disease spread in patients could be better determined. This would be especially beneficial if the site of initial injury is known, as spread of disease could be accurately mapped.

Multiple other avenues of related research are also available. For example, size and chronicity of foreign objects have important effects on their visibility when using any imaging

modality. However, the precise effects (such as minimal visible size) remain poorly understood. Comparing the impact of foreign body size and chronicity on conspicuity with multiple imaging modalities would be of value. This would be especially valuable in MR imaging, where the inflammatory response may help highlight a foreign object, but the amount of time required to sufficiently increase the contrast between the object and the surrounding tissues is unknown. Also, it is known that the composition of the metacarpal pad changes as dogs age, but the effects of this change on imaging appearance (which would influence foreign body detection) are unknown. Thus, evaluating these changes over time may be beneficial.

Patterns of lymphatic drainage are important considerations when evaluating any pathology of the limb, including inflammation and neoplasia. While the axillary lymph node is considered the sentinel lymph node for the thoracic limb in dogs, lymphatic drainage beyond this point is less well understood. Because of this, mapping of lymphatic drainage using lymphoscintigraphy or dye studies could help determine which lymph nodes are most important to evaluate when assessing disease spread.

Implications of compartment syndrome should also be considered when regarding the distal limb. Although clinical cases of compartment syndrome have been reported in dogs and compartment syndrome has also been experimentally produced in dogs, the overall clinical importance of compartment syndrome in the dog is unknown as this clinical entity is quite uncommon when compared to reports in humans. Further evaluation of the clinical pertinence of compartment syndrome in dogs could be performed by measuring intracompartmental pressures in dogs with predisposing conditions (fracture, other trauma, tight splints) and associating these pressure values with the development of clinical signs. Arteriography and venography could also be performed in these cases, or in experimentally induced cases of compartment syndrome, to

determine if the low incidence of clinical signs may be due to better collateral circulation. Additionally, the effects of increased intracompartmental pressure on imaging characteristics could also be evaluated.

The results of the current research will aid in the diagnosis and surgical management of foreign objects and infection in the canine manus, but further study will be necessary to refine these findings.

References

1. Slensky KA, Drobatz KJ, Downend AB, et al. Deployment morbidity among search-and-rescue dogs used after the September 11, 2001, terrorist attacks. *Journal of the American Veterinary Medical Association* 2004;225:868-873.

2. Fox PR, Puschner B, Ebel JG. Assessment of acute injuries, exposure to environmental toxins, and five-year health surveillance of New York Police Department working dogs following the September 11, 2001, World Trade Center terrorist attack. *Journal of the American Veterinary Medical Association* 2008;233:48-59.

3. Flom LL, Ellis GL. Radiologic evaluation of foreign bodies. *Emergency Medicine Clinics of North America* 1992;10:163-177.

4. Lamb CR, White RN, McEvoy FJ. Sinography in the investigation of draining tracts in small animals: retrospective review of 25 cases. *Veterinary Surgery* 1994;23:129-134.

5. Anderson MA, Newmeyer WL, III, Kilgore ES, Jr. Diagnosis and treatment of retained foreign bodies in the hand. *The American Journal of Surgery* 1982;144:63-67.

6. Brennan KE, Ihrke PJ. Grass awn migration in dogs and cats: a retrospective study of 182 cases. *Journal of the American Veterinary Medical Association* 1983;182:1201-1204.

7. Russell RC, Williamson DA, Sullivan JW, et al. Detection of foreign bodies in the hand. *The Journal of Hand Surgery* 1991;16A:2-11.

8. Horton LK, Jacobson JA, Powell A, et al. Sonography and radiography of soft-tissue foreign bodies. *American Journal of Roentgenology* 2001;176:1155-1159.

9. Oikarinen KS, Nieminen TM, Mäkäräinen H, et al. Visibility of foreign bodies in soft tissue in plain radiographs, computed tomography, magnetic resonance imaging, and ultrasound: an *in vitro* study. *International Journal of Oral and Maxillofacial Surgery* 1993;22:119-124.

10. Manthey DE, Storrow AB, Milbourn JM, et al. Ultrasound versus radiography in the detection of soft-tissue foreign bodies. *Annals of Emergency Medicine* 1996;28:7-9.

11. Ng SY, Songra AK, Bradley PF. A new approach using intraoperative ultrasound imaging for the localization and removal of multiple foreign bodies in the neck. *International Journal of Oral and Maxillofacial Surgery* 2003;32:433-436.

12. Leung A, Patton A, Navoy J, et al. Intraoperative sonography-guided removal of radiolucent foreign bodies. *Journal of Pediatric Orthopaedics* 1998;18:259-261.

13. Graham DD, Jr. Ultrasound in the emergency department: detection of wooden foreign bodies in the soft tissues. *The Journal of Emergency Medicine* 2002;22:75-79.

14. Dean AJ, Gronczewski CA, Costantino TG. Technique for emergency medicine bedside ultrasound identification of a radiolucent foreign body. *The Journal of Emergency Medicine* 2003;24:303-308.

15. Boyse TD, Fessell DP, Jacobson JA, et al. US of soft-tissue foreign bodies and associated complications with surgical correlation. *RadioGraphics* 2001;21:1251-1256.

16. Holmes P-J, Miller JR, Gutta R, et al. Intraoperative imaging techniques: a guide to retrieval of foreign bodies. *Oral Surgery, Oral Medicine, Oral Pathology, Oral Radiology, and Endodontology* 2005;100:614-618.

17. Bushberg JT, Seibert JA, Leidholdt EM, Jr., et al. *The Essential Physics of Medical Imaging*. 2nd ed. Philadelphia: Lippincott Williams & Wilkins, 2002.

18. Ginsberg LE, Williams DW, III, Mathews VP. CT in penetrating craniocervical injury by wooden foreign bodies: reminder of a pitfall. *American Journal of Neuroradiology* 1993;14:892-895.

19. Bodne D, Quinn SF, Cochran CF. Imaging foreign glass and wooden bodies of the extremities with CT and MR. *Journal of Computer Assisted Tomography* 1988;12:608-611.

20. Imokawa H, Tazawa T, Sugiura N, et al. Penetrating neck injuries involving wooden foreign bodies: the role of MRI and the misinterpretation of CT images. *Auris, Nasus, Larynx* 2003;30:S145-147.

21. Charney DB, Manzi JA, Turlik M, et al. Nonmetallic foreign bodies in the foot: radiography *versus* xeroradiography. *Journal of Foot Surgery* 1986;25:44-49.

22. Crawford R, Matheson AB. Clinical value of ultrasonography in the detection and removal of radiolucent foreign bodies. *Injury* 1989;20:341-343.

23. Bray PW, Mahoney JL, Campbell JP. Sensitivity and specificity of ultrasound in the diagnosis of foreign bodies in the hand. *Journal of Hand Surgery (American version)* 1995;20A:661-666.

24. Jacobson JA, Powell A, Craig JG, et al. Wooden foreign bodies in soft tissue: detection at US. *Radiology* 1998;206:45-48.

25. Mizel MS, Steinmetz ND, Trepman E. Detection of wooden foreign bodies in muscle tissue: experimental comparison of computed tomography, magnetic resonance imaging, and ultrasonography. *Foot and Ankle International* 1994;15:437-443.

26. Venter NG, Jamel N, Marques RG, et al. Avaliação de métodos radiológicos na detecção de corpo estranho de madeira em modelo animal. *Acta Cirúrgica Brasileira* 2005;20:19-26.

27. Koutinas CK, Papazoglou LG, Saridomichelakis MN, et al. Caudal mediastinal abscess due to a grass awn (*Hordeum* spp) in a cat. *Journal of Feline Medicine and Surgery* 2003;5:43-46.

28. Johnson MD, Magnusson KD, Shmon CL, et al. Porcupine quill injuries in dogs: a retrospective of 296 cases (1998-2002). *Canadian Veterinary Journal* 2006;47:677-682.

29. Ledermann HP, Morrison WB, Schweitzer ME. Is soft-tissue inflammation in pedal infection contained by fascial planes? MR analysis of compartmental involvement in 115 feet. *American Journal of Roentgenology* 2002;178:605-612.

30. Doyle JR. Anatomy of the upper extremity muscle compartments. *Hand Clinics* 1998;14:343-364.

31. DiFelice A, Jr., Seiler JG, III, Whitesides TE, Jr. The compartments of the hand: an anatomic study. *Journal of Hand Surgery (American version)* 1998;23A:682-686.

32. Guyton GP, Shearman CM, Saltzman CL. Compartmental divisions of the hand revisited: rethinking the validity of cadaver infusion experiments. *Journal of Bone and Joint Surgery (British volume)* 2001;83-B:241-244.

33. Grodinsky M, Holyoke EA. The fasciae and fascial spaces of the palm. *Anatomical Record* 1941;79:435-450.

34. Kamel R, Sakla FB. Anatomical compartments of the sole of the human foot. *Anatomical Record* 1961;140:57-60.

35. Guyton GP, Shearman CM, Saltzman CL. The compartments of the foot revisited: rethinking the validity of cadaver infusion experiments. *Journal of Bone and Joint Surgery (British volume)* 2001;83-B:245-249.

36. Seidel U, Bade H, Koebke J. Studies of the topography of the compartments of the foot. *Fuss & Sprunggelenk* 2003;1:191-198.

37. Toomayan GA, Robertson F, Major NM, et al. Upper extremity compartmental anatomy: clinical relevance to radiologists. *Skeletal Radiology* 2006;35:195-201.

38. Abrams RA, Botte MJ. Hand infections: treatment recommendations for specific types. *Journal of the American Academy of Orthopaedic Surgeons* 1996;4:219-230.

39. Pemberton PA. Infection of fascial spaces of the palm. *American Journal of Surgery* 1940;50:512-515.

40. Beye HL. Deep palmar hand infections: a clinical study of the diagnosis and treatment of these conditions. *Annals of Surgery* 1918;67:152-162.

41. Rauwerda JA. Foot debridement: anatomic knowledge is mandatory. *Diabetes/Metabolism Research and Reviews* 2000;16 (Suppl 1):S23-S26.

42. Sisson S. Carnivore osteology. In: Getty R, ed. *Sisson and Grossman's The Anatomy of the Domestic Animals*. 5th ed. Philadelphia: W.B. Saunders Co., 1975;1427-1503.

43. Evans HE. The skeleton. In: Evans HE, ed. *Miller's Anatomy of the Dog*. 3rd ed. Philadelphia: W.B. Saunders Co., 1993;122-218.

44. Dyce KM, Sack WO, Wensing CJG. *Textbook of Veterinary Anatomy*. 3rd ed. Philadelphia: Saunders, 2002.

45. Nickel R, Schummer A, Wille K-H, et al. Passive locomotor system, skeletal system. In: Nickel R, Schummer A,Seiferle E, eds. *The Anatomy of the Domestic Animals*. New York: Springer-Verlag, 1986;9-213.

46. Evans HE. Prenatal development. In: Evans HE, ed. *Miller's Anatomy of the Dog*. 3rd ed. Philadelphia: W.B. Saunders Co., 1993;32-97.

47. Hermanson JW, Evans HE. The muscular system. In: Evans HE, ed. *Miller's Anatomy of the Dog*. 3rd ed. Philadelphia: W.B. Saunders Co., 1993;258-384.

48. Seiferle E, Frewein J. Active locomotor system, muscular system, myologia. In: Nickel R, Schummer A,Seiferle E, eds. *The Anatomy of the Domestic Animals*. New York: Springer-Verlag, 1986;214-466.

49. Sisson S. Carnivore syndesmology. In: Getty R, ed. *Sisson and Grossman's The Anatomy of the Domestic Animals*. 5th ed. Philadelphia: W.B. Saunders Co., 1975;1504-1506.

50. St. Clair LE. Carnivore myology. In: Getty R, ed. *Sisson and Grossman's The Anatomy of the Domestic Animals*. Philadelphia: W.B. Saunders Co., 1975;1507-1537.

51. Evans HE. Arthrology. In: Evans HE, ed. *Miller's Anatomy of the Dog*. 3rd ed. Philadelphia: W.B. Saunders Co., 1993;219-257.

52. Nordberg CC, Johnson KA. Magnetic resonance imaging of normal canine carpal ligaments. *Veterinary Radiology and Ultrasound* 1998;39:128-136.

53. *Nomina Anatomica Veterinaria*. 4th ed. Ithaca, NY: International Committee on Veterinary Gross Anatomical Nomenclature, 1994.

54. Evans HE. The heart and arteries. In: Evans HE, ed. *Miller's Anatomy of the Dog*. 3rd ed. Philadelphia: W.B. Saunders Co., 1993;586-681.

55. Ghoshal NG. Carnivore heart and arteries. In: Getty R, ed. *Sisson and Grossman's The Anatomy of Domestic Animals*. 5th ed. Philadelphia: W.B. Saunders Co., 1975;1594-1651.

56. Evans HE. The veins. In: Evans HE, ed. *Miller's Anatomy of the Dog*. 3rd ed. Philadelphia: W.B. Saunders Co., 1993;682-716.

57. Kitchell RL, Evans HE. The spinal nerves. In: Evans HE, ed. *Miller's Anatomy of the Dog*. 3rd ed. Philadelphia: W.B. Saunders Co., 1993;829-893.

58. Dellman H-D, McClure RC. Carnivore neurology. In: Getty R, ed. *Sisson and Grossman's The Anatomy of the Domestic Animals*. 5th ed. Philadelphia: W.B. Saunders Co., 1975;1671-1740.

59. Netter FH. *Atlas of Human Anatomy*. Summit, New Jersey: Ciba-Geigy Corporation, 1989.

60. Al-Bagdadi F. The integument. In: Evans HE, ed. *Miller's Anatomy of the Dog*. 3rd ed. Philadelphia: W.B. Saunders Co., 1993;98-121.

61. Sisson S. Carnivore sense organs and common integument: common integument. In: Getty R, ed. *Sisson and Grossman's The Anatomy of the Domestic Animals*. 5th ed. Philadelphia: W.B. Saunders Co., 1975;1782-1783.

62. Habermehl K-H. Skin and cutaneous organs. In: Nickel R, Schummer A,Seiferle E, eds. *The Anatomy of the Domestic Animals*. New York: Springer-Verlag, 1981;441-557.

63. Basher A. Foot injuries in dogs and cats. *Compendium on Continuing Education for the Practicing Veterinarian* 1994;16:1159-1176.

64. Besancon MF, Conzemius MG, Evans RB, et al. Distribution of vertical forces in the pads of Greyhounds and Labrador Retrievers during walking. *American Journal of Veterinary Research* 2004;65:1497-1501.

65. Doyle JR, Tornetta P, Einhorn TA. Compartment syndrome. In: Doyle JR, Tornetta P,Einhorn TA, eds. *Hand and Wrist*. Philadelphia: Lippincott, Williams, and Wilkins, 2005.

66. Seiler JG, III, Olvey SP. Compartment syndromes of the hand and forearm. *Journal of the American Society for Surgery of the Hand* 2003;3:184-198.

67. McDonald AP, III, Lourie GM. Complex surgical conditions of the hand: avoiding the pitfalls. *Clinical Orthopaedics and Related Research* 2005;433:65-71.

68. Ouellette EA, Kelly R. Compartment syndromes of the hand. *Journal of Bone and Joint Surgery (American volume)* 1996;78:1515-1522.

69. Kumar R, Trikha V. Compartment syndrome of the hand in an infant. *Injury Extra* 2005;36:127-129.

70. Sharma H, Rana B, Naik M. Bipedal compartment syndrome following bilateral intra-articular calcaneal fractures. *Foot and Ankle Surgery* 2004;10:93-96.

71. Maharaj D, Bahadursingh S, Shah D, et al. Sepsis and the scalpel: anatomic compartments and the diabetic foot. *Vascular and Endovascular Surgery* 2005;39:421-423.

72. Andermahr J, Helling HJ, Tsironis K, et al. Compartment syndrome of the foot. *Clinical Anatomy* 2001;14:184-189.

73. Adelaar RS. Complications of forefoot and midfoot fractures. *Clinical Orthopaedics and Related Research* 2001;391:26-32.

74. Blick SS, Brumback RJ, Poka A, et al. Compartment syndrome in open tibial fractures. *Journal of Bone and Joint Surgery (American volume)* 1986;68-A:1348-1353.

75. Konstantakos EK, Dalstrom DJ, Nelles ME, et al. Diagnosis and management of extremity compartment syndromes: an orthopaedic perspective. *American Surgeon* 2007;73:1199-1209.

76. Department of Defense USA. Injuries to the Hands and Feet. *Emergency War Surgery*. Third United States Revision ed, 2004.

77. Ascer E, Strauch B, Calligaro KD, et al. Ankle and foot fasciotomy: an adjunctive technique to optimize limb salvage after revascularization for acute ischemia. *Journal of Vascular Surgery* 1989;9:594-597.

78. Holstege CP, Miller MB, Wermuth M, et al. Crotalid snake envenomation. *Critical Care Clinics* 1997;13:889-921.

79. Selek H, Özer H, Aygencel G, et al. Compartment syndrome in the hand due to extravasation of contrast material. *Archives of Orthopaedic and Trauma Surgery* 2007;127:425-427.

80. Seiler JG, III, Valadie AL, III, Drvaric DM, et al. Perioperative compartment syndrome: a report of four cases. *Journal of Bone and Joint Surgery (American volume)* 1996;78-A:600-602.

81. Matava MJ, Whitesides TE, Jr., Seiler JG, III, et al. Determination of the compartment pressure threshold of muscle ischemia in a canine model. *Journal of Trauma* 1994;37:50-58.

82. Kumar PR, Jenkins JPR, Hodgson SP. Bilateral chronic exertional compartment syndrome of the dorsal part of the forearm: the role of magnetic resonance imaging in diagnosis. *Journal of Bone and Joint Surgery (American volume)* 2003;85:1557-1559.

83. Colosimo AJ, Ireland ML. Thigh compartment syndrome in a football athlete: a case report and review of the literature. *Medicine and Science in Sports and Exercise* 1992;24:958-963.

84. Reach JS, Jr., Amrami KK, Felmlee JP, et al. Anatomic compartments of the foot: a 3-Tesla magnetic resonance imaging study. *Clinical Anatomy* 2007;20:201-208.

85. Goodwin DW, Salonen DC, Yu JS, et al. Plantar compartments of the foot: MR appearance in cadavers and diabetic patients. *Radiology* 1995;196:623-630.

86. Gest TR, Schlesinger J. *MedCharts Anatomy*. New York: ILOC, Inc., 1995.

87. Kingston R, Sparkes J, Keogh P, et al. Midpalmar space hematoma mimicking compartment syndrome of the hand. *Journal of Orthopaedic Trauma* 2002;16:56-57.

88. Schnall SB, Vu-Rose T, Holtom PD, et al. Tissue pressures in pyogenic flexor tenosynovitis of the finger: compartment syndrome and its management. *Journal of Bone and Joint Surgery (British volume)* 1996;78-B:793-795.

89. Manoli A, II, Weber TG. Fasciotomy of the foot: an anatomical study with special reference to release of the calcaneal compartment. *Foot and Ankle* 1990;10:268-275.

90. Fulkerson E, Razi A, Tejwani N. Review: acute compartment syndrome of the foot. *Foot and Ankle International* 2003;24:180-187.

91. Daniels JM, II, Zook EG, Lynch JM. Hand and wrist injuries: Part II. Emergent evaluation. *American Family Physician* 2004;69:1949-1956.

92. Devor M, Sørby R. Fibrotic contracture of the canine infraspinatus muscle. *Veterinary and Comparative Orthopaedics and Traumatology* 2006;19:117-121.

93. McQueen MM, Court-Brown CM. Compartment monitoring in tibial fractures: the pressure threshold for decompression. *Journal of Bone and Joint Surgery (British volume)* 1996;78-B:99-104.

94. Strauss MB, Hargens AR, Gershuni DH, et al. Delayed use of hyperbaric oxygen for treatment of a model anterior compartment syndrome. *Journal of Orthopaedic Research* 1986;4:108-111.

95. Better OS, Rubinstein I, Winaver JM, et al. Mannitol therapy revisited (1940-1997). *Kidney International* 1997;51:886-894.

96. Olivieri M, Suter PF. Compartmental syndrome of the front leg of a dog due to rupture of the median artery. *Journal of the American Animal Hospital Association* 1978;14:210-218.

97. Basinger RR, Aron DN, Crowe DT, et al. Osteofascial compartment syndrome in the dog. *Veterinary Surgery* 1987;16:427-434.

98. de Haan JJ, Beale BS. Compartment syndrome in the dog: case report and literature review. *Journal of the American Animal Hospital Association* 1993;29:134-140.

99. Williams J, Bailey MQ, Schertel ER, et al. Compartment syndrome in a Labrador Retriever. *Veterinary Radiology and Ultrasound* 1993;34:244-248.

100. Moed BR, Strom DE. Compartment syndrome after closed intramedullary nailing of the tibia: a canine model and report of two cases. *Journal of Orthopaedic Trauma* 1991;5:71-77.

101. Low VHS, Killius JS. Animal, vegetable, or mineral: a collection of abdominal and alimentary foreign bodies. *Applied Radiology* 2000;29:23-30.

102. Applegate KE, Dardinger JT, Lieber ML, et al. Spiral CT scanning technique in the detection of aspiration of LEGO foreign bodies. *Pediatric Radiology* 2001;31:836-840.

103. Ayantunde AA, Oke T. A review of gastrointestinal foreign bodies. *International Journal of Clinical Practice* 2006;60:735-739.

104. Root CR, Lord PF. Linear radiolucent gastrointestinal foreign bodies in cats and dogs: their radiographic appearance. *Veterinary Radiology* 1971;12:45-53.

105. Papazoglou LG, Patsikas MN, Rallis T. Intestinal foreign bodies in dogs and cats. *Compendium: Continuing Education for Veterinarians* 2003;25:830-843.

106. Hunter TB, Taljanovic MS. Foreign bodies. *RadioGraphics* 2003;23:731-757.

107. Jones JC, Ober CP. Computed tomographic diagnosis of non-gastrointestinal foreign bodies in dogs. *Journal of the American Animal Hospital Association* 2007;43:99-111.

108. Erne JB. Nasal foreign body in a dog. *Veterinary Forum* 2008;25:56-60.

109. Gupta AK, Berry M. Detection of a radiolucent bronchial foreign body by computed tomography. *Pediatric Radiology* 1991;21:307-308.

110. Hasegawa J, Watanabe K-i, Kunitomo M, et al. Foreign body in the maxillary sinus - possible plastic tube: a case report. *Auris, Nasus, Larynx* 2003;30:299-301.

111. Tivers M, Moore AH. Tracheal foreign bodies in the cat and the use of fluoroscopy for removal: 12 cases. *Journal of Small Animal Practice* 2006;47:155-159.

112. Cotran RS, Kumar V, Collins T. *Robbins Pathologic Basis of Disease*. 6th ed. Philadelphia: W.B. Saunders Company, 1999.

113. Luttikhuizen DT, Harmsen MC, Van Luyn MJA. Cellular and molecular dynamics in the foreign body reaction. *Tissue Engineering* 2006;12:1955-1970.

114. Cracchiolo A, III, Goldberg L. Local and systemic reactions to puncture injuries by the sea urchin spine and the date palm thorn. *Arthritis and Rheumatism* 1977;20:1206-1212.

115. Qiu HH, Hedlund LW, Neuman MR, et al. Measuring the progression of foreign-body reaction to silicone implants using *in vivo* MR microscopy. *IEEE Transactions on Biomedical Engineering* 1998;45:921-927.

116. Zimmerli W, Lew PD, Waldvogel FA. Pathogenesis of foreign body infection: evidence for a local granulocyte defect. *Journal of Clinical Investigation* 1984;73:1191-1200.

117. Phlegmon. *Merriam-Webster Online Medical Dictionary*: Merriam-Webster Online, 2009.

118. Ralls PW, Boswell W, Henderson R, et al. CT of inflammatory disease of the psoas muscle. *American Journal of Roentgenology* 1980;134:767-770.

119. Moizhess TG. Carcinogenesis induced by foreign bodies. *Biochemistry (Moscow)* 2008;73:763-775.

120. Gnudi G, Volta A, Bonazzi M, et al. Ultrasonographic features of grass awn migration in the dog. *Veterinary Radiology and Ultrasound* 2005;46:423-426.

121. Blankstein A, Cohen I, Heiman Z, et al. Localization, detection and guided removal of soft tissue in the hands using sonography. *Archives of Orthopaedic and Traumatic Surgery* 2000;120:514-517.

122. Levine MR, Gorman SM, Young CF, et al. Clinical characteristics and management of wound foreign bodies in the ED. *American Journal of Emergency Medicine* 2008;26:918-922.

123. O'Reilly A, Beck C, Mouatt JG, et al. Exophthalmos due to a wooden foreign body in a dog. *Australian Veterinary Journal* 2002;80:268-271.

124. Peterson JJ, Bancroft LW, Kransdorf MJ. Wooden foreign bodies: imaging appearance. *American Journal of Roentgenology* 2002;178:557-562.

125. Imoisili MA, Bonwit AM, Bulas DI. Toothpick puncture injuries of the foot in children. *Pediatric Infectious Disease Journal* 2004;23:80-82.

126. Newman JT, Hunt DW. Toothpick foreign body in the foot: a case report. *Journal of the American Podiatric Medical Association* 1989;79:458-461.

127. Ik Yang, Hayes CW, Jacobson JA, et al. Unique foreign body injury: bamboo penetration fo thigh and pelvis while skiing. *Emergency Radiology* 2002;9:243-246.

128. Boncoeur-Martel MP, Adenis JP, Rulfi JY, et al. CT appearances of chronically retained wooden intraorbital foreign bodies. *Neuroradiology* 2001;43:165-168.

129. Krimmel M, Cornelius CP, Stojadinovic S, et al. Wooden foreign bodies in facial injury: a radiological pitfall. *International Journal of Oral and Maxillofacial Surgery* 2001;30:445-447.

130. Uchino A, Kato A, Takase Y, et al. Intraorbital wooden and bamboo foreign bodies: CT. *Neuroradiology* 1997;39:213-215.

131. Van Thong Ho, McGuckin JF, Jr., Smergel EM. Intraorbital wooden foreign body: CT and MR appearance. *American Journal of Neuroradiology* 1996;17:134-136.

132. Yoshii M, Enoki T, Mizukawa A, et al. Intraorbital wooden foreign body. *Acta Ophthalmologica Scandinavica* 2004;82:492-493.

133. Robinson PD, Rajayogeswaran V, Orr R. Unlikely foreign bodies in unusual facial sites. *British Journal of Oral and Maxillofacial Surgery* 1997;35:36-39.

134. Nishio Y, Hayashi N, Hamada H, et al. A case of delayed brain abscess due to a retained intracranial wooden foreign body: a case report and review of the last 20 years. *Acta Neurochirurgica* 2004;146:847-850.

135. Pal D, Timothy J, Marks P. Penetrating spinal injury with wooden fragments causing cauda equina syndrome: case report and literature review. *European Spine Journal* 2006;15:574-577.

136. Green BF, Kraft SP, Carter KD, et al. Intraorbital wood: detection by magnetic resonance imaging. *Ophthalmology* 1990;97:608-611.

137. Weinacht S, Zaunbauer W, Gottlob I. Optic atrophy induced by an intraorbital foreign body: the role of CT and MRI. *Journal of Pediatric Ophthalmology and Strabismus* 1998;35:179-181.

138. Robaei D, Fernando GT, Branley MG, et al. Orbitocranial penetration by a fragment of wood. *Medical Journal of Australia* 2004;181:329-330.

139. Dalley RW. Intraorbital wood foreign bodies on CT: Use of wide bone window settings to distinguish wood from air. *American Journal of Roentgenology* 1995;164:434-435.

140. Specht CS, Varga JH, Jalali MM, et al. Orbitocranial wooden foreign body diagnosed by magnetic resonance imaging. Dry wood can be isodense with air and fat by computed tomography. *Survey of Ophthalmology* 1992;36:341-344.

141. Stevens MA, de Coster TA, Renwick SE. Cactus thorn embedded in the cartilaginous proximal tibia. *The Western Journal of Medicine* 1995;162:57-59.

142. Adams CD, Timms FJ, Hanlon M. Phoenix date palm injuries: a review of injuries from the Phoenix date palm treated at Starship Children's Hospital. *Australian and New Zealand Journal of Surgery* 2000;70:355-357.

143. Pyhtinen J, Ilkko E, Lähde S. Wooden foreign bodies in CT: case reports and experimental studies. *Acta Radiologica* 1995;36:148-151.

144. Roberts CF, Leehey PJ, III. Intraorbital wood foreign body mimicking air at CT. *Radiology* 1992;185:507-508.

145. Narita N, Yamada T, Imoto Y, et al. Treatment of scattered glass foreign bodies in both the superficial and deep neck: a case report. *Auris, Nasus, Larynx* 2005;32:295-299.

146. Wilson AJ. Gunshot injuries: what does a radiologist need to know? *RadioGraphics* 1999;19:1358-1368.

147. Kerkhoffs GMMJ, op den Akker JW, Hammacher ER. Surfer wipe out by predator fish. *British Journal of Sports Medicine* 2003;37:537-539.

148. Uguz MZ, Kazikdas KC, Erdogan N, et al. An unusual foreign body in the floor of the mouth presenting as a gradually growing mass. *European Archive of Oto-Rhino-Laryngology* 2005;262:875-877.

149. Chao-Jung Lin, Wan-Fu Su, Chih-Hung Wang. A foreign body embedded in the mobile tongue masquerading as a neoplasm. *European Archive of Oto-Rhino-Laryngology* 2003;260:277-279.

150. Soubhia AMP, Ribiero ACP, Martins LD, et al. Unusual wooden foreign body in the palate. *British Dental Journal* 2007;203:573-574.

151. Montano JB, Steele MT, Watson WA. Foreign body retention in glass-caused wounds. *Annals of Emergency Medicine* 1992;21:1360-1363.

152. Hubbell KC. Plantar puncture wounds. In: Slaven EM, Stone SC,Lopez FA, eds. *Infectious Diseases: Emergency Department Diagnosis & Management*. 1st ed. New York: McGraw-Hill, 2007;293-299.

153. Giraldo L, Redding WR. Radiographic diagnosis: foreign body in the distal interphalangeal joint. *Veterinary Radiology and Ultrasound* 2005;46:304-305.

154. Modransky PD, Welker B, Moon ML. Subcutaneous foreign body in a horse resembling fistulous withers. *Veterinary Radiology and Ultrasound* 1989;30:282-283.

155. Gerros TC, McGuirk SM, Biller DS, et al. Choledocholithiasis attributable to a foreign body in a horse. *Journal of the American Veterinary Medical Association* 1993;202:301-303.

156. Maï W, Ledieu D, Venturini L, et al. Ultrasonographic appearance of intra-abdominal granuloma secondary to retained surgical sponge. *Veterinary Radiology and Ultrasound* 2001;42:157-160.

157. Miller MA, Aper RL, Fauber A, et al. Extraskeletal osteosarcoma associated with retained surgical sponge in a dog. *Journal of Veterinary Diagnostic Investigation* 2006;18:224-228.

158. Merlo M, Lamb CR. Radiographic and ultrasonographic features of retained surgical sponge in eight dogs. *Veterinary Radiology and Ultrasound* 2000;41:279-283.

159. Cima RR, Kollengode A, Garnatz J, et al. Incidence and characteristics of potential and actual retained foreign object events in surgical patients. *Journal of the American College of Surgeons* 2008;207:80-87.

160. Kominami M, Fujikawa A, Tamura T, et al. Retained surgical sponge in the thigh: report of the third known case in the limb. *Radiation Medicine* 2003;21:220-222.

161. Kalbermatten DF, Kalbermatten NT, Hertel R. Cotton-induced pseudotumor of the femur. *Skeletal Radiology* 2001;30:415-417.

162. Catalano OA, Dal Pozzo F, Nizzi Grifi D, et al. Paraffinoma of the knee. *Skeletal Radiology* 2003;32:485-488.

163. Kim SR, Baik HK, Park YW. Retained surgical sponge presenting as a pelvic tumor after 25 years. *International Journal of Gynecology and Obstetrics* 2003;82:223-225.

164. Brown M, Schabel S. Case of the month: retained laparotomy sponge (gossypiboma). *Applied Radiology* 2004;33.

165. Vento JA, Karak PK, Henken EM. Gossypiboma as an incidentaloma. *Clinical Nuclear Medicine* 2006;31:176-177.

166. Chung-Ping Lo, Chia-Chun Hsu, Tsun-Hou Chang. Gossypiboma of the leg: MR imaging characteristics. A case report. *Korean Journal of Radiology* 2003;4:191-193.

167. Ribalta T, McCutcheon IE, Neto AG, et al. Textiloma (gossypiboma) mimicking recurrent intracranial tumor. *Archives of Pathology & Laboratory Medicine* 2004;128:749-758.

168. Karçaaltincaba M, Demirkazik FB, İmamoğlu T, et al. Breast abscess mimicking malignant mass due to retained penrose drain: diagnosis by mammography and MRI. *Journal of Clinical Imaging* 2004;28:278-279.

169. Sakayama K, Fujibuchi T, Sugawara Y, et al. A 40-year-old gossypiboma (foreign body granuloma) mimicking a malignant femoral surface tumor. *Skeletal Radiology* 2005;34:221-224.

170. Yi-Ying Lu, Yun-Chung Cheung, Sheung-Fat Ko, et al. Calcified reticulate rind sign: a characteristic feature of gossypiboma on computed tomography. *World Journal of Gastroenterology* 2005;11:4927-4929.

171. Johnson-Neitman JL, Bahr RJ, Broaddus KD. Fistula formation secondary to a nylon cable band in a dog. *Veterinary Radiology and Ultrasound* 2006;47:355-357.

172. Werner RE, Straughan AJ, Vezin D. Nylon cable band reactions in ovariohysterectomized bitches. *Journal of the American Veterinary Medical Association* 1992;200:64-66.

173. Kopka L, Fischer U, Gross AJ, et al. CT of retained surgical sponges (textilomas): pitfalls in detection and evaluation. *Journal of Computer Assisted Tomography* 1996;20:919-923.

174. Penninck D, Mitchell SL. Ultrasonographic detection of ingested and perforating wooden foreign bodies in four dogs. *Journal of the American Veterinary Medical Association* 2003;223:206-209.

175. Hunt GB, Worth A, Marchevsky A. Migration of wooden skewer foreign bodies from the gastrointestinal tract in eight dogs. *Journal of Small Animal Practice* 2004;45:362-367.

176. Nielsen C. Gastrocutaneous fistula secondary to wooden foreign body. *Veterinary Forum* 2007;24:54-58.

177. Jackson AH, Degner DA. Cutaneopulmonary fistula in a dog caused by migration of a toothpick. *Journal of the American Animal Hospital Association* 2002;38:545-547.

178. White RAS, Lane JG. Pharyngeal stick penetration injuries in the dog. *Journal of Small Animal Practice* 1988;29:13-35.

179. Isaacs DL. Detection of a ballpoint pen in a patient's abdomen by sonography. *Journal of Ultrasound in Medicine* 2006;25:1095-1098.

180. Chachad S, Kamat D. Management of plantar puncture wounds in children. *Clinical Pediatrics* 2004;43:213-216.

181. Janda JM, Abbott SL, Brenden RA. Overview of the etiology of wound infections with particular emphasis on community-acquired illnesses. *European Journal of Clinical Microbiology and Infectious Diseases* 1997;16:189-201.

182. Houshian S, Seyedipour S, Wedderkopp N. Epidemiology of bacterial hand infections. *International Journal of Infectious Diseases* 2006;10:315-319.

183. Green RA, Carter WA. Animal bites and rabies. In: Slaven EM, Stone SC,Lopez FA, eds. *Infectious Diseases: Emergency Department Diagnosis & Management*. 1st ed. New York: McGraw-Hill, 2007;313-326.

184. von Graevenitz A, Zbinden R, Mutters R. *Actinobacillus, Capnocytophaga, Eikenella, Kingella, Pasteurella,* and other fastidious or rarely encountered Gram-negative rods. In: Murray PR, Baron EJ, Jorgensen JH, et al., eds. *Manual of Clinical Microbiology*. 9th ed. New York: American Society for Microbiology Press, 2007;621-635.

185. Smith PF, Meadowcroft AM, May DB. Treating mammalian bite wounds. *Journal of Clinical Pharmacy and Therapeutics* 2000;25:85-99.

186. Könönen E, Wade WG. *Propionibacterium, Lactobacillus, Actinomyces,* and other non-spore-forming anaerobic Gram-positive rods. In: Murray PR, Baron EJ, Jorgensen JH, et al., eds. *Manual of Clinical Microbiology*. 9th ed. New York: American Society for Microbiology Press, 2007;872-888.

187. Ming-Chau Chang, Yuan-Lung Huang, Yih Liu, et al. Infectious complications associated with toothpick injuries of the hand. *Journal of Hand Surgery (American version)* 2003;28A:327-331.

188. Mostert L, Groenewald JZ, Summerbell RC, et al. Species of *Phaeoacremonium* associated with infections in humans and environmental reservoirs in infected woody plants. *Journal of Clinical Microbiology* 2005;43:1752-1767.

189. McNab ISH. Hand infections. *Surgery* 2005;23:19-24.

190. Eo S, Jones NF. Fungal infections of the hand and upper extremity. *Journal of the American Society for Surgery of the Hand* 2004;4:250-255.

191. Elhassan BT, Wynn SW, Gonzalez MH. Atypical infections of the hand. *Journal of the American Society for Surgery of the Hand* 2004;4:42-49.

192. Kann SE, Jacquemin JB, Stern PJ. Instructional course lectures, the American Academy of Orthopaedic Surgeons - Simulators of hand infections. *Journal of Bone and Joint Surgery (American volume)* 1996;78-A:1114-1128.

193. Frendin J, Funkquist B, Hansson K, et al. Diagnostic imaging of foreign body reactions in dogs with diffuse back pain. *Journal of Small Animal Practice* 1999;40:278-285.

194. Flynn JE. Clinical and anatomical investigations of deep fascial space infections of the hand. *American Journal of Surgery* 1942;55:467-475.

195. Colonna PC. Infections of the tendon sheaths. *American Journal of Surgery* 1940;50:509-511.

196. Schultz RM, Zwingenberger A. Radiographic, computed tomographic, and ultrasonographic findings with migrating intrathoracic grass awns in dogs and cats. *Veterinary Radiology and Ultrasound* 2008;49:249-255.

197. Radlinsky MG, Homco LD, Blount WC. Ultrasonographic diagnosis - radiolucent pulmonary foreign body. *Veterinary Radiology and Ultrasound* 1998;39:150-153.

198. Dennis MM, Pearce LK, Norrdin RW, et al. Bacterial meningoencephalitis and ventriculitis due to migrating plant foreign bodies in three dogs. *Veterinary Pathology* 2005;42:840-844.

199. Mateo I, Lorenzo V, Muñoz A, et al. Brainstem abscess due to plant foreign body in a dog. *Journal of Veterinary Internal Medicine* 2007;21:535-538.

200. McEvoy FJ, Lamb CR, White RN. An application of sinography in small animal practice. *The Veterinary Record* 1993;132:183-185.

201. Armbrust LJ, Biller DS, Radlinsky MG, et al. Ultrasonographic diagnosis of foreign bodies associated with chronic draining tracts and abscesses in dogs. *Veterinary Radiology and Ultrasound* 2003;44:66-70.

202. Nicholson I, Halfacree Z, Whatmough C, et al. Computed tomography as an aid to management of chronic oropharyngeal stick injury in the dog. *Journal of Small Animal Practice* 2008;49:451-457.

203. Otto CM, Franz MA, Kellogg B, et al. Field treatment of search dogs: lessons learned from the World Trade Center disaster. *Journal of Veterinary Emergency and Critical Care* 2002;12:33-42.

204. Bonatz E, Robbin ML, Weingold MA. Ultrasound for the diagnosis of retained splinters in the soft tissue of the hand. *The American Journal of Orthopedics* 1998;27:455-459.

205. Makary MA. Reported incidence of injuries caused by street glass among urban children in Philadelphia. *Injury Prevention* 1998;4:148-149.

206. Abu Hassan FO. Retained toothpick causing pseudotumor of the first metatarsal: a case report and literature review. *Foot and Ankle Surgery* 2008;14:32-35.

207. Rosenberg NM, Debaker K. Incidence of infection in pediatric patients with laceration. *Pediatric Emergency Care* 1987;3:239-241.

208. Rutherford WH, Spence RAJ. Infection in wounds sutured in the accident and emergency department. *Annals of Emergency Medicine* 1980;9:350-352.

209. Ochiai H, Yamakawa Y, Fukushima T, et al. Neuroimaging of a wooden foreign body retained for 5 months in the temporalis muscle following penetrating trauma with a chopstick. *Neurologia Medico-Chirurgica* 1999;39:744-747.

210. Smely C, Orszagh M. Intracranial transorbital injury by a wooden foreign body: re-evaluation of CT and MRI findings. *British Journal of Neurosurgery* 1999;13:206-211.

211. Inci S, Karakoc E, Saygi S, et al. Unrecognized intracerebral glass particle mimicking cavernoma: case report. *Neurosurgery* 2006;58:E203 (201-204).

212. Weissberg D, Weissberg-Kasav D. Foreign bodies in pleura and chest wall. *Annals of Thoracic Surgery* 2008;86:958-961.

213. Kanavel AB. *Infections of the Hand*. 4th ed. Philadelphia: Lea & Febiger, 1921.

214. Hoon LW, Ross GJ. Infections of the hand. *Annals of Surgery* 1913;57:561-568.

215. Beye HL. Deep palmar hand infections: an experimental and clinical study of the surgical anatomy of these conditions. *Annals of Surgery* 1917;66:24-42.

216. Anson BJ, Ashley FL. The midpalmar compartment, associated spaces and limiting layers. *Anatomical Record* 1940;78:389-407.

217. Jamieson JG. The fascial spaces of the palm: with special reference to their significance in infections of the hand. *British Journal of Surgery* 1950;38:193-199.

218. Bojsen-Møller F, Schmidt L. The palmar aponeurosis and the central spaces of the hand. *Journal of Anatomy* 1974;117:55-68.

219. Pus in the hands and feet. *Primary Surgery Online*: German Society for Tropical Surgery, 2008.

220. Belcher HJCR, Clare TD. Mini-symposium: the elective hand: (iv) hand infections. *Current Orthopaedics* 2003;17:28-43.

221. Thurmüller P, Schubert M, Bade H, et al. Functional gliding spaces of the dorsal side of the human hand. *Anatomical Record* 2002;267:242-251.

222. Spann M, Talmor M, Nolan WB. Hand infections: basic principles and management. *Surgical Infections* 2004;5:210-220.

223. Ramanathan EBS, Luiz CPJ. Date palm thorn synovitis. *Journal of Bone and Joint Surgery (British volume)* 1990;72-B:512-513.

224. Doig SG, Cole WG. Plant thorn synovitis: resolution following total synovectomy. *Journal of Bone and Joint Surgery (British volume)* 1990;72-B:514-515.

225. Piermattei DL, Johnson KA. *An Atlas of Surgical Approaches to the Bones and Joints of the Dog and Cat*. 4th ed. Philadelphia: Elsevier, 2004.

226. Probst CW, Millis DL. Carpus and digits. In: Slatter D, ed. *Textbook of Small Animal Surgery*. 3rd ed. Philadelphia: Elsevier Science (USA), 2003;1974-1988.

227. Stevens DL, Bisno AL, Chambers HF, et al. Practice guidelines for the diagnosis and management of skin and soft-tissue infections. *Clinical Infectious Diseases* 2005;41:1373-1406.

228. Citron DM, Hecht DW. Susceptibility test methods: anaerobic bacteria. In: Murray PR, Baron EJ, Jorgensen JH, et al., eds. *Manual of Clinical Microbiology*. 9th ed. New York: American Society for Microbiology Press, 2007;1214-1222.

229. Hernandez R, Henderson S. Tetanus. In: Slaven EM, Stone SC,Lopez FA, eds. *Infectious Diseases: Emergency Department Diagnosis & Management*. 1st ed. New York: McGraw-Hill, 2007;327-334.

230. Johnson EA, Summanen P, Finegold SM. *Clostridium*. In: Murray PR, Baron EJ, Jorgensen JH, et al., eds. *Manual of Clinical Microbiology*. 9th ed. New York: American Society for Microbiology Press, 2007;889-910.

231. Hsu SS, Groleau G. Tetanus in the emergency department: a current review. *Journal of Emergency Medicine* 2001;20:357-365.

232. Blondel-Hill E, Henry DA, Speert DP. *Pseudomonas*. In: Murray PR, Baron EJ, Jorgensen JH, et al., eds. *Manual of Clinical Microbiology*. 9th ed. New York: American Society for Microbiology Press, 2007;734-748.

233. Kauffman CA, Hajjeh R, Chapman SW. Practice guidelines for the management of patients with sporotrichosis. *Clinical Infectious Diseases* 2000;30:684-687.

234. Bannerman TL, Peacock SJ. *Staphylococcus, Micrococcus,* and other catalase-positive cocci. In: Murray PR, Baron EJ, Jorgensen JH, et al., eds. *Manual of Clinical Microbiology*. 9th ed. Washington, D.C.: American Society for Microbiology Press, 2007;390-411.

235. Nielsen C, Todd JM, Cronk DE, et al. What is your diagnosis? *Journal of the American Veterinary Medical Association* 2005;226:1055-1056.

236. Grain E, Jr., Evans JE, Jr. What is your diagnosis? *Journal of the American Veterinary Medical Association* 1981;179:1024-1026.

237. Mellema LM, Samii VF, Vernau KM, et al. Meningeal enhancement on magnetic resonance imaging in 15 dogs and 3 cats. *Veterinary Radiology and Ultrasound* 2002;43:10-15.

238. Brisson BA, Bersenas A, Etue SM. Ultrasonographic diagnosis of septic arthritis secondary to porcupine quill migration in a dog. *Journal of the American Veterinary Medical Association* 2004;224:1467-1470.

239. Choudhari KA, Muthu T, Tan MH. Progressive ulnar neuropathy caused by delayed migration of a foreign body. *British Journal of Neurosurgery* 2001;15:263-265.

240. Yang SS, Bear BJ, Weiland AJ. Rupture of the flexor pollicis longus tendon after 30 years due to migration of a retained foreign body. *Journal of Hand Surgery (British and European Volume)* 1995;20B:803-805.

241. Whittaker J-P, Kelly CP. Glass foreign body in a healed fracture. *Injury: International Journal of the Care of the Injured* 2001;32:80-81.

242. Brisson BA, Théoret M-C. Osteolysis of the radius and ulna induced by a circumferential foreign body in a cat. *Journal of the American Veterinary Medical Association* 2008;233:1117-1120.

243. Berry CR, Thrall DE. Introduction to radiographic interpretation. In: Thrall DE, ed. *Textbook of Veterinary Diagnostic Radiology*. 5th ed. St. Louis: Saunders, 2007;78-92.

244. Lagalla R, Manfrè L, Caronia A, et al. Plain film, CT and MRI sensibility in the evaluation of intraorbital foreign bodies in an *in vitro* model of the orbit and in pig eyes. *European Radiology* 2000;10:1338-1341.

245. Cawthon LA, Meza MP, Eggleston DE. The radiolucent wooden foreign body. *Pediatric Emergency Care* 1991;7:224-225.

246. O'Driscoll SW. Glass is detectable on plain radiographs. *Canadian Medical Association Journal* 1988;139:643-644.

247. Lamb CR. Contrast radiography of equine joints, tendon sheaths, and draining tracts. *Veterinary Clinics of North America: Equine Practice* 1991;7:241-257.

248. Tandberg D. Glass in the hand and foot: will an x-ray film show it? *Journal of the American Medical Association* 1982;248:1872-1874.

249. Matteucci ML, Spaulding K, Dassler C, et al. Ultrasound diagnosis: intra-abdominal wood foreign body. *Veterinary Radiology and Ultrasound* 1999;40:513-516.

250. Turkcuer I, Atilla R, Topacoglu H, et al. Do we really need plain and soft-tissue radiographies to detect radiolucent foreign bodies in the ED? *American Journal of Emergency Medicine* 2006;24:763-768.

251. Levine MR, Yarnold PR, Michelson EA. A training program in portable fluoroscopy for the detection of glass in soft tissues. *Academic Emergency Medicine* 2002;9:858-862.

252. Curry TS, III, Dowdey JE, Murry RC, Jr. *Christensen's Physics of Diagnostic Radiology*. 4th ed. Philadelphia: Lea & Febiger, 1990.

253. Barber DL. Imaging: radiography - II. *Veterinary Radiology* 1981;22:149-158.

254. Woesner ME, Sanders I. Xeroradiography: a significant modality in the detection on nonmetallic foreign bodies in soft tissues. *American Journal of Roentgenology, Radium Therapy, and Nuclear Medicine* 1972;115:636-640.

255. Kuhns LR, Borlaza GS, Seigel RS, et al. An *in vitro* comparison of computed tomography, xeroradiography, and radiography in the detection of soft-tissue foreign bodies. *Radiology* 1979;132:218-219.

256. Fistula. *Stedman's Online Medical Dictionary*: Lippincott Williams & Wilkins, 2008.

257. Fistula. *Merriam-Webster Online Dictionary*: Merriam-Webster Online, 2008.

258. Sinus. *Merriam-Webster Online Dictionary*: Merriam-Webster Online, 2008.

259. Kowalsky RJ. Radioactive decay, radioactivity, Tc-99m generator, and radiopharmaceuticals. In: Daniel GB,Berry CR, eds. *Textbook of Veterinary Nuclear Medicine*. 2nd ed. Harrisburg, PA: American College of Veterinary Radiology, 2006;1-24.

260. Berry CR, Daniel GB. Radiation detectors. In: Daniel GB,Berry CR, eds. *Textbook of Veterinary Nuclear Medicine*. 2nd ed. Harrisburg, PA: American College of Veterinary Radiology, 2006;25-37.

261. Berry CR, Daniel GB. Principles of image interpretation, nuclear medicine counting statistics, and an introduction to kinetic modeling. In: Daniel GB,Berry CR, eds. *Textbook of Veterinary Nuclear Medicine*. 2nd ed. Harrisburg, PA: American College of Veterinary Radiology, 2006;129-141.

262. Berry CR, Daniel GB. Radiation safety, personnel radiation monitoring, and licensing issues. In: Daniel GB,Berry CR, eds. *Textbook of Veterinary Nuclear Medicine*. 2nd ed. Harrisburg, PA: American College of Veterinary Radiology, 2006;121-128.

263. Love C, Palestro CJ. Radionuclide imaging of infection. *Journal of Nuclear Medicine Technology* 2004;32:47-57.

264. Poteet B. Small animal skeletal scintigraphy. In: Daniel GB,Berry CR, eds. *Textbook of Veterinary Nuclear Medicine*. 2nd ed. Harrisburg, PA: American College of Veterinary Radiology, 2006;143-164.

265. McCarthy K, Velchik MG, Alavi A, et al. Indium-111-labeled white blood cells in the detection of osteomyelitis complicated by a pre-existing condition. *Journal of Nuclear Medicine* 1988;29:1015-1021.

266. Schauwecker DS, Hee-Myung Park, Mock BH, et al. Evaluation of complicating osteomyelitis with Tc-99m MDP, In-111 granulocytes, and Ga-67 citrate. *Journal of Nuclear Medicine* 1984;25:849-853.

267. Koblik PD, Lofstedt J, Jakowski RM, et al. Use of ^{111}In-labeled autologous leukocytes to image an abdominal abscess in a horse. *Journal of the American Veterinary Medical Association* 1985;186:1319-1322.

268. Alexander K, Drost WT, Mattoon JS, et al. ^{99m}Tc-ciprofloxacin in imaging of clinical infections in camelids and a goat. *Veterinary Radiology and Ultrasound* 2005;46:340-347.

269. Sonmezoglu K, Sonmezoglu M, Halac M, et al. Usefulness of ^{99m}Tc-ciprofloxacin (Infecton) scan in diagnosis of chronic orthopedic infections: comparative study with ^{99m}Tc-HMPAO leukocyte scintigraphy. *Journal of Nuclear Medicine* 2001;42:567-574.

270. Yapar Z, Kibar M, Yapar AF, et al. The efficacy of technetium-99m ciprofloxacin (Infecton) imaging in suspected orthopaedic infection: a comparison with sequential bone/gallium imaging. *European Journal of Nuclear Medicine* 2001;28:822-830.

271. Malamitsi J, Giamarellou H, Kanellakopoulou K, et al. Infecton: a ^{99m}Tc-ciprofloxacin radiopharmaceutical for the detection of bone infection. *Clinical Microbiology and Infection* 2003;9:101-109.

272. Matwichuk-Bassett CL, Berry CR. Single photon emission (computed) tomography and positron emission tomography. In: Daniel GB,Berry CR, eds. *Textbook of Veterinary Nuclear Medicine*. 2nd ed. Harrisburg, PA: American College of Veterinary Radiology, 2006;39-52.

273. Kremkau FW. *Diagnostic Ultrasound: Principles and Instruments*. 6th ed. Philadelphia: W.B. Saunders, 2002.

274. Staudte KL, Hopper BJ, Gibson NR, et al. Use of ultrasonography to facilitate surgical removal of non-enteric foreign bodies in 17 dogs. *Journal of Small Animal Practice* 2004;45:395-400.

275. Dumarey A, de Maeseneer M, Ernst C. Large wooden foreign body in the hand: recognition of occult fragments with ultrasound. *Emergency Radiology* 2004;10:337-339.

276. Lyon M, Brannam L, Johnson D, et al. Detection of soft tissue foreign bodies in the presence of soft tissue gas. *Journal of Ultrasound in Medicine* 2004;23:677-681.

277. Erol Ö, Özçakar L, Çetin A. Sonography streamlines the diagnosis in hand injuries with small foreign bodies. *Journal of Emergency Medicine* 2009;[Epub ahead of print].

278. Della Santa D, Rossi F, Carlucci F, et al. Ultrasound-guided retrieval of plant awns. *Veterinary Radiology and Ultrasound* 2008;49:484-486.

279. McDicken WN, Hoskins PR. Physics: Principles, practice, and artefacts. In: Allan PL, Dubbins PA, Pozniak MA, et al., eds. *Clinical Doppler Ultrasound*. London: Churchill Livingstone, 2000;1-25.

280. Nyman HT, Kristensen AT, Flagstad A, et al. A review of the sonographic assessment of tumor metastases in liver and superficial lymph nodes. *Veterinary Radiology and Ultrasound* 2004;45:438-448.

281. Nyman HT, Kristensen AT, Kjelgaard-Hansen M, et al. Contrast-enhanced ultrasonography in normal canine liver. Evaluation of imaging and safety parameters. *Veterinary Radiology and Ultrasound* 2005;46:243-250.

282. Haers H, Saunders JH. Review of clinical characteristics and applications of contrast-enhanced ultrasonography in dogs. *Journal of the American Veterinary Medical Association* 2009;234:460-470.

283. Hall TJ. Beyond the basics: elasticity imaging with US. *RadioGraphics* 2003;23:1657-1671.

284. Teefey SA, Middleton WD, Boyer MI. Sonography of the hand and wrist. *Seminars in Ultrasound, CT, and MRI* 2000;21:192-204.

285. Rubin JM, Adler RS, Bude RO, et al. Clean and dirty shadowing at US: a reappraisal. *Radiology* 1991;181:231-236.

286. Shah ZR, Crass JR, Oravec DC, et al. Ultrasonographic detection of foreign bodies in soft tissues using turkey muscle as a model. *Veterinary Radiology and Ultrasound* 1992;33:94-100.

287. Blyme PJH, Lind T, Schantz K, et al. Ultrasonographic detection of foreign bodies in soft tissue: a human cadaver study. *Archives of Orthopaedic and Trauma Surgery* 1990;110:24-25.

288. Schlager D, Sanders AB, Wiggins D, et al. Ultrasound for the detection of foreign bodies. *Annals of Emergency Medicine* 1991;20:189-191.

289. Wisner ER, Nyland TG, Mattoon JS. Ultrasonographic examination of cervical masses in the dog and cat. *Veterinary Radiology and Ultrasound* 1994;35:310-315.

290. Samii VF, Long CD. Musculoskeletal system. In: Nyland TG,Mattoon JS, eds. *Small Animal Diagnostic Ultrasound*. 2nd ed. Philadelphia: Saunders, 2002;267-284.

291. Kramer M, d'Anjou M-A. Musculoskeletal system. In: Penninck D,d'Anjou M-A, eds. *Atlas of Small Animal Ultrasonography*. Ames, Iowa: Blackwell Publishing, 2008;465-510.

292. Wilson DJ. Soft tissue and joint infection. *European Radiology* 2004;14:E64-E71.

293. Mattoon JS, Nyland TG. Abdominal fluid, lymph nodes, masses, peritoneal cavity, and great vessel thrombosis. In: Nyland TG,Mattoon JS, eds. *Small Animal Diagnostic Ultrasound*. 2nd ed. Philadelphia: Saunders, 2002;82-91.

294. Lin J, Jacobson JA, Fessell DP, et al. An illustrated tutorial of musculoskeletal sonography: Part 4, musculoskeletal masses, sonographically guided interventions, and miscellaneous topics. *American Journal of Roentgenology* 2000;175:1711-1719.

295. Matwiyoff NA, Brooks WM. Instrumentation. In: Stark DD,Bradley WG, Jr., eds. *Magnetic Resonance Imaging*. 3rd ed. St. Lous: Mosby, 1999;15-32.

296. Jacobs MA, Ibrahim TS, Ouwerkerk R. MR imaging: brief overview and emerging applications. *RadioGraphics* 2007;27:1213-1229.

297. Wood ML, Wehrli FW. Principles of magnetic resonance imaging. In: Stark DD,Bradley WG, Jr., eds. *Magnetic Resonance Imaging*. 3rd ed. St. Louis: Mosby, 1999;1-14.

298. Hagmann P, Jonasson L, Maeder P, et al. Understanding diffusion MR imaging techniques: from scalar diffusion-weighted imaging to diffusion tensor imaging and beyond. *RadioGraphics* 2006;26:S205-S223.

299. Bitar R, Leung G, Perng R, et al. MR pulse sequences: what every radiologist wants to know but is afraid to ask. *RadioGraphics* 2006;26:513-537.

300. Bradley WG, Jr., Dar-Yeong Chen, Atkinson DJ, et al. Fast spin-echo and echo-planar imaging. In: Stark DD,Bradley WG, Jr., eds. *Magnetic Resonance Imaging*. 3rd ed. St. Louis: Mosby, 1999;125-157.

301. Pierpaoli C, Jezzard P, Basser PJ, et al. Diffusion tensor MR imaging of the human brain. *Radiology* 1996;201:637-648.

302. Boesch C. Musculoskeletal spectroscopy. *Journal of Magnetic Resonance Imaging* 2007;25:321-338.

303. Matson GB, Weiner MW. Spectroscopy. In: Stark DD,Bradley WG, Jr., eds. *Magnetic Resonance Imaging*. 3rd ed. St. Louis: Mosby, 1999;181-214.

304. Foerster BR, Thurnher MM, Malani PN, et al. Intracranial infections: clinical and imaging characteristics. *Acta Radiologica* 2007;48:875-893.

305. Tidwell AS, Jones JC. Advanced imaging concepts: a pictorial glossary of CT and MRI technology. *Clinical Techniques in Small Animal Practice* 1999;14:65-111.

306. Moseley ME, Butts K. Diffusion and perfusion. In: Stark DD,Bradley WG, Jr., eds. *Magnetic Resonance Imaging*. 3rd ed. St. Louis: Mosby, 1999;1515-1538.

307. Mock BJ, Lowe MJ, Turski PA. Functional magnetic resonance imaging. In: Stark DD,Bradley WG, Jr., eds. *Magnetic Resonance Imaging*. 3rd ed. St. Louis: Mosby, 1999;1555-1574.

308. Teresi LM, Dar-Yeong Chen, Atkinson DJ, et al. Optimizing scanning techniques and protocols. In: Stark DD,Bradley WG, Jr., eds. *Magnetic Resonance Imaging*. 3rd ed. St. Louis: Mosby, 1999;A1-A13.

309. Drapé J-L, Tardif-Chastenet de Gery S, Silbermann-Hoffman O, et al. Closed ruptures of the flexor digitorum tendons: MRI evaluation. *Skeletal Radiology* 1998;27:617-624.

310. Bydder M, Rahal A, Fullerton GD, et al. The magic angle effect: a source of artifact, determinant of image contrast, and technique for imaging. *Journal of Magnetic Resonance Imaging* 2007;25:290-300.

311. Spriet M, Mai W, McKnight A. Asymmetric signal intensity in normal collateral ligaments of the distal interphalangeal joint in horses with a low-field MRI system due to the magic angle effect. *Veterinary Radiology and Ultrasound* 2007;48:95-100.

312. McGuckin JF, Jr., Akhtar N, Ho VT, et al. CT and MR evaluation of a wooden foreign body in an *in vitro* model of the orbit. *American Journal of Neuroradiology* 1996;17:129-133.

313. Glatt HJ, Custer PL, Barrett L, et al. Magnetic resonance imaging and computed tomography in a model of wooden foreign bodies in the orbit. *Ophthalmic Plastic and Reconstructive Surgery* 1990;6:108-114.

314. Young B, Klopp L, Albrecht M, et al. Imaging diagnosis: magnetic resonance imaging of a cervical wooden foreign body in a dog. *Veterinary Radiology and Ultrasound* 2004;45:538-541.

315. Woolfson JM, Wesley RE. Magnetic resonance imaging and computed tomographic scanning of fresh (green) wood foreign bodies in dog orbits. *Ophthalmic Plastic and Reconstructive Surgery* 1990;6:237-240.

316. Monu JUV, McManus CM, Ward WG, et al. Soft-tissue masses caused by long-standing foreign bodies in the extremities: MR imaging findings. *American Journal of Roentgenology* 1995;165:395-397.

317. Sang Yong Lee, Nae Ho Lee, Myong Ja Chung, et al. Foreign-body granuloma caused by dispersed oil droplets simulating subcutaneous fat tissue on MR images. *American Journal of Roentgenology* 2004;182:1090-1091.

318. Ledermann HP, Morrison WB, Schweitzer ME. Pedal abscesses in patients suspected of having pedal osteomyelitis: analysis with MR imaging. *Radiology* 2002;224:649-655.

319. Spaeth HJ, Jr., Dardani M. Magnetic resonance imaging of the diabetic foot. *MRI Clinics of North America* 1994;2:123-130.

320. Tang JSH, Gold RH, Bassett LW, et al. Musculoskeletal infection of the extremities: evaluation with MR imaging. *Radiology* 1988;166:205-209.

321. Sage MR. Blood-brain barrier: phenomenon of increasing importance to the imaging clinician. *American Journal of Roentgenology* 1982;138:887-898.

322. Laster DW, Moody DM, Ball MR. Resolving intracerebral hematoma: alteration of the "ring sign" with steroids. *American Journal of Roentgenology* 1978;130:935-939.

323. Kuperman VY, Alley MT. Differentiation between the effects of T_1 and T_2* shortening in contrast-enhanced MRI of the breast. *Journal of Magnetic Resonance Imaging* 1999;9:172-176.

324. Dangman BC, Hoffer FA, Rand FF, et al. Osteomyelitis in children: gadolinium-enhanced MR imaging. *Radiology* 1992;182:743-747.

325. Nagy JA, Benjamin L, Huiyan Zeng, et al. Vascular permeability, vascular hyperpermeability, and angiogenesis. *Angiogenesis* 2008;11:109-119.

326. Weis SM. Vascular permeability in cardiovascular disease and cancer. *Current Opinion in Hematology* 2008;15:243-249.

327. Suzuki T, Nakamura Y, Moriya T, et al. Effects of steroid hormones on vascular functions. *Microscopy Research and Techniques* 2003;60:76-84.

328. Balci NC, Semelka RC, Noone TC, et al. Pyogenic hepatic abscesses: MRI findings on T1- and T2-weighted and serial gadolinium-enhanced gradient-echo images. *Journal of Magnetic Resonance Imaging* 1999;9:285-290.

329. Wall SD, Fisher MR, Amparo EG, et al. Magnetic resonance imaging in the evaluation of abscesses. *American Journal of Roentgenology* 1985;144:1217-1221.

330. Smirniotopoulos JG, Murphy FM, Rushing EJ, et al. Patterns of contrast enhancement in the brain and meninges. *RadioGraphics* 2007;27:525-551.

331. Abuhamed M, Xiao Bo, Cai Yan. Central nervous system tuberculomas: a review article. *American Journal of Infectious Diseases* 2008;4:168-173.

332. Özateş M, Özkan Ü, Kemaloglu S, et al. Spinal subdural tuberculous abscess. *Spinal Cord* 2000;38:56-58.

333. Kastrup O, Wanke I, Maschke M. Neuroimaging of infections of the central nervous system. *Seminars in Neurology* 2008;28:511-522.

334. Prakash M, Gupta RK, Jha D, et al. Brain abscess: MRI demonstration of rare cause of intraventricular hemorrhage. *European Journal of Radiology Extra* 2004;51:91-93.

335. Shih-Chin Chang, Ping-Hong Lai, Wei-Liang Chen, et al. Diffusion-weighted MRI features of brain abscess and cystic or necrotic brain tumors: comparison with conventional MRI. *Journal of Clinical Imaging* 2002;26:227-236.

336. Bükte Y, Paksoy Y, Genç E, et al. Role of diffusion-weighted MR in differential diagnosis of intracranial cystic lesions. *Clinical Radiology* 2005;60:375-383.

337. Kingsley PB, Shah TC, Woldenberg R. Identification of diffuse and focal brain lesions by clinical magnetic resonance spectroscopy. *NMR in Biomedicine* 2006;19:435-462.

338. Kimura T, Sako K, Gotoh T, et al. In vivo single-voxel proton MR spectroscopy in brain lesions with ring-like enhancement. *NMR in Biomedicine* 2001;14:339-349.

339. Bradley WG, Jr. MR appearance of hemorrhage in the brain. *Radiology* 1993;189:15-26.

340. Thomas WB. Nonneoplastic disorders of the brain. *Clinical Techniques in Small Animal Practice* 1999;14:125-147.

341. Clark RA, Watanabe AT, Bradley WG, Jr., et al. Acute hematomas: effects of deoxygenation, hematocrit, and fibrin-clot formation and retraction on T2 shortening. *Radiology* 1990;175:201-206.

342. Atlas SW, Mark AS, Grossman RI, et al. Intracranial hemorrhage: gradient-echo MR imaging at 1.5 T. *Radiology* 1988;168:803-807.

343. Atlas SW, DuBois P, Singer MB, et al. Diffusion measurements in intracranial hematomas: implications for MR imaging of acute stroke. *American Journal of Neuroradiology* 2000;21:1190-1194.

344. Hiwatashi A, Kinoshita T, Moritani T, et al. Hypointensity on diffusion-weighted MRI of the brain related to T2 shortening and susceptibility effects. *American Journal of Roentgenology* 2003;181:1705-1709.

345. Tong KA, Ashwal S, Obenaus A, et al. Susceptibility-weighted MR imaging: a review of clinical applications in children. *American Journal of Neuroradiology* 2008;29:9-17.

346. Srinivasan A, Goyal M, Al Azri F, et al. State-of-the-art imaging of acute stroke. *RadioGraphics* 2006;26:S75-S95.

347. Dainer HM, Smirniotopoulos JG. Neuroimaging of hemorrhage and vascular malformations. *Seminars in Neurology* 2008;28:533-547.

348. Berland LL. *Practical CT: Technology and Techniques*. New York: Raven Press, 1987.

349. Flohr TG, Schaller S, Stierstorfer K, et al. Multi-detector row CT systems and image-reconstruction techniques. *Radiology* 2005;235:756-773.

350. Hunter TB. Letter to the editor: CT units. *Radiology* 1982;144:942.

351. Carter R. Gray scale and achromatic color difference. *Journal of the Optical Society of America A, Optics, image science, and vision* 1993;10:1380-1391.

352. Carter R. Gray-scale perceptions calculated: optimum display background luminance. *Applied Optics* 1997;36:1705-1717.

353. Krauskopf J, Gegenfurtner K. Color discrimination and adaptation. *Vision Research* 1992;32:2165-2175.

354. Yamaguchi M, Fujita H, Uemura M, et al. Development and evaluation of a new gray-scale test pattern to adjust gradients of thoracic CT imaging. *European Radiology* 2004;14:2357-2361.

355. Vaiman M, Bekerman I, Puterman M. 3D computer-assisted assessment of complicated penetrating foreign bodies cases in ENT practice. *European Archive of Oto-Rhino-Laryngology* 2009;[Epub ahead of print].

356. Salvolini L, Secchi EB, Costarelli L, et al. Clinical applications of 2D and 3D CT imaging of the airways - a review. *European Journal of Radiology* 2000;34:9-25.

357. Takhtani D. CT neuroangiography: a glance at the common pitfalls and their prevention. *American Journal of Roentgenology* 2005;185:772-783.

358. Ming-Yue Luo, Hong Shan, Li-Qing Yao, et al. Postprocessing techniques of CT colonography in detection of colorectal carcinoma. *World Journal of Gastroenterology* 2004;10:1574-1577.

359. Burgess AE. The Rose model, revisited. *Journal of the Optical Society of America A, Optics, image science, and vision* 1999;16:633-646.

360. Yucel EK, Silver MS, Carter AP. MR angiography of normal pelvic arteries: comparison of signal intensity and contrast-to-noise ratio for three different inflow techniques. *American Journal of Roentgenology* 1994;163:197-201.

361. Watts R, Yi Wang. k-Space interpretation of the Rose model: noise limitation on the detectable resolution in MRI. *Magnetic Resonance in Medicine* 2002;48:550-554.

362. Wagner RF. Toward a unified view of radiological imaging systems. Part II: noisy images. *Medical Physics* 1977;4:279-296.

363. Ariz C, Horton KM, Fishman EK. 3D CT evaluation of retained foreign bodies. *Emergency Radiology* 2004;11:95-99.

364. LoBue TD, Deutsch TA, Lobick J, et al. Detection and localization of nonmetallic intraocular foreign bodies by magnetic resonance imaging. *Archives of Ophthalmology* 1988;106:260-261.

365. Hansen JE, Gudeman SK, Holgate RC, et al. Penetrating intracranial wood wounds: clinical limitations of computerized tomography. *Journal of Neurosurgery* 1988;68:752-756.

366. Pliura A, Zhang SY, MacKay J, et al. Genotypic variation in wood density and growth traits of poplar hybrids at four clonal trials. *Forest Ecology and Management* 2007;238:92-106.

367. Slik JWF. Estimating species-specific wood density from the genus average in Indonesian trees. *Journal of Tropical Biology* 2006;22:481-482.

368. Chave J, Muller-Landau HC, Baker TR, et al. Regional and phylogenetic variation of wood density across 2456 neotropical tree species. *Ecological Applications* 2006;16:2356-2367.

369. Macedo A, Vaz CMP, Pereira JCD, et al. Wood density determination by X- and gamma-ray tomography. *Holzforschung* 2002;56:535-540.

370. Mäkinen H, Saranpää P, Linder S. Wood-density variation of Norway spruce in relation to nutrient optimization and fibre dimensions. *Canadian Journal of Forest Research* 2002;32:185-194.

371. Knapic S, Louzada JL, Leal S, et al. Radial variation of wood density components and ring width in cork oak trees. *Annals of Forest Science* 2007;64:211-218.

372. Bouriaud O, Bréda N, Le Moguédec G, et al. Modelling variability of wood density in beech as affected by ring age, radial growth and climate. *Trees* 2004;18:264-276.

373. Repola J. Models for vertical wood density of Scots pine, Norway spruce, and birch stems, and their application to determine average wood density. *Silva Fennica* 2006;40:673-685.

374. Wright IJ, Ackerly DD, Bongers F, et al. Relationships among ecologically important dimensions of plant trait variation in seven neotropical forests. *Annals of Botany* 2007;99:1003-1015.

375. Mayo GL, Long LS, Fitzsimmons T, et al. Delayed orbital foreign body reaction to dicotyledon (hardwood) libriform fibers. *Archives of Ophthalmology* 2002;120:1770-1771.

376. Fayad LM, Carrino JA, Fishman EK. Musculoskeletal infection: role of CT in the emergency department. *RadioGraphics* 2007;27:1723-1736.

377. New PFJ, Aronow S. Attenuation measurements of whole blood and blood fractions in computed tomography. *Radiology* 1976;121:635-640.

378. Bergström M, Ericson K, Levander B, et al. Variation with time of the attenuation values of intracranial hematomas. *Journal of Computer Assisted Tomography* 1977;1:57-63.

379. Dolinskas CA, Bilaniuk LT, Zimmerman RA, et al. Computed tomography of intracerebral hematomas. I. Transmission CT observations on hematoma resolution. *American Journal of Roentgenology* 1977;129:681-688.

380. Swensen SJ, McLeod RA, Stephens DH. CT of extracranial hemorrhage and hematomas. *American Journal of Roentgenology* 1984;143:907-912.

381. Ginsburg MJ, Ellis GL, Flom LL. Detection of soft-tissue foreign bodies by plain radiography, xerography, computed tomography, and ultrasonography. *Annals of Emergency Medicine* 1990;19:701-703.

382. Eggers G, Welzel T, Mukhamadiev D, et al. X-ray-based volumetric imaging of foreign bodies: a comparison of computed tomography and digital volume tomography. *Journal of Oral and Maxillofacial Surgery* 2007;65:1880-1885.

383. Manickavasagam J, Bateman N, Street I, et al. Radio opacity of various ENT foreign bodies in sheep's neck preparation. *European Archive of Oto-Rhino-Laryngology* 2008;[Epub ahead of print].

384. Orlinsky M, Knittel P, Feit T, et al. The comparative accuracy of radiolucent foreign body detection using ultrasonography. *The American Journal of Emergency Medicine* 2000;18:401-403.

385. Crystal CS, Masneri DA, Hellums JS, et al. Bedside ultrasound for the detection of soft tissue foreign bodies: a cadaveric study. *Ultrasound in Emergency Medicine* 2008;[Epub ahead of print].

386. Breathnach RM, Fanning S, Mulcahy G, et al. Canine pododermatitis and idiopathic disease. *Veterinary Journal* 2008;176:146-157.

387. Marino DJ, Matthiesen DT, Stefanacci JD, et al. Evaluation of dogs with digit masses: 117 cases (1981-1991). *Journal of the American Veterinary Medical Association* 1995;207:726-728.

388. Assheuer J, Sager M. *MRI and CT Atlas of the Dog*. Berlin: Blackwell Science, 1997.

389. Ober CP, Jones JC, Larson MM, et al. Comparison of ultrasound, computed tomography, and magnetic resonance imaging in detection of acute wooden foreign bodies in the canine manus. *Veterinary Radiology and Ultrasound* 2008;49:411-418.

390. Totty WG, Murphy WA, Lee JKT. Soft-tissue tumors: MR imaging. *Radiology* 1986;160:135-141.

391. Tehranzadeh J, Mnaymneh W, Ghavam C, et al. Comparison of CT and MR imaging in musculoskeletal neoplasms. *Journal of Computer Assisted Tomography* 1989;13:466-472.

392. Evans HE. *Miller's Anatomy of the Dog*. Philadelphia: W.B. Saunders Co., 1993.

393. Wetzel LH, Levine E, Murphey MD. A comparison of MR imaging and CT in the evaluation of musculoskeletal masses. *RadioGraphics* 1987;7:851-874.

394. Bucur V. *Nondestructive Characterization and Imaging of Wood*. Berlin: Springer-Verlag, 2003.

395. Kelsey CA, Moseley RD, Mettler FA, Jr., et al. Observer performance as a function of viewing distance. *Investigative Radiology* 1981;16:435-437.

396. Samei E, Flynn MJ, Eyler WR. Detection of subtle lung nodules: relative influence of quantum and anatomic noise on chest radiographs. *Radiology* 1999;213:727-734.

397. Samei E, Flynn MJ, Peterson E, et al. Subtle lung nodules: influence of local anatomic variations on detection. *Radiology* 2003;228:76-84.

398. de Flaviis L, Scaglione P, del Bo P, et al. Detection of foreign bodies in soft tissues: experimental comparison of ultrasonography and xeroradiography. *Journal of Trauma* 1988;28:400-404.

Appendix A

Sectional Anatomy of the Normal Canine Manus

Transverse slices (Figure A.1)
4 mm thickness
Right manus from distal to proximal

Table A.1: Key to Transverse Images

Code	Structure	Code	Structure
A APPD3	Axial palmar proper digital a. III	DAL	Proximal digital annular ligament
A APPD4	Axial palmar proper digital a. IV	DDF	Deep digital flexor
A CI	Caudal (palmar) interosseous a.	DP	Digital pad
A M	Median a.	DS	Dorsal sesamoid bone
A PCD2	Palmar common digital a. II	ECR	Extensor carpi radialis
A PCD3	Palmar common digital a. III	FCR	Flexor carpi radialis
A PCD4	Palmar common digital a. IV	FCU	Flexor carpi ulnaris
ADQ	Abductor digiti quinti	FPB	Flexor pollicis brevis
AP	Adductor pollicis	IL	Intersesamoidean ligament
APB	Abductor pollicis brevis	IO	Interosseous muscle
APL	Abductor pollicis longus	LDE	Lateral digital extensor
AS	Sesamoid bone in APL tendon	MC1	Metacarpal bone I
C1	Carpal bone 1	MC2	Metacarpal bone II
C2	Carpal bone 2	MC3	Metacarpal bone III
C3	Carpal bone 3	MC4	Metacarpal bone IV
C4	Carpal bone 4	MC5	Metacarpal bone V
Ca	Accessory carpal bone	MCP	Metacarpal pad
CDE	Common digital extensor	Pd	Distal phalanx
CL	Collateral ligament	Pm	Middle phalanx
CP	Carpal pad	Pp	Proximal phalanx
Cr	Radial (radiointermedial) carpal bone	PS	Proximal sesamoid bone
Cu	Ulnar carpal bone	R	Radius
D1	Digit I	SDF	Superficial digital flexor
D2	Digit II	U	Ulna
D3	Digit III	UL	Ulnaris lateralis
D4	Digit IV	V AC	Accessory cephalic v.
D5	Digit V		

Notes: a. = artery, v. = vein


Pd D4
Pd D3
DP

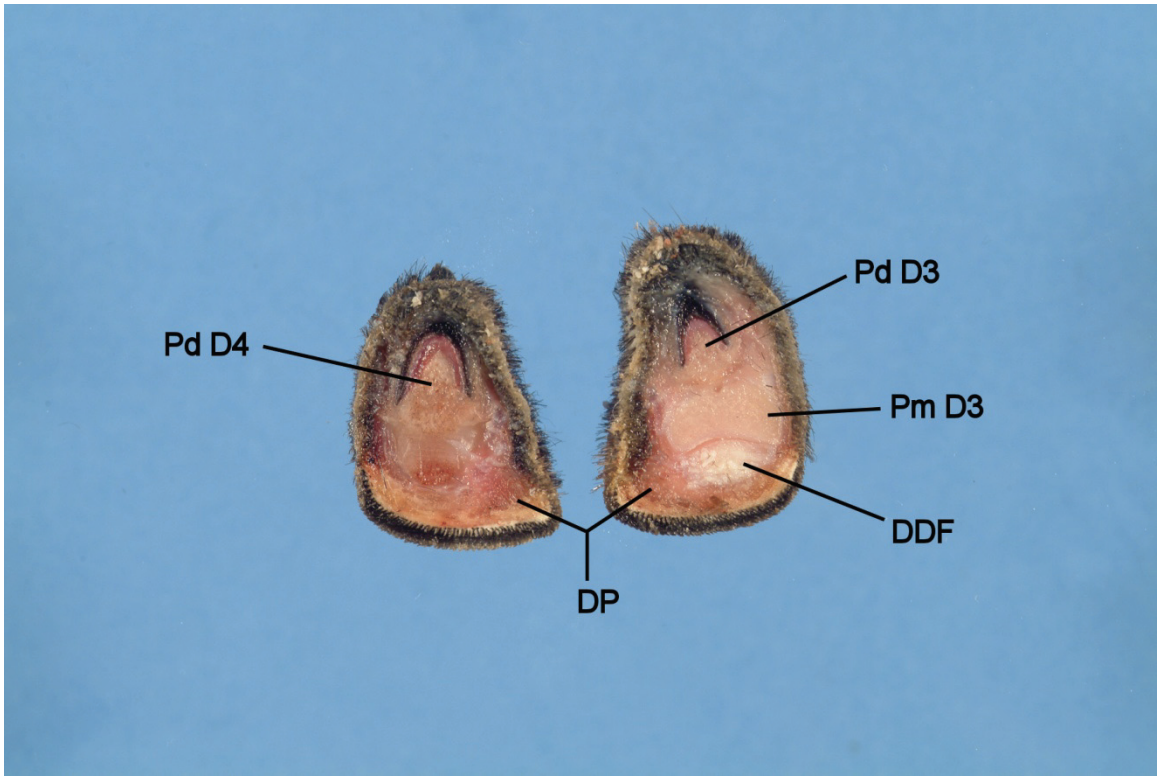
Pd D4
Pd D3
Pm D3
DDF
DP

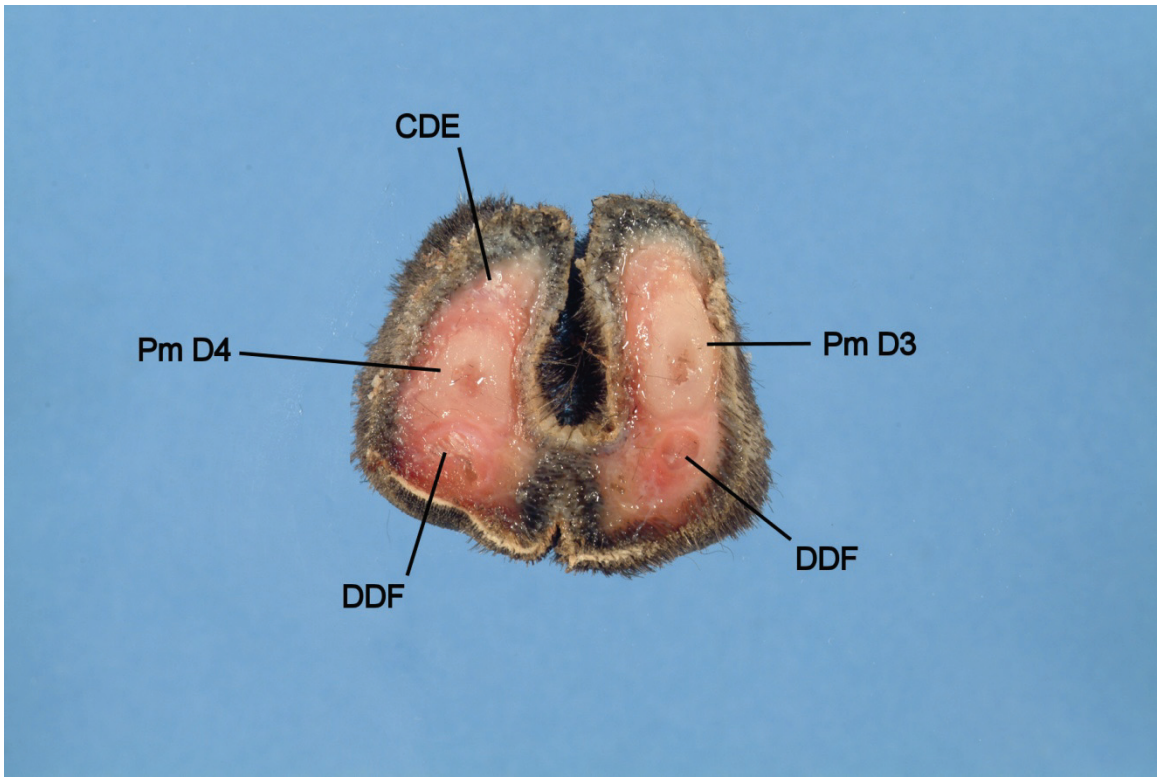
CDE
Pm D4
Pm D3
DDF
DDF

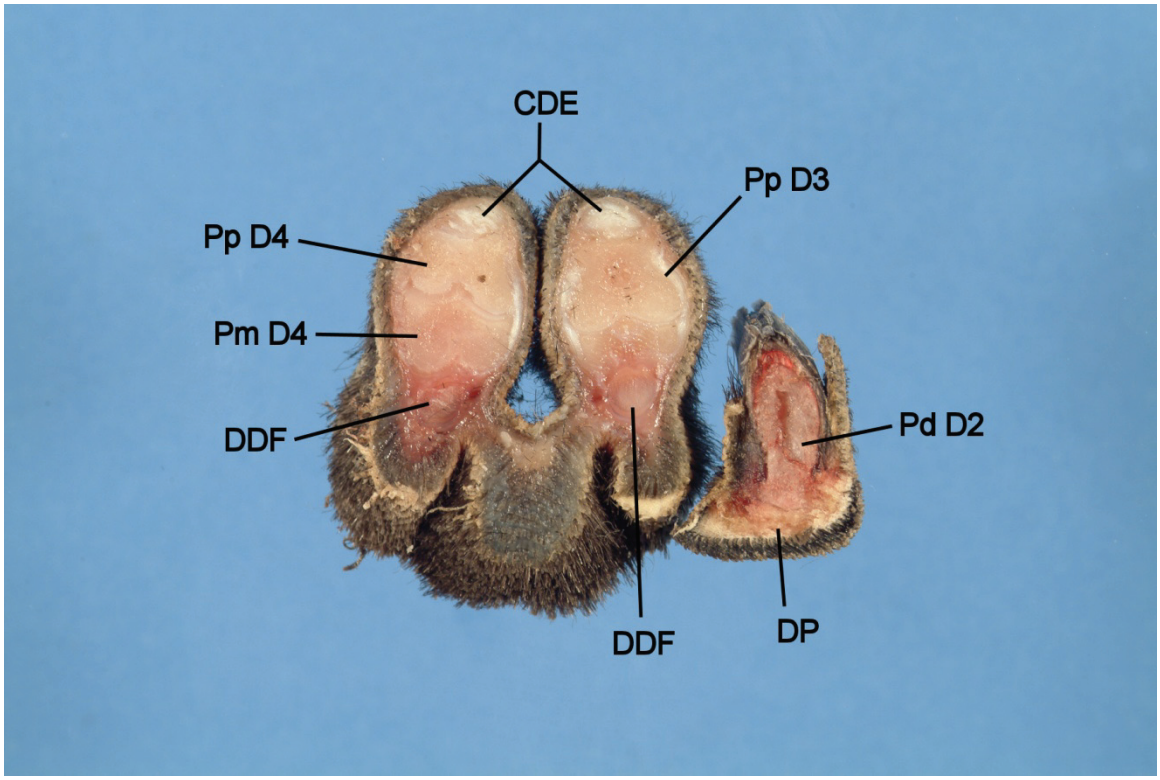
CDE
Pp D3
Pp D4
Pm D4
DDF
Pd D2
DDF
DP

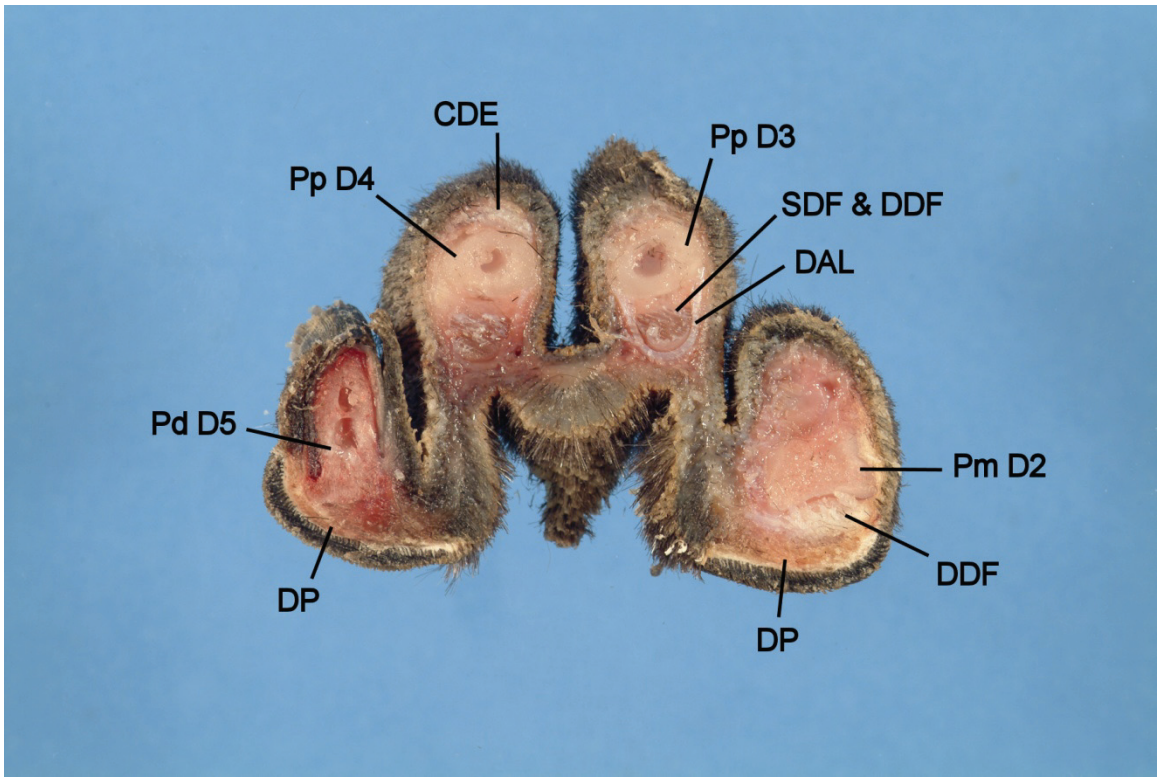
CDE
Pp D4
Pp D3
SDF & DDF
DAL
Pd D5
Pm D2
DDF
DP
DP

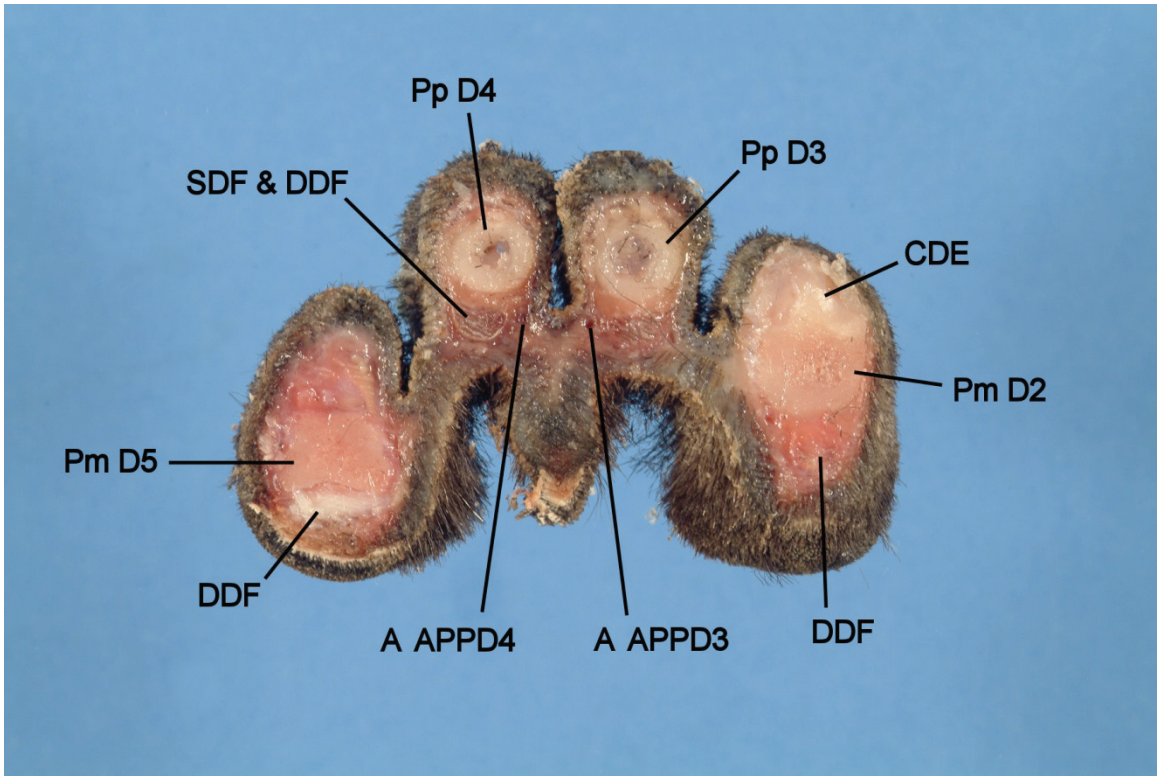
Pp D4
Pp D3
SDF & DDF
CDE
Pm D2
Pm D5
DDF
A APPD4
A APPD3
DDF

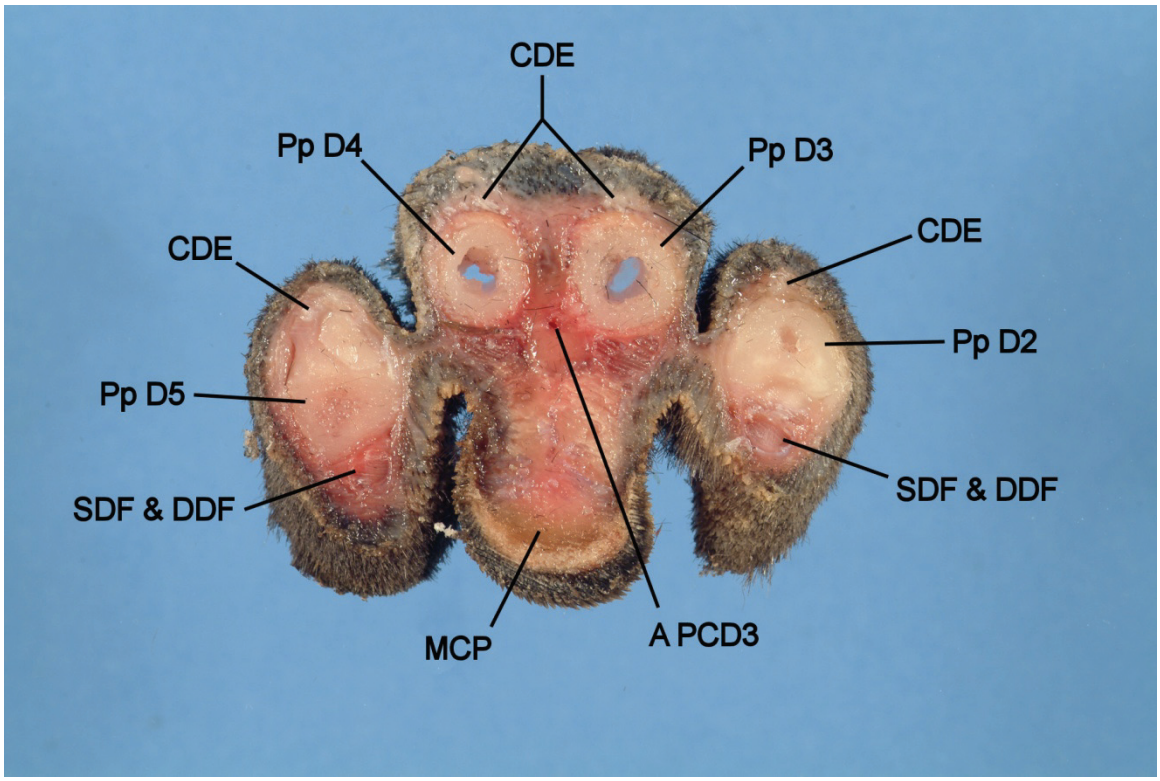
CDE
Pp D4
Pp D3
CDE
CDE
Pp D2
Pp D5
SDF & DDF
SDF & DDF
MCP
A PCD3

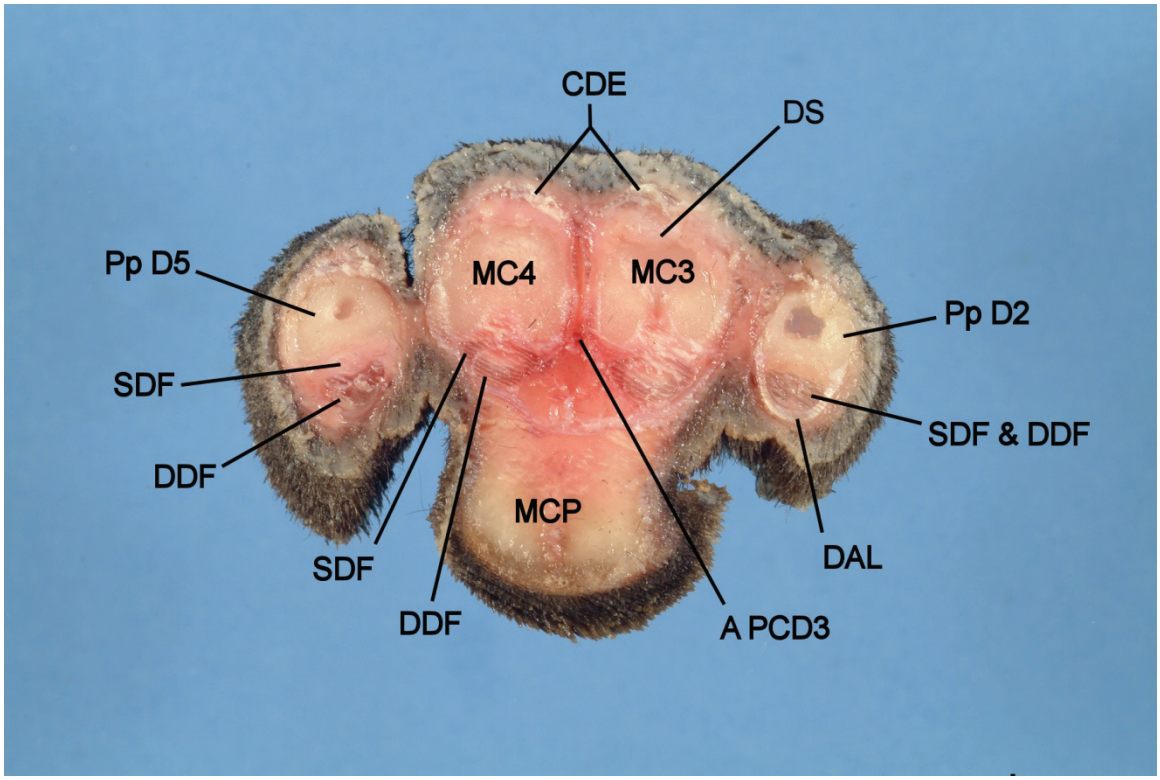
CDE
DS
Pp D5
MC4
MC3
Pp D2
SDF
SDF & DDF
DDF
MCP
DAL
SDF
DDF
A PCD3

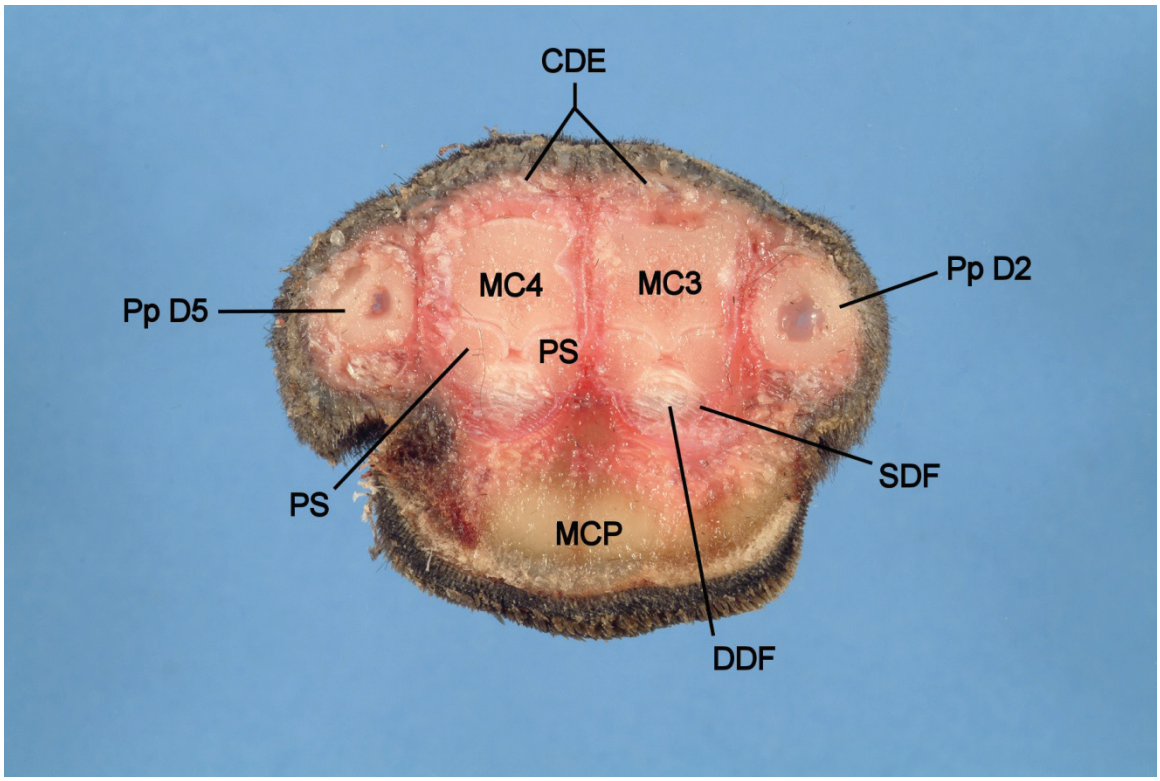
CDE
Pp D5
MC4
MC3
Pp D2
PS
PS
SDF
MCP
DDF

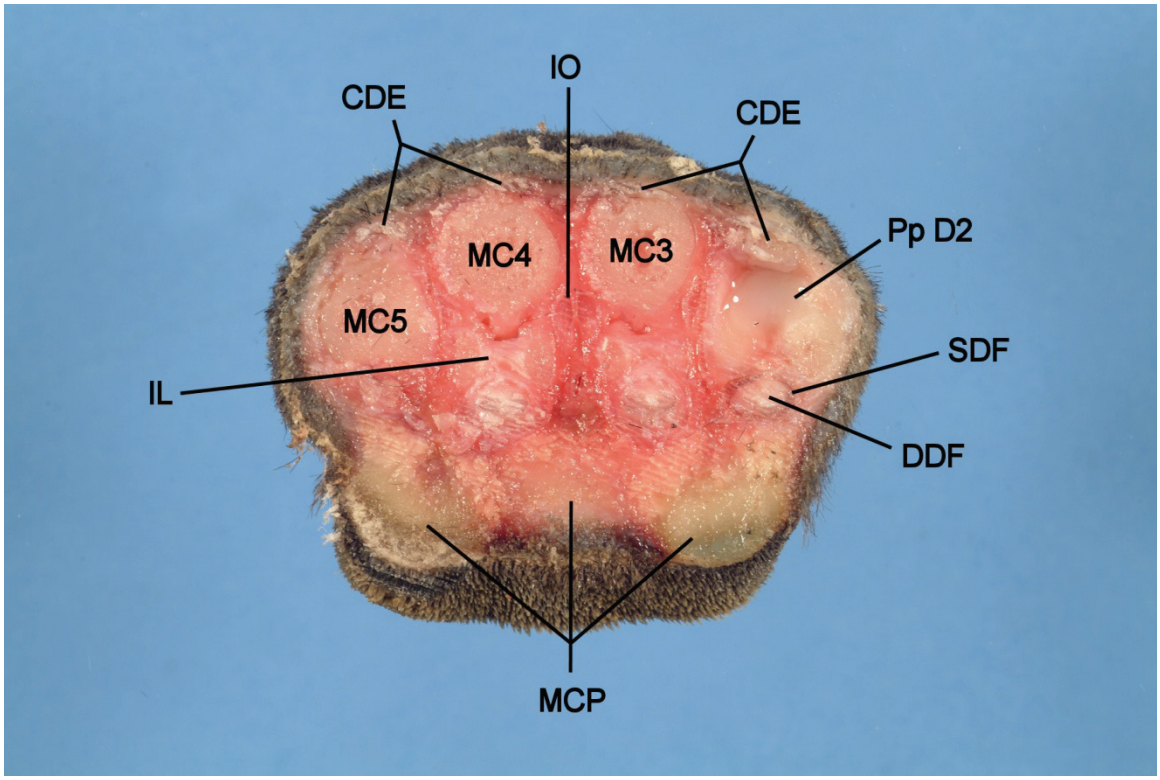
IO
CDE
CDE
Pp D2
MC4
MC3
MC5
SDF
IL
DDF
MCP

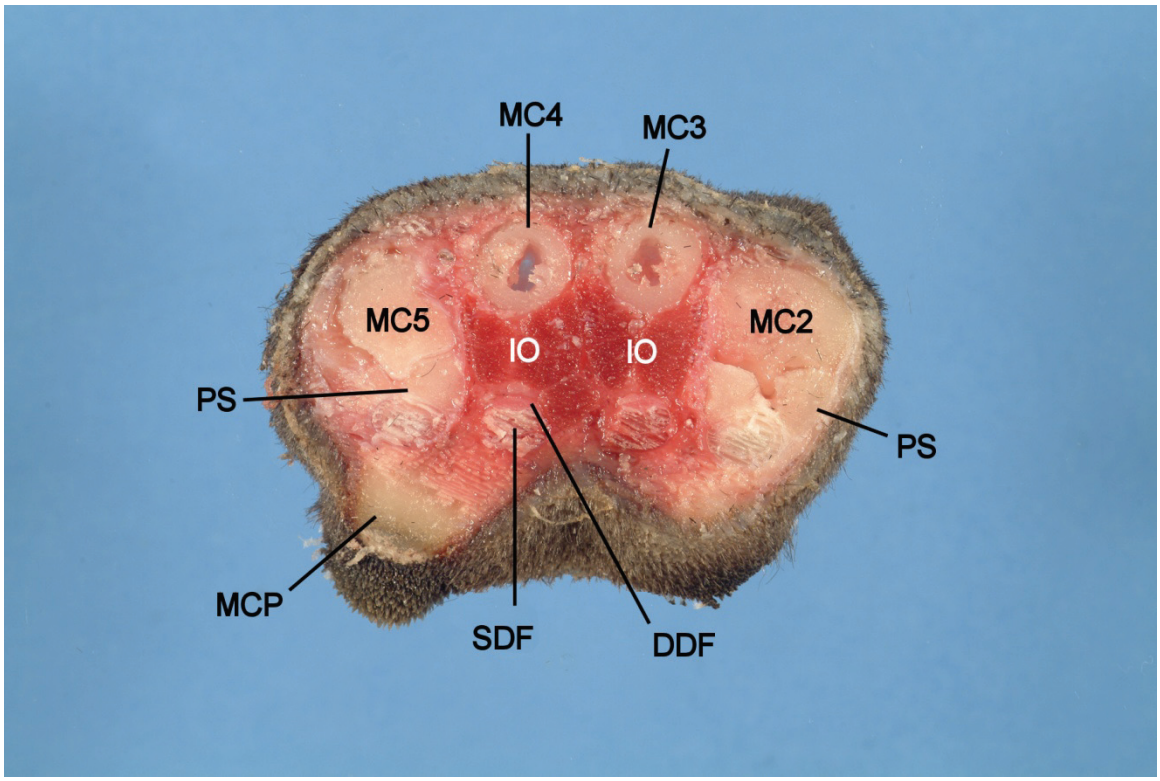
MC4
MC3
MC5
IO
IO
MC2
PS
PS
MCP
SDF
DDF

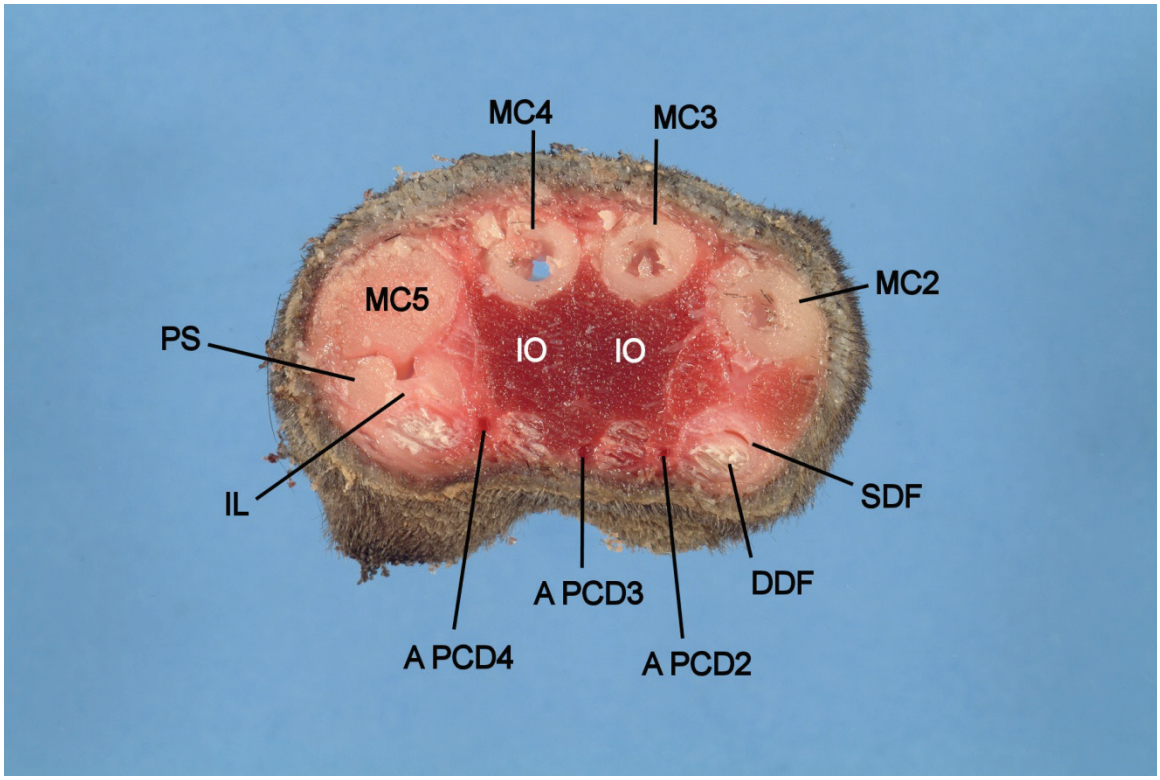
MC4
MC3
MC2
MC5
PS
IO
IO
IL
SDF
DDF
A PCD3
A PCD4
A PCD2

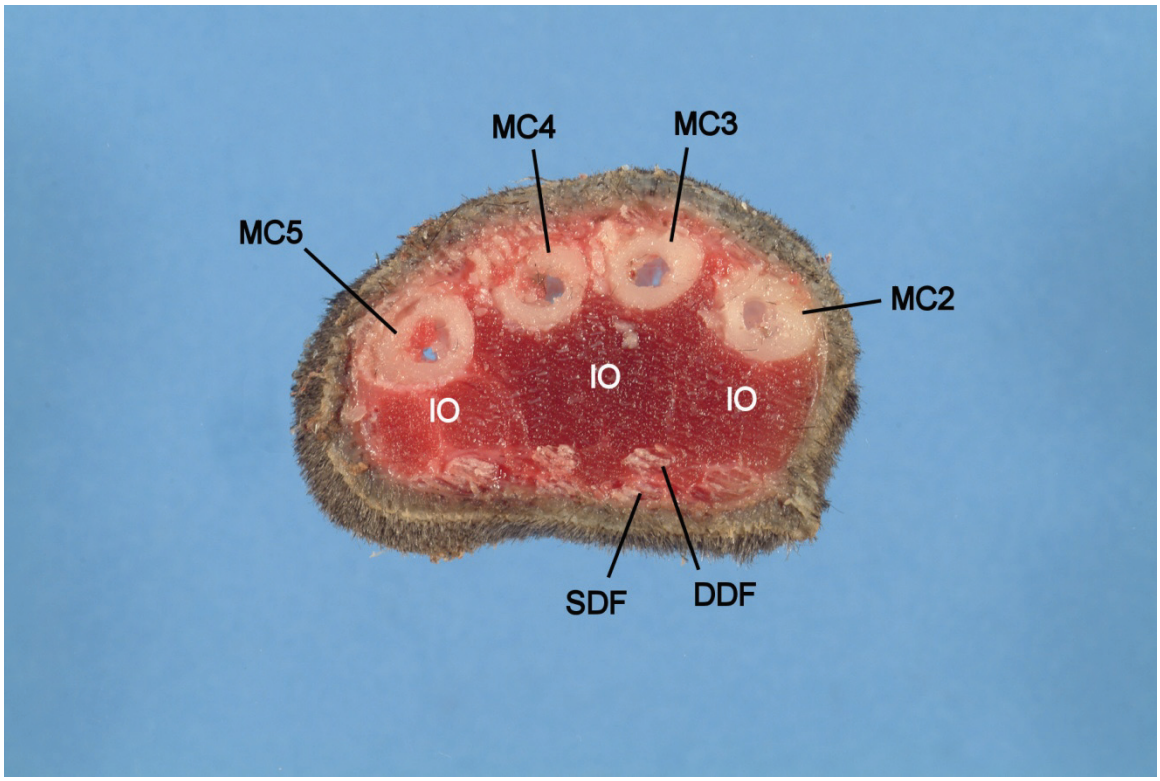
MC4
MC3
MC5
MC2
IO
IO
IO
SDF
DDF

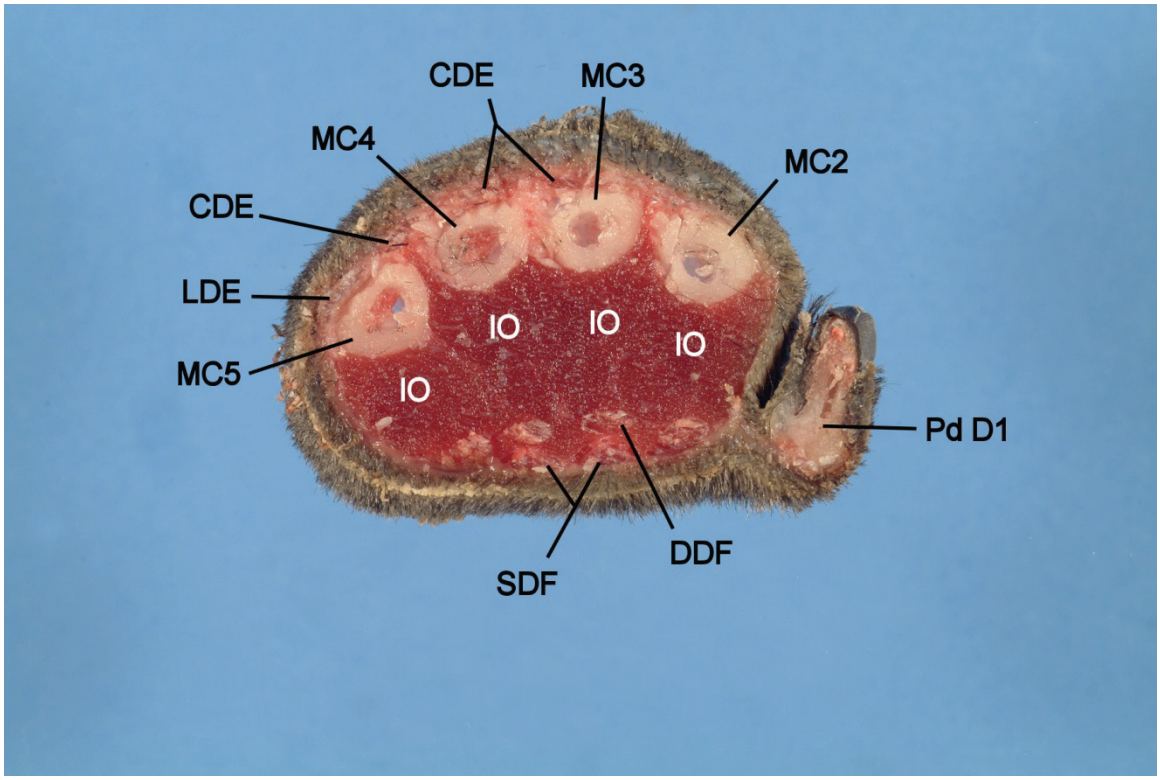
CDE
MC3
MC4
MC2
CDE
LDE
IO
IO
IO
MC5
IO
Pd D1
DDF
SDF

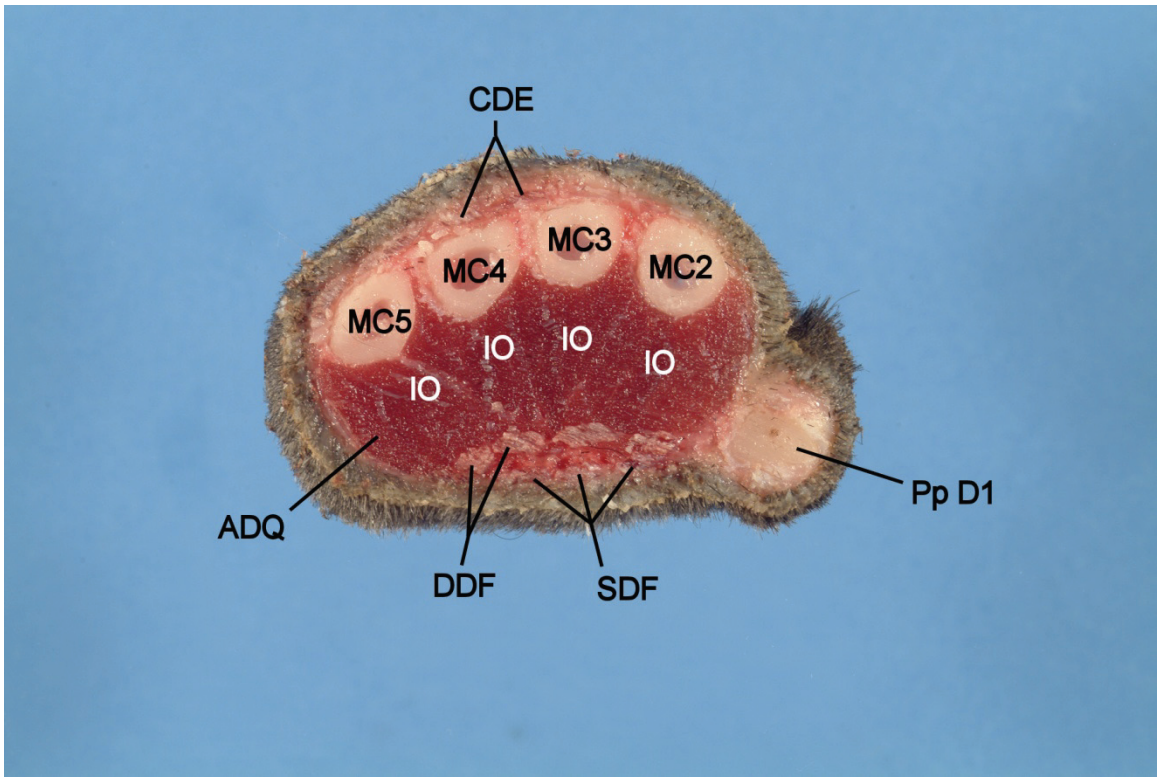
CDE
MC3
MC4
MC2
MC5
IO
IO
IO
IO
ADQ
Pp D1
DDF
SDF

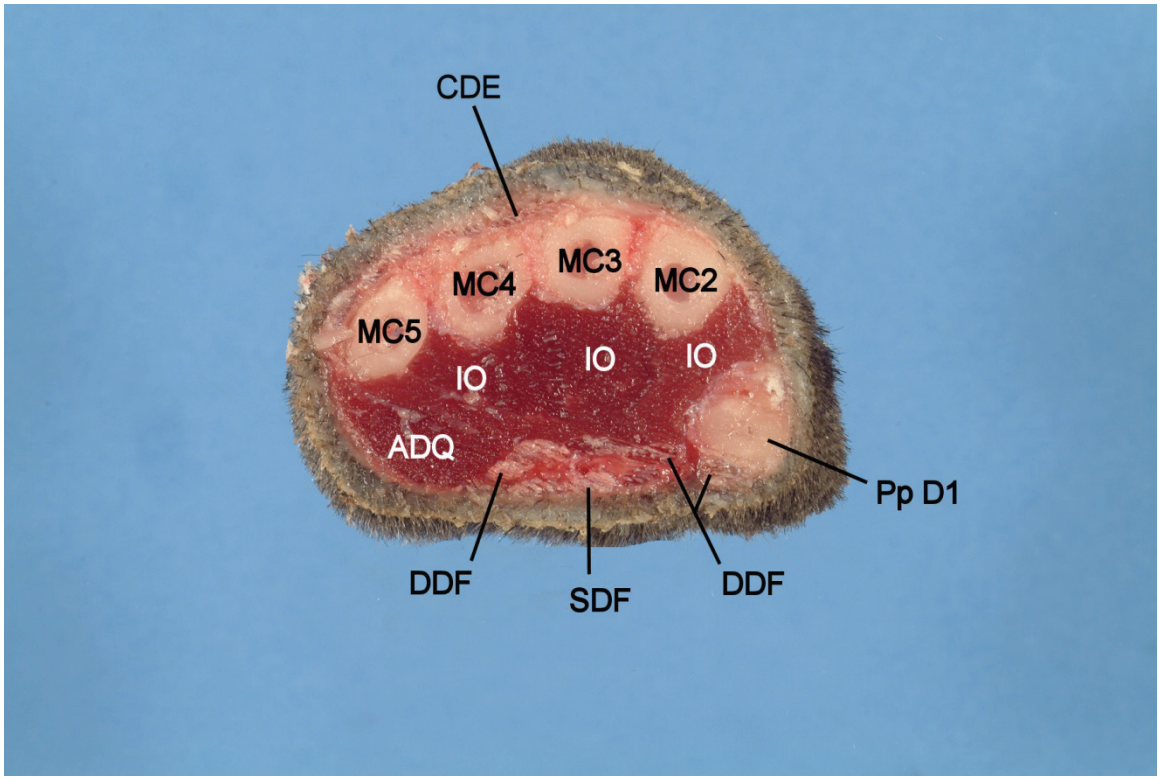
CDE
MC3
MC4
MC2
MC5
IO
IO
IO
ADQ
Pp D1
DDF
SDF
DDF

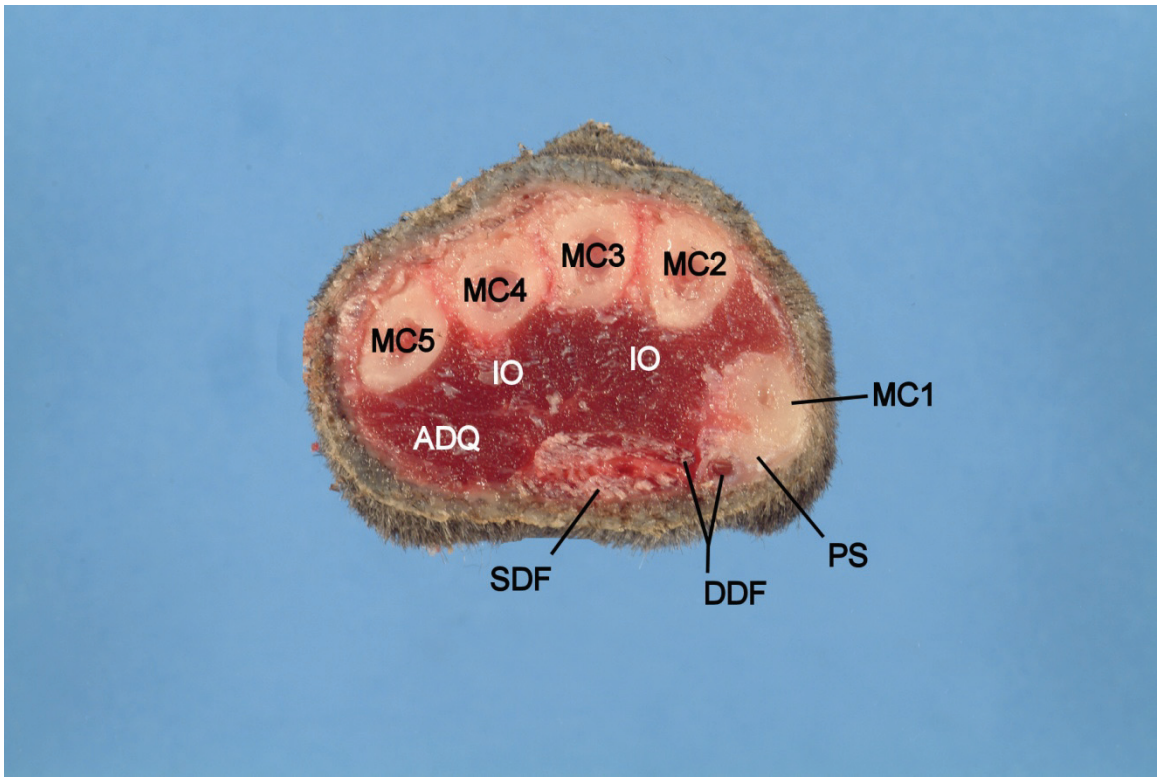
MC3
MC2
MC4
MC5
IO
IO
MC1
ADQ
SDF
DDF
PS

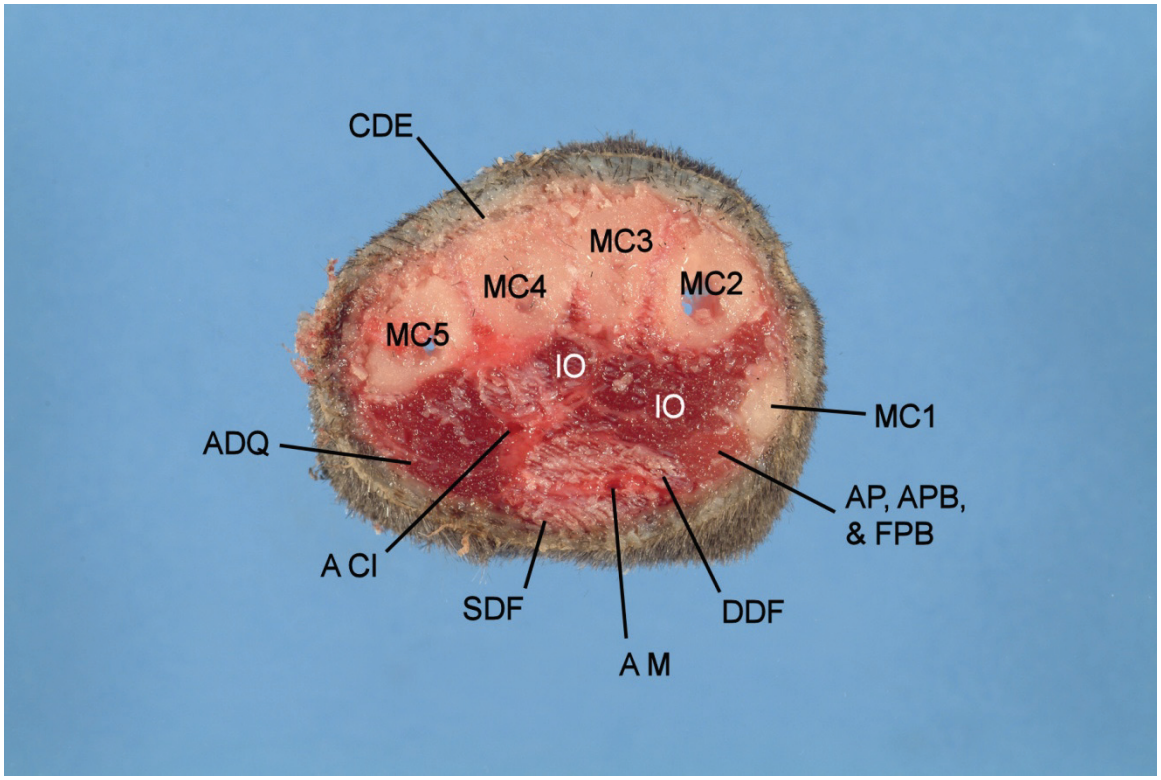
CDE
MC3
MC4
MC2
MC5
IO
IO
MC1
ADQ
AP, APB,
& FPB
A CI
SDF
DDF
A M

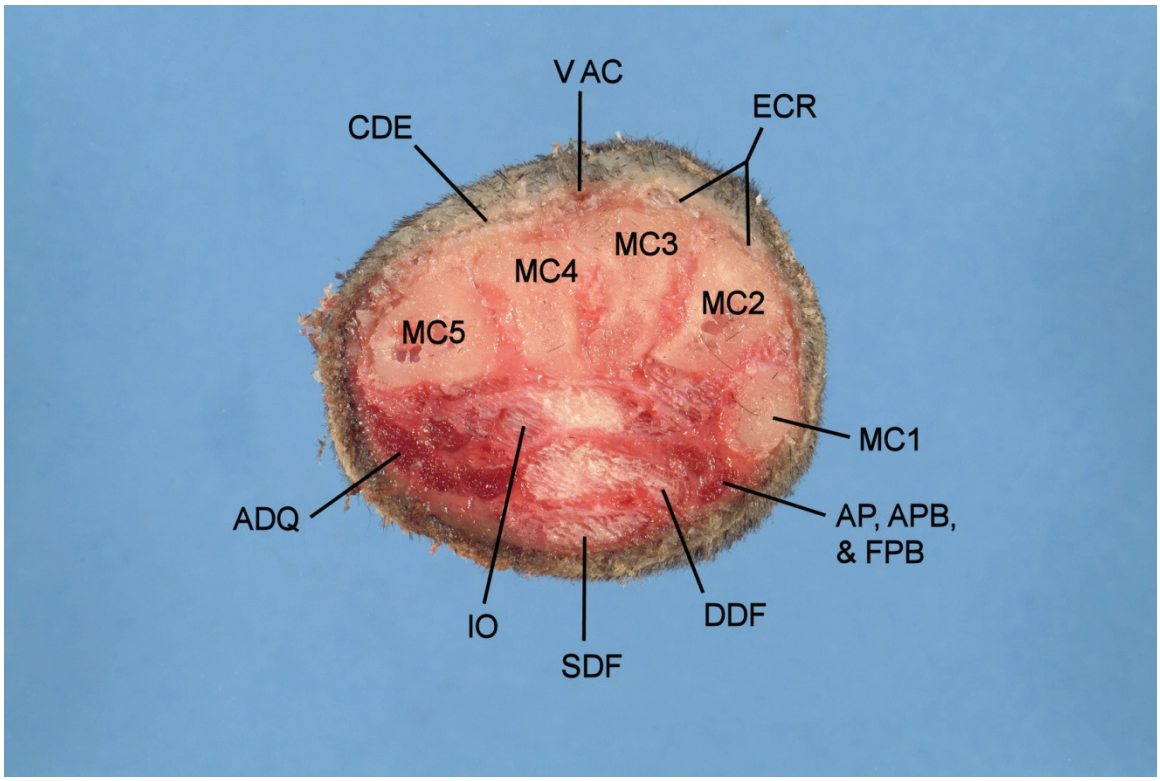
V AC
CDE
ECR
MC3
MC4
MC2
MC5
MC1
ADQ
AP, APB,
& FPB
IO
DDF
SDF

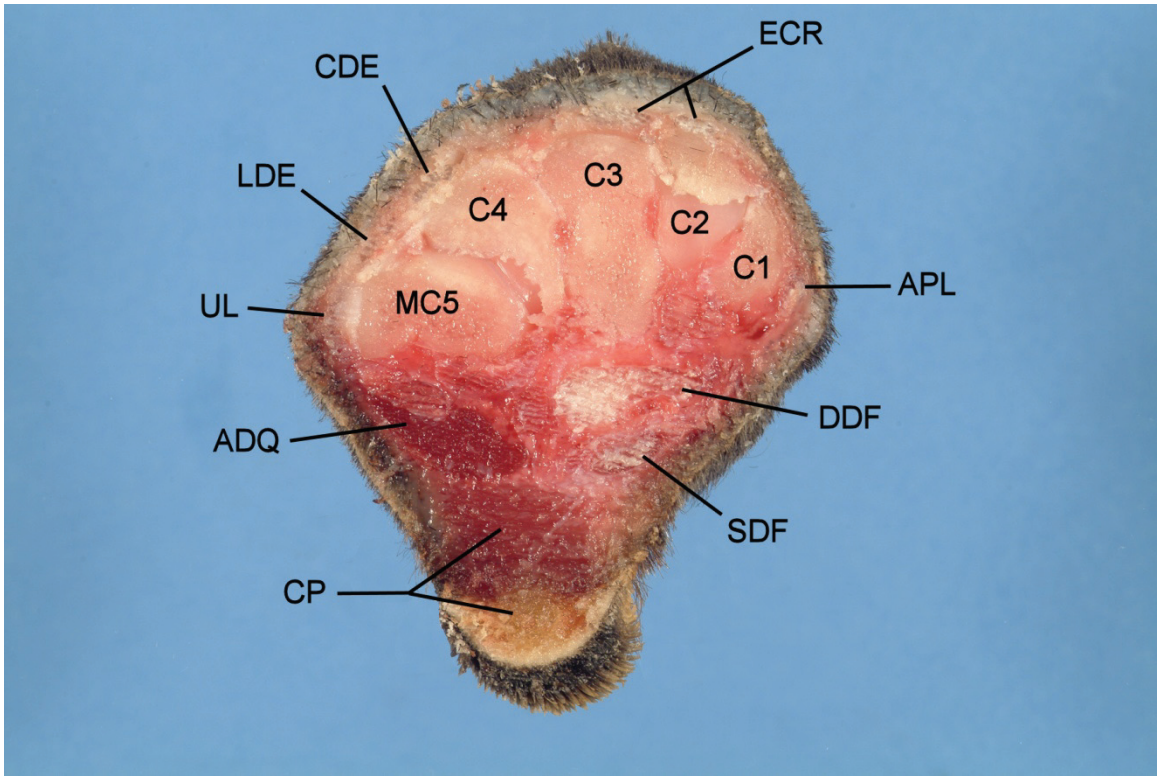
ECR
CDE
LDE
C3
C4
C2
C1
APL
UL
MC5
DDF
ADQ
SDF
CP

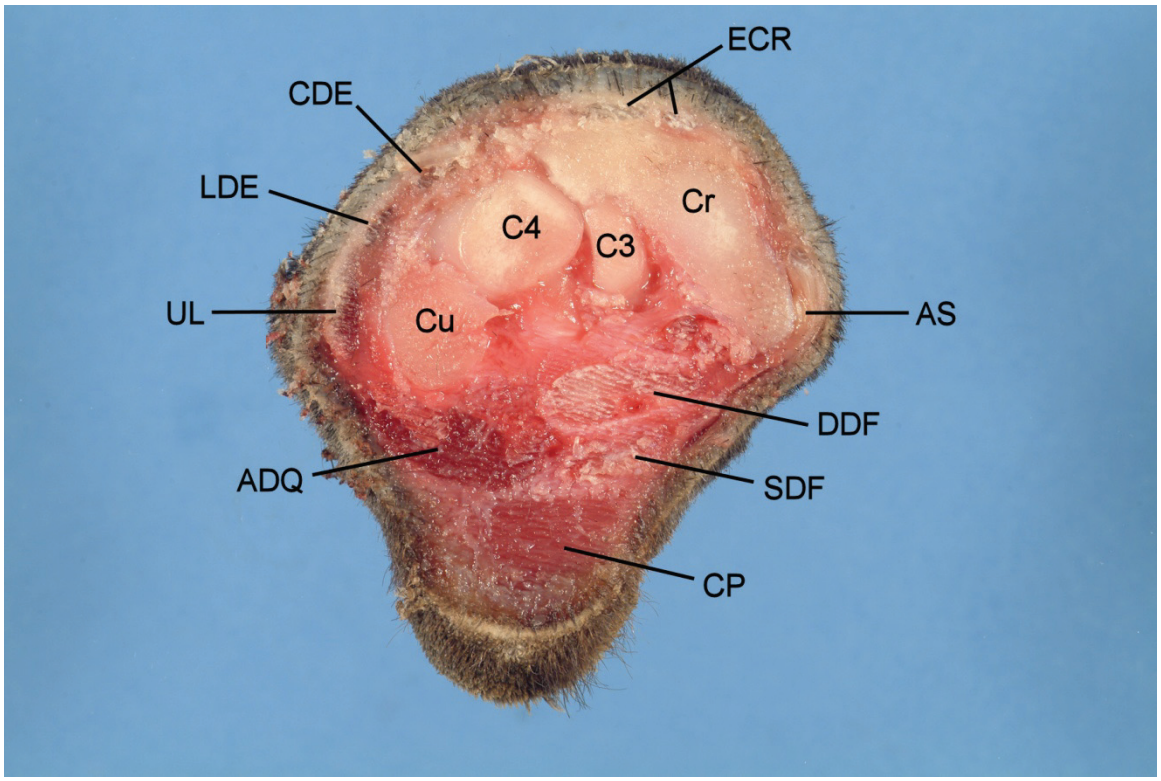
ECR
CDE
LDE
C4
C3
Cr
UL
Cu
AS
DDF
ADQ
SDF
CP

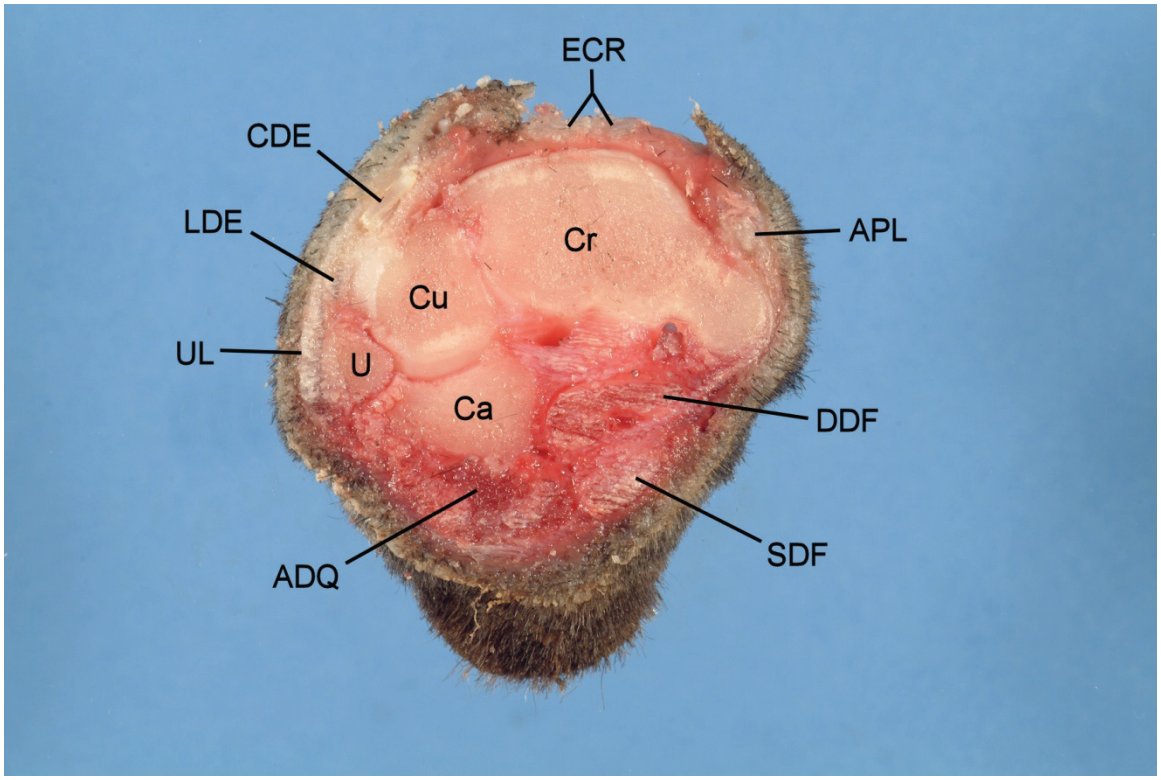
ECR
CDE
LDE
Cr
APL
Cu
UL
U
Ca
DDF
ADQ
SDF

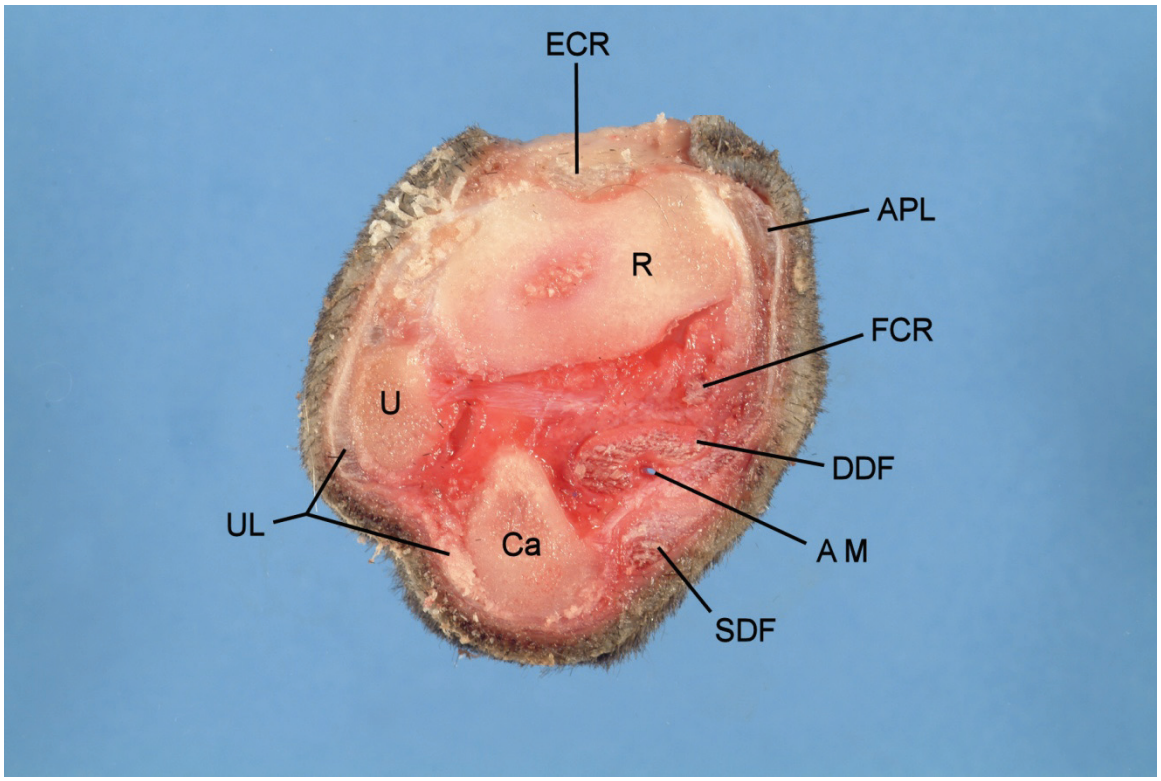
ECR
APL
R
FCR
U
DDF
UL
Ca
A M
SDF

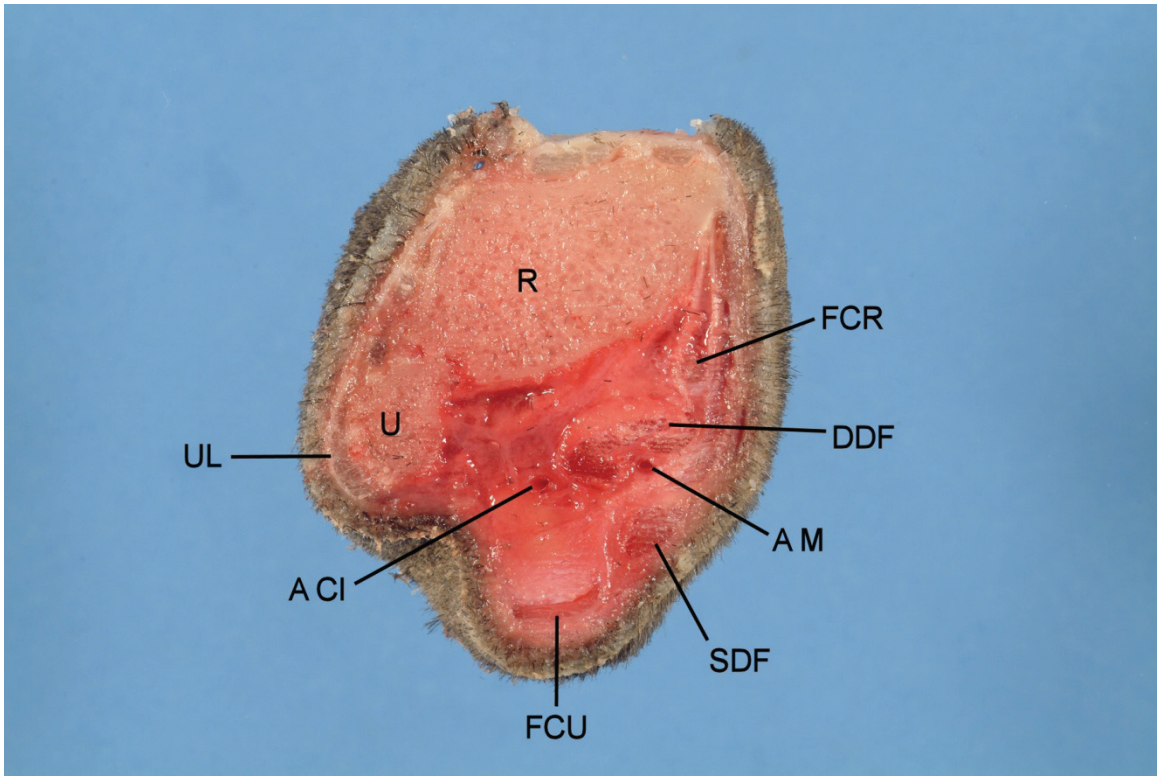
R
FCR
U
DDF
UL
A M
A CI
SDF
FCU

Dorsal slices (Figure A.2)
4 mm thickness
Right manus from dorsal to palmar

Table A.2: Key to Dorsal Images

Code	Structure	Code	Structure
A APPD3	Axial palmar proper digital a. III	DAL	Proximal digital annular ligament
A APPD4	Axial palmar proper digital a. IV	DDF	Deep digital flexor
A CI	Caudal (palmar) interosseous a.	DP	Digital pad
A M	Median a.	DS	Dorsal sesamoid bone
A PCD2	Palmar common digital a. II	ECR	Extensor carpi radialis
A PCD3	Palmar common digital a. III	FCR	Flexor carpi radialis
A PCD4	Palmar common digital a. IV	FCU	Flexor carpi ulnaris
ADQ	Abductor digiti quinti	FPB	Flexor pollicis brevis
AP	Adductor pollicis	IL	Intersesamoidean ligament
APB	Abductor pollicis brevis	IO	Interosseous muscle
APL	Abductor pollicis longus	LDE	Lateral digital extensor
AS	Sesamoid bone in APL tendon	MC1	Metacarpal bone I
C1	Carpal bone 1	MC2	Metacarpal bone II
C2	Carpal bone 2	MC3	Metacarpal bone III
C3	Carpal bone 3	MC4	Metacarpal bone IV
C4	Carpal bone 4	MC5	Metacarpal bone V
Ca	Accessory carpal bone	MCP	Metacarpal pad
CDE	Common digital extensor	Pd	Distal phalanx
CL	Collateral ligament	Pm	Middle phalanx
CP	Carpal pad	Pp	Proximal phalanx
Cr	Radial (radiointermedial) carpal bone	PS	Proximal sesamoid bone
Cu	Ulnar carpal bone	R	Radius
D1	Digit I	SDF	Superficial digital flexor
D2	Digit II	U	Ulna
D3	Digit III	UL	Ulnaris lateralis
D4	Digit IV	V AC	Accessory cephalic v.
D5	Digit V		

Notes: a. = artery, v. = vein

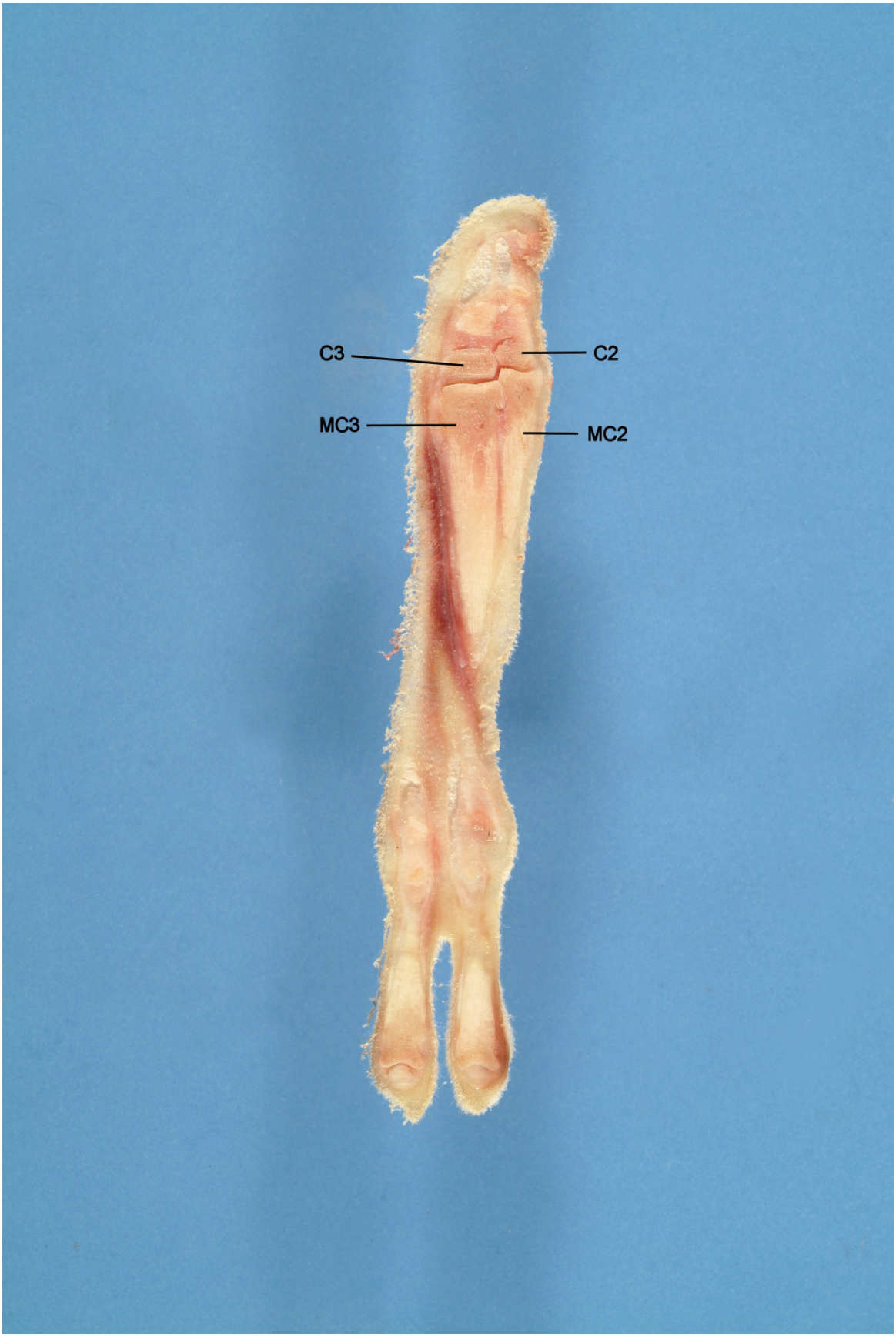
C3
C2
MC3
MC2

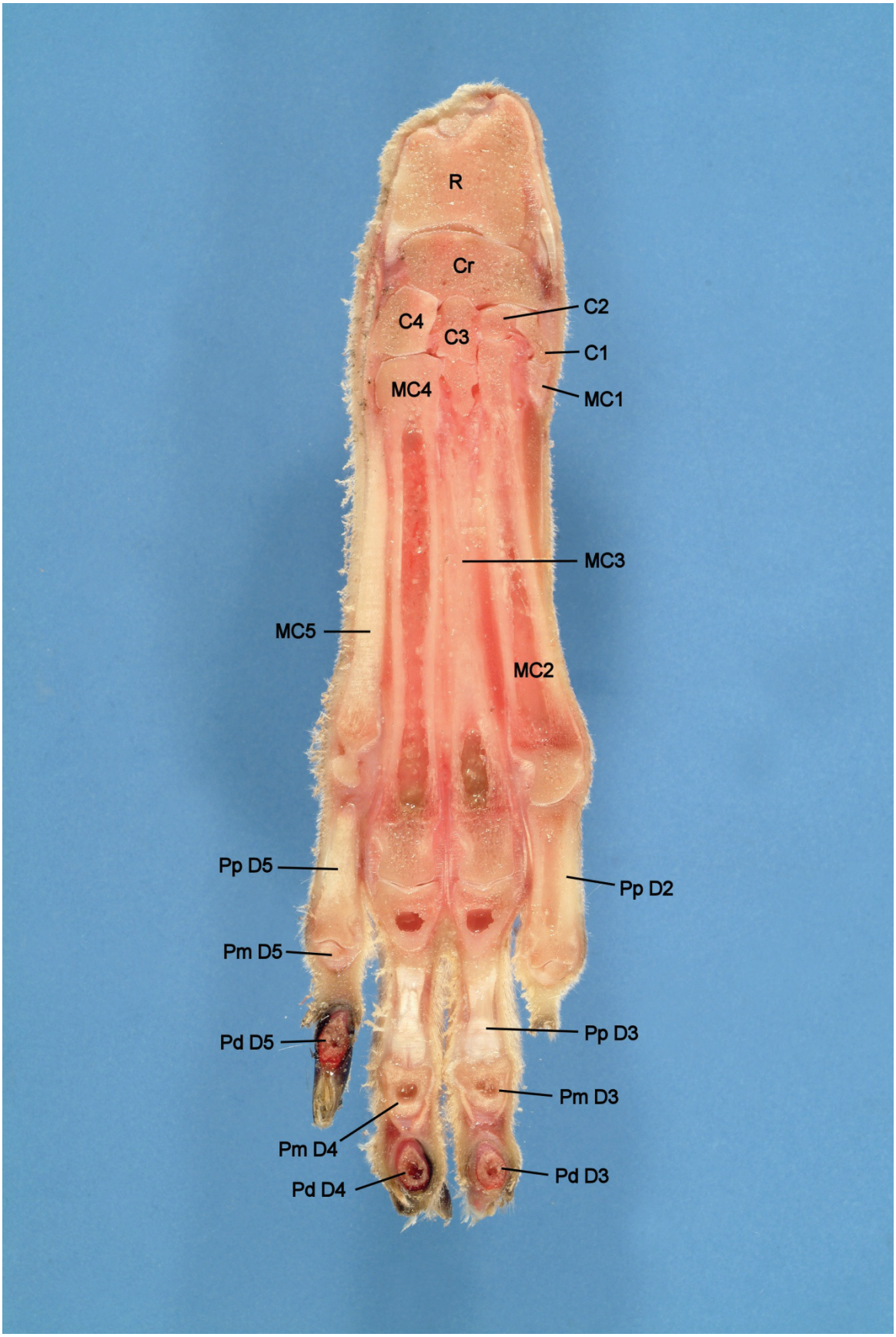
R
Cr
C2
C4
C3
C1
MC4
MC1
MC3
MC5
MC2
Pp D5
Pp D2
Pm D5
Pd D5
Pp D3
Pm D3
Pm D4
Pd D3
Pd D4

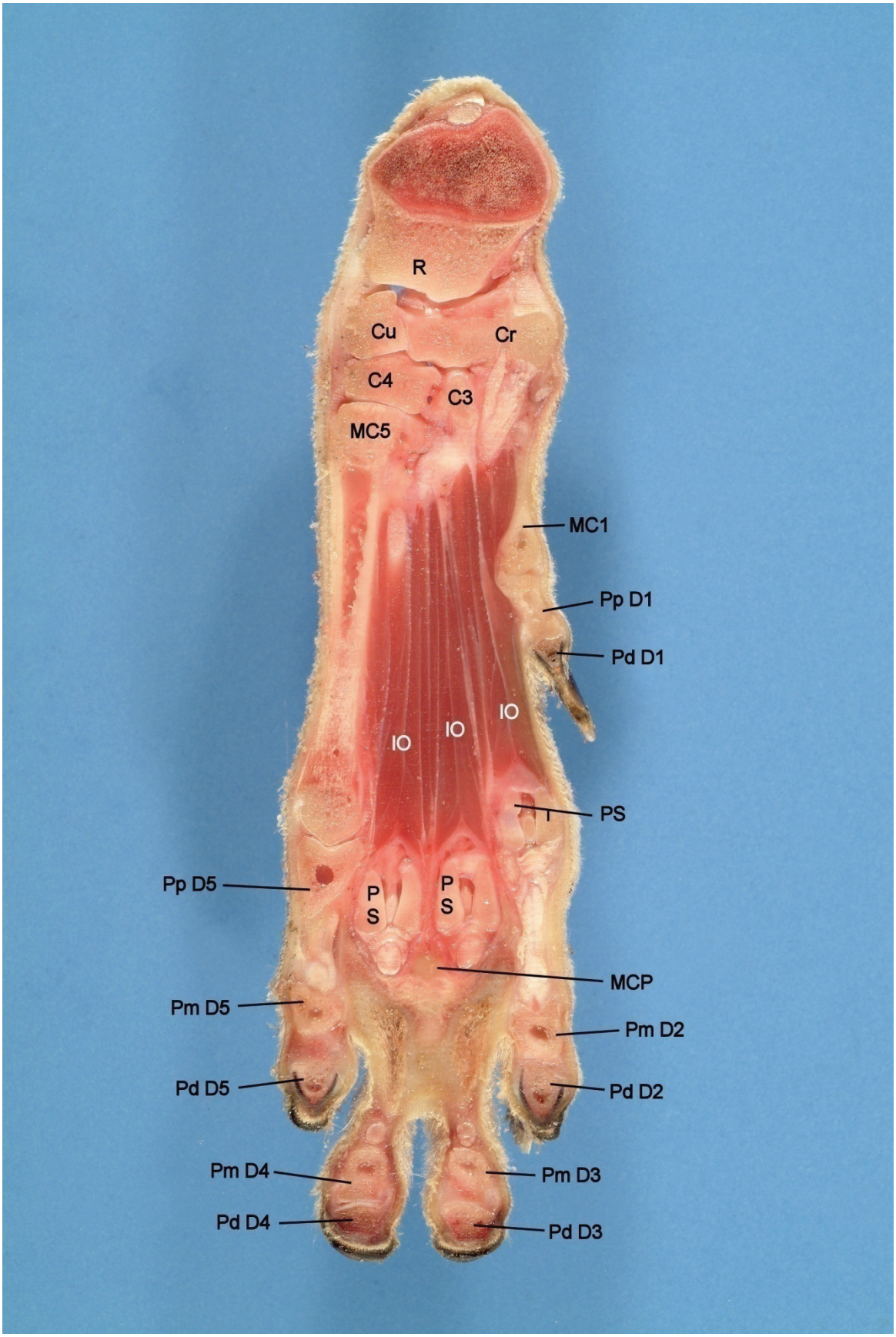
R
Cu
Cr
C4
C3
MC5
MC1
Pp D1
Pd D1
IO
IO
IO
PS
Pp D5
P
S
P
S
MCP
Pm D5
Pm D2
Pd D5
Pd D2
Pm D4
Pm D3
Pd D4
Pd D3

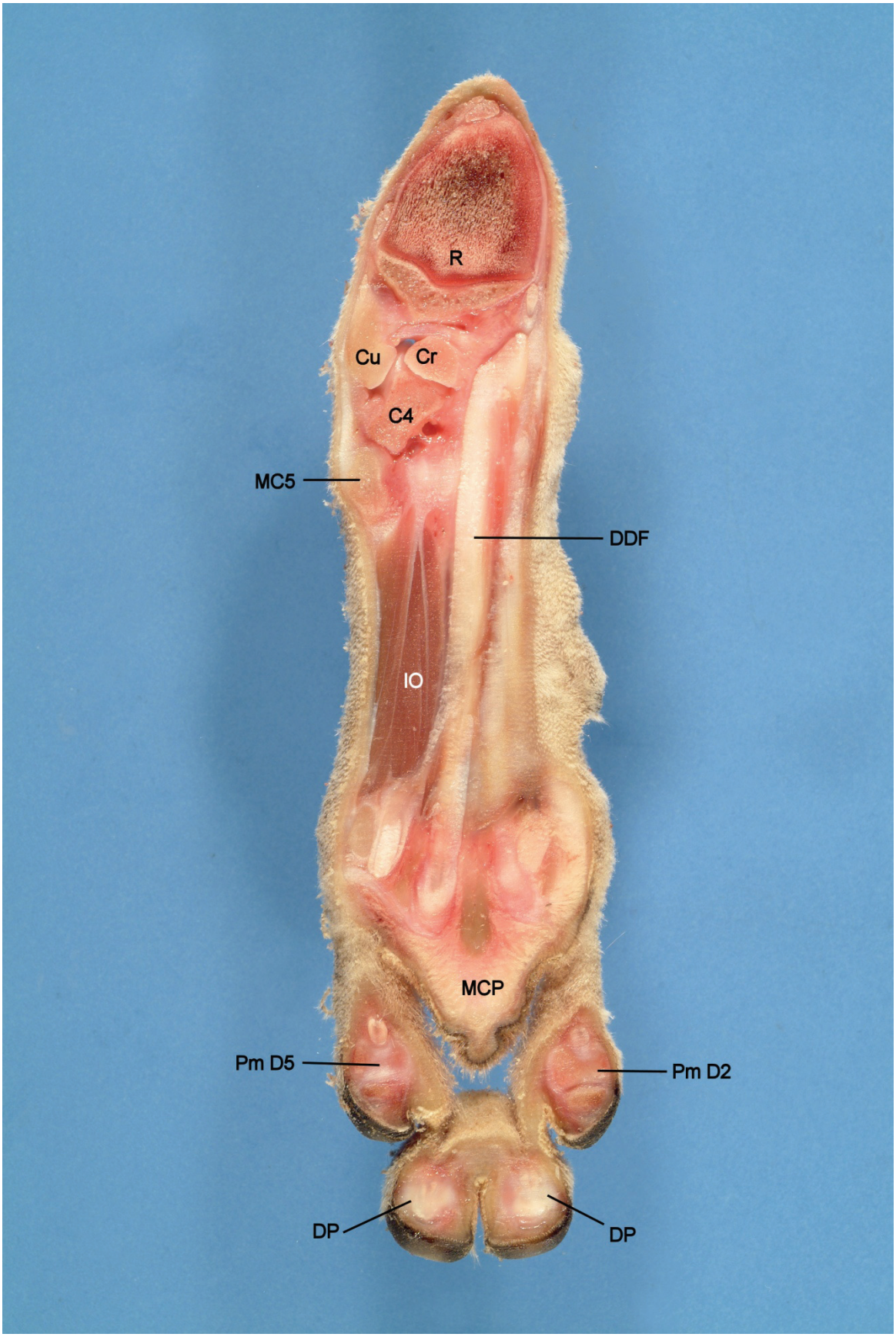
R
Cu
Cr
C4
MC5
DDF
IO
MCP
Pm D5
Pm D2
DP
DP


R
U
Ca
MCP
DP
DP

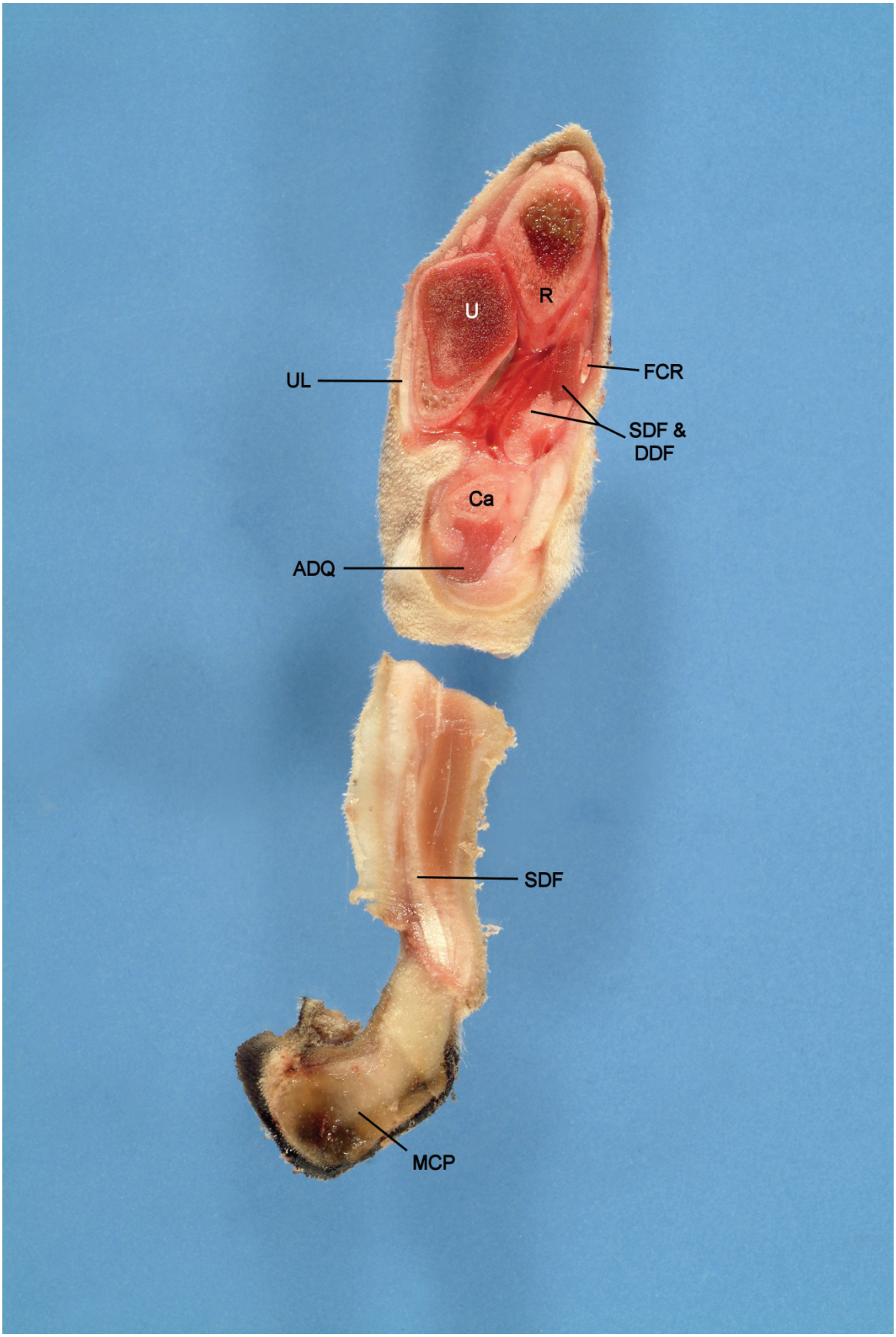
U
R
UL
FCR
SDF &
DDF
Ca
ADQ
SDF
MCP

Sagittal slices (Figure A.3)
4 mm thickness
Right manus from lateral to medial

Table A.3: Key to Sagittal Images

Code	Structure	Code	Structure
A APPD3	Axial palmar proper digital a. III	DAL	Proximal digital annular ligament
A APPD4	Axial palmar proper digital a. IV	DDF	Deep digital flexor
A CI	Caudal (palmar) interosseous a.	DP	Digital pad
A M	Median a.	DS	Dorsal sesamoid bone
A PCD2	Palmar common digital a. II	ECR	Extensor carpi radialis
A PCD3	Palmar common digital a. III	FCR	Flexor carpi radialis
A PCD4	Palmar common digital a. IV	FCU	Flexor carpi ulnaris
ADQ	Abductor digiti quinti	FPB	Flexor pollicis brevis
AP	Adductor pollicis	IL	Intersesamoidean ligament
APB	Abductor pollicis brevis	IO	Interosseous muscle
APL	Abductor pollicis longus	LDE	Lateral digital extensor
AS	Sesamoid bone in APL tendon	MC1	Metacarpal bone I
C1	Carpal bone 1	MC2	Metacarpal bone II
C2	Carpal bone 2	MC3	Metacarpal bone III
C3	Carpal bone 3	MC4	Metacarpal bone IV
C4	Carpal bone 4	MC5	Metacarpal bone V
Ca	Accessory carpal bone	MCP	Metacarpal pad
CDE	Common digital extensor	Pd	Distal phalanx
CL	Collateral ligament	Pm	Middle phalanx
CP	Carpal pad	Pp	Proximal phalanx
Cr	Radial (radiointermedial) carpal bone	PS	Proximal sesamoid bone
Cu	Ulnar carpal bone	R	Radius
D1	Digit I	SDF	Superficial digital flexor
D2	Digit II	U	Ulna
D3	Digit III	UL	Ulnaris lateralis
D4	Digit IV	V AC	Accessory cephalic v.
D5	Digit V		

Notes: a. = artery, v. = vein

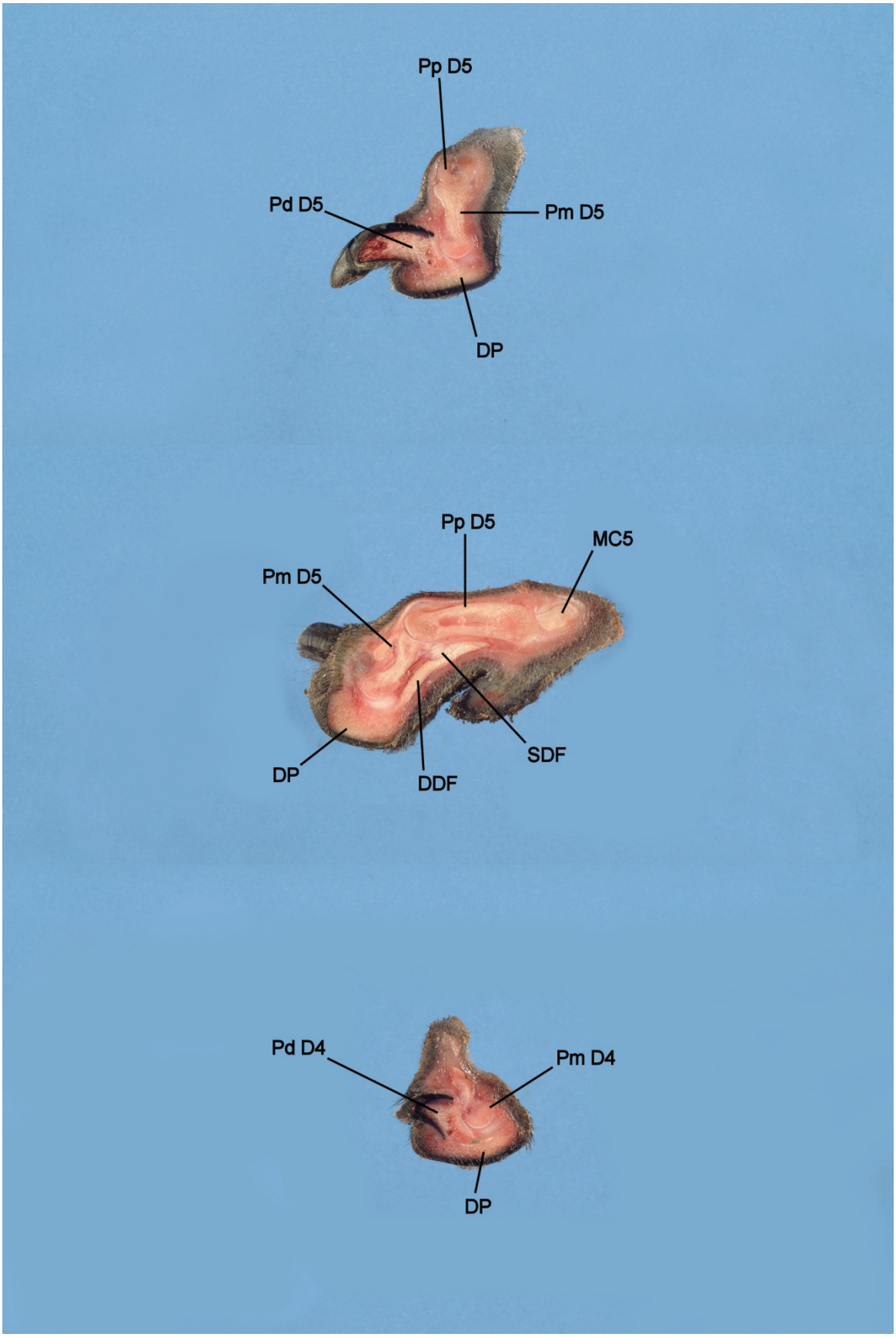
Pp D5
Pd D5
Pm D5
DP
Pp D5
MC5
Pm D5
SDF
DP
DDF
Pd D4
Pm D4
DP

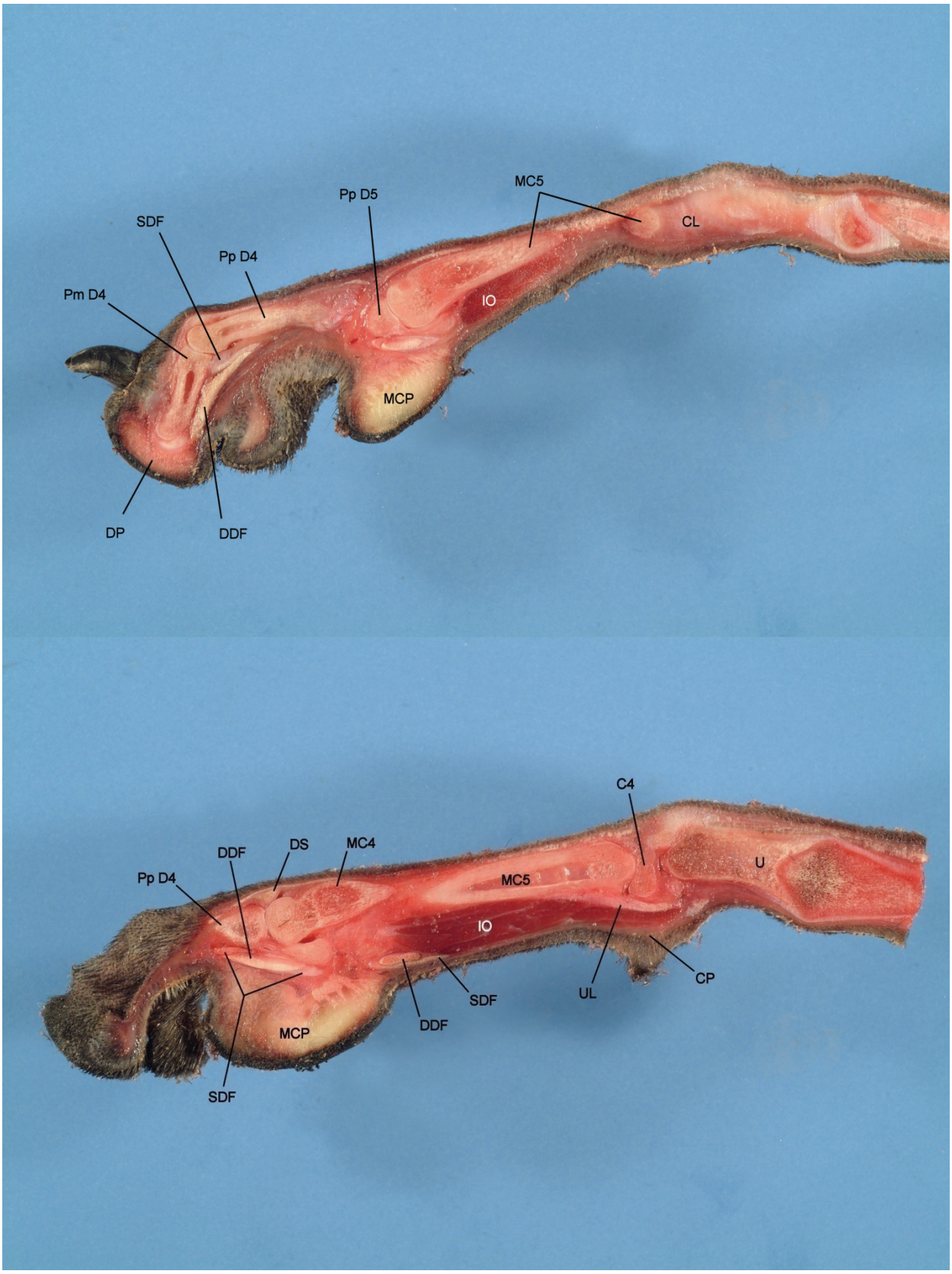
MC5
Pp D5
SDF
CL
Pp D4
Pm D4
IO
MCP
DP
DDF
C4
DDF
DS
MC4
U
Pp D4
MC5
IO
CP
UL
SDF
DDF
MCP
SDF

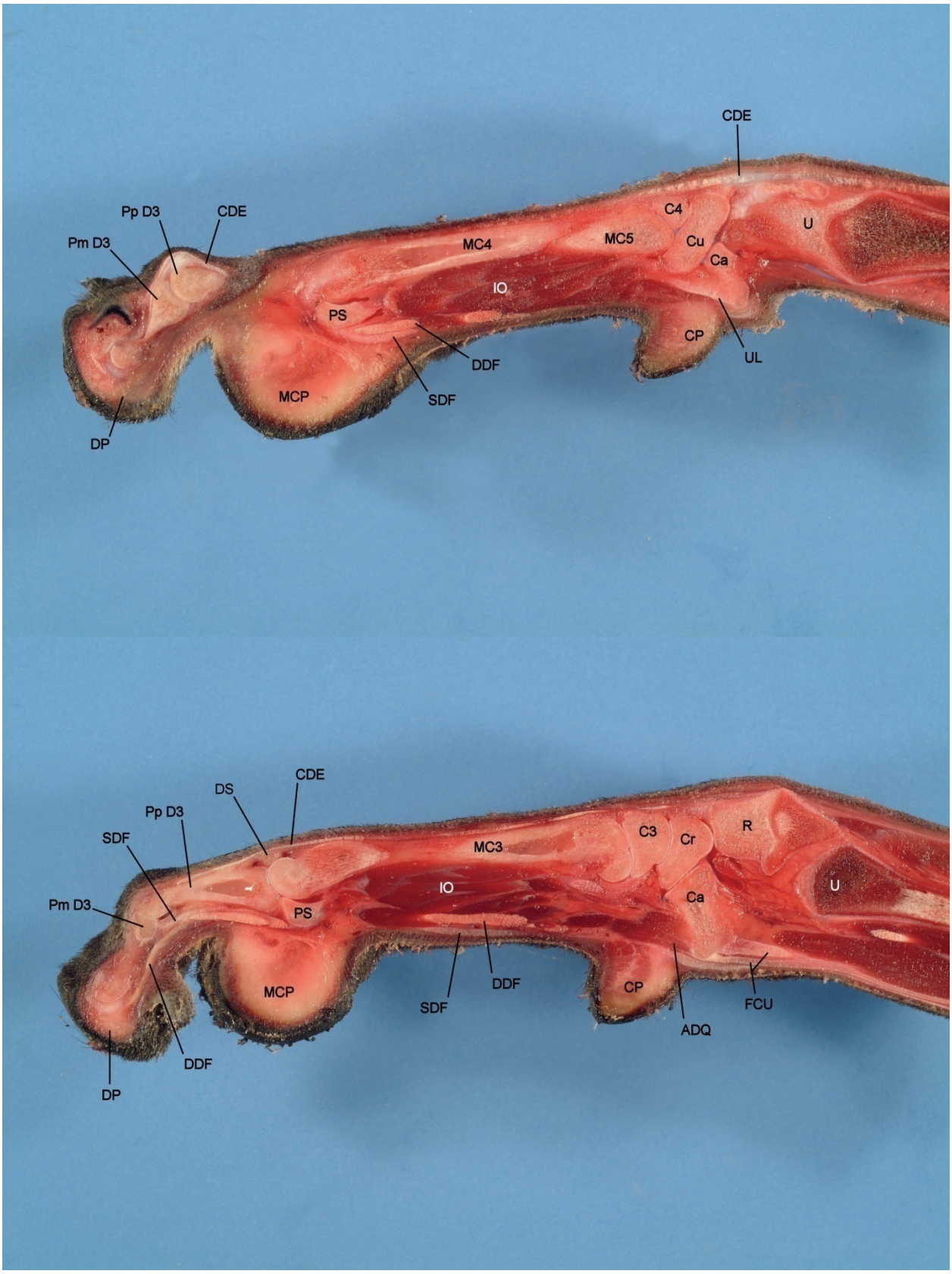
CDE
Pp D3
CDE
Pm D3
C4
U
MC4
MC5
Cu
Ca
IO
PS
CP
UL
DDF
MCP
SDF
DP
CDE
DS
Pp D3
SDF
C3
Cr
R
MC3
IO
U
Pm D3
PS
Ca
MCP
DDF
SDF
CP
FCU
ADQ
DDF
DP

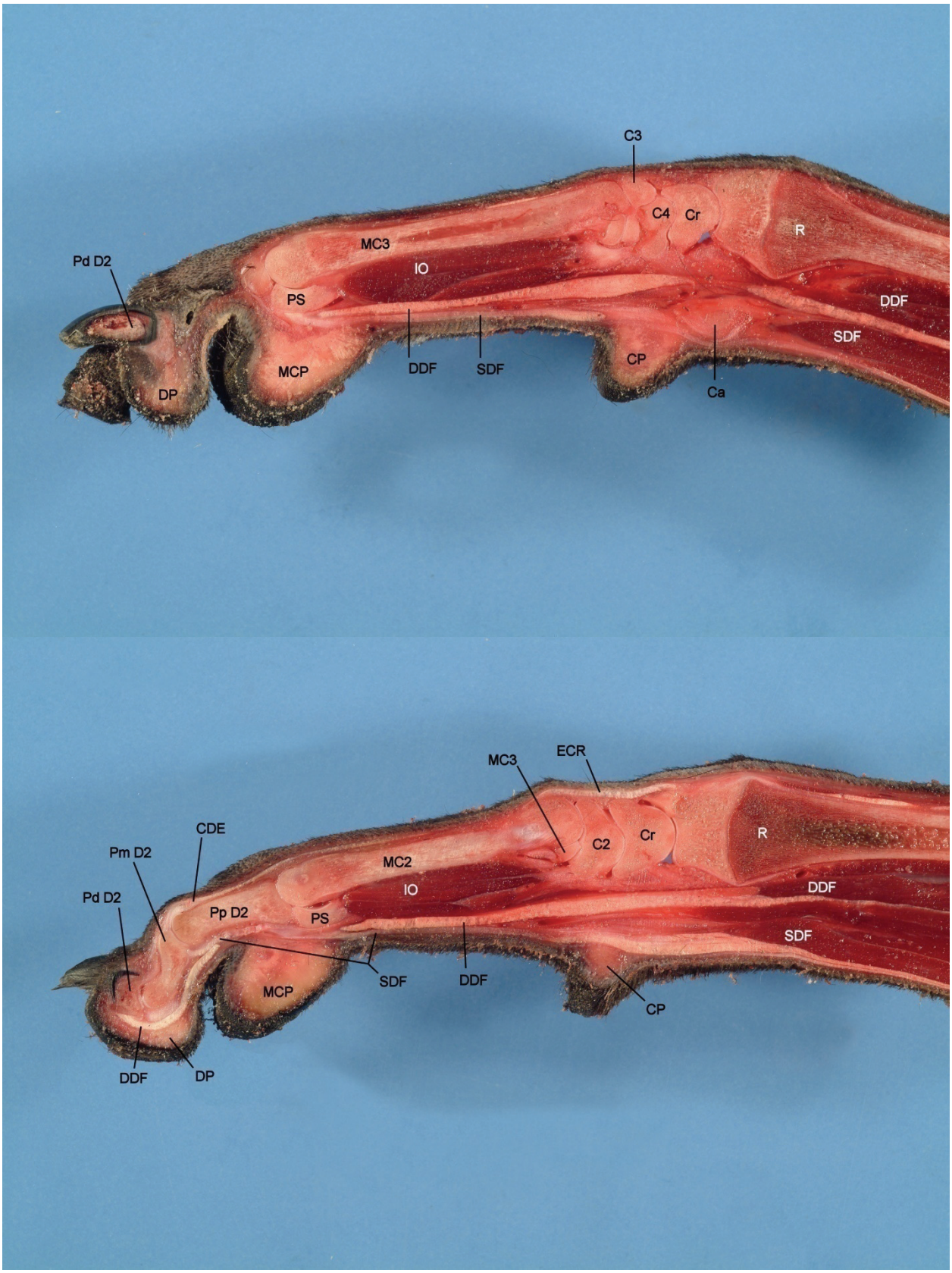
C3
C4
Cr
R
MC3
IO
Pd D2
PS
DDF
SDF
MCP
DP
CP
Ca
ECR
CDE
Pm D2
Pp D2
C2
MC2


ECR
MC1
C2
Cr
R
Pp D2
MC2
IO
PS
PS
Pp D1
FCR
DDF
SDF
MCP
DP
CL
C1
R
Cr
MC2
Pp D1
Pd D1

Appendix B

Foreign Body Imaging Comparisons in the Literature

The tables in this section are derived from data presented in multiple different articles and are presented chronologically. Some tables are modified directly from the results presented in the manuscripts, while other tables represent an extrapolation of descriptors used by the authors. In tables depicting visibility of objects, foreign bodies with more plus signs (+) were considered more easily visualized, and those with a zero (0) were not visualized.

Table B.1: Woesner and Sanders. (1972).[254] Tissue: Water phantom and lamb shank
(Table is extrapolated from descriptions in text of article)

	Visualization			
	Water Phantom		Lamb Shank	
Foreign object	Radiography	Xeroradiography	Radiography	Xeroradiography
Metal	++++	++++	++++	++++
Glass	++++	++++	++++	++++
Wood	++	+++	0	++
Plastic	++	+++	+	+++
Gravel	++++	++++	++++	++++
Rubber	+	+	0	+
Gauze pad	0	+	0	0
Chicken bone	++++	++++	++++	++++
Fish bone	++++	++++	++++	++++
Graphite	++	+++	+	+++
Palm thorn	+	+	0	0
Polyethylene tube	+++	+++	+++	+++
Cotton ball	0	0	0	0

Table B.2: Kuhns, *et al*. (1979).[255] Tissue: Human cadaver limb

	Visualized?		
Foreign object	Mammography	Xeroradiography	CT
Dry toothpick	No	No	Yes
Soaked toothpick	No	No	Yes

Table B.3: Anderson, *et al*. (1982).[5] Tissue: Human hands (clinical patients)

	Radiography		Xeroradiography	
Foreign object	Positive cases	Negative cases	Positive cases	Negative cases
Metal	58		4	
Glass	34	2	12	
Wood	2	13	2	10
Pencil	2			
Bone	1			
Gravel	1		1	
Fiberglass			1	
Plastic				1

Table B.4: Charney, *et al*. (1986).[21] Tissue: Human cadaver feet

	Visibility	
Foreign object	Radiography	Xeroradiography
Oak (4mm x 6cm)	++	+
Cedar (4mm x 6cm)	++	+
Pine (4mm x 6cm)	++	+
Maple (4mm x 6cm)	++	+
Cedar (2mm x 5cm)	0	0
Pine – untreated	+	0
Pine – varnished	+	+
Pine – epoxy stain	+	0
Pine – oil stain	+	+
Pine – epoxy enamel	++	++
Pine – oil paint	+	+
Glass	+++	+++
Gravel	+++	+++
Plastic cylinder	++	++
Flat plastic	+	+
Tile	+++	+++
Clay	+++	+++
Toothpick	+	+

Table B.5: de Flaviis, *et al*. (1988).[398] Tissue: Veal meat

	Visibility	
Foreign object	Xeroradiography	Ultrasound
Fish bone	0	Good
Sea urchin spine	Poor	Good
Rose thorn	0	Good
Wood	0	Good
Plastic splinter	0	Poor
Glass	Good	Good
Needle	Good	Good
Metal wire	Good	Good
Pebble	Good	Good
Suture material	0	Good

Table B.6: LoBue, *et al*. (1988).[364] Tissue: Enucleated sheep eyes
Foreign objects: Wood, glass, plastic, rock (each in two sizes)

	CT (%)	MRI (%)
Sensitivity	87.5	100
Specificity	100	100

Table B.7: Crawford and Matheson. (1989).[22] Tissue: Human hands (clinical patients)

	Ultrasound diagnosis			
Foreign object	True Positive	False Positive	True Negative	False Negative
Wood	17	1	3	1
Thorn	2	0	2	0
Other	0	1	12	0

Ultrasound sensitivity: 95.0%
Ultrasound specificity: 89.5%

Table B.8: Blyme, *et al*. (1990).[287] Tissue: Human cadaver thighs

	Ultrasound visualization	
Foreign object	Correct (%)	Incorrect (%)
Wood	89	11
Plastic	83	17
Glass	100	0
Empty wound	89	11

Overall sensitivity: 89%
Overall specificity: 93%

Table B.9: Ginsburg, *et al*. (1990).[381] Tissue: Steak strips

	Visualized?			
Foreign object	Radiography	Xeroradiography	Ultrasound	CT
Wood	No	No	Yes	No
Glass	Yes	Yes	Yes	Yes
Plastic	No	No	Yes	No

Table B.10: Glatt, *et al*. (1990).[313] Tissue: Vegetable oil phantom

	Visibility	
Foreign object	CT	MRI
Balsa (3 mm^2)	++	++
Balsa (1 mm^2)	0	+
Oak (4 mm^2)	+	+++
Oak (0.5 mm^2)	0	+

Table B.11: Russell, *et al*. (1991).[7] Tissue: Human cadaver hands

	Visualized?			
Foreign object	Radiography	Xeroradiography	CT	MRI
Glass	Yes	Yes	Yes	Yes
Gravel	Yes	Yes	Yes	Ferromagnetic artifacts
Plastic	No / minimal	No	Yes	Yes
Dry wood	No / minimal	Minimal	Yes	Yes
Wet wood	No	No	Poor	Yes

Table B.12: Schlager, *et al*. (1991).[288] Tissue: Beef cubes

	Ultrasound	
Foreign object	True Positives (%)	True Negatives (%)
Gravel	100	100
Cactus spine	100	100
Glass	90	90
Metal	100	100
Wood	100	100
Plastic	100	100

Overall sensitivity, specificity, PPV, and NPV: 98%

Table B.13: Shah, *et al*. (1992).[286] Tissue: Turkey breast and thigh

	Visibility	
Foreign object	Radiography	Ultrasound
Wood	0	++
BB pellet	++++	++++
Steel wire	++++	++++
Graphite (0.25 mm diam.)	0	++
Graphite (1 mm diam.)	++	+++
Rock/gravel	+++	++++
Glass	++	++++
Plastic	0	++++
Nail	++++	++++

Table B.14: Oikarinen, *et al*. (1993).[9] Tissue: Cow tongue

	Visualized?			
Foreign object	Radiography	Ultrasound	CT	MRI
Tooth	Yes	Yes	Yes	Yes
Amalgam	Yes	Yes	Hyperattenuation artifact	Ferromagnetic artifact
Glass	Yes	Yes	Yes	Yes
Asphalt	Yes	Yes	Yes	Yes
Composite	Yes	Yes	Yes	Yes
Wood	No	Yes	Yes	Yes
Stone	Yes	Yes	Yes	Ferromagnetic artifact

Table B.15: Mizel, *et al*. (1994).[25] Tissue: Porcine shoulders
Foreign objects: Wood splinters of clinically relevant size

Object characteristics		Object visibility			
Soaked	Location	Radiography	Ultrasound	CT	MRI
3 days	Near bone	0	+	++	++
3 days	Far from bone	0	+++	++	++
5 months	Near bone	0	+	0/+	+++
5 months	Far from bone	0	+++	0/+	+++

Table B.16: Bray, *et al*. (1995).[23] Tissue: Human cadaver hands

	Ultrasound sensitivity (%)	
Foreign object	Phalanges	Palm
Wood (small)	95	100
Wood (large)	100	100
Glass (small)	93	77
Glass (large)	100	100
Metal (small)	79	100
Metal (large)	93	100

Table B.17: Manthey, *et al*. (1996).[10] Tissue: Chicken thighs

	Foreign body detection rate (%)	
Foreign object	Radiography	Ultrasound
Rock	100	40
Glass	95	50
Metal	100	45
Wood	0	50
Plastic	0	40
Cactus spine	0	30
False positive rate	2	30
False negative rate	NA	50

Ultrasound sensitivity: 43%, specificity: 70%
NA: Not available

Table B.18: Jacobson, *et al*. (1998).[24] Tissue: Human cadaver feet (plantar tissues)

Wooden object size	Ultrasound (%)				
	Sensitivity	Specificity	Accuracy	PPV	NPV
2.5 x 1.0 mm	86.7	96.7			
5.0 x 1.0 mm	93.3	96.7			
Overall	90.0	96.7	92.3	98.0	83.0

Table B.19: Lagalla, *et al*. (2000).[244] Tissue: Enucleated pig eyes

	Visualized?		
Foreign object	Radiography	CT	MRI
Dry wood	No	Yes	Yes
Fresh wood	No	Yes	Yes
Glass	Yes	Yes	Moderate artifact
Iron	Yes	Yes	Ferromagnetic artifact
Plastic	No	Yes	Moderate artifact
Graphite	Yes	Yes	Moderate artifact
Air bubble	Yes	Yes	Yes

Table B.20: Orlinsky, *et al*. (2000).[384] Tissue: Chicken thighs
Foreign object: Toothpick segment

	Ultrasound				
Sonographer	Sensitivity	Specificity	Accuracy	PPV	NPV
Radiologist	83	83	83	83	83
US Tech.	85	85	85	86	84
Emerg. MD	74	87	80	85	77
Overall	79	86	82	85	80

Table B.21: Horton, *et al*. (2001).[8] Tissue: Human cadaver feet (heel pad)

	Visualized?	
Foreign Object	Ultrasound	Radiography
Windshield glass	Yes	Yes
Bottle glass	Yes	Yes
Wooden toothpick	Yes	No
Pencil fragment	Yes	Yes
Sewing needle	Yes	Yes
Galvanized steel	Yes	Yes
BB shot pellet	Yes	Yes
Stone	Yes	Yes
Plastic	Yes	No

Table B.22: Levine, *et al*. (2002).[251] Tissue: Chicken legs

	Fluoroscopy	
Glass foreign body detection	Before training (%)	After training (%)
Sensitivity	40	93
Specificity	61	91

Table B.23 a & b: Lyon, *et al*. (2004).[276] Tissue: Turkey breasts

	Correct localization with Ultrasound	
Foreign object	Without soft tissue air (%)	With soft tissue air (%)
Metal	100	100
Glass	100	100
Bone	100	100

	Characterization with Ultrasound					
	Without soft tissue air (%)			With soft tissue air (%)		
Foreign object	Accuracy	Sensitivity	Specificity	Accuracy	Sensitivity	Specificity
Metal	64	41	75	78	0	93
Glass	69	33	81	64	17	73
Bone	94	100	93	81	67	85

Table B.24: Venter, *et al*. (2005).[26] Tissue: Live chicken thighs
Foreign object: Wooden splinter

	Radiography (%)	Ultrasound (%)	CT (%)	MRI (%)
Sensitivity	13.6	63.6	72.7	59.1
Specificity	100	100	95.5	95.5
Accuracy	56.8	81.8	84.1	77.3
Pos. Pred. Val.	100	100	95	93.8
Neg. Pred. Val.	53.7	73.7	78.3	70.1

Table B.25: Turkcuer, *et al*. (2006).[250] Tissue: Chicken thighs

	Correct diagnosis (%)		
Foreign object	Plain Radiography	Soft Tissue Radiogr.	Ultrasound
Wood (positive)	0	0	85
Wood (negative)	90	90	80
Rubber (positive)	10	10	95
Rubber (negative)	90	90	80
Sensitivity	5	5	90
Specificity	90	90	80

Table B.26: Eggers, *et al*. (2007).[382] Tissue: Air, porcine muscle, porcine muscle/bone interface

Foreign object	Smallest foreign object detected (mm^3)				$3mm^3$ object detected?	
	Air		Muscle		Muscle/bone interface	
	DVT	CT	DVT	CT	DVT	CT
Amalgam	0.05	0.05	0.05	0.05	Yes	Yes
Glass	0.23	0.13	0.32	0.13	Yes	Yes
Asphalt	0.31	0.12	0.31	0.12	Yes	Yes
Tooth	0.37	0.2	0.47	0.2	Yes	Yes
Resin	0.39	0.22	3	0.39	No	No
Dry wood	0.8	0.8	18.5	2.75	No	No

DVT = digital volume tomography

Table B.27: Levine, *et al*. (2008).[122] Tissue: Human soft tissues (clinical patients)

	Radiography		
Foreign object	True positive cases	False negative cases	Sensitivity (%)
Glass	74	24	75.5
Metal	72	1	98.6
Gravel	5	0	100.0
Wood	2	25	7.4

Table B.28: Crystal, *et al*. (2008).[385] Tissue: Human cadaver arms and legs

Foreign object	Ultrasound – Correct diagnosis (%)
Glass	52.2
Metal	48.6
Plastic	53.9
Wood	55.6
None	52.8

Overall ultrasound sensitivity: 52.6%, specificity: 47.2%

Table B.29: Manickavasagam, *et al*. (2008).[383] Tissue: Sheep necks

Foreign object	Radiographic visibility
Glass	++
Hard plastic	0
Soft plastic	+
Rubber	++
Foam	0
Chicken bone	++
3mm fish bone	++
1mm fish bone	+
Safety pin	+++
Aluminum (foil and can lid)	0

Note: objects were placed in the esophagus, and could have been partially surrounded by air

Appendix C

Foreign Body Imaging:

A Pictorial Exhibit

This section is intended to give examples of the appearance of different types of foreign objects using different imaging modalities. This is not an exhaustive study of foreign objects, but all examples are characteristic in their appearance.

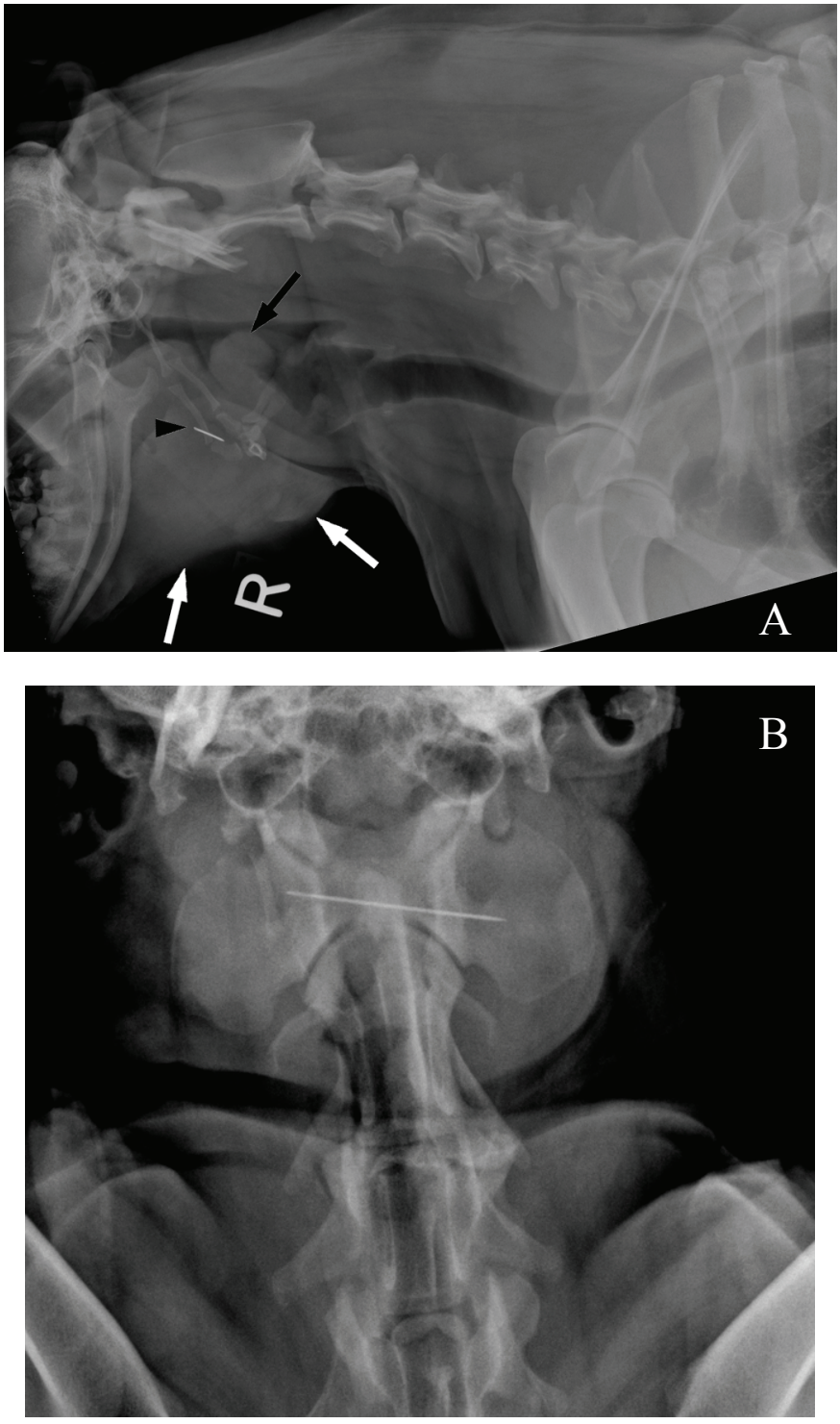

Figure C.1: Radiographs of a dog with a needle foreign body in the ventral cervical soft tissues. (A) The needle is seen nearly end-on as a metallic opacity (arrowhead) near the hyoid apparatus. There is marked regional soft tissue swelling (white arrows) as well as swelling of the epiglottis (black arrow). (B) The needle can be recognized as a linear metal opacity structure superimposed over C1.

Figure C.2: Images of a horse with a curved suture needle foreign body adjacent to the mandible. (A) Lateral oblique radiograph demonstrating the metal opacity needle (arrow) adjacent to the left mandibular ramus. (B) Ultrasound image of the curved needle (arrow) in the soft tissues. Note the comet tail artifact extending from the portion of the needle that is oriented perpendicular to the ultrasound beam.

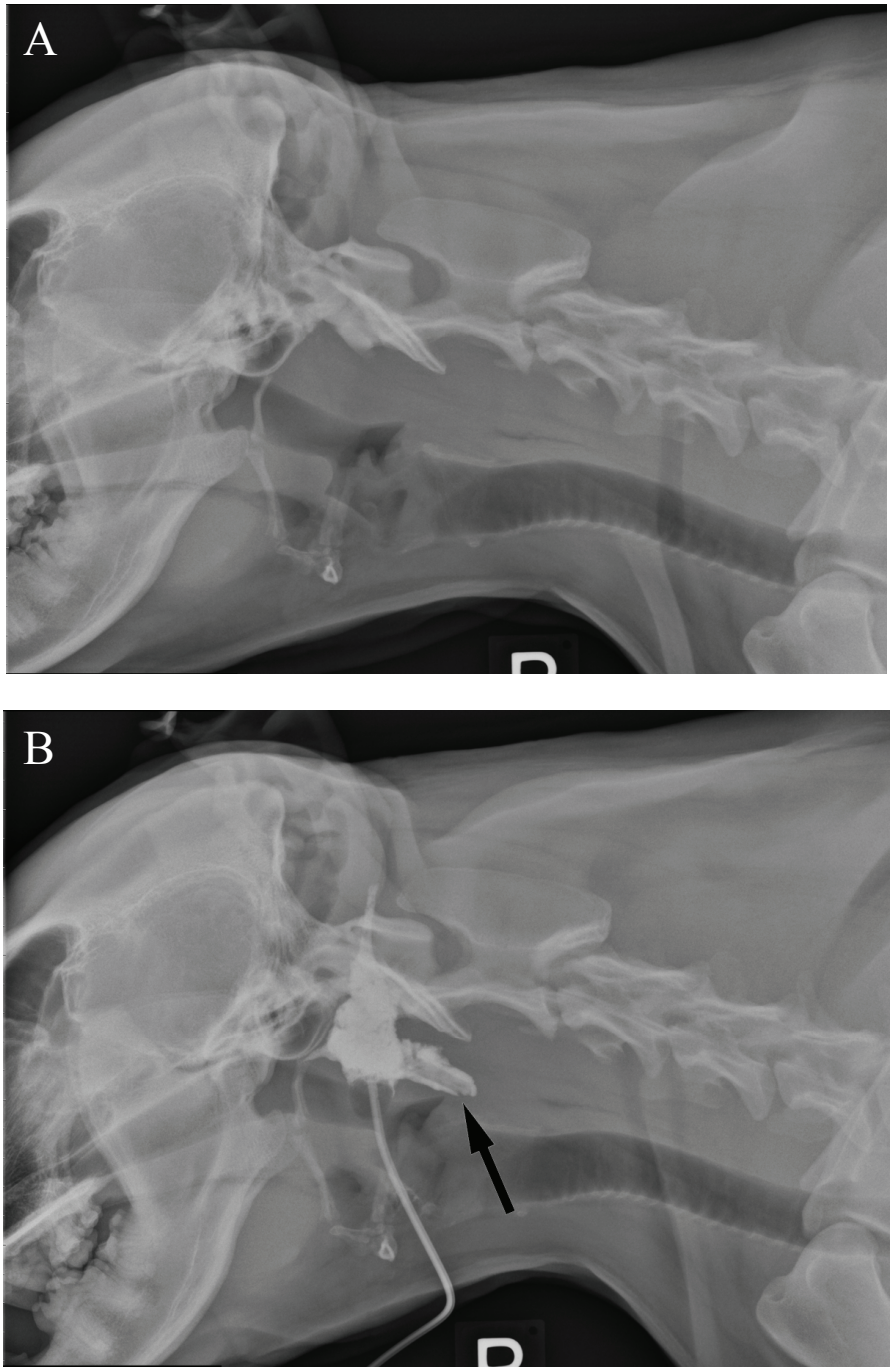

Figure C.3: Images of a dog with a wooden foreign body in the parapharyngeal soft tissues. The patient was presented for evaluation of a cervical draining tract. (A) Survey lateral radiograph of the cervical region. Only the impression of minimal soft tissue swelling dorsal to the caudal nasopharynx is noted. (B) Lateral radiograph of the cervical region following sinography. A large collection of contrast medium is present, and a filling defect (arrow) is present in one extension of the contrast medium.

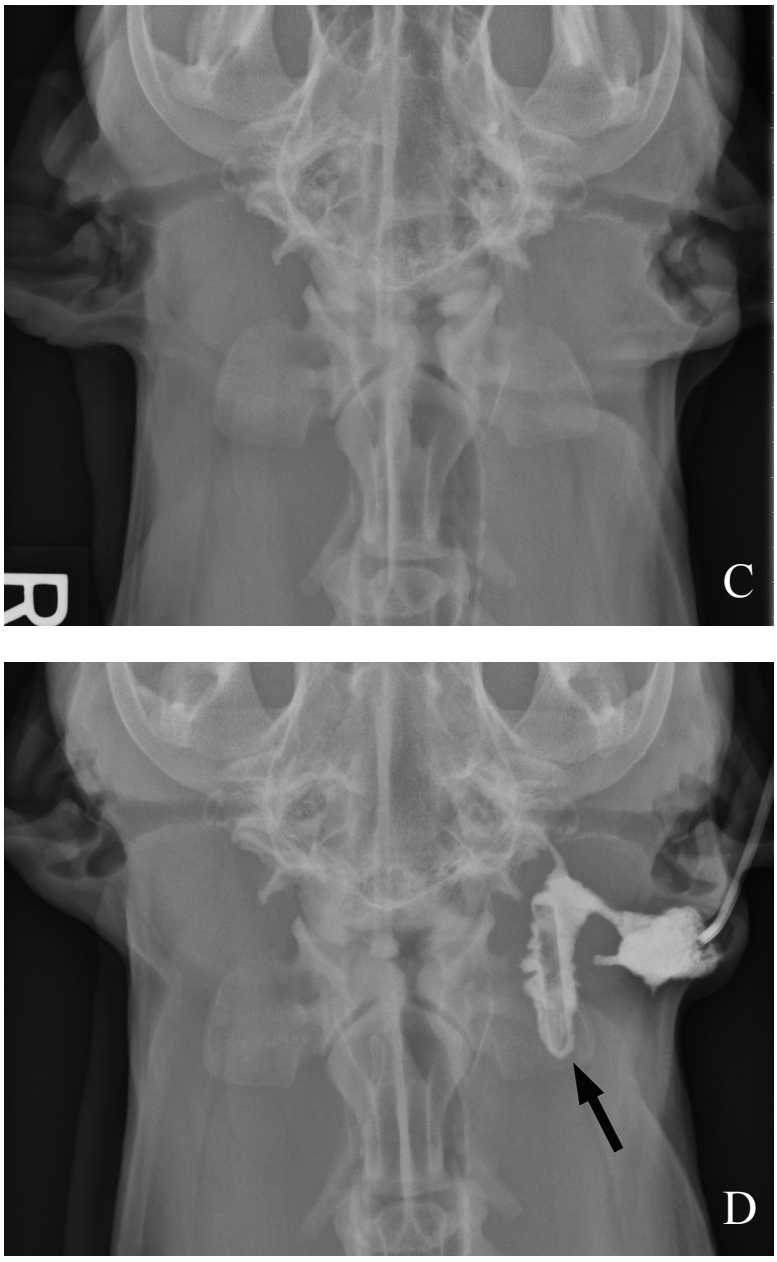

Figure C.3 (cont.): (C) Survey ventrodorsal radiograph of the cranial cervical region. No abnormalities are detected. (D) Ventrodorsal radiograph of the cranial cervical region following sinography. A collection of contrast medium is present laterally, and a filling defect can be seen within the medial portion of the contrast medium collection (arrow).

Figure C.3 (cont.): (E) Non-enhanced transverse CT image through caudal C1. The wooden foreign body is seen as a hyperattenuating ovoid structure in cross-section (arrow). Note the hypoattenuating region of inflammation and edema surrounding the foreign object. (F) Non-enhanced dorsal planar CT reconstruction. The wooden foreign body (arrow) is hyperattenuating to the surrounding soft tissues, though the opacity difference was not sufficient to visualize it on the radiographs.

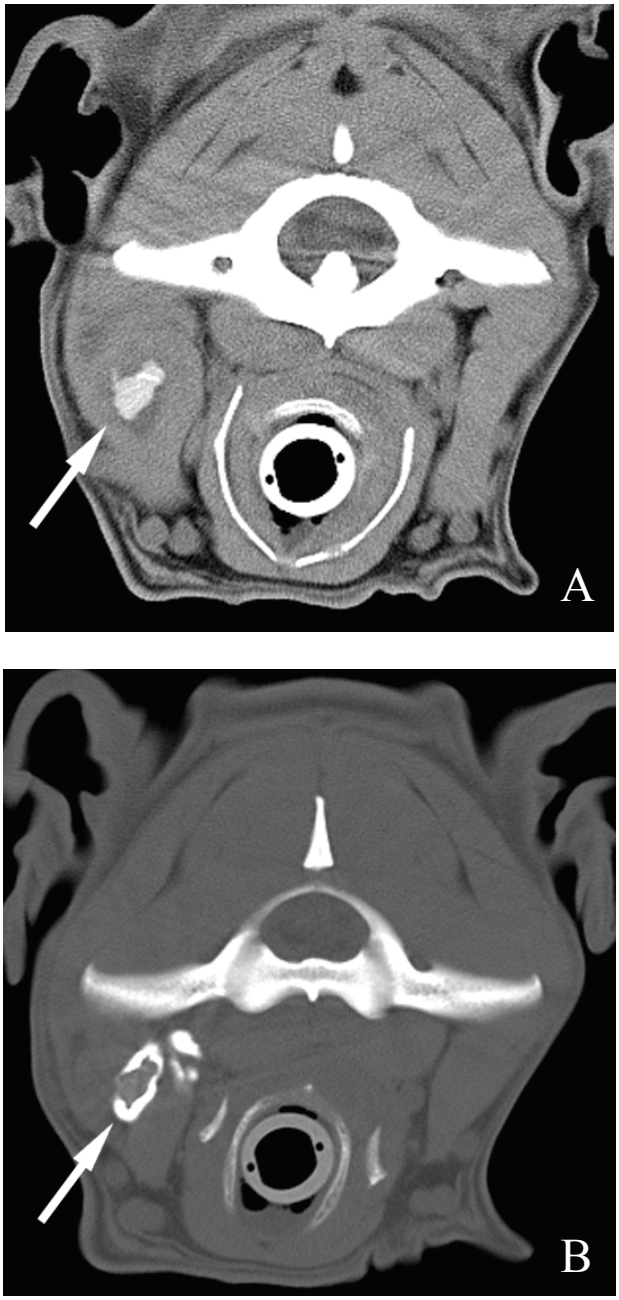

Figure C.4: CT images of a dog with a draining sinus and a wooden foreign body in the cervical soft tissues. (A) Transverse pre-contrast CT image. The wooden foreign body can be seen as an irregular hyperattenuating structure lateral to the hyoid apparatus (arrow). There is soft tissue swelling surrounding the foreign object and hypoattenuating edematous tissue immediately adjacent to the object. (B) Transverse CT image following sinography. The foreign object is seen as a filling defect within the collection of contrast medium (arrow).

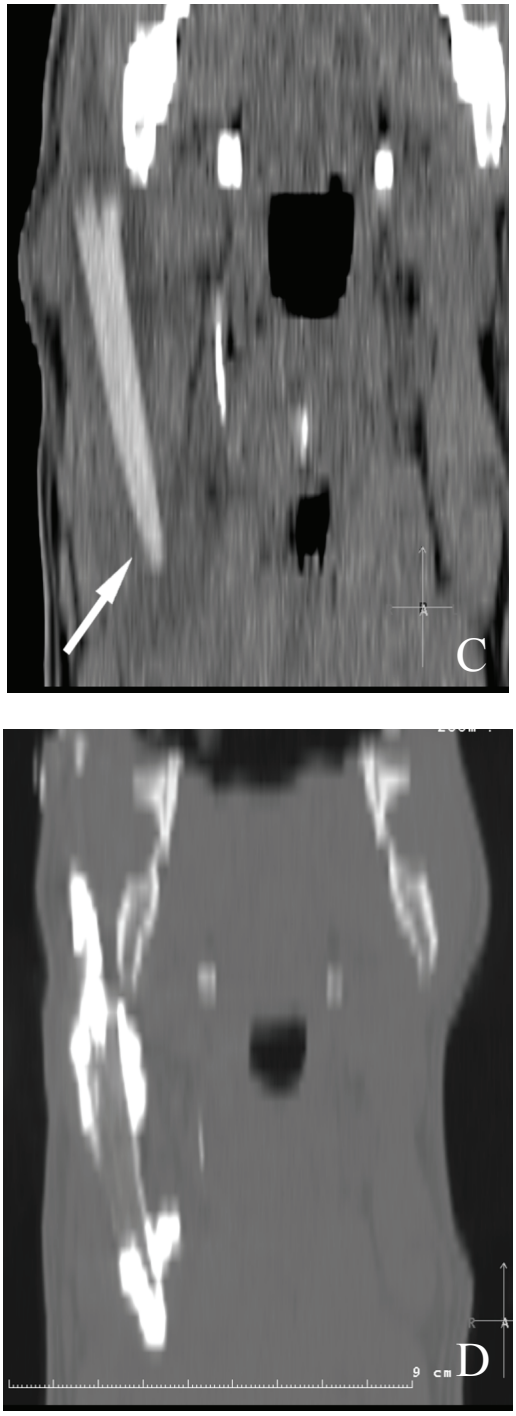

Figure C.4 (cont.): (C) Pre-contrast dorsal planar CT reconstruction of the ventral cervical tissues. The hyperattenuating wooden object (arrow) is apparent. (D) Dorsal planar reconstruction of the ventral cervical soft tissues at the same level as C following sinography. The extent of the draining sinus can be seen as an elongated collection of contrast medium. The wooden foreign object is a linear filling defect within the contrast medium pool.

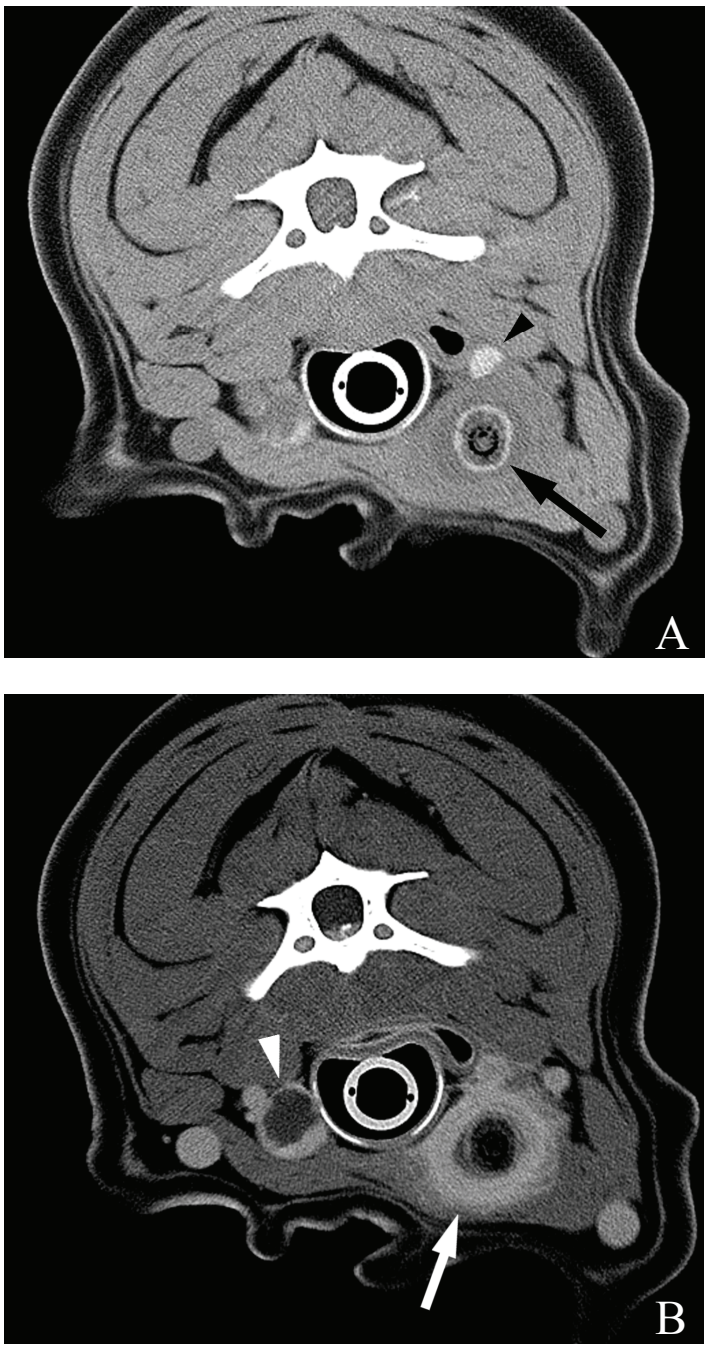

Figure C.5: Images of a dog with a stick foreign body embedded in the ventral cervical soft tissues. (A) Pre-contrast transverse CT image. The stick (arrow) is seen as a target-shaped structure with a hypoattenuating (gas) ring near the center and a hyperattenuating ring at the periphery. There is swelling and decreased attenuation of the surrounding tissues, and the left thyroid (arrowhead) is dorsally displaced. (B) Transverse CT image following intravenous administration of contrast medium. The inflamed tissues are seen as a ring of marked homogeneous contrast enhancement surrounding the stick (arrow). The fluid-filled rim-enhancing structure to the right of the trachea likely represents an abscess (arrowhead).

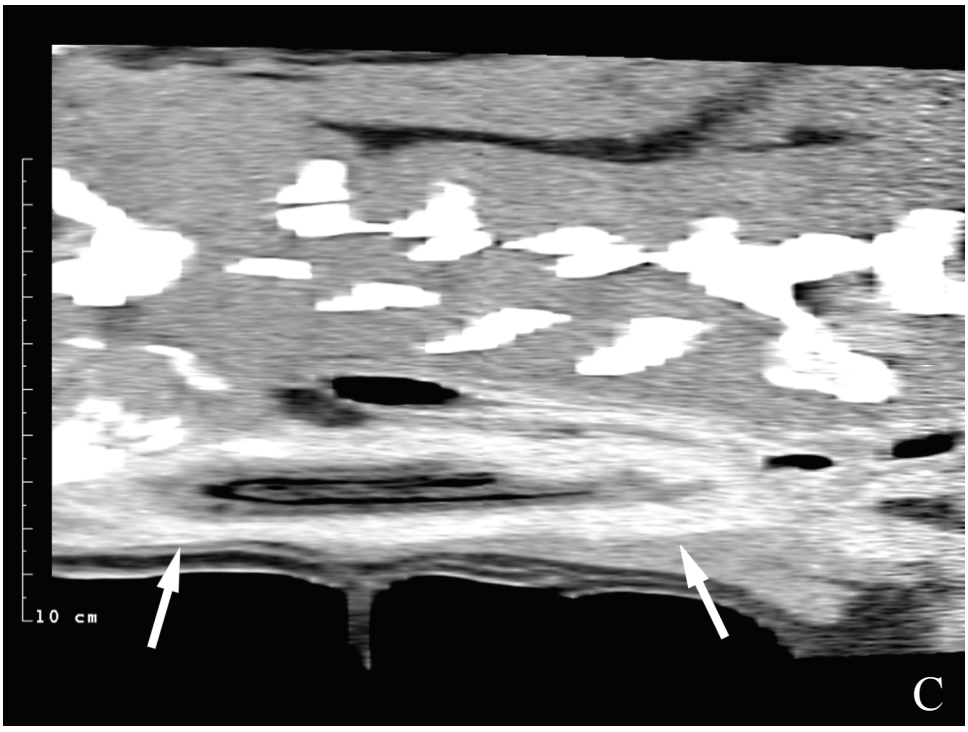

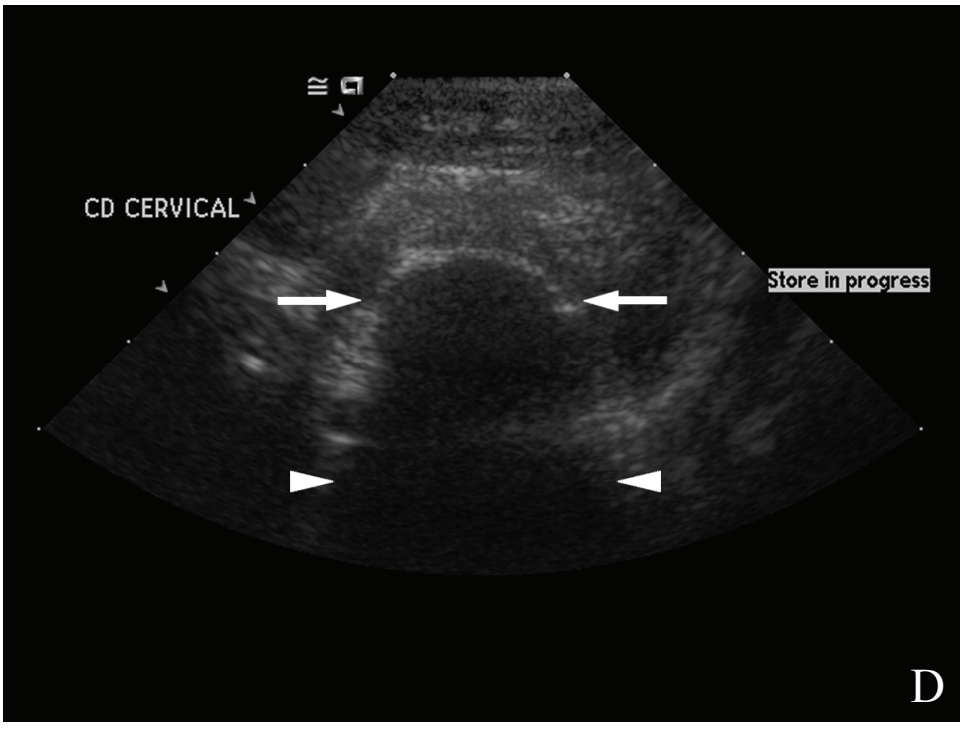

Figure C.5 (cont.): (C) Sagittal planar reconstructed CT image following IV contrast administration. Homogeneous contrast-enhancing tissues (arrows) surround the striated hypoattenuating stick foreign body. (D) Transverse ultrasound image of the cervical soft tissues. The near surface of the wooden stick is seen in cross-section as a curved echogenic interface (arrows); the far surface cannot be seen due to the marked acoustic shadowing (arrowheads).

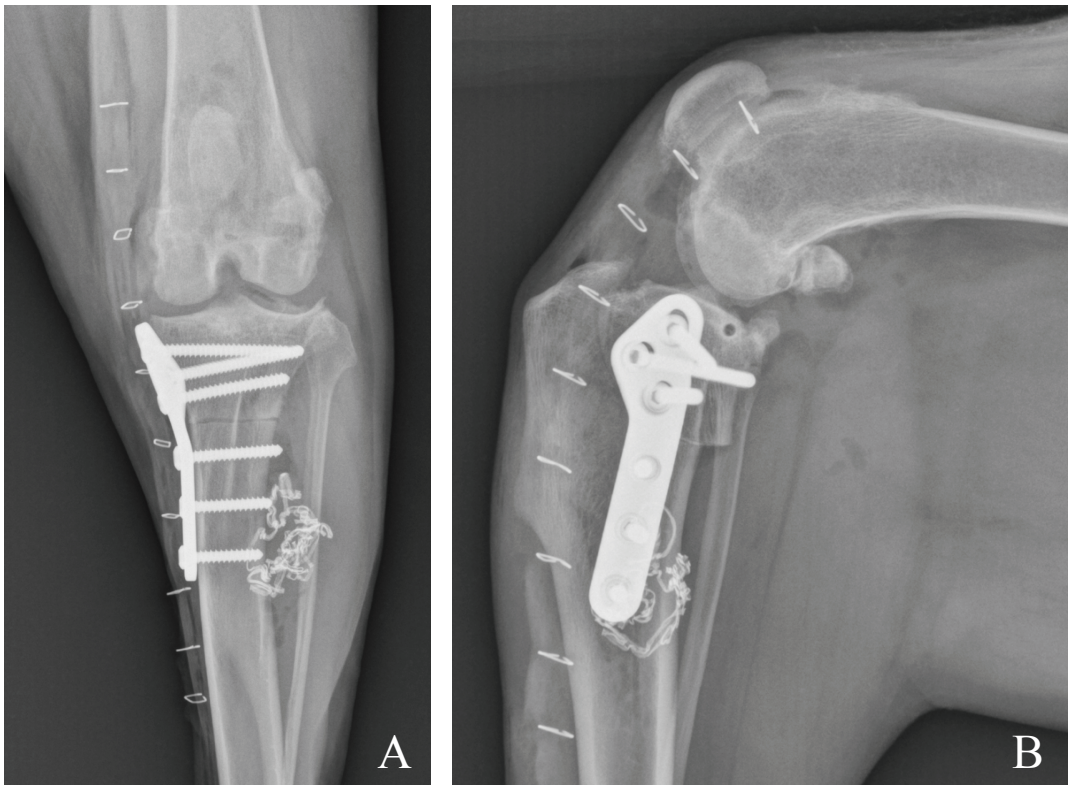

Figure C.6: Craniocaudal (A) and lateral (B) radiographs of a dog's stifle made immediately following tibial plateau leveling osteotomy surgery. The tortuous linear opacity immediately lateral to the proximal diaphysis of the tibia represents the radiopaque marker found in a surgical sponge; note that the sponge is otherwise not visible radiographically. The patient was returned to surgery following radiography and the retained surgical sponge was removed.

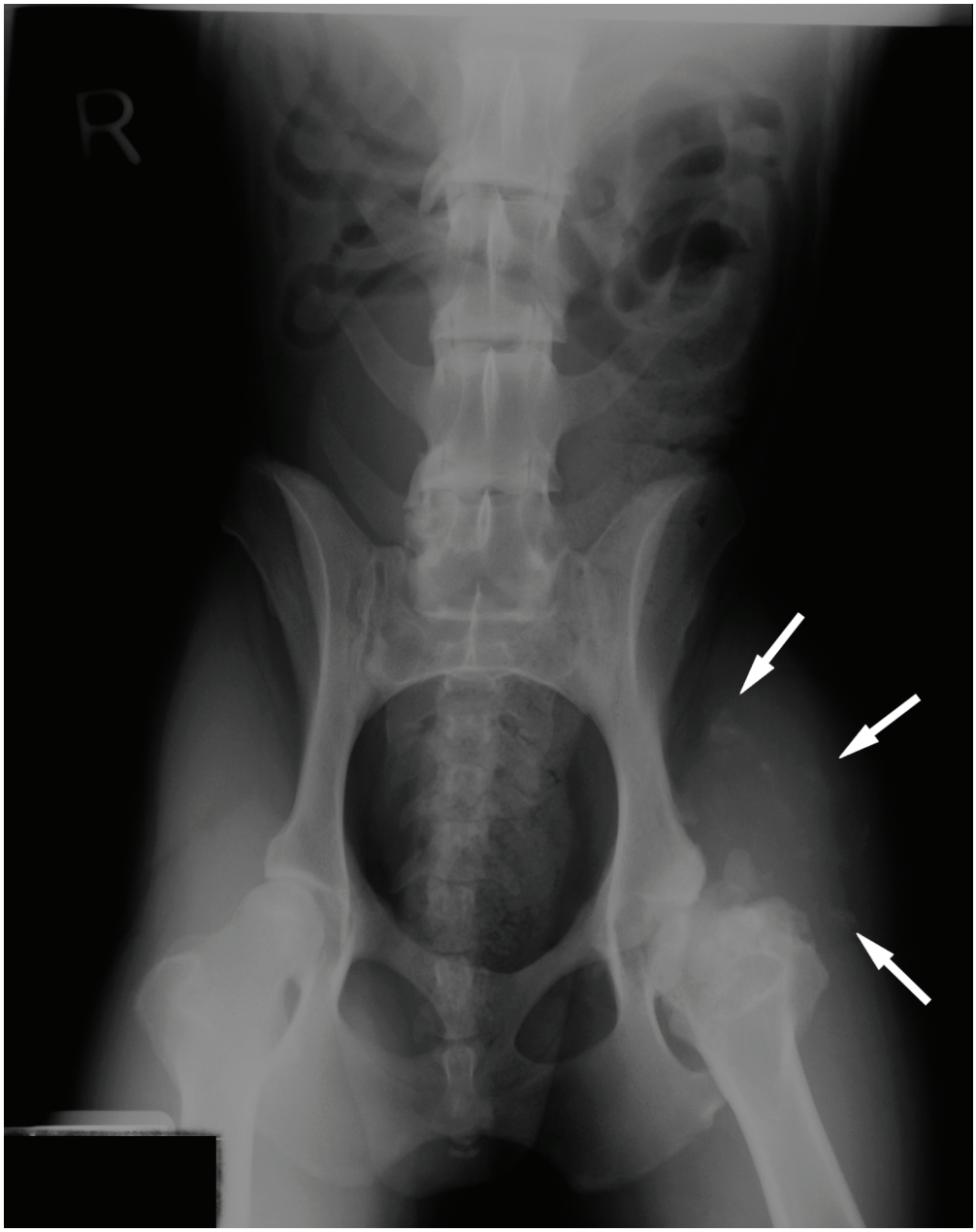

Figure C.7: Ventrodorsal pelvic radiograph of a six-year-old dog with progressive swelling around the left coxofemoral joint. A femoral head and neck ostectomy had been performed five years previously. Radiographically there is soft tissue swelling and multiple foci of soft tissue mineralization around the ilium and femur. There is also chronic remodeling of the proximal femur and acetabulum. Neoplasia was suspected based on the radiographic findings. At exploratory surgery a gossypiboma was identified, and four surgical sponges were removed. Note that the sponges are not radiographically visible because they did not include radiopaque markers.

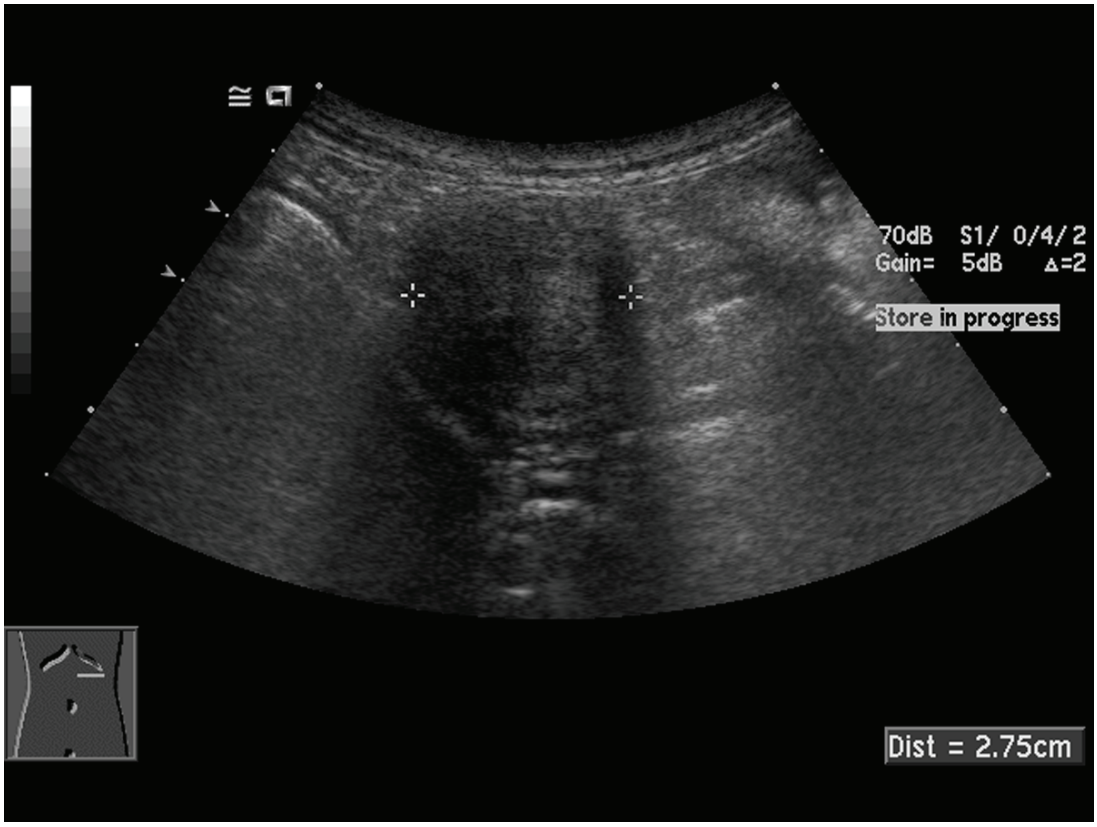

Figure C.8: Abdominal ultrasound image of a dog who was presented for chronic vomiting. Exploratory laparotomy had been performed several years prior. A heterogeneous mass with distal acoustic shadowing and reverberation artifact was identified in the cranial abdomen. Upon surgical exploration, two surgical sponges were identified in the middle of a granuloma, and there were multiple adhesions to the small intestine.